DIPARTIMENTO
DI GEOSCIENZE

UNIVERSITÀ
DEGLI STUDI
DI PADOVA

via Gradenigo,6
35131 Padova
tel +39 049 8279110
fax +39 049 8279134
CF 80006480281
P.IVA 00742430283

Padova, 29/11/2018

TO WHOM IT MAY CONCERN,

I would like to thank the reviewers of my PhD thesis, Prof. Giuliana Villa and Prof. Agata di Stefano, for their careful reading and positive evaluation of my research work entitled “Early to middle Eocene calcareous nannoplankton evolution: paleoclimatic forcing or casual pattern?”.

As I have received two positive evaluations, the regulation of the University of Padova indicates that I can only make editorial changes so that the final version that I have uploaded only contains formal edits to the text.

Kind regards,

PhD Candidate Carlotta Cappelli

Carlotta Cappelli

UNIVERSITÀ
DEGLI STUDI
DI PADOVA

Sede Amministrativa: Università degli Studi di Padova

Dipartimento di Geoscienze

CORSO DI DOTTORATO DI RICERCA IN: Scienze della Terra
CURRICOLO: Curricula-UNICO
CICLO XXXI

Early to middle Eocene calcareous nannoplankton evolution: paleoclimatic forcing or casual pattern?

Evoluzione del nannoplancton calcareo durante l'Eocene inferiore-medio: forcing paleoclimatico o pattern casuale?

Tesi redatta con il contributo finanziario della Fondazione Cassa di Risparmio di Padova e Rovigo

Coordinatore: Prof.ssa Claudia Agnini
Supervisore: Prof.ssa Claudia Agnini
Co-Supervisore: Prof. Paul R. Bown

Dottorando: Carlotta Cappelli

Contents

Chapter 3

A reassessment of middle Eocene large coccolithaceans: biostratigraphic implications and paleoclimatic clues

Chapter 4

The evolution of early middle Eocene sphenoliths: a record from Southeast Newfoundland Ridge (Site U1410)

Chapter 5

Abstract

This PhD thesis focuses on ecological and evolutionary dynamics of calcareous nannoplankton communities during the early-middle Eocene, when the extreme warmth condition of the Early Eocene Climatic Optimum progressively switched towards the long-term middle Eocene cooling. This time interval represents a crucial transitional phase in the long-term global Paleogene climate evolution, but the relationship between climate and calcareous nannoplankton are poorly constrained due to the lack of high resolution records. We present calcareous nannofossil data combined with stable isotope of bulk sediments and carbonate records from the deep-sea succession recovered at Site U1410 (IODP Exp. 342, northwest Atlantic). The continuous stratigraphic record and the exceptional preservation of calcareous nannofossils at Site U1410 enabled us to improve the biostratigraphic framework and to document the temporal relationship between changes in paleoenvironmental trends and modification in calcareous nannofossil assemblage. Throughout the study interval, the general long-term evolution of calcareous nannofossil assemblages is characterized by the onset and successively the dominance of family *Noelaerhabdaceae*. In particular, genus *Reticulofenestra* emerged during the EECO and became established as the prominent component of Eocene assemblages by the early Lutetian. The prominent increase in abundance observed during the latest Ypresian was concomitant with the decline of other important components of the assemblage such as *Zygrhablithus, Discoaster* and *Sphenolithus* and appears to have been favoured by a combination of different biotic and abiotic factors, such as the long-term effect of EECO coupled with minor environmental changes recorded as a positive step of $\delta^{18}O$. On a short-term perspective, the early Lutetian at Site U1410 is characterized by a distinctive short-term negative perturbation in the stable isotope records that have been tentatively interpreted as a warming episode that interrupted the initial post-EECO cooling phase (Chapter 2). Calcareous nannofossil assemblages seems to respond to this transient event with changes in abundance observed both in *Sphenolithus* and *Discoaster.* In addition, the exceptionally preservation of middle Eocene calcareous nannofossils enabled a comprehensive taxonomic revision of middle Eocene *Coccolithus*-like placoliths; the SEM analyses highlighted the development of cross or X-shaped structures in the central area (Chapter 3), which eventually lead to the description a new genus *Pletolithus* and a new species *(Pletolithus giganteus).* Finally, a taxonomic reassessment of the middle Eocene *Sphenolithus furcatolithoides* group was the case study of Chapter 4. Based on the morphology and extinction pattern we described the successive steps observed in this lineage that led to comprehensive understanding of the stepped evolution of this group. More importantly, these taxonomic studies improve the stability of middle Eocene biostratigraphic schemes and highlight that the appearance of reiterative characters, a apical spine within sphenoliths and a robust structure in the central area within coccolithaceans, have occurred during a phase of relatively stable conditions during the Lutetian.

Riassunto

Questa tesi di Dottorato è incentrata sullo studio delle dinamiche ecologiche ed evolutive entro le comunità dei nannofossili calcarei durante l'Eocene inferiore-medio, che coincide con l'intervallo di tempo in cui le estreme condizioni di "greenhouse" raggiunte durante l'Early Eocene Climatic Optimum progressivamente sono passate alla fase di raffreddamento a lungo temine che caratterizza l'Eocene medio. Questo intervallo di tempo rappresenta una fase di transizione cruciale nell'evoluzione climatica globale a lungo termine del Paleogene, ma ad oggi, i dettagli dell'evoluzione climatica e di quella delle associazioni a nannofossili calcarei sono poco definiti a causa della carenza di record ad alta risoluzione. In questo studio noi presentiamo i dati delle associazioni a nannofossili calcarei insieme ai record degli isotopi stabili di carbonio e ossigeno della successione sedimentaria recuperata al Site U1410 (IODP Exp. 342, Atlantico nord-occidentale), dove a partire dall'Eocene medio si sono depositate espanse successioni di drift ricche in argilla. Il record stratigrafico continuo e l'eccezionale qualità di preservazione dei nannofossil calcarei al Site U1410 hanno permesso di fornire dei dati che servono a migliorare la biostratigrafia dell'Eocene e di documentare le relazioni temporali tra i trend paleoambientali e quelli delle associazioni a nannofossili calcarei. Durante l'intero intervallo studiato l'evoluzione generale delle associazioni a nannofossili calcarei è caratterizzata dall'ingresso e aumento in abbondanza fino alla dominanza della famiglia *Noelaerhabdaceae.* In particolare, il genere *Reticulofenestra*, entra nell' associazione fossile durante l'EECO e diventa entro la fine dell'Eocene inferiore la componente dominante. Il significativo aumento in abbondanza di *Reticulofenestra* durante la fase terminale dell'Ypresiano coincide anche con la diminuzione in abbondanza dei generi *Zygrhablithus, Discoaster* e *Sphenolithus* e sembra essere legato ad un insieme di diversi fattori sia biotici che abiotici, come l'effetto a lungo termine dell'EECO sulle associazioni associato ad un spostamento di piccola entità verso valori più positivi nel record del $\delta^{18}O$. Il record degli isotopi stabili al Site U1410 è caratterizzato da una distintiva escursione negativa alla base del Luteziano che è stata interpretata come un possibile segnale legato ad un episodio di riscaldamento che ha interrotto la fase di iniziale raffreddamento a lungo termine. In corrispondenza di questa escursione negativa le associazioni a nannofossili calcarei registrano variazioni in abbondanza nei generi *Discoaster* e *Sphenolithus.* Inoltre, l'eccezionale preservazione dei nannofossili calcarei ci ha permesso di effettuare una revisione tassonomica approfondita di forme di placoliti che hanno una struttura simile a quella del genere *Coccolithus.* L'analisi al SEM di queste forme ha evidenziato lo sviluppo di strutture a croce o ad X nell'area centrale (Capitolo 3), che hanno portato alla descrizione di un nuovo genere *(Pletolithus)* e di una nuova specie *(Pletolithus giganteus).* Infine, il caso di studio presentato nel Capitolo 4 è principalmente incentrato su una revisione tassonomica degli sphenoliti dell'Eocene medio che appartengo al gruppo di *Sphenolithus furcatolithoides.* Sulla base della morfologia e del loro pattern di estinzione è stata descritta la successione degli step evolutivi all'interno di questo gruppo. Lo studio tassonomico di questi due gruppi ha consentito di migliorare la stabilità degli schemi biostratigrafici standard e ha evidenziato che la comparsa di caratteri reiterativi, come la spina apicale tra gli sphenoliti e robuste strutture nell'area centrale nelle coccolithaceae, sia avvenuta durante una fase di condizioni paleambientali relativamente stabili nel Luteziano.

Chapter 1

Introduction

1.1 OVERVIEW

The Eocene (56- 34 Ma) is an intriguing time interval of the Cenozoic that represents a paradigm of how the Earth experienced profound climate and global carbon cycle perturbations on both short-and long-timescales. It is well established that the early Eocene represents the climax of a long-term warming phase culminating in the so-called Early Eocene Climatic Optimum (~ 50-52 Ma) (Zachos et al. 2001, 2008; Bijl et al. 2009; Hollis et al. 2009, 2012), when average temperatures were about 14 ± 3 °C warmer than during pre-industrial times (Caballero and Huber et al., 2013; Cramwinkel et al., 2018). After the EECO, surface and bottom water temperatures cooled over the middle Eocene and drove the Earth's climate into a glacial regime with the inception of permanent Antarctic ice sheet at the Eocene-Oligocene boundary (e.g., Coxall et al., 2005).

In the last 2-3 centuries, geocientists have used a wide range of geochemical and paleontological proxies in order to unravel the Earth's climate history. To this aim, calcareous nannoplankton are particularly relevant when trying to reconstruct paleooceanographic and paleoenviromental conditions. Calcareous nannoplankton thrive in the photic zone of the ocean where they occupy the base of the marine food chain and their calcareous skeletons represent geochemical proxies of the past conditions (e.g., temperature, productivity of surface oceans). Calcareous nannofossils are particularly useful because of their high abundance and continuous fossil record that allow to interpret their modifications in assemblages as a response/adaptation to climate changes.

In particular, one of the most fascinating subject in current calcareous nannoplankton research is the study of the importance of biotic versus environmental factors to force evolutionary trends. This topic is receiving considerable attention because it may provide insights into the response of one of the major oceanic primary producers to significant changes in atmospheric greenhouse gas levels and projected climate changes that are expected in the near future as a consequence of anthropogenic carbon emissions. This is even more important if we consider that calcareous nannoplankton affect climate, playing a fundamental role in the organic (biomass) and inorganic ($CaCO_3$ test) carbon cycle as well as in albedo feedbacks (Tyrrell and Young, 2008).

This research focused on calcareous nannofossil biostratigraphy, evolutionary trends and paleoecological response during the early and middle Eocene transition. Interestingly, the deterioration of the extreme greenhouse condition of EECO coincided with a general reassessment of

nannoplankton communities that evolved toward a modern like structure with the appearance of important nannoplankton genera. We studied calcareous nannofossil assemblages from Integrated Ocean Drilling Program (IODP) Site U1410 (Southeast Newfoundland Ridge), that represents one of the most complete and well-preserved section yet recovered for this time interval worldwide. This unique record will be investigated in order to describe the mode and tempo of major calcareous nannofossil evolutionary trends and assemblages shifts across the early-middle Eocene transition and to provide additional insights into the critical issue concerning the influence of environmental forcing on biotic evolution.

1.2. PALEOGENE CLIMATIC EVOLUTION

The Paleogene (66-23 Ma) is often referred as one of the most dynamic period of the Earth's climate history. In contrast to the present day, much of this Epoch was characterized by the absence of permanent ice sheets at poles, much warmer mean global temperatures and higher concentrations of greenhouse gases (Zachos et al., 2001; 2008; Cramwinkel et al., 2018). Our current knowledge on past climate evolution is largely based on multi-site composite benthic foraminiferal stable isotope oxygen ($\delta^{18}O$) and carbon ($\delta^{13}C$) records (Figure 1.1).

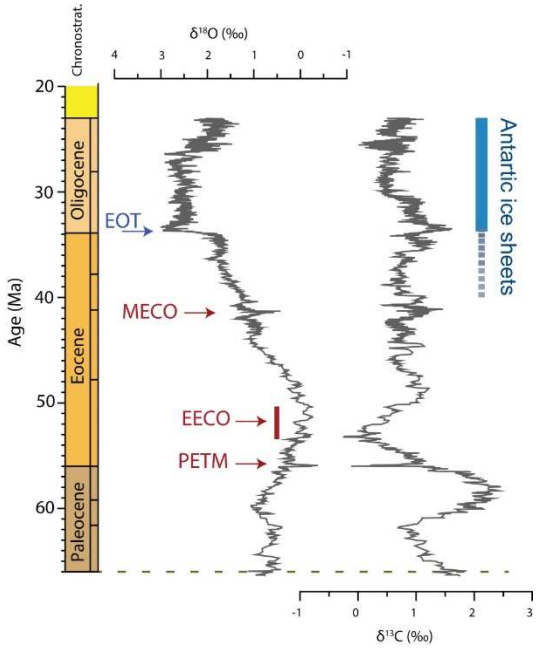

Figure 1.1: Global oxygen and carbon isotope compilations for the Paleogene (Zachos et al., 2001 converted to the Geological Time Scale 2012 (GTS12); Gradstein et al., 2012).Transient events, the Paleocene-Eocene Thermal Maximum (PETM), the Early Eocene Climatic Optimum (EECO), the Middle Eocene Climatic Optimum (MECO) are highlighted. The Eocene-Oligocene Transition (EOT) marks the culmination of the greenhouse to icehouse climatic shift.

During the early Paleogene, benthic foraminiferal $\delta^{18}O$ serves as proxy for deep-water temperature, whereas the $\delta^{13}C$ records the composition of deep-water dissolved inorganic carbon (DIC). Global $\delta^{18}O$ isotope compilation indicates that the warmest phase of the Cenozoic, the EECO, was followed

by a long-term climatic cooling that eventually led to the appearance of the first permanent ice-sheet in Antarctica at the Eocene-Oligocene transition (EOT). The long-term post EECO cooling has been documented in the benthic foraminiferal $\delta^{18}O$ records (Figure 1.1) (Cramer et al., 2003; Zachos et al., 2001, 2008; Westerhold et al.,2018), but also from other geochemical proxies, such as benthic foraminifera Mg/Ca ratio (Lear et al., 2000, Dutton et al., 2005; Hollis et al., 2012), and TEX_{86} (Bijl et al., 2009, 2013; Hollis et al., 2012; Inglis et al., 2015, Cramwinckel et al., 2018).

The increase in the mean surface temperatures during the EECO is thought to have been primary triggered by an increase of greenhouse gas concentrations (Zachos et al., 2008, Anagnostou et al., 2016); and there are growing evidences supporting the hypothesis that decreasing greenhouse gas concentrations (mainly CO_2) was the principal forcing mechanism for the Eocene cooling (Pagani et al., 2005; Zachos et al., 2008; Inglis et al., 2015; Cramwinckel et al., 2018).

Alternatively, changes in ocean circulation and meridional heat transport associated with opening of ocean gateways, specifically the opening of the Tasmania gateway or the Drake Passage, have been proposed as primary drivers of Eocene cooling (Kennet at al., 1977; Lawver and Gahagan, 2003; Lagabrielle et al., 2009, Bijl et al., 2013). The long transition to a cooler climate state was also punctuated by transient events of warming, the most pronounced occurred during the middle Eocene (Middle Eocene Climatic Optimum (MECO), Bohaty et al., 2009; Bijl et al., 2010).

Somehow related to the climate evolution, the early Paleogene is characterized by large magnitude changes in global carbon cycling that are expressed by long secular trends in $\delta^{13}C$ values (Figure 1.1). The mean global $\delta^{13}C$ values increased through most of the Paleocene (from ~ 62 Ma) and reached the maximum value at ~58 Ma where the Paleocene Carbon Isotope Maximum (PCIM) was defined (Westerhold et al., 2011). From this point, the $\delta^{13}C$ profile declined over the following ~5 Myrs towards a minimum recorded near the onset of the EECO (~53 Ma). Both long and short-term variations in the $\delta^{13}C$ trend reflect major changes in organic carbon fluxes to and from the ocean-atmosphere system. (Dickens et al., 1995; Kurtz et al., 2003; Komar et al., 2013). Specifically, the rise of $\delta^{13}C$ toward the PCIM and after EECO reflect a net removal of ^{13}C-depleted carbon from to the exogenic carbon pool (Dickens, 2000, 2003).

Superimposed on the long-term climate trend, there were a series of geologically brief (10^4-10^5 yrs) episodes of warming (termed hyperthermals). The largest of the hyperthermals was the Paleocene-Eocene Thermal Maximum (PETM at ~56 Ma), which caused a global warming of the bottom waters of more than 5 °C (Kennett and Stott, 1991; Sluijs et al., 2006; Thomas and Shackleton, 1996; Tripati and Elderfield, 2005; Zachos et al., 2010). The latest Ypresian is punctuated by numerous hyperthermals of variable magnitude (Cramer et al., 2003; Lourens et al., 2005; Agnini et al., 2009; Galeotti et al., 2010; Leon-Rodriguez and Dickens 2010; Stap et al., 2010; Zachos et al., 2010; Sexton

et al., 2011; Slotnick et al., 2012; Littler et al., 2014; Kirtland Turner et al., 2014; Lauretano et al., 2015, 2016; Westerhold et al., 2017, 2018). Hallmarks of early Cenozoic hyperthermal events are negative carbon isotope excursions (CIEs) and dissolution of carbonates at the seafloor due to acidification related to shallowing of carbonate compensation depth (e.g. Zachos et al., 2005, Kirtland-Turner et al., 2014). Hyperthermals and associated CIEs have been related to the release of massive amounts of isotopically light carbon into the ocean-atmosphere system from a ^{13}C-depleted carbon reservoir (Zachos et. al. 2005, Lourens et al. 2005, Agnini et al. 2007, Nicolo et al. 2007). Proposed carbon sources for hyperthermals are gas hydrates (Dickens et al., 1995); oceanic dissolved organic carbon (Sexton et al., 2011; Kirtland Turner, 2014) and permafrost (DeConto et al., 2012). In addition, numerous studies support the idea that most of the early Eocene hyperthermals are paced by Earth's orbital parameters, suggesting a strong orbital forcing on the carbon cycle during the super greenhouse period (Sexton et al., 2011; Littler et al., 2014; Lauretano et al., 2015, 2016; Galeotti et al., 2017; Westerhold et al., 2017; 2018). Based on the relationships between the magnitude of CIEs and the degree of inferred warming, it has been suggested that certain hyperthermals (e.g., PETM) were caused by carbon injections from a slowly recharged and more negative reservoirs (Westerhold et al., 2018). However, causes and magnitudes of carbon flux variations and the total number of hyperthermals are still focus of major research efforts (e.g. Komar et al., 2013).

1.3. THE EECO AND THE YPRESIAN-LUTETIAN BOUNDARY IN THE STRATIGRAPHIC RECORD

In order to fully understand the global climate and carbon cycle dynamics it is crucially important to reconstruct a robust chronostratigraphic framework. From this point of view, the early-middle Eocene transition is a poorly studied time interval, essentially due to the lack of highly resolved records.

The EECO was first introduced by Zachos et al. (2001), based on a 1.5 ‰ decrease in the global compilation $\delta^{18}O$ curve. However, this long-lasting event lacks of a formal definition due to several reasons (Slotnick et al., 2015; Luciani et al., 2016; Westerhold et al., 2018): (I) the age model used by Zachos et al. (2001) is now out of date; (II) using temperature (i.e., $\delta^{18}O$) to correlate records at different locations might be inaccurate because warming as cooling trends may have occurred at different times; (III) there are relatively few records of past temperatures that can be clearly linked to geopolarity time scale during the early Eocene.

Recently, it has been proposed to place the onset of the EECO in correspondence of the prominent CIE termed J event (Luciani et al., 2016). This suggestion is based on observations from stable benthic foraminifera isotope data from deep-sea Site 1263 (Walvis Ridge, Lauretano et al., 2015), and on lithological and carbon isotope data from land-based Mead Stream section (New Zealand, Stoltnick

et al., 2012). Specifically, in this succession, the J event and the onset of the EECO correspond to a significant shift in the sedimentary regime, which led to the deposition of a marl-rich unit (Lower Marl Unit). At Mead Stream, the increase in terrigenous sedimentation and carbonate dilution in correspondence of the Lower Marl Unit has been related to an acceleration of the hydrological cycle and to enhanced seasonality due to warmer surface temperatures throughout the EECO (Slotnick et al., 2012, Dallanave et al., 2015). In this section, the end of EECO is characterized by the decrease of the terrigenous component that lithologically coincides with transition between the Lower Marl and the overlying Upper Limestone units. This transition occurred in the upper part of Chron C22n (Dallanave et al., 2015). Luciani et al., (2016) noted that the first appaerance of the calcareous nannofossil *Discoaster sublodoensis* lies in a similar position respect to magentostratigraphy (Agnini et al., 2014), suggesting to use this biohorizon for stratigraphic correlation purposes. Following this definition, the EECO lasted ~ 4 Myr (calcareous nannofossil Zone CNE3-CNE5), spanning from 53 Ma to 49 Ma if the Geological Time Scale 2012 (GTS2012) is adopted, but its formal definition is still matter of discussion.

Another important chronostratigraphic issue is the ambiguous bio-magnetostratigraphic framework across the Ypresian-Lutetian boundary. The Global Stratigraphic Section and Point (GSSP) for the base of the Lutetian is placed in a dark marly level in the Gorrondaxte section (Spain). This level coincides with the firs appaerance of the calcareous nannofossil *Blackites inflatus* (Molina et al., 2011). However, the position of this biohorizon with respect to magnetostratigraphy is controversial (Agnini et al., 2017). In detail, the base of *B. inflatus* shows an offset of more than 600 kyr between data from IODP Atlantic sites (1258, 109-1410) and the Gorrondatxe section (Norris et al., 2012; Westerhold et al., 2017). More interestingly, previous data from Gorrondatxe section and northwest Pacific Ocean (ODP Site 1209, Westerhold et al., 2018) provide evidences for significant stable isotope perturbation close the Ypresian- Lutetian boundary (Payros et al., 2012; Intxauspe-Zubiaurre et al., 2017 a, b). However, as a consequence of the unclear bio-magnetostratigraphicc framework of the latest Ypresian and early Lutetian, any correlation between different datasets remains at present speculative.

1.4. CALCAREOUS NANNOFOSSILS

Calcareous nannofossils are a collective term that includes calcareous fossils smaller than 30 µm (Bown and Young, 1998). A great variety of organisms therefore can be ascribed to calcareous nannofossils (e.g. spicules, calcareous cysts, small foraminifera), however the dominant group that produces calcareous remains are the coccolithophores (or calcareous nannoplankton). They are single-celled calcifying phytoplankton secreting a tiny composite exoskeleton, the coccosphere that

is made of multiple coccoliths. Although morphologically highly diverse, all coccoliths have a calcite composition, only very few aragonitic coccoliths have been documented (Manton and Oates, 1980; Cros and Fortuno, 2002). Calcareous nannoplankton first appeared in the Triassic and reached rock-forming abundance since the early Jurassic (ca. 150 Mya) (Bown et al., 2004), if not even before (Preto et al., 2013). From this moment, calcareous nannoplankton have had a major impact on marine biogeochemical cycles, acting on different time scales and processes. During photosynthesis CO_2 is stored in organic compounds ("organic carbon pump"), while the biomineralization is a short-term source of CO_2 for the atmosphere and the upper ocean ("carbonate counter pump"). On geological time scales, the burial of coccoliths is the main mechanism to store carbon into sediments, and consequently it contributes to remove CO_2 from the ocean-atmosphere system (e.g. DeVargas et al., 2007). This is of particular relevance considering that coccoliths are thought to be responsible for about half of all modern precipitation of $CaCO_3$ in the oceans (Milliman, 1993). Today, as in the past, variations in productivity (C_{org} and $CaCO_3$) may result in significant changes in carbon fluxes between different reservoirs, and in turn in the global carbon cycle.

1.4.1 Calcareous nannofossil taxonomy

The taxonomy of calcareous nannofossils is primarily based on the complex morphology of coccoliths/nannoliths and ideally rely on the use of homologous structural elements. The paleontological species concept adopted for calcareous nannofossils is substantially different to that used for other modern no-calcifying haptophyte algae, which is based on cell cytology, biology and molecular genetic (Saez et al., 2003).

Based on their morphostrucutures, coccoliths have long been classified in two broad groups: heterecoccoliths and holococcoliths (Braarud et al., 1995). The structure of heteroccoliths is complicated and consists of strongly modified crystals with different sizes and shapes arranged in interlocking cycles with different crystallographic orientations. By converse, holococcoliths usually have simpler structures, formed by non-hinterlocking rhomboehedrical crystallites of uniform size (~0.1 μm) (Billard, 1994; Young et al., 1999).

Other biogenic calcareous structures of similar size but lacking the characteristic features of either heterococcoliths and holococcoliths and like secreted by haptophytes, are defined as calcareous nannofossil of uncertain affinities. A common collective term for these forms is nannolith (*e.g.* Perch-Nielsen, 1985a, b; Bown, 1987.). This group includes important extinct taxa.

Heterococcoliths are the dominant group in fossil and modern assemblages. The identification of major clades within this group is based on the V-R model. The V/R biomeralization is characterized by an initial nucleation of a proto-coccolith ring that is formed of regularly spaced calcite crystals

with alternating sub-vertical (V-units) and sub-radial (R-units) c-axis orientations (Young et al., 1992). For species levels taxonomy variable characters that are formed later in the coccolith biomeralizations (e.g., central area structures, processes spine morphologies) are used. Concerning holoccoliths and nannoliths, their systematic is more controversial from a formal perspective (Young et al., 1997). However, their definition as separated taxonomic units is extremely useful for several applications.

A major outcome from modern culture observations is that coccolithophores have an heteromorphic life cycle during which they produce distinct coccoliths with diverse biomineralization modes in the two phases of their haplo-diplotic life cycle. Heterococcoliths are produced in the diploid phase of the life-cycle within the cytoplasm in the coccolith vesicle (Young and Henriksen, 2003). The calcite secreted to produce heterococcoliths is chemically different from abiotic calcite, suggesting a strong physiological control on the intracellular calcification processes (Cros et al., 2013). Holococcoliths are associated with the haploid phase of the life-cycle and they are produced within membrane-bound space but outside the cell wall (Rowson et al., 1986). Although the most common heteromorphic life cycle is that in which heteroccoccoliths are produced during the diploid phase and holococcoliths during the haploid phase, many exceptions exist. For example, the coccolithophore family of Noelearhabdaceae appears to not calcify during the haploid phase and the Ceratolithaceae and Alicosphaeraceae are known to produce both heteroccoliths and nannoliths within their life cycles (Alcober and Jordan 1997; Sprengel and Young 2000; Cros et al. 2000; Cros and Fortuno 2002; Young et al. 2003). The morphologic affinity of extinct taxa is sometime very difficult to reconstruct, especially for those with no clear modern descendants. A special attention is deserved to nannoliths that are considered a polyphyletic group including modified heterococcoliths, modified holococcoliths and nannoliths formed by entirely different biomeralization mechanism (Bown and Young, 1997).

The complicated biological cycle displayed by extant forms suggest that all inferred taxonomic affinities of fossil species are largely based on morphological features, and that biological affinities are only supposed. In the common practice, each biominiralizated phase observed in the fossil record is considered as a single independent species, although it might have been produced by the same organism in different phases of its life-cycle. A further potential complication is related to polymorphism, i.e. have two or more coccoliths types on a single coccosphere. Several modern coccosphere types (sensu Young et al., 2005) display polymorphism, but coccospheres are not commonly preserved in the fossil assemblages and therefore assessing the possible extent of polymorphism is difficult in the fossil record. On the other hand, it might happen that two similar coccoliths do not belong to the same species but represent cryptospecies (DeVargas et al., 2004),

since (pseudo)cryptic speciation has been recently documented in certain modern coccolithophores (Saez et al., 2013).

Modern taxonomic practice encourages to avoid the use of group that are thought to be polyphyletic/artificial. It is noteworthy that evolutionary trends have always stimulated the interest of nannofossil micropaleontologists that have provided strong basis for the modern Paleogene calcareous nannofossil taxonomy (i.e. Gartner, 1970; Prins, 1971; Bukry, 1971). Essential requirements to undertake rigorous evolutionary studies on nannofossil are (I) the detailed documentation (step by step) of the evolutionary transition given by the presence of forms with intergrading morphological features between two end-members and (II) the availability of continuous and expanded sections containing abundant and well-preserved nannofossils.

The importance of taxonomy expands into diverse applications of calcareous nannofossils, i.e. biostratigraphy, where application of rigorous taxonomic concept is crucial to gain reliable results.

1.4.2 Calcareous nannofossil biostratigraphy

Calcareous nannofossils are present in the fossil record from 220 My ago (or even before), when calcareous nannoplankton presumably started to calcify (Bown, 1998). The rapid evolution, the wide geographic distribution (from tropics to polar regions) and the abundance in marine sediments (millions of individuals per gram of calcareous sediments) of calcareous nannofossils have made them one of the best fossil groups for stratigraphic correlations. Though the effectiveness of calcareous nannofossil taxonomy is possibly biased by their complicated life cycle, the use of this group as a biostratigraphic tool benefits of several advantages such as the high evolutionary rates that in principle could provide a large number of biohorizons. Bramlette and Riedel (1954) first recognized the biostratigraphic usefulness of this group. From that time onwards, numerous biostratigraphic schemes were developed for part of the Cenozoic, but only with the availability of numerous deep-sea successions recovered by ocean research drillings, calcareous nannofossil zonations have become more refined (e.g. Martini 1971; Sissingh and Prins 1977; Roth 1978; Okada & Bukry, 1980).

Over four decades later, calcareous nannofossil biozonations of Martini (1971) and Okada & Bukry (1980) are still widely used. Recently, Agnini et al. (2014) have published a new low-middle latitude zonation for the Paleogene, which presents a combination of reliable biohorizons from previous schemes and new biohorizons (Figure 1.2). The principal aim of the new biozonation was to provide a robust biostratigraphic framework that relies on reproducible and trackable biohorizons.

Biostratigraphy is a very complicated discipline and it is becoming clear that having quantitative and highly resolved datasets is an essential requisite to provide the correct position and to discuss the

reliability and the correlativity of a certain biohorizon. Indeed, markers used in the standard biozonantion schemes may show complicated abundance patterns, being consistently rare-absent in specific settings or showing sporadic abundances around their level of evolutionary emergence and/or extinction. All these features can led to significant inconsistences in biostratigraphic results.

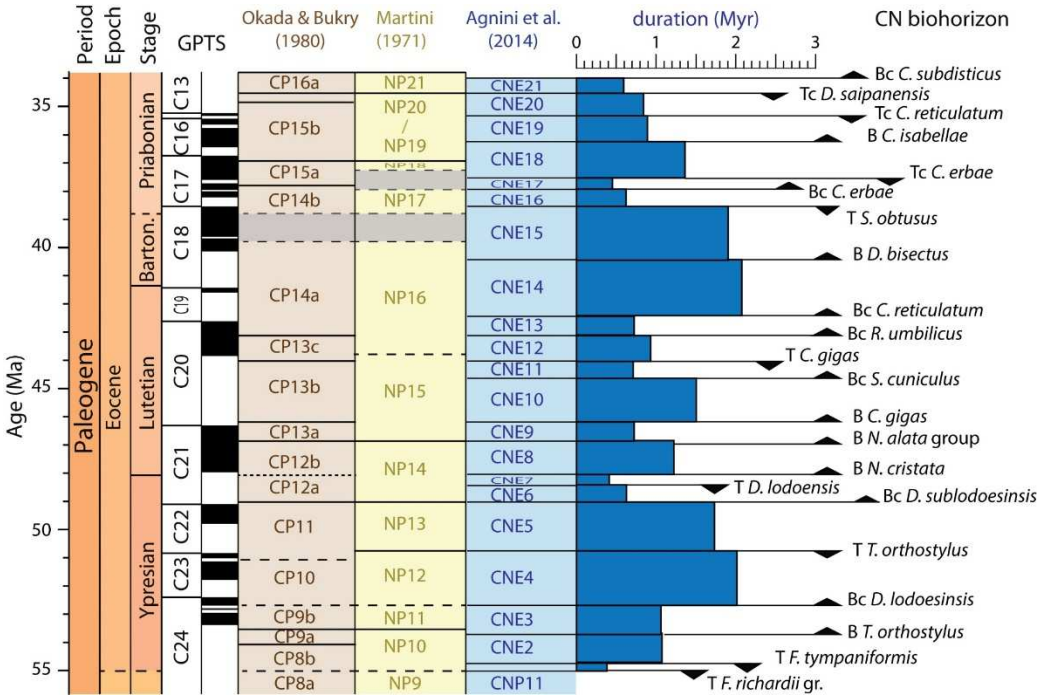

Figure 1.2: Paleogene calcareous nannofossil biozonations (CP, Okada & Bukry 1980; NP, Martini 1971; CN, Agnini et al. 2014) and primay biohorizons used in Agnini et al. (2014) are plotted versus the chronostratigraphic scale and the Geomagnetic Polarity Time Scale (GPTS; Lourens et al., 2004). Biohorizons: B=Base, Bc= Base Common; T=Top, Tc= Top Common. The duration of CNE zones is also reported. Modified from Agnini et al. (2104).

An additional potential problem in biostratigraphy is the taxonomic effect. Different species concept among workers, related to ambiguities in the formal original descriptions or to highly variable morphologies, caused inconsistencies. A stable and unambiguous taxonomy of marker index species is essential in order to guarantee stability and reliability in the available biozonation schemes.

1.4.3 Calcareous nannofossil paleoecology

The evolutionary history of calcareous nannoplankton suggests an intrinsic relationship with Paleogene climate evolution, both on the short and long time scales. After the Cretaceous-Paleogene boundary, which coincides with a massive extinction in calcareous nannofossils, nannoplankton diversity increased up to reach the Cenozoic maximum in the early Paleogene and then significantly declined to the Cenozoic minimum in the Oligocene (Bown et al., 2004; Bown, 2005). The diversity decline through the middle Eocene cooling results from an elevated rates of extinction and a low rate of speciation. The significant diversity loss of nannofossils has been interpreted to be linked to middle Eocene cooling, which presumably resulted in the establishment of new unfavourable habitats for

nannoplankton, in which they could not flourish as in the past (Bown et al., 2004, Bown et al., 2005). Besides temperature, other factors, such as competitive interactions with other planktonic groups and nutrient availability and light, might have played an important role in the long-term processes of diversity loss (Bown et al., 2005).

In addition, numerous studies have shown that calcareous nannoplankton populations were also affected by environmental changes that took place over short timescales. Calcareous nannofossil response to transient environmental perturbations might include relative changes in assemblage compositions, evolutionary turnover and, in the case of the extreme PETM conditions, the appearance of short-lived excursion taxa.

The distribution of extant coccolithophores is largely controlled by temperature and water-mass nutrient concentrations (e.g. Okada and Honjo, 1973; Winter et al., 1994). The composition and diversity of modern nannoplankton assemblages fluctuates with thermal and nutrient structure of water column and, by analogy, changes in calcareous nannofossil assemblages are considered an excellent proxy to assess past variations in sea-surface temperatures and nutrient levels (Lees et al., 2005.).

Our current knowledge of paleoecological preferences of nannofossil taxa is largely based on pioneering studies of paleobiogeography (e.g., Haq and Lohmann, 1976; Roth and Bowdler, 1981; Roth and Krumbach, 1986; Watkins, 1986; Wei and Wise, 1990; Wei, Villa and Wise; 1992; Aubry, 1992) and calcareous nannofossil assemblage data are usually interpreted in the context of a Trophic Resources Continuum (TRC- Hallock, 1987). Fossil taxa that thrived in cold water assemblages have been interpreted as adapted to eutrophic environments, likewise taxa that are more common in warm water assemblages have been interpreted as more adapted to oligotrophic environments. However, the concept of TRC implies that a wide range of mesotrophic communities exists.

Over the past years, several studies have compared assemblage data with geochemical proxies for paleotemperature and paleoproductivity ($\delta^{18}O$, Ca/Mg, $\delta^{13}C$, Sr/Ca), improving the paleonvironmental interpretation of specific taxa that have become established as indicators of paleotemperature and /or paleofertility in a variety of situations. However, although some species are relatively well understood, others appears to have more complicated ecologies and have shown contradictory behaviours (Villa et al., 2008; Bown and Pearson, 2009; Schneider et al., 2011). Additional uncertainties are related to the difficulty to disentangle the temperature effect from the control played by nutrients availability, as well as to determine the role of other biotic factors (grazing, bacterial infection, competition).

1.5. EARLY-MIDDLE EOCENE OCEANOGRAPHY AND THE NORTH ATLANTIC SITE U1410

Alongside significant changes in the global climate, the Paleogene experienced crucial variations in deep ocean currents that have contributed to the formation of the modern circulation system. Modern North Atlantic Deep Water (NADW) production accounts for ~40% to 50% of Atlantic Meridional Overturning Circulation (AMOC), which in turn implies a fundamental role in the regulation of global climate (Broecker, 1998). In the modern ocean, the NADW forms in the Labrador and Nordic Seas as surface waters. The sinking of NADW is largely controlled by the balance between warm salty water from low latitudes and cold freshwater from the Antarctic Ocean at convection sites and by the wind-driven upwelling in the Southern Ocean (Coxall et al., 2018). During the Paleogene, deep-water circulation was substantially different from today due to warmer global temperature and different paleoceanographic configuration. The onset of the NADW is thought to have coincided with the Antarctic ice sheet growth at the Eocene-Oligocene boundary (Davis et al., 2001; Via et al., 2006), but the onset of a deep current activity in the North Atlantic is thought to be older (Coxall et al., 2018). Based on the presence of drift sediments at the Greenland-Scotland Ridge, Hohbein et al. (2012) suggested that deep current activity in the Northeast Atlantic initiated close the early-middle Eocene boundary. This age estimation coincides also with the onset of drift sedimentation observed at northwest Atlantic sites retrieved during Integrated Ocean Drilling Program (IODP) Expedition 342 (Boyle et al., 2017), which thus corroborates previous studies focused on the formation of the northern hemisphere deep-water mass. Major changes in deep ocean circulation at the early-middle Eocene transition has been evidenced also by changes in the global inter-basinal $\delta^{13}C$ gradient (Sexton et al., 2006), warming of the Atlantic relative to the Pacific (Cramer et al., 2009) and enhanced global productivity (Nielsen et al., 2009).

The Site investigated in this PhD thesis, Site U1410, is one of the nine sites (Sites U1403-U1411) that were drilled during IODP Exp. 342 (Norris et al.; 2014) (Figure 1.3a). Specifically, Site U1410 is located on the Southeast Newfoundland Ridge (SERN), a positive bathymetric feature extending southeast from Grand Banks. Today, this Site is positioned on the path of the Deep Western Boundary Current and the Gulf Stream (Figure 1.3b). SERN has been interpreted as a volcanic edifice overlying the intersection of the transform margin and the axis of the rift between Newfoundland and Iberia that led to the opening of the Labrador Sea and the northwest Atlantic Ocean starting from the end of Jurassic (Tucholke and Ludwig, 1982; Tucholke et al., 2007). The oceanic basement of SERN is capped by a rudist reef of Barremian/early Aptian age, which presumably were exposed above sea level before subsiding to abyssal depth by the late Cretaceous (Tucholke and Vogt, 1979), when pelagic sediment began to cover the ridge.

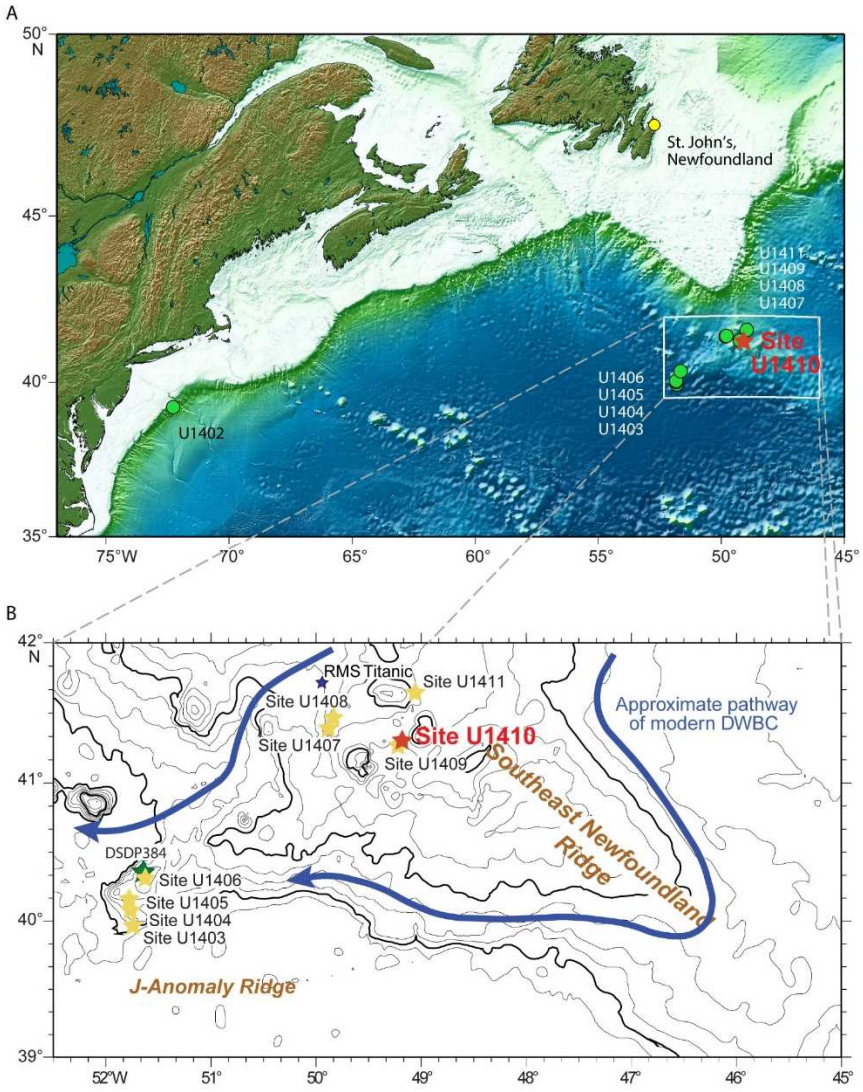

Figure 1.3: A) Location map of the sites drilled during Expedition 342 in the northwest Atlantic, off the coast of Newfoundland. B) Bathymetric map showing the pathways of modern Deep Western Boundary Current (DWBC). Modified from Norris et al. (2014).

At Site U1410 a 260 m thick sedimentary succession of deep-sea sediments was recovered. These sediments comprise short Pleistocene sequences overlying higher sedimentation-rate Oligocene through early Eocene succesions. As with other sites drilled on the Southeast Newfoundland Ridge, the most prominent change in the sedimentary succession at Site U1410 is a severe drop in calcium carbonate content close the early middle Eocene boundary. This drop marks the transition from nannofossil chalk sedimentation to greenish grey nannofossil clay and nannofossil ooze deposition (Figure 1.4).

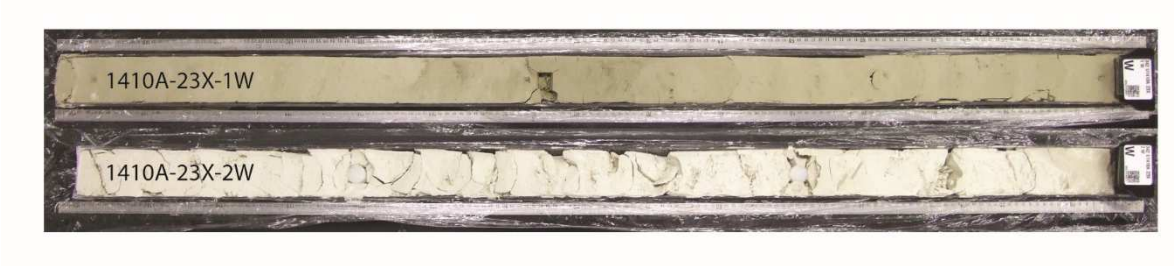

Figure 1.4: Core images showing the boundary defined by the transition from white to pinkish white nannofossil chalk (lithostratigraphic Subunit IVa, Norris et al., 2014) to greenish grey nannofossil ooze (lithostratigraphic Unit III, Norris et al., 2014) in correspondence of the early-middle Eocene transition.

The change in sedimentary regime has been interpreted to mark the onset of significant deep current activity that was able to transport sediments from source along the northeast Canadian continental margin southward to the Newfoundland Ridge (Boyle et al., 2017).

The primary objective of IODP Exp.342 was to acquire contourite drift sediments (Norris et al., 2014), which can provide high-resolution (MAR = 1.3-2.6 cm /kyr) archives of oceanographic and climatic changes throughout the Paleogene. A great value of Newfoundland sediments drifts is the good to exceptional preservation of microfossils. These sediments are therefore suitable for trace element geochemistry, isotope geochemistry and microfossil assemblage studies.

1.6. OBJECTIVES

A series of questions are still open as to whether calcareous nannofossil evolutionary changes were controlled by intrinsic evolutionary trends or if these changes were partially driven by major trends in the climate evolution (Van Valen, 1973; Stenseth & Maynard, 1984; Thierstein et al., 2004). Try answering to these big questions is really difficult but the early-middle Eocene is an ideal case study because it encompasses a dramatic shift in the global climate state which has passed from the climax of the early Eocene to the post-EECO long-term cooling. During this time of climate reversal, the calcareous nannofossil assemblages underwent a profound renovation which includes the entry and expansion of the very successful Noelaerhabdaceae family (i.e, *Reticulofenestra/Dictyococcites*), marking the first step toward the modern-like assemblage structure (Agnini et al., 2006). The early-middle Eocene was therefore one of most significant interval of both climate and calcareous nannoplankton evolutions, but, as yet, the details of these crucial changes are uncertain because few stratigraphic records with appropriate resolution have been studied.

The principal objective of this study is contributing to address this gap, with detailed analysis of calcareous nannofossils alongside comparable investigation of environmental proxies. Specifically, this study is focused on the most remarkable events in the early middle-Eocene nannofossil assemblages, including fluctuations in abundance patterns, biostratigraphy and evolutionary changes displayed by different calcareous nannofossil groups.

To this purpose, the sedimentary succession recovered at Site U1410 represents an extraordinary archive, with the most complete succession yet recovered in the North Atlantic Ocean across the early-middle Eocene transition. This is a unique succession because of the exquisite preservation of calcareous nannofossil assemblages which was favoured by the presence of clay-rich drift sediments. More in detail, the principal objectives of this research can be summarized as follows:

1) Analyse the possible long-lasting impacts of the extreme global warmth of the EECO and the successive shift towards cooling on calcareous nannofossil evolution, including significant assemblage shifts and morphostructural innovation within groups.

2) Improve the stability of existing calcareous nannofossil biozonation schemes by providing abundance patterns of selected taxa, which include standard markers and additional species. This investigation aims to point out already known or potential problems concerning the reliability of certain nannofossil biohorizons, and to provide new promising additionally biohorizons.

3) Reassess the taxonomy of taxa belonging to two important middle Eocene taxonomic groups. The high sedimentation rates and the exquisite preservation of calcareous nannofossils at Site U1410 are essential requisites to study fine morphological features and evolutionary trends. Specifically, the present study aims to provide a robust and comprehensive revision of the evolutionary trends displayed by coccolithaceans and sphenoliths during the middle Eocene and their possible correlation with paleoenvironmental conditions. A better characterization of these lineages and of the taxonomy of specific taxa may also serve to improve the reliability of these species as biostratigraphic tool.

REFERENCES

Agnini, C., Muttoni, G., Kent, D. V., & Rio, D. (2006). Eocene biostratigraphy and magnetic stratigraphy from Possagno, Italy: The calcareous nannofossil response to climate variability. *Earth and Planetary Science Letters*, 241(3-4), 815-830. https://doi.org/10.1016/j.epsl.2005.11.00

Agnini, C., Fornaciari, E., Rio, D., Tateo, F., Backman, J., & Giusberti, L. (2007). Responses of calcareous nannofossil assemblages, mineralogy and geochemistry to the environmental perturbations across the Paleocene/Eocene boundary in the Venetian Pre-Alps. *Marine Micropaleontology,* 63(1-2), 19-38. https://doi.org/10.1016/j.marmicro.2006.10.002

Agnini, C., Macri, P., Backman, J., Brinkhuis, H., Fornaciari, E., Giusberti, L., Speranza, F. (2009). An early Eocene carbon cycle perturbation at ~52.5 ma in the Southern Alps: Chronology and biotic response. *Paleoceanography*, 24(2) https://doi.org/10.1029/2008PA001649

Agnini, C., Fornaciari, E., Raffi, I., Catanzariti, R., Pälike, H., Backman, J., & Rio, D. (2014). Biozonation and biochronology of Paleogene calcareous nannofossils from low and middle latitudes. *Newsletters on Stratigraphy,* 47(2), 131-181. https://doi.org/10.1127/0078-0421/2014/004

Agnini, C., Monechi, S., & Raffi, I. (2017). Calcareous nannofossil biostratigraphy: Historical background and application in Cenozoic chronostratigraphy. *Lethaia,* 50(3), 447-463. https://doi.org/10.1111/let.12218

Alcober, J., & Jordan, R. W. (1997). An interesting association between *Neosphaera coccolithomorpha* and *Ceratolithus cristatus* (Haptophyta). *European Journal of Phycology*, 32(1), 91-93. https://doi.org/10.1017/S0967026296001047

Anagnostou, E., John, E. H., Edgar, K. M., Foster, G. L., Ridgwell, A., Inglis, G. N., Pearson, P. N. (2016). Changing atmospheric CO_2 concentration was the primary driver of early Cenozoic climate. *Nature,* 533, 380-384. https://doi.org/10.1038/nature17423

Aubry, M.-P. (1992). Late Paleogene calcareous nannoplankton evolution: a tale of climatic deterioration, in: Prothero, D.R., Berggren, W.A. (Eds.), Eocene- Oligocene Climatic and Biotic Evolution. Princeton *University Press, Princeton*, pp. 272–309

Aubry, M.-P.(1998): Early Paleogene calcareous nannoplankton evolution: a tale of climatic amelioration, in: Late Paleocene–early Eocene Biotic and Climatic Events in the Marine and Terrestrial Records, *Columbia University Press,* New York, 158–201.

Bijl, P. K., Schouten, S., Sluijs, A., Reichart, G. -.J, Zachos, J. C., & Brinkhuis, H. (2009). Early Palaeogene temperature evolution of the Southwest Pacific Ocean. Nature, 461(7265), 776-779. https://doi.org/10.1038/nature08399

Bijl, P. K., Houben, A. J. P., Schouten, S., Bohaty, S. M., Sluijs, A., Reichart, G., Sinninghe Damsté, J.S., Brinkhuis, H. (2010). Transient middle Eocene atmospheric CO_2 and temperature variations. *Science*, 330(6005), 819-821. https://doi.org/10.1126/science.1193654

Bijl, P. K., Bendle, J. A. P., Bohaty, S. M., Pross, J., Schouten, S., Tauxe, L., Brinkhuis, H. (2013). Eocene cooling linked to early flow across the Tasmanian gateway. *Proceedings of the National Academy of Sciences of the United States of America*, 110(24), 9645-9650. https://doi.org/10.1073/pnas.1220872110

Billard, C. and Innouye, I. (2004). What is new in coccolithophore biology? in: Coccolithophores – From Molecular Processes to Global Impact, Springer, Berlin, 1–29, 2004

Bohaty, S. M., Zachos, J. C., Florindo, F., & Delaney, M. L. (2009). Coupled greenhouse warming and deep-sea acidification in the middle Eocene. *Paleoceanography*, 24(2) https://doi.org/10.1029/2008PA001676

Boyle, P. R., Romans, B. W., Tucholke, B. E., Norris, R. D., Swift, S. A., & Sexton, P. F. (2017). Cenozoic North Atlantic deep circulation history recorded in contourite drifts, offshore Newfoundland, Canada. *Marine Geology*, 385, 185-203. https://doi.org/10.1016/j.margeo.2016.12.01

Bown, P.R. (1987). Taxonomy, evolution, and biostratigraphy of Late Triassic-Early Jurassic calcareous nannofossils. *Special Papers in Palaeontology*, 38, 118.

Bown, P. R. & Young, J.R. (1997. Proposal for a revided classification system for calcareous nannoplankton. Journal of Nannoplankton Research, 19 (1)15-47.

Bown, P. R. & Young, J.R. (1998). Introduction. In Bown, P.R. (ed.): Calcareous Nannofossil Biostratigraphy, 1–15. Chapman and Hall, London

Bown PR (1998) Triassic. *In:* Calcareous Nannofossil Biostratigraphy. Bown PR (ed) Chapman & Hall, London, p 29-33

Bown, P.R., Lees, J.A., Young, J.R., 2004. Calcareous nannofossil evolution and diversity through time, in: Thierstein, H.R., Young, J.R. (Eds.), Coccolithophores: From Molecular Processes to Global Impact. Springer-Verlag, pp. 481–508.

Bown, P. R. (2005). Calcareous nannoplankton evolution: A tale of two oceans. *Micropaleontology, 51*(4), 299-308. https://doi.org/10.2113/gsmicropal.51.4.299

Broecker, W. S. (1998). Paleocean circulation during the last deglaciation: A bipolar seesaw? *Paleoceanography*, 13(2), 119-121. https://doi.org/10.1029/97PA03707

Braarud, T., Deflandre, G., Halldal, P., and Kamptner, E. (1955). Terminology, nomenclature, and systematics of the Coccolithophoridae. *Micropaleontology* 1: 157-159.

Bramlette, M. N., & Riedel, W. R. (1954). Stratigraphic value of discoasters and some other microfossils related to recent coccolithophores. *Journal of Paleontology,* 28(4), 385–403.

Caballero, R., & Huber, M. (2013). State-dependent climate sensitivity in past warm climates and its implications for future climate projections. Proceedings of the National Academy of Sciences of the United States of America, 110(35), 14162-14167. https://doi.org/10.1073/pnas.1303365110

Coxall, H. K., Wilson, P. A., Pälike, H., Lear, C. H., & Backman, J. (2005). Rapid stepwise onset of Antarctic glaciation and deeper calcite compensation in the Pacific Ocean. *Nature,* 433(7021), 53-57. doi:10.1038/nature03135

Coxall, H. K., Huck, C. E., Huber, M., Lear, C. H., Legarda-Lisarri, A., O'Regan, M., Sliwinska, K.K, van de Flierdt, T., de Boer, A. G., Zachos, J.C., Backman, J. (2018). Export of nutrient rich Northern Component Water preceded early Oligocene Antarctic glaciation. *Nature Geoscience,* 11(3), 190-196. doi:10.1038/s41561-018-0069-9

Cramer, B. S., Wright, J. D., Kent, D. V., & Aubry, M.P. (2003). Orbital climate forcing of $\delta^{13}C$ excursions in the late Paleocene-early Eocene (Chrons C24n-C25n). *Paleoceanography*, 18(4) https://doi.org/10.1029/2003PA000909

Cramer, B. S., Toggweiler, J. R., Wright, J. D., Katz, M. E., & Miller, K. G. (2009). Ocean overturning since the late Cretaceous: Inferences from a new benthic foraminiferal isotope compilation. Paleoceanography, 24(4) https://doi.org/10.1029/2008PA001683

Cramwinckel, M. J., Huber, M., Kocken, I. J., Agnini, C., Bijl, P. K., Bohaty, S. M., Sluijs, A. (2018). Synchronous tropical and polar temperature evolution in the Eocene. *Nature,* 559(7714), 382-386. https://doi.org/10.1038/s41586-018-0272-2

Cros, L., Kleijne, A., Zeltner, A., Billard, C., & Young, J. R. (2000). New examples of holococcolith-heterococcolith combination coccospheres and their implications for coccolithophorid biology. *Marine Micropaleontology*, 39(1-4), 1-34. https://doi.org/10.1016/S0377-8398(00)00010-4

Cros, L., and Fortuno, J.M. (2002). Atlas of northwestern Mediterranean coccolithophores. *Scientia Marina* 66: 1-70.

Cros, L., Fortuño, J. -., & Estrada, M. (2013). Elemental composition of coccoliths: Mg/Ca relationships. [Composición elemental de cocolitos. Relaciones Mg/Ca] *Scientia Marina*, 77(SUPPL. 1), 63-67. https://doi.org/10.3989/scimar.03727.27E

Dallanave, E., Bachtadse, V., Crouch, E. M., Tauxe, L., Shepherd, C. L., Morgans, H. E. G., Sugisaki, S. (2016). Constraining early to middle Eocene climate evolution of the Southwest Pacific and Southern Ocean. *Earth and Planetary Science Letters,* 433, 380-392. https://doi.org/10.1016/j.epsl.2015.11.010

Davies, R., Cartwright, J., Pike, J. & Line, C. (2001).Early Oligocene initiation of North Atlantic Deep Water formation. *Nature* 410, 917–920.

Deconto, R. M., Galeotti, S., Pagani, M., Tracy, D., Schaefer, K., Zhang, T., Beerling, D. J. (2012). Past extreme warming events linked to massive carbon release from thawing permafrost. *Nature*, 490(7419), 292. https://doi.org/10.1038/nature11424

De Vargas, C., Aubry, M. P., Probert, I. & Young, J. R. (2007). Origin and evolution of coccolithophores: from coastal hunters to oceanic farmers. Pp. 251-287 *in* P. G. Falkowski & A. H. Knoll (eds) *Evolution of Primary Producers in the Sea. Elsevier Academic Press, Amsterdam, Boston.*

Dickens, G. R., O'Neil, J. R., Rea, D. K., & Owen, R. M. (1995). Dissociation of oceanic methane hydrate as a cause of the carbon isotope excursion at the end of the Paleocene. *Paleoceanography*, 10(6), 965-971. https://doi.org/10.1029/95PA0208

Dickens, G. R. (2000). Modeling the global carbon cycle with a gas hydrate capacitor: Significance for the latest Paleocene Thermal Maximum. *Geophysical Monograph Series*, 124 (200), 19-38 https://doi.org/10.1029/GM124p0019

Dickens, G. R. (2003). Rethinking the global carbon cycle with a large, dynamic and microbially mediated gas hydrate capacitor. *Earth and Planetary Science Letters*, 213(3-4), 169-183. https://doi.org/10.1016/S0012-821X(03)00325-X

Dutton, A., Lohmann, K. C., & Leckie, R. M. (2005). Data report: Stable isotope and Mg/Ca of Paleocene and Eocene foraminifers, ODP site 1209, Shatsky Rise. Proceedings of the Ocean Drilling Program: Scientific Results,

Gartner, S. (1970). Phylogenetic lineages in the Lower Tertiary Coccolith genus *Chiasmolithus*. Proc. N. Am. Paleontol. Conv., 1969, Part G, pp. 930–957.

Gradstein, F.M., Ogg, J.G., Schmitz, M.D., Ogg, G.M. (Eds.), (2012). The Geologic Time Scale 2012. Elsevier, Amsterdam pp. 1144. doi:10.1016/B978-0-444-59425-9.01001-5

Greenwood, D. R., & Wing, S. L. (1995). Eocene continental climates and latitudinal temperature gradients. *Geology*, 23(11), 1044-1048. https://doi.org/10.1130/0091-7613(1995)023<1044:ECCALT>2.3.CO;2

Galeotti, S., Krishnan, S., Pagani, M., Lanci, L., Gaudio, A., Zachos, J. C., Lourens, L. (2010). Orbital chronology of early Eocene hyperthermals from the Contessa Road section, Central Italy. *Earth and Planetary Science Letters, 290*(1-2), 192-200. https://doi.org/10.1016/j.epsl.2009.12.021

Haq, B. U., & Lohmann, G. P. (1976). Early Cenozoic calcareous nannoplankton biogeography of the Atlantic Ocean. *Marine Micropaleontology,1*(C), 119-194. https://doi.org/10.1016/0377-8398(76)90008-6

Hay, W. W.(2004). Carbonate fluxes and calcareous nannoplankton, in: Coccolithophores – From Molecular Processes to Global Impact, Springer, Berlin, 508–528.

Hohbein, M. W., Sexton, P. F., & Cartwright, J. A. (2012). Onset of North Atlantic deep water production coincident with inception of the Cenozoic global cooling trend. *Geology*, 40(3), 255-258. https://doi.org/10.1130/G32461.1

Hollis, C. J., Handley, L., Crouch, E. M., Morgans, H. E. G., Baker, J. A., Creech, J., Pancost, R. D. (2009). Tropical sea temperatures in the high-latitude South Pacific during the Eocene.*Geology,* 37(2), 99-102. https://doi.org/10.1130/G25200A.1

Hollis, C. J., Taylor, K. W. R., Handley, L., Pancost, R. D., Huber, M., Creech, J. B., Zachos, J. C. (2012). Early Paleogene temperature history of the southwest Pacific Ocean: Reconciling proxies and models. *Earth and Planetary Science Letters*, 349-350, 53-66. https://doi.org/10.1016/j.epsl.2012.06.024

Huber, M., & Caballero, R. (2011). The early Eocene equable climate problem revisited. *Climate of the Past*, 7(2), 603-633. https://doi.org/10.5194/cp-7-603-2011

Inglis, G. N., Farnsworth, A., Lunt, D., Foster, G. L., Hollis, C. J., Pagani, M., Pancost, R. D. (2015). Descent toward the icehouse: Eocene sea surface cooling inferred from GDGT distributions. *Paleoceanography*, 30(7), 1000-1020. https://doi.org/10.1002/2014PA002723

Intxauspe-Zubiaurre, B., Flores, J., Payros, A. (2017a). Variations to calcareous nannofossil $CaCO_3$ content during the middle Eocene C21r-H6 Hyperthermal Event (~ 47.4 ma) in the Gorrondatxe section (Bay of Biscay, Western Pyrenees). *Palaeogeography, Palaeoclimatology, Palaeoecology,* 487, 296-306. https://doi.org/10.1016/j.palaeo.2017.09.015

Intxauspe-Zubiaurre, B., Payros, A., Flores, J., & Apellaniz, E. (2017b). Changes to sea-surface characteristics during the middle Eocene (47.4 ma) C21r-H6 Event: Evidence from calcareous nannofossil assemblages of the Gorrondatxe section (Western Pyrenees). *Newsletters on Stratigraphy*, 50(3), 245-267. https://doi.org/10.1127/nos/2017/0305

Kennett, J.P., Stott, L.D.(1991). Abrupt deep-sea warming, paleoceanographic changes and benthic extinctions at the end of the Palaeocene. *Nature* 353, 225–229, http://dx.doi.org/10.1038/353225a0

Komar, N., Zeebe, R. E., & Dickens, G. R. (2013). Understanding long-term carbon cycle trends: The late Paleocene through the early Eocene. *Paleoceanography*, 28(4), 650-662. https://doi.org/10.1002/palo.20060

Kennett, J. P. (1977). Cenozoic evolution of Antarctic glaciation, the circum-Antarctic Ocean, and their impact on global paleoceanography. *J. Geophys. Res*. 82, 3843–3860.

Kurtz, A. C., Kump, L. R., Arthur, M. A., Zachos, J. C., & Paytan, A. (2003). Early Cenozoic decoupling of the global carbon and sulfur cycles. *Paleoceanography*, 18(4). https://doi.org/10.1029/2003PA000908

Lagabrielle, Y., Goddéris, Y., Donnadieu, Y., Malavieille, J., & Suarez, M. (2009). The tectonic history of Drake Passage and its possible impacts on global climate. *Earth and Planetary Science Letters*, 279(3-4), 197-211. https://doi.org/10.1016/j.epsl.2008.12.03

Lourens, L. J., Hilgen, F. J., Shackleton, N. J., Laskar, J., Wilson, D., (2004). The Neogene Period. In: Gradstein, F. M., Ogg, J. G., Smith, A. G. (Eds.), A Geological Time Scale 2004. Cambridge University Press, Cambridge, 409–440.

Lauretano, V., Littler, K., Polling, M., Zachos, J. C., & Lourens, L. J. (2015). Frequency, magnitude and character of hyperthermal events at the onset of the Early Eocene Climatic Optimum. *Climate of the Past, 11*(10), 1313-1324. https://doi.org/10.5194/cp-11-1313-2015

Lauretano, V., Hilgen, F. J., Zachos, J. C., & Lourens, L. J. (2016). Astronomically tuned age model for the early Eocene carbon isotope events: A new high-resolution $\delta^{13}C$ benthic record of ODP Site 1263 between ~ 49 and ~ 54 ma. *Newsletters on Stratigraphy*, 49(2), 383-400. https://doi.org/10.1127/nos/2016/0077

Lawver, L. A., & Gahagan, L. M. (2003). Evolution of Cenozoic seaways in the circum-Antarctic region. *Palaeogeography, Palaeoclimatology, Palaeoecology*, 198(1-2), 11-37. https://doi.org/10.1016/S0031-0182(03)00392-4

Lear, C. H., Elderfield, H., & Wilson, P. A. (2000). Cenozoic deep-sea temperatures and global ice volumes from Mg/Ca in benthic foraminiferal calcite. *Science*, 287(5451), 269-272. https://doi.org/10.1126/science.287.5451.269

Lees, J. A., Bown, P. R., & Mattioli, E. (2005). Problems with proxies? Cautionary tales of calcareous nannofossil paleoenvironmental indicators. *Micropaleontology*, 51(4), 333-343. doi:10.2113/gsmicropal.51.4.333

Leon-Rodriguez, L., & Dickens, G. R. (2010). Constraints on ocean acidification associated with rapid and massive carbon injections: The early Paleogene record at Ocean Drilling Program Site 1215, Equatorial Pacific Ocean. *Palaeogeography, Palaeoclimatology, Palaeoecology*, 298(3-4), 409-420. https://doi.org/10.1016/j.palaeo.2010.10.029

Lourens, L. J., Sluijs, A., Kroon, D., Zachos, J. C., Thomas, E., Röhl, U., Raffi, I. (2005). Astronomical pacing of late Palaeocene to early Eocene global warming events. *Nature, 435*(7045), 1083-1087. https://doi.org/10.1038/nature03814

Luciani, V., Dickens, R. G., Backman, J., Fornaciari, E., Giusberti, L., Agnini, C., & D'Onofrio, R. (2016). Major perturbations in the global carbon cycle and photosymbiont-bearing planktic foraminifera during the early Eocene. *Climate of the Past*, 12(4), 981-1007. https://doi.org/10.5194/cp-12-981-2016

Lunt, D. J., Jones, T. D., Heinemann, M., Huber, M., LeGrande, A., Winguth, A., Loptson, C., Marotzke, J., Roberts, C.D., Tindall, J., Valdes, P., Winguth, C. (2012). A model-data comparison for a multi-model ensemble of early Eocene atmosphere-ocean simulations: EoMIP. *Climate of the Past*, 8(5), 1717-1736. https://doi.org/10.5194/cp-8-1717-2012

Manton, I., and Oates, K. (1980). *Polycrater galapagensis* gen. et sp. nov., a putative coccolithophorid from the Galapagos Islands with an unusual aragonitic periplast. *Br. PhycoI. J.* 15, 95-103.

Martini, E. (1971). Standard Tertiary and Quaternary calcareous nannoplankton zonation, in: Proceedings of the 2nd Planktonic Conference, 2, Tecnoscienza, Roma, 739–785, 1971.

Milliman, J. D. (1993). Production and accumulation of calcium carbonate in the ocean: Budget of a nonsteady state. *Global Biogeochemical Cycles*, 7(4), 927-957. https://doi.org/10.1029/93GB02524

Molina, E., Alegret, L., Apellaniz, E., Bernaola, G., Caballero, F., Dinarès-Turell, J., Uchman, A. (2011). The Global Stratotype Section and Point (GSSP) for the base of the Lutetian Stage at the Gorrondatxe section, Spain. *Episodes, 34*(2), 86-108

Nicolo, M. J., Dickens, G. R., Hollis, C. J., & Zachos, J. C. (2007). Multiple early Eocene hyperthermals: Their sedimentary expression on the New Zealand continental margin and in the deep sea. *Geology*, 35(8), 699-702. https://doi.org/10.1130/G23648A.1

Nielsen, S. G., Mar-Gerrison, S., Gannoun, A., LaRowe, D., Klemm, V., Halliday, A. N., Hein, J. R. (2009). Thallium isotope evidence for a permanent increase in marine organic carbon export in the early Eocene. *Earth and Planetary Science Letters*, 278(3-4), 297-307. https://doi.org/10.1016/j.epsl.2008.12.010

Norris, R.D., Wilson, P.A., Blum, P., Scientists, E. 342, (2014). Paleogene Newfoundland Sediment Drifts and MDHDS Test, in: Proceedings of the Integrated Ocean Drilling Program, 342: College Station, TX (Integrated Ocean Drilling Program). https://doi.org/10.2204/iodp.proc.342.2014

Okada, H., & Honjo, S. (1973). The distribution of oceanic coccolithophorids in the Pacific. *Deep-Sea Research and Oceanographic Abstracts, 20*(4), 355-364,IN3-IN4,365-374. https://doi.org/10.1016/0011-7471(73)90059-4

Okada, H., & Bukry, D. (1980). Supplementary modification and introduction of code numbers to the low-latitude coccolith biostratigraphic zonation (Bukry, 1973; 1975). *Marine Micropaleontology*, 5(C), 321-325. https://doi.org/10.1016/0377-8398(80)90016-X

Pagani, M., Zachos, J. C., Freeman, K. H., Tipple, B., & Bohaty, S. (2005). Atmospheric science: Marked decline in atmospheric carbon dioxide concentrations during the Paleogene. *Science*, 309(5734), 600-603. https://doi.org/10.1126/science.1110063

Payros, A., Ortiz, S., Alegret, L., Orue-Etxebarria, X., Apellaniz, E., & Molina, E. (2012). An early Lutetian carbon-cycle perturbation: Insights from the Gorrondatxe section (Western Pyrenees, Bay of Biscay). *Paleoceanography*, 27(2) https://doi.org/10.1029/2012PA002300

Perch-Nielsen, K. (1985). Cenozoic calcareous nannofossils, in: Bolli, H.M., Saunders, J.B., Perch-Nielsen, K. (Eds.), Plankton Stratigraphy. Cambridge University Press, Cambridge, pp. 427–554

Preto, N., Agnini, C., Rigo, M., Sprovieri, M., Westphal, H. (2013). The calcareous nannofossil *Prinsiosphaera* achieved rock-forming abundances in the latest Triassic of western Tethys: Consequences for the $\delta^{13}C$ of bulk carbonate. *Biogeosciences*, 10(9), 6053-6068. https://doi.org/10.5194/bg-10-6053-2013

Prins, B. (1971). Speculations on relations, evolution, and stratigraphic distribution of *Discoasters*. In: Farinacci, A. (Ed.), Proc. II Planktonic Conference, Rome, 1970. Tecnoscienza, Rome, Vol. 2, pp. 1017–1039.

Rost, B. and Riebesell, U. (2004) Coccolithophores and the biological pump: responses to environmental changes, in: Coccolithophores – From Molecular Processes to Global Impact, Springer, Berlin, 99–125, 2004.

Roth, P.H. (1978): Cretaceous nannoplankton biostratigraphy and oceanography of the Northwestern Atlantic Ocean. Initial Reports of the Deep Sea Drilling Project 44, 731–759.

Roth, P. H., & Bowdler, J. L. (1981). Middle Cretaceous calcareous nannoplankton biogeography and oceanography of the Atlantic Ocean. The Deep Sea Drilling Project: A Decade of Progress, 517-546

Roth, P. H., & Krumbach, K. R. (1986). Middle Cretaceous calcareous nannofossil biogeography and preservation in the Atlantic and Indian Oceans: Implications for paleoceanography. *Marine Micropaleontology*, 10(1-3), 235-266. https://doi.org/10.1016/0377-8398(86)90031-9

Rowson, J. D., Leadbeater, B. S. C., & Green, J. C. (1986). Calcium carbonate deposition in the motile *(Crystallolithus*) phase of *Coccolithus pelagicus* (Prymnesiophyceae). *British Phycological Journal*, 21(4), 359-370. https://doi.org/10.1080/00071618600650431

Sexton, P. F., Wilson, P. A., & Norris, R. D. (2006). Testing the Cenozoic multisite composite $\delta^{18}O$ and $\delta^{13}C$ curves: New monospecific Eocene records from a single locality, Demerara Rise (Ocean Drilling Program leg 207). *Paleoceanography*, 21(2) https://doi.org/10.1029/2005PA001253

Sexton, P. F., Norris, R. D., Wilson, P. A., Pälike, H., Westerhold, T., Röhl, U., Gibbs, S. (2011). Eocene global warming events driven by ventilation of oceanic dissolved organic carbon. *Nature*, 471(7338), 349-353. https://doi.org/10.1038/nature09826

Sáez, A. G., Probert, I., Geisen, M., Quinn, P., Young, J. R., & Medlin, L. K. (2003). Pseudo-cryptic speciation in coccolithophores. Proceedings of the National Academy of Sciences of the United States of America, 100(12), 7163-7168. https://doi.org/10.1073/pnas.1132069100

Schneider, L. J., Bralower, T. J., & Kump, L. R. (2011). Response of nannoplankton to early Eocene ocean destratification. *Palaeogeography, Palaeoclimatology, Palaeoecology*, 310(3-4), 152-162. https://doi.org/10.1016/j.palaeo.2011.06.018

Sissingh, W., & Prins, B. (1977). Biostratigraphy of cretaceous calcareous nannoplankton. Geologie En Mijnbouw, 56(1), 37-65.

Slotnick, B. S., Dickens, G. R., Nicolo, M. J., Hollis, C. J., Crampton, J. S., Zachos, J. C., & Sluijs, A. (2012). Large-amplitude variations in carbon cycling and terrestrial weathering during the latest Paleocene and earliest Eocene: The record at Mead Stream, New Zealand. *Journal of Geology, 120*(5), 487-505. https://doi.org/10.1086/666743

Slotnick, B. S., Dickens, G. R., Hollis, C. J., Crampton, J. S., Percy Strong, C., & Phillips, A. (2015). The onset of the Early Eocene Climatic Optimum at Branch Stream, Clarence River Valley, New Zealand. *New Zealand Journal of Geology and Geophysics,* 58(3), 262-280. https://doi.org/10.1080/00288306.2015.1063514

Sluijs, A., Schouten, S., Pagani, M., Woltering, M., Brinkhuis, H., Damsté, J. S. S., Yamamoto, M. (2006). Subtropical Arctic Ocean temperatures during the Palaeocene/Eocene thermal maximum. *Nature*, 441(7093), 610-613. https://doi.org/10.1038/nature04668

Sprengel, C., & Young, J. R. (2000). First direct documentation of associations of *Ceratolithus cristatus* ceratoliths, hoop-coccoliths and *Neosphaera coccolithomorpha* planoliths. *Marine Micropaleontology*, 39(1-4), 39-41. https://doi.org/10.1016/S0377-8398(00)00012-8

Stap, L., Lourens, L. J., Thomas, E., Sluijs, A., Bohaty, S., & Zachos, J. C. (2010). High-resolution deep-sea carbon and oxygen isotope records of Eocene thermal maximum 2 and H2. *Geology*, 38(7), 607-610. https://doi.org/10.1130/G30777.1

Stenseth, N.C., Maynard Smith, J. (1984). Coevolution in ecosystems: Red Queen evolution or stasis? *Evolution* 38, 870–880.

Taylor, K. W. R., Huber, M., Hollis, C. J., Hernandez-Sanchez, M. T., & Pancost, R. D. (2013). Re-evaluating modern and Palaeogene GDGT distributions: Implications for SST reconstructions. *Global and Planetary Change*, 108, 158-174. https://doi.org/10.1016/j.gloplacha.2013.06.011

Thomas, E., & Shackleton, N. J. (1996). The Paleocene-Eocene benthic foraminiferal extinction and stable isotope anomalies. Correlation of the Early Paleogene in Northwest Europe, 401-441

Tierney, J. E., & Tingley, M. P. (2015). A TEX 86 surface sediment database and extended bayesian calibration. Scientific Data, 2 https://doi.org/10.1038/sdata.2015.29

Tripati, A., & Elderfield, H. (2005). Paleoclimate: Deep-sea temperature and circulation changes at the Paleocene-Eocene Thermal Maximum. Science, 308(5730), 1894-1898. https://doi.org/10.1126/science.1109202

Tucholke, B. E., & Vogt, P. R. (1979). (DSDP) western North Atlantic: Sedimentary evolution and aspects of tectonic history. Initial Reports of the Deep Sea Drilling Project, Leg 43, Instanbul, Turkey to Norfolk, Virginia, 1975, (Scripps Institution of Oceanography; UK Distributors IPOD Committee, NERC, Swindon), , 791-826.

Tucholke, B. E., & Ludwig, W. J. (1982). Structure and origin of the J anomaly ridge, western North Atlantic Ocean. *Journal of Geophysical Research*, 87(B11), 9389-9407. https://doi.org/10.1029/JB087iB11p09389

Tucholke, B.E., Sawyer, D.S., Sibuet, J.-C. (2007). Breakup of the Newfoundland Iberia rift. In: Karner, G.D., Manatschal, G., Pinheiro, L.M. (Eds.), Imaging, Mapping and Modelling Continental Lithosphere Extension and Breakup, Geological Society London, Special Publication. Vol. 282:pp. 9–46. http://dx.doi.org/10.1144/SP282.2.

Turner, S. K., Sexton, P. F., Charles, C. D., & Norris, R. D. (2014). Persistence of carbon release events through the peak of early Eocene global warmth. *Nature Geoscience*, 7(10), 748-751. https://doi.org/10.1038/NGEO2240

Thierstein, H.R., Cortés, M.Y., Haidar, A.T. (2004). Plankton community behavior on ecological end evolutionary timescales: when models confront evidence. In: Thierstein, H.R., Young, J.R. (Eds.), Coccolithophores, From Molecular Processes to Global Impact. Springer Verlag, Berlin, Germany, pp. 455–480.

Tyrrell, T. and Young, J. R. (2008). Coccolithophores. In Steele, J. H., Thorpe, S. A and Turekian, K. K., (2nd Edition.). Encyclopedia of Ocean Sciences. Academic Press, San Diego, US, pp. 606–614.

Van Valen, L. (1973). A new evolutionary law. Evol. *Theory* 1, 1–30

Villa, G., Fioroni, C., Pea, L., Bohaty, S., & Persico, D. (2008). Middle Eocene-late Oligocene climate variability: Calcareous nannofossil response at Kerguelen Plateau, Site 748. *Marine Micropaleontology*, 69(2), 173-192. https://doi.org/10.1016/j.marmicro.2008.07.00

Via, R. K. & Thomas, D. J. (2006). Evolution of Atlantic thermohaline circulation: early Oligocene onset of deep-water production in the North Atlantic. *Geology* 34, 441–444.

Watkins, D. K. (1986). Calcareous nannofossil paleoceanography of the Cretaceous Greenhorn Sea (USA). *Geological Society of America Bulletin*, 97(10), 1239-1249. https://doi.org/10.1130/0016-7606(1986)97<1239:CNPOTC>2.0.CO;2

Wei, W., & Wise Jr., S. W. (1990). Biogeographic gradients of middle Eocene-Oligocene calcareous nannoplankton in the South Atlantic Ocean. *Palaeogeography, Palaeoclimatology, Palaeoecology*, 79(1-2), 29-61. https://doi.org/10.1016/0031-0182(90)90104-F

Wei, W., Villa, G., & Wise Jr, S. W. (1992). Paleoceanographic implications of Eocene-Oligocene calcareous nannofossils from Sites 711 and 748 in the Indian Ocean. *Proc., Scientific Results, ODP, Leg 120, Central Kerguelen Plateau,* 979-999.

Westerhold, T., Rhl, U., Donner, B., McCarren, H. K., & Zachos, J. C. (2011). A complete high-resolution Paleocene benthic stable isotope record for the central pacific (ODP site 1209). *Paleoceanography*, 26(2) https://doi.org/10.1029/2010PA00209

Westerhold, T., Röhl, U., Frederichs, T., Agnini, C., Raffi, I., Zachos, J. C., & Wilkens, R. H. (2017). Astronomical calibration of the Ypresian timescale: Implications for seafloor spreading rates and the chaotic behavior of the solar system? *Climate of the Past,* 13(9), 1129-1152. https://doi.org/10.5194/cp-13-1129-201

Westerhold, T., Röhl, U., Donner, B., & Zachos, J. C. (2018). Global extent of early Eocene hyperthermal events: A new Pacific benthic foraminiferal isotope record from Shatsky Rise (ODP Site 1209).*Paleoceanography and Paleoclimatology,* 33(6), 626-642. https://doi.org/10.1029/2017PA003306

Winter, A., Jordan, R. W., and Roth, P. H.(1994) Biogeography of living coccolithophores, in: Coccolithophores, edited by: Winter, A. and Siesser, W. G., Cambridge Univ. Press, Cambridge, 161– 17.

Young, J. R., Didymus, J. M., Brown, P. R., Prins, B., & Mann, S. (1992). Crystal assembly and phylogenetic evolution in heterococcoliths. *Nature*, 356(6369), 516-518. https://doi.org/10.1038/356516a0

Young, J. R., Bergen, J. A., Bown, P. R., Burnett, J. A., Fiorentino, A., Jordan, R. W., Von Salis, K. (1997). Guidelines for coccolith and calcardous nannofossil terminology. *Palaeontology*, 40(4), 875-912.

Young, J. R., Davis, S. A., Bown, P. R., & Mann, S. (1999). Coccolith ultrastructure and biomineralisation. *Journal of Structural Biology*, 126(3), 195-215. https://doi.org/10.1006/jsbi.1999.4132

Young, J. R. and Henriksen K. (2003). Biomineralization within vesicles: the calcite of coccoliths. In: Dove P.M., De Yoreo J. J., Weiner S., Eds., Biomineralisation. *Reviews in Mineralogy and Geochemistry,* 54, 189-215.

Young, J.R., Geisen, M., Cros, L., Kleijne, A., Probert, I., and Ostergaard, J.B. (2003). A guide to extant coccolithophore taxonomy. *Journal of Nannoplankton Research, Special Issue,* 1, 1-132.

Young, J. R., Geisen, M., & Probert, I. (2005). A review of selected aspects of coccolithophore biology with implications for paleobiodiversity estimation. *Micropaleontology*, 51(4), 267-288. https://doi.org/10.1649/772

Zachos, J., Pagani, H., Sloan, L., Thomas, E., & Billups, K. (2001). Trends, rhythms, and aberrations in global climate 65 Ma to present. *Science*, 292(5517), 686-693. https://doi.org/10.1126/science.1059412

Zachos, J. C., & Kump, L. R. (2005). Carbon cycle feedbacks and the initiation of Antarctic glaciation in the earliest Oligocene. *Global and Planetary Change*, 47(1), 51-66. https://doi.org/10.1016/j.gloplacha.2005.01.001

Zachos, J. C., Dickens, G. R., & Zeebe, R. E. (2008). An early Cenozoic perspective on greenhouse warming and carbon-cycle dynamics. *Nature*, 451(7176), 279-283. https://doi.org/10.1038/nature06588

Ziveri, P., Young, J., and van Hinte, J. E. (1999) Coccolithophore export production and accumulation rates, in: On determination of sediment accumulation rates, GeoResearch Forum, Trans Tech Publications LTD, Switzerland, 5, 41–56.

Chapter 2

The early-middle Eocene transition: an integrated calcareous nannofossil and stable isotope record from Northwest Atlantic (IODP Site U1410)

Abstract

The interval comprised between the Early Eocene Climatic Optimum and the onset of the long-term cooling in the middle Eocene is marked by prominent changes in calcareous nannoplankton communities and coincides with a fundametal reorganization in the North Atlantic deep circulation. In order to better understand the potential interplay between modifications in the physical environment and changes in calcareous nannofossil assemblages the sedimentary succession recovered at Site U1410 (Southeast Newfoundland Ridge, northwest Atlantic) represents the ideal case study to investigate. Site U1410 provides one of the most complete record across the early-middle Eocene transition in the North Atlantic and documents the onset of a persistent contour-following deep current from the middle Eocene that has led to the deposition of expanded clay-rich sediments. We documented the abundance patterns of selected biostratigraphically relevant taxa encompassing Zones CNE4-CNE12 and we discussed their reliability as biostratigraphic tools in order to strengthen the middle Eocene biostratigraphic framework. In addition, the evolution of calcareous nannoplankton was investigated and compared with stable isotope records from bulk sediments. Our study reveals both long- and short-term trends that allowed us to analyze the temporal relationships between plaeoenvironmental trends and calcareous nannofossil changes. On a long-term perspective, the most prominent changes observed in the study interval are the evolutionary emergence of *Noelaerhabdaceae* during EECO and their successive dominance in the middle Eocene cooling phase. The notable expansion of this family occurred at the expense of *Toweius, Zygrhablithus, Discoaster* and *Sphenolithus* and was associated with a new steady state characterized by more stability in the physical and chemical surface water conditions. At the Ypresian-Lutetian boundary, stable isotope records show a distinctive trend that might indicate a short-term warming perturbation, This event is associated with a peak in abundance of *Discoaster sublodoensis.* Overall, results from Site U1410 suggest that a combination of different factors, such as the long-term effect of EECO, minor environmental changes and biotic controls, may have played a crucial role in the development of the modern-like assemblage, where *Noelaerhabdaceae* still represents the main component of extant populations.

2.1 INTRODUCTION

Throughout the early and middle Eocene, the global climate system crossed a critical turning point shifting from the warmest global temperature of the past 65 million years to a long phase of global cooling that culminated in the early Oligocene Glacial Maximum (OGM). The long-lived climatic phase known as Early Eocene Climatic Optimum (EECO) was a long lasting extreme warmth interval (Zachos et al., 2001, 2008; Bijl et al., 2009; Hollis et al., 2009; 2012), with very high levels of atmospheric *p*CO2 (Pagani et al., 2005; Zachos et al., 2008; Beerling and Royer, 2011) and subdued Equator-to-Pole temperature gradients (Greenwood and Wing, 1995; Bijl et al., 2009; Cramwinckel et al., 2018). This event was originally descripted as a ca. 2 Myr phase characterized by low values

in the global stable isotope oxygen (Zachos et al., 2001). Superimposed on extreme warmth condition documented during the early Eocene, the climate system underwent numerous events of rapid warming (hyperthermals) which are recorded as transient carbon negative excursions (CIEs) related to huge releases of ^{13}C-depleted carbon in the ocean-atmosphere system (Agnini et al., 2009; 2016; Dickens, 2011; Thomas and Zachos, 2000; Cramer et al., 2003; Zachos et al., 2004, Kirtland Turner et al, 2014; Nicolò et al., 2007; Quilléveré et al., 2008; Sexton et al., 2011; Lunt et al, 2011). Hyperthermals are also associated with dissolution of marine carbonates in deep-sea settings that acted as a buffering mechanism to counterbalance the large input of CO_2 into the ocean. Last but not least, since we are dealing with hyperthermals, negative excursions in oxygen stable isotopes are the fingerprints of these events. During the early Eocene, the multiple occurrence of hyperthermals are not randomly spaced rather they are distributed through time in predictable positions because they are triggered by orbital forcing (Cramer et al., 2003; Lourens et al., 2005; Galeotti et al., 2010; Lunt et al., 2011, Littler et al., 2014; Lauretano et al., 2015; Galeotti et al., 2017; Westehold et al., 2017, 2018). Although hyperthermals are typically documented during the middle Paleocene-early Eocene interval, the EECO represents their climax in terms of frequency (Lunt et al., 2011). The demise of the extreme warmth conditions following the EECO coincides with the onset of deep ocean and global cooling, but perturbations in carbon cycle associated with increased temperature persisted in the middle Eocene (Figure 2.1) (Sexton et al. 2011, Kirtland et al, 2014). Eventually, the long lasting cooling of the Earth system passed a climatic threshold at the Eocene-Oligocene transition (EOT) when the onset permanent ice sheets caps took place in Antarctica (Coxall and Pearson, 2007). Variations in ocean paleocirculation related to the tectonic evolution of the Southern Hemisphere (Kennet et al., 1977; Bijl et al., 2013) as well as the decline in atmospheric greenhouse gases concentrations (Pagani et al., 2005; Anagnostou et al., 2016; Cramwinckel et al., 2018) are suggested as primary drivers for global cooling, even scientists has continued to lively discuss on which mechanism was the most determining in controlling the climate evolution.

The articulated nature of the Paleogene climate evolution and the related modifications of the physical parameters of the past environments have been used to understand the relationship and the relative timing between the changes observed in the geosphere and the evolution of the biosphere. Calcareous nannoplankton are of particular interest because, as all the living organisms, they are sensitive to changes in the physical conditions and, even more importantly, they lie at the base of the food chain of the oceans. Any change observed in the calcareous nannoplankton could be thus related to global paleooceanographic modifications and affect the higher levels of the food web.

Reconstructing the evolutionary history of this important marine calcareous phytoplankton group could on one hand shed light on the details of their evolutionary patterns and, on the other hand,

provide an important dataset to test how the nannoplankton evolution and climate changes interact. In particular, the late early-middle Eocene, is an understudied time interval that includes the tail of the early Eocene hypethermal events and the relatively stable early Lutetian giving the opportunity to observe the evolutionary patterns during dramatic perturbations of the global system as well as across the so-called background conditions.

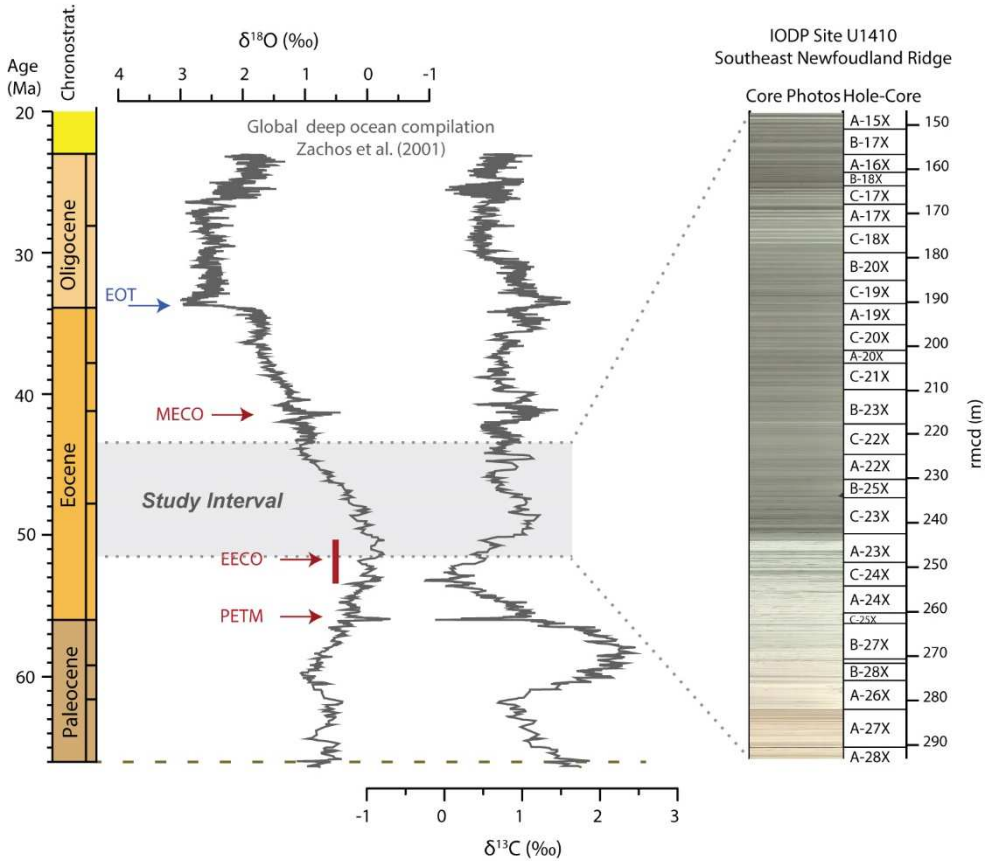

Figure 2.1: Global deep-sea benthic foraminiferal oxygen and carbon isotope ($\delta^{18}O$ and $\delta^{13}C$) records for the Paleogene (Zachos et al., 2001, recalibrated to the Geological Time Scale 2012; Gradstein et al., 2012). Red arrows indicate the major warming episodes throughout the Eocene: the short -lived Paleocene-Eocene Thermal Maximum (PETM), the long-standing Early Eocene Climatic Optimum (EECO), the Mid-Eocene Climatic Optimum (MECO). Blue arrow indicates the Eocene-Oligocene transition (EOT), which coincides with a sharp cooling and the emplacement of permanent ice-sheets in Antarctica. Grey band highlights the study interval, which encompasses the upper part of EECO and the initial phase of the long-term cooling. To the right, core images and the depth splice (rmcd; Vahlenkamp et al., 2018) of the study interval at IODP SiteU1410.

For calcareous nannoplankton, the EECO was a time of significant biotic turnovers (Agnini et al., 2006; Luciani et al., 2016; Oreshkina, 2012). In particular, the assemblages underwent a permanent change with the extinction of the Paleocene *Prinsiaceae* family and the appearance and successive spreading of the modern-like coccoliths belonging to *Noelaerhabdaceae* family (i.e. *Reticulofenestra/Dictyococcites* group) (Agnini et al., 2006; Schneider et al., 2011). The expansion of this new group was accompanied by an increase in nannofossil diversity, which reached the maximum value in the middle Eocene (Bown et al., 2004, 2005).

A debate among specialists is still on as to whether the strong environmental pressure during and shortly after the EECO was directly responsible for the changes observed in calcareous nannoplankton communities. Numerous evidences support the idea that key transient paleoclimatic events throughout the Eocene (PETM, MECO, EOT) have induced both permanent and temporary modifications in nannofossil assemblages (e.g. Bralower et al., 2002, Gibbs et al., 2006; Agnini et al., 2007, Toffanin et al., 2011; Jones et al., 2008; Villa et al., 2008). The transition from the extreme warmth of greenhouse condition of the early Eocene to the long-term cooling trend of the middle Eocene is one of the most profound perturbation of the global climate state, but major uncertainty still exists on the mode and tempo of environmental deterioration and calcareous nannofossil assemblage dynamics across this long interval (52-34 Ma; Aubry et al., 1992, 1998). The lack of a comprehensive understanding of this crucial passage is mainly due to the scarcity of well-preserved, continuous and expanded successions where the early-middle Eocene is documented (Schneider et al., 2011). In this interval, the sedimentary sequences recovered at deep-sea sites in the North Atlantic Ocean (ODP Leg 171b, Norris et al., 2001; Leg 207, Erbacher et al., 2004) are typically characterized by chert horizons in the lower Eocene, which eventually result in condensed sequence or in the presence of major hiatus across the early-middle Eocene transition (Aubry et al., 1995; Norris et al., 2001a, b; Muttoni and Kent, 2007).

Here we present a long-term geochemical ($\delta^{13}C$, $\delta^{18}O$ and $CaCO_3$ content) record from the North Atlantic IODP Site U1410 (Southeast Newfoundland Ridge) spanning from the final phase of EECO to the lower middle Eocene (Figure 2.1) (51-43 Ma), which is combined with a highly resolved calcareous nannofossil dataset. This Site represents the most well-preserved and continuous deep-sea record of the early middle Eocene transition (Norris et al., 2014) and is thus ideal to be investigated (1) to document principal and additional biostratigraphic biohorizons by means of semi-quantitative trends of selected taxa, which will provide an improved time framework; (2) to acquire assemblage data in order to highlight the major changes in the main components of the assemblages on a long- and short term perspective; (3) to interpret the changes in calcareous nannofossils and geochemical proxies (stable oxygen and carbonate data from bulk sediments) in term of modification in paleotemperature, paleoproductivity or other environmental parameters; (4) to compare the biotic perturbations observed in calcareous nannofossils to the well-known or putative global environmental/climate changes across the early-middle Eocene transition.

2.2 MATERIAL AND METHODS

2.2.1 IODP Site U1410

Site U1410 (41°19.6993′N, 49°10.1847′W) was drilled during Integrated Ocean Drilling Program (IODP) Expedition 342 on the Southeast Newfoundland Ridge, offshore Newfoundland, Canada (Figure 2.2). Today, the oceanography of this area of the North Atlantic is strongly influenced by the passage of the warm Gulf Stream and the modern Deep Western Boundary Current, which is the primary southerly flow component of the deep current system along the western North Atlantic Ocean basin. Site U1410 is at a current water depth of ~3400m and it was estimated to have been ~2950m at 50 Ma (Norris et al., 2014). At this Site, a composite sedimentary succession was generated from drilling three holes, spanning from the early Eocene to the Pleistocene (Norris et al., 2014). In this study, we adopt the latest version of the splice (from Hole A Core 27 to Hola A Core 15), recently proposed by Vahlenkamp et al. (2018), which is mainly based on onshore-acquired XRF data. This age model also affects the depth of chron boundaries (Yamamoto et al., 2018).

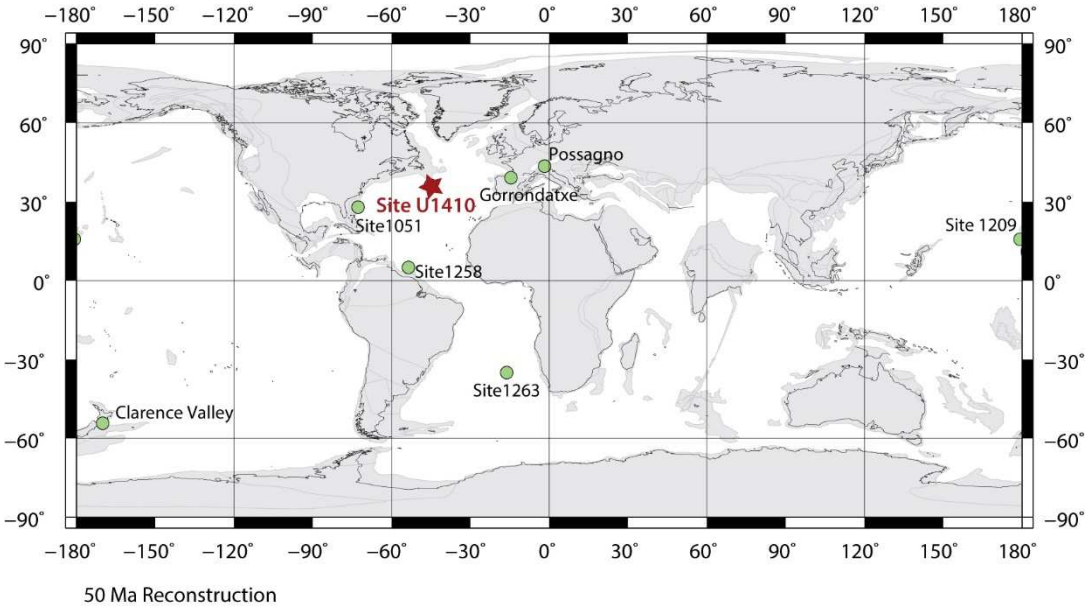

Figure 2.2*:* Location map at 50 Ma showing the position of IODP Site U1410 (solid red star) during the early-middle Eocene. The locations of key sites documenting the early-middle Eocene transition are also reported (solid green circle): Gorrondatxe section (Spain, Global Stratigraphic Section and Point for the base of Lutetian, Molina et al., 2011); the Possagno section (NE Italy, Agnini et al., 2006, 2014); ODP Site 1051 (Blake Nose, Agnini et al., 2014); ODP Site 1258 (Demerara Rise, Sexton et al., 2011; Westerhold et al., 2018); ODP Site 1209 (Shatsky Rise, Westerhold et al., 2018;), ODP Site 1263 (Walvis Ridge, Westerhold et al., 2017, 2018) and Clarence valley (New Zealand, Slotnick et al., 2012, 2015b). Base map is from http://www.odsn.de/odsn/services/paleomap/paleomap.html

The study interval encompasses the transition from white to pinkish white nannofossil chalk (lithologic unit IV) of early Eocene age to greenish nannofossil clay of middle Eocene age (lithologic unit III) (Norris et al., 2014). This prominent lithologic change likely reflects the onset of a drift sedimentation regime also suggested by the enhancement in the deposition of terrigenous clay-rich sediments (Boyle et al., 2017). The onset of a contour-following deep currents produced different

depositional features at the sea floor, where erosional unconformities and sedimentation of contourites have been documented just above the early-middle Eocene boundary. This oceanographic change has been associated with the establishment of a new deep current system, referred as to Northern Component Water (NCW), which has been interpreted as the predecessor/progenitor of the modern North Atlantic Deep Water (Vahlenkamp et al., 2018; Coxall et al., 2018). This sedimentary regime caused a significant shift in the sedimentation rates, which shifted from on average ca. 0.6 cm/k.y.in the early Eocene, typical of truly pelagic environments, to 1.3-2.6 cm/k.y. in the middle Eocene (Norris et al., 2014), confirming the onset of contourite drifts.

2.2.2 Calcareous nannofossil assemblage data

The study on calcareous nannofossil assemblages has been carried out on 208 samples spanning an interval of 147.46 m that documents the early-middle Eocene transition. Smear-slides were prepared from raw sediment samples using standard techniques (Bown and Young, 1998) and then investigated at light microscope at a magnification of 1250X. The taxonomic concepts adopted are described in Aubry (1982, 1988, 1989, 1990, 1999), Perch-Nielsen (1985), Bown (2005); Bown and Dunkley Jones (2006, 2012); Bown and Newsam (2017) except for *Dictyoccocites* and *Reticulofenstra* for which we follow Agnini et al., (2014) and large coccolithaceans and sphenoliths for which we use the concepts recently proposed by Cappelli et al. (see Chapter 3).

Counts of the relative abundance of taxa were performed by counting a minimum of 300 specimens from the whole assemblage. The abundance patterns of index species were determined by counting the number of specimens in a prefixed area (modified after Backman and Shackleton, 1983). This counting was performed on 1mm^2, but for rare index taxa (*Nannotetrina, Pletolithus gigas, Reticulofenestra umbilicus*) we extended the counts to 2 mm^2 and then normalised to the prefixed area (e.g., 1 mm^2). The position of biohorizons recognized in this study are based on abundance patterns of index species and, according to Backman (2012) and Agnini et al. (2014), they are defined as follows: Base (B) and Top (T) are used to describe the stratigraphic lowest and highest occurrences of taxa; Base common and continuous (Bc) and Top common and continuous (Tc) were used to define the first/last continuous presence of a specific taxon, which is usually preceded/succeed by an interval of sporadic occurrence. The biostratigraphic schemes adopted here are those of Martini (1971), Okada and Bukry (1980) and Agnini et al. (2014).

In order to evaluate the main factors affecting variations in assemblage composition, principal component analysis (PCA) was performed using the free statistical software PAST (PAleontological Statistic; Hammer et al., 2011). The analysis was carried out on a dataset based the relative abundance of 16 informal subgroups: *Blackites, Campylosphaera, Chiasmolithus, Clausicoccus,*

Cyclicargolithus, Dictyococcites, Discoaster, Ericsonia, Girgisia, Helicosphaera, Pontosphaera, Reticulofenestra, Sphenolithus, Toweius, Zygrhablithus and "others".

2.2.3 Paleoecological significance of calcareous nannofossils

In this study, the paleoecological interpretation is based on fluctuations of selected paleoecologically sensitive taxa, for which environmental preferences are relatively well established from the literature. Selected temperate waters and/or mesotrophic favouring taxa include *Reticulofenestra, Toweius, Coccolithus pelagicus* (Haq & Lohmann, 1976; Monechi et al., 2000; Gibbs et al., 2006; Persico & Villa, 2004; Villa et al., 2008), whereas selected warm water and /or oligotrophic taxa are *Discoaster, Sphenolithus, Zygrhablithus* and *Ericsonia* (Haq & Lohmann, 1976; Backman, 1986; Wei & Wise, 1990; Monechi et al., 2000; Bralower, 2002; Gibbs et al., 2006; Agnini et al., 2007a; Villa et al., 2014). We applied a common approach used in paleoenvironmental studies, calculating a paleoevironmental index (PEI) based on the abundances of the two contrasting groups (Villa et al., 2008). Here the PaleoEnvironmental Index (PEI) is defined as [temperate-mesotrophic group/ (temperate-mesotrophic group+warm-oligotrophic group)].

2.2.4 Geochemical data

A total of 329 samples were powdered and analysed for bulk sediment stable isotope composition and percent calcium carbonate ($CaCO_3$). The analyses were carried out in the Stable Isotope Laboratory of the Department of Geosciences at the University of Padova using a Delta V Advance Isotopic Ratio Mass Spectrometer equipped with a Gas Bench II device. A known mass of sample (0.25-0.75 mg) was placed into headspace vials and flushed with helium. Each sample was treated with 10 mL of 100% phosphoric acid (EMSURE ® ≥ 99 %) at 70 °C for ca. 3 hours and reacted with orthophosphoric acid at 70 °C. Isotopic values are reported in standard delta notation relative to the Vienna Pee Dee Belemnite (VPDB). An internal standard (white Carrara marble Maq 1: $\delta^{13}C = 2.58‰$; $\delta^{18}O = -1.15‰$ VPDB) periodically calibrated to NBS-19 IAEA reference material (Coplen et al., 2006) was used to normalize raw $\delta^{13}C$ and $\delta^{18}O$ values. A third internal standard (marble Gr1: $\delta^{13}C = 0.68$ ‰; $\delta^{18}O = -10.44$ ‰ VPDB) was run for quality assurance, and repeated with precisions better than 0.07‰ for $\delta^{13}C$, and better than 0.09‰ for $\delta^{18}O$.

The calcium carbonate content of each sample was calculated based on the beam height obtained during isotope mass spectrometer analysis (Spofforth et al., 2010). The beam height depends on the pressure of CO_2 liberated from the sample, which in turn is a function of the carbonate content of the sample. Apart from the Maq 1 samples used to calibrate each sequence, every run contained at least 10 samples of Maq1 (weights range from 50 to 500 mg) distributed along the run. These standard

samples serve to construct a linear fit line based on the beam height / standard weight ratio (with a r^2 always > 0.99) that is used to calculate the carbonate content of the analyzed samples.

2.3. RESULTS

2.3.1 Calcareous nannofossil assemblage data

Calcareous nannofossil assemblages are rich and well diversified. In the study succession the preservation varies from moderate to good and it is strictly related with the lithology. In particular, calcareous nannofossils are moderately to well-preserved in nannofossil chalk through the lower Eocene, where they typically are (especially *Disocoaster* and *Zygrhablithus*) affected by overgrowth of secondary calcite. The fossil assemblages are generally very well preserved in the overlying clay-rich drift sediments. The exceptional preservation observed in study material recovered during Expedition 342 is a distinctive feature that makes these successions different from most of Paleogene deep-sea sites (Bown and Newsam, 2017) and allows for the perfect preservation of very delicate structures (central area nets in *Reticulofenetsra*) and high abundance of small placoliths (reticulofenestrids) and fragile taxa (*Blackites)* (see Appendix I).

Nannofossil assemblages from Site U1410 display several general trends and prominent changes in their composition (Figure 2.3):

- *Reticulofenestra* accounts for on average ~ 8% in the lower part of its distribution range, and it increases in abundance from 260.77 rmcd, reaching on average values of 60% that remain substantially the same for the rest of the study interval.
- *Dictyococcites* is present from 278.14 rmcd. A sudden increase in abundance occurs at 271.23 rmcd (from less than 1 % to 11 %) and high values are maintained up to 251.69 rmcd (~12% on average). Above this interval, *Dictyococcites* decreases and remains relatively constant showing values around ~ 2 %.
- *Toweius* are consistently present from the base of the study interval to 280.45 rmcd. *Toweius* is common in the basal part of the section, showing a spike in abundance between 290.55 and 288 rmcd (~ 16 %). Above this level, *Toweius* exhibits a progressive decrease to values <1% from 281.69 rmcd.
- *Coccolithus* displays an average abundance of ~ 16 %, with higher values (~26 %) recorded before the origination of *Reticulofenestra.*
- *Discoaster* represents ~ 8 % of the assemblages through the lower Eocene. This genus peaks to ~13 % during the turnover between *Toweius* and *Reticulofenstra-Dictyoccocites* (284.18 - 278.72 rmcd) and shows a second spike in abundance (~11 %) in the upper part of the early Eocene (between 268.50 and 261.96 rmcd). *Discoaster* shows an overall decrease in

abundance from the early-middle Eocene transition, with values never exceeding ~2 % of the assemblages in middle Eocene samples.

- *Sphenolithus* is relatively common (on average ~7 %) at Site U1410. The genus is relatively abundant during the early Eocene where it reaches values around ~ 12 %, but it undergoes a significant decrease (up to ~4 %) in the middle Eocene.
- *Zyghrablithus* has a highly variable abundance pattern during the study interval. It is a common component of the assemblages during the lower Eocene, accounting for ~ 33%, but its abundance dramatically declines across the early-middle Eocene transition. In middle Eocene samples, the abundance of this genus is only ~ 1%.
- *Cyclicargolithus* constitutes a minor component of the assemblages. Higher values are recorded in the basal part of the study interval, where the most common species is *Cyclicargolithus luminis*.
- *Ericsonia* and *Clausicoccus* are present from the base of the section and represent a minor component of the assemblages, with low abundances (~3% and ~2%, respectively) observed throughout the study section. These genera display a slight increase from ~ 203 rmcd upward.
- *Chiasmolithus* is rare component of the assemblages throughout the study section but it shows an increase in abundance right in coincidence with the base of the Lutetian.

A slight increase in abundance is recorded from 241.75 rmcd to 231.91, where the mean relative abundance values averages around ~5%.

- *Campylosphaera, Helicosphaera* and *Pontosphaera* always display very rare abundances in the early Eocene samples. They display a very slight increase in abundance with an average value of ~ 1% in the middle Eocene samples.
- *Blackites* is a minor component of the nannofossil assemblages and it displays an increase in abundance (up to 3-4%) close the base of Chron C21n.

From the evolutionary point of view, the study interval is marked by a number of appearance and extinction, which serve as primary and additional marker biostratigraphic events. The description and discussions of the standard biohorizons of the Paleogene Zonation (Martini, 1971; Okada and Bukry, 1980 and Agnini et al., 2014) and additional events are presented below.

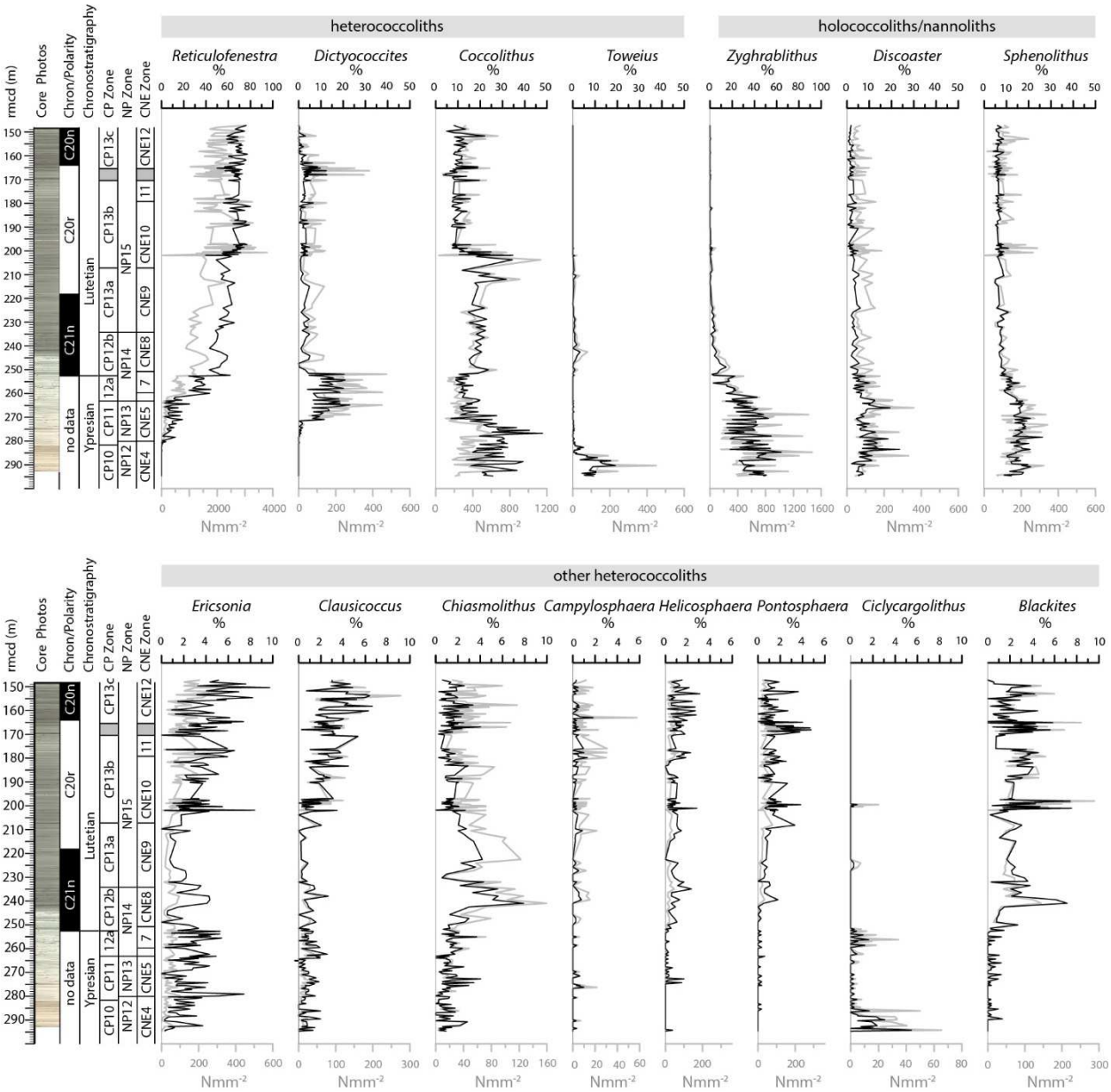

Figure 2.3*:* Relative (%, black line) and semi-quantitative (N mm^{-2}, grey line) abundances of selected calcareous nannofossil genera from IODP Site U1410 are plotted against chronostratigraphy, magnetostratigraphy (Yamamoto et al., 2018) and calcareous nannofossil biostratigraphy: NP Zone (Martini; 1971) CP Zone (Okada and Bukry, 1980); CNE Zone (Agnini et al., 2014).

The PCA analyses on the census data show that two significant principal components (PCA1 and PCA2) explain ~78% of the variance (Figure 2.4). The PCA factor 1 (PC1, 65.47% of the variance) is characterized by a high negative loading of *Reticulofenestra,* whereas it is positively loaded by *Zygrhablithus* (0.64)*,* and, to a lesser extent, by *Sphenolithus* (0.21)*, Discoaster* (0.21) and *Toweius* (0.18). The loadings of the others species are considered too low to be significant. The trend of PC1scores displays a gradual decrease along the section, marked by two negative shifts at ~280 rmcd and at the early-middle Eocene boundary. Early Eocene samples are generally characterized by positive values, whereas middle Eocene samples display negative values, except for a short interval

just above the boundary. The PCA factor 2 (PC2, 12.84% of the variance) is dominated by a very high positive component loading of *Dictyoccicites* (0.77) and, to lesser extent, it is influenced by *Zygrhablithus* (0.34), *Reticulofenetsra* (0.34) and *Discoaster* (0.15). The main negative loading on PC2 is that of *Toweius* (0.32). The trend of PC2 scores records an abrupt variation between 270.94 rmcd and 250.08 rmcd.

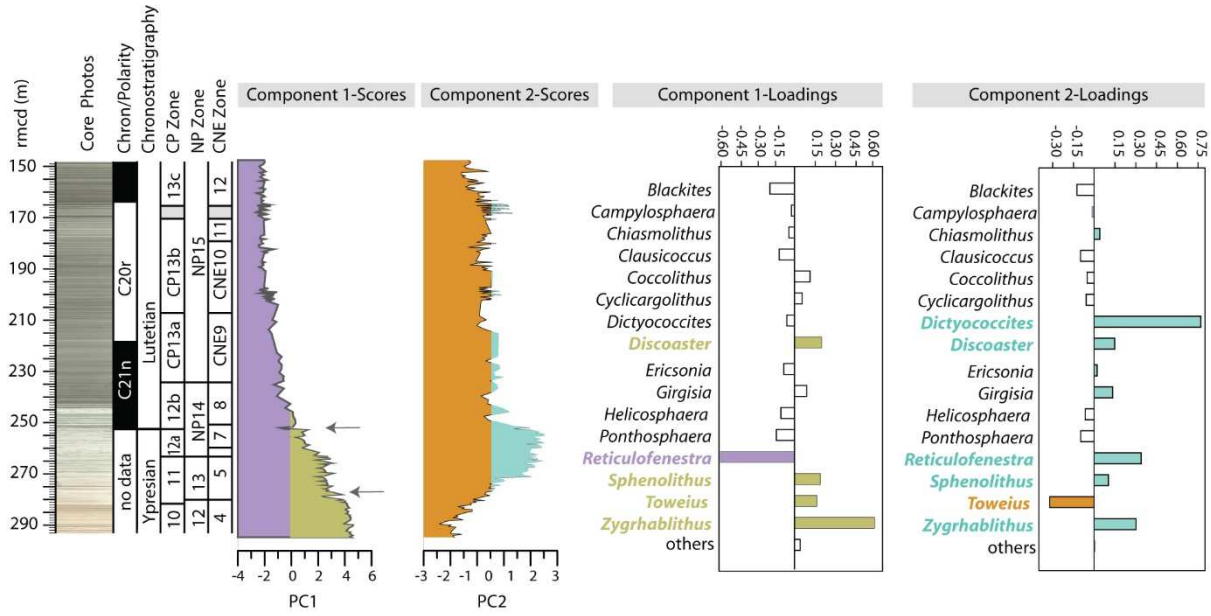

Figure 2.4: Distribution patterns of PC1 and PC2 are plotted against core images, chronostratigraphy, magnetostratigraphy (Yamamoto et al., 2018) and calcareous nannofossil biostratigraphy: NP Zone (Martini; 1971) CP Zone (Okada and Bukry, 1980); CNE Zone (Agnini et al., 2014).

2.3.2 The PEI and long-term paleoecological evolution

During the early-middle Eocene, the trend of PEI suggests a significant change in the relative abundances of two groups of taxa with contrasting paleoecological affinities (Figure 2.6). From the base of the study interval to ~267 rmcd, the PEI shows broad fluctuations around a mean value of 0.37, suggesting that warm-waters oligotrophic taxa were slight favoured. In this interval, the PEI, is characterized by two increases in abundance of the warm-water / oligotrophic group, a feature shaped by the high abundances displayed by only one species, *Discoaster kuepperi.* From 264 rmcd up to the early-middle Eocene boundary, the PEI values progressively increase up to 0.8, reflecting both the relevant increase of temperate-water/mesotrophic group *(*mainly *Reticulofenestra)* and the decline of the warm-water/oligotrophic taxa. The PEI remains high and constant through the middle Eocene with a mean value of 0.88 and a very low standard deviation (0.04), this is the result of the very high relative abundances of temperate water / meso-eutrophic taxa and low abundances displayed by the warm-water/oligotrophic group, which never exceeds 20% of the entire assemblages.

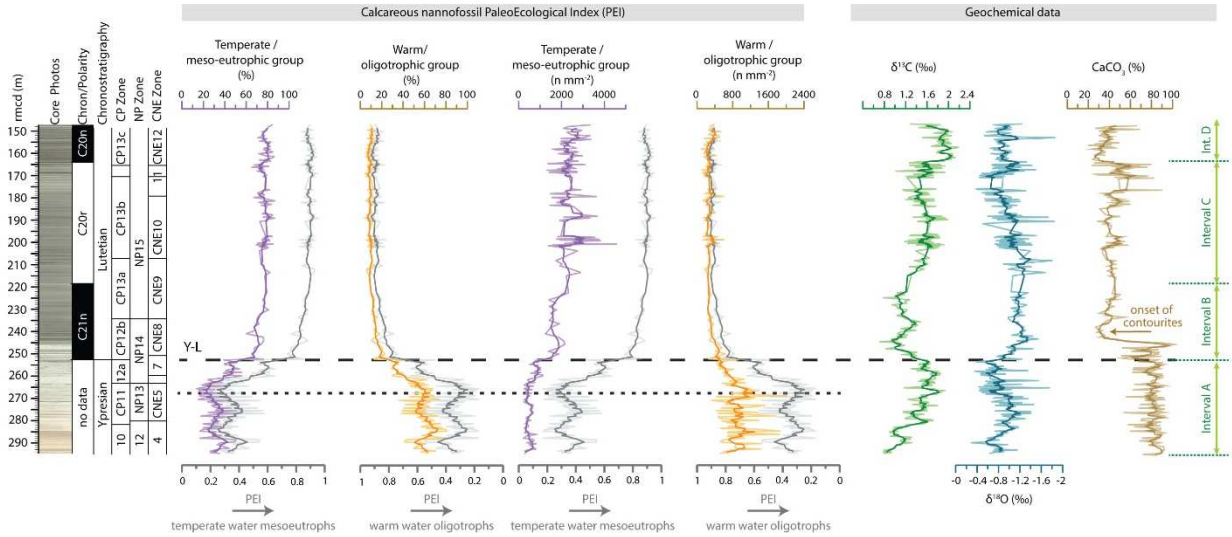

Figure 2.3: Calcareous nannofossil PaleoEcological Index (PEI) is plotted against relative abundance (%) and semi-quantitative abundance (N mm^{-2}) of nannofossil paleoecological groups. To the right stable carbon ($\delta^{13}C$) and oxygen ($\delta^{18}C$) isotope records and calcium carbonate content ($CaCO_3$) from bulk sediments. Darker lines are 5 point moving average dataset. Dotted lines highlight key intervals for the paleoecological interpretations. Y-L = Ypresian – Lutetian. To the left Core images, chronostratigraphy, magnetostratigraphy (Yamamoto et al., 2018) and calcareous nannofossil biostratigraphy: NP Zone (Martini; 1971), CP Zone (Okada and Bukry, 1980), CNE Zone (Agnini et al., 2014).

2.3.3 Bulk stable isotope data and $CaCO_3$ content

Bulk carbon ($\delta^{13}C$) and oxygen ($\delta^{18}O$) isotopes, and carbonate content ($CaCO_3$) data show distinctive trends and several minor excursions that allow for a fourfold subdivision (A to D) of the study section (Figure 2.6).

2.3.3.1 Carbon isotopes

Carbon isotope values range between 0.71 and 2.19 ‰ with an average of 1.48 with a standard deviation (1σ) of 0.31‰. From the base of the succession to 252.53 mcd we identify an interval (Interval A) where the $\delta^{13}C$ values have an average of 1.41 ‰ and a standard deviation of 0.28 ‰. Superimposed on a long-term increasing trend, the $\delta^{13}C$ record shows several small negative carbon isotope excursions (CIEs) with magnitudes ranging from 0.28 to 0.57 ‰. The second interval (Interval B: 252.53 - 218.56 rmcd, broadly corresponding to Chron C21n) is characterized by the lowest values in $\delta^{13}C$ (mean value = 1.17 ± 0.16‰ 1σ) and three significant negative CIEs with magnitudes of ca. 0.5 ‰, that lie at 247.67, 244.55, 224.77 rmcd, respectively. Above this interval from 218.56 to 163.71 rmcd (Interval C), the $\delta^{13}C$ curve displays a trend towards higher values (average 1.54 ‰ ± 0.2 1σ). Just above the base of Chron C20n (163.71 rmcd) the curve shows a second abrupt shift towards higher values (average = 1.89 ‰ ± 0.17 1σ) (Interval D).

2.3.3.2 Oxygen isotopes

Oxygen isotopes of bulk carbonate vary between -0.29 and -1.88 ‰, with a mean value of -0.96 ‰ ± 0.28 1σ. In the lower part of the study section (Interval A), the $\delta^{18}O$ curve is characterized by the highest mean values of the entire succession (- 0.84 ‰). In the lower part of Interval A, $\delta^{18}O$ mean values are around -1.01‰, but sharply increase by of 0.3 ‰ throughout the interval between 267.67 and 253.49 rmcd. At the base of Interval B, values rapidly decrease to -1.54 ‰ at 243.32 rmcd. From this point to 169.02 rmcd, values display a long-term increase with an average value of ca. -1.05 ‰ and a standard deviation of 0.28 ‰. The general increase in $\delta^{18}O$ values is followed by a slight decrease in the uppermost part of interval C. A shift toward higher values is observed from 163.71 rmcd upward (Interval D) where values remains stable ca. -0.90‰.

2.3.3.3 Carbonate content

The lower 50 meters of the study succession (Interval A and lower Interval B), are characterized by high $CaCO_3$ content, varying between 50 and 100 % with a mean value of 81%. This long interval is followed by a prominent and abrupt drop in the carbonate content to ~60%. From 242.42 rmcd and in the following 76 meters the carbonate content remains stable with a mean value of 41.54% and a limited variance (6.84 % 1σ). At 176.01 rmcd the $CaCO_3$ shows an abrupt increase from 44% to 90%. From this level and in the following ~11 meters the curve shows several prominent peaks reaching values between 76 and 90%. This wide variability gives a high standard deviation (15 % 1σ) around a mean value of ca. 53%. An important shift towards lower values is observed at 163.71 rmcd at the base of Interval D, where $CaCO_3$ content averages around 35% with a lower standard deviation.

2.4 BIOSTRATIGRAPHY

Calcareous nannofossil biostratigraphy is based on the recognition of biohorizons, which derive from changes in the abundance pattern and first and last occurences of taxa. Providing quantitative highly resolved dataset is therefore essential to discuss the reliability of biostratigraphic events (Agnini et al., 2017). This is particularly relevant for early-middle Eocene interval, where numerous standard markers have been found to be rare or even absent in some depositional settings or show scattered abundance patterns around their level of evolutionary emergence and/or extinction. In general, the study interval suffers for the scarcity of semi-quantitative datasets of index species and consequently the quality and reliability of some biostratigraphic events are still uncertain and need to be further checked (Agnini et al., 2014). Here we present the abundance patterns of marker species used in Paleogene calcareous nannofossil zonations (Martini, 1971; Okada & Bukry, 1980; Agnini et al., 2014) as well as the abundance of several taxa that might provide useful additional biohoriozons

(Figure 2.6). In the following, we provide a comprehensive discussion of selected biohorizons, which are listed in stratigraphic order and summarized in Table 2.1 and in Figure 2.7.

-The Base and Base common of *Discoaster lodoensis*

The B of *D. lodoensis* is used to define the base of Zones CP10 (Okada and Bukry, 1980) and NP12 (Martini, 1971). Instead, the base of Zone CNE4 (Agnini et al., 2014), is marked by the base common and continuous of this species which is usually found ca. 700 Kyr after the very first appearance (Agnini et al., 2016) but, according to the authors, provides a more reliable event. The sample at the base of the study section contains *D. lodoensis.* Although its occurrence is not continuous up to 289.10 rmcd, this taxon displays a relative good continuity (Figure 2.7). This datum indicates that the base of the section belongs to Zone CNE4 (NP12 or CP10).

-Turnover *Toweius* spp. /*Dictyoccocites + Reticulofenestra* spp.

At Site U1410, the interval between 285.20 and 280.45 rmcd documents the turnover in abundance between *Toweius* spp., one of the main component of the Paleocene assemblages, and *Dictyococcites + Reticulofenestra* spp. (family *Noelaerhabdaceae*), a group that will dominate the Eocene/Oligocene times (Figure 2.7). Looking in detail at this turnover, we observe that genus *Toweius*, which accounts for ~40% of the nannofossil assemblages at 290.12 rmcd, relatively sharply declines to less than 5% at 285.02 rmcd. The common and continuous presence of *Noelaerhabdaceae* (Bc) occurs at 279.48 rmcd, but rare and scattered occurrences of members of this family are recorded from well below (284.28 rmcd) almost in coincidence with the decline *Toweius*. The turnover is associated with high abundances of the genus *Discoaster*, in particular *D. kuepperi* dominates within this genus. In the Newfoundland region, this event is recorded in the uppermost part of Zone CNE8 (Agnini et al., 2014) or NP12 (Martini, 1971). This datum is in agreement with other data from the Tethyan domain, the Indian Ocean and the Goban Spur sites (Agnini et al., 2006; Schneider et al., 2011; Shamrock and Watkins, 2012.), however data from Maud Rise area may suggest a possible anticipation of this important evolutionary step at high latitudes (Schneider et al., 2011).

-The Base of *Coccolithus crassus*

The Base of *C. crassus* defines the base of Zone CP11 of Okada & Bukry (1980). At Site U1410, this event occurs at 281.65 rmcd, in coincidence with the turnover between *Toweius* and *Dictyoccocites + Reticulofenestra* (Figue 2.7, 2.8). This position is consistent with that observed in the middle latitude Possagno section (Agnini et al., 2006). At Site U1410 the ranking and spacing of two relatively close biohorizons, the Base of *C. crassus* and the Top of *T. orthostylus*, display that the

former slightly predates the latter and this datum is consistent with several datasets from different depositional settings (Agnini et al., 2006; Tori and Monechi, 2013; Shamrock and Watkins, 2012; Westerhold et al., 2017).

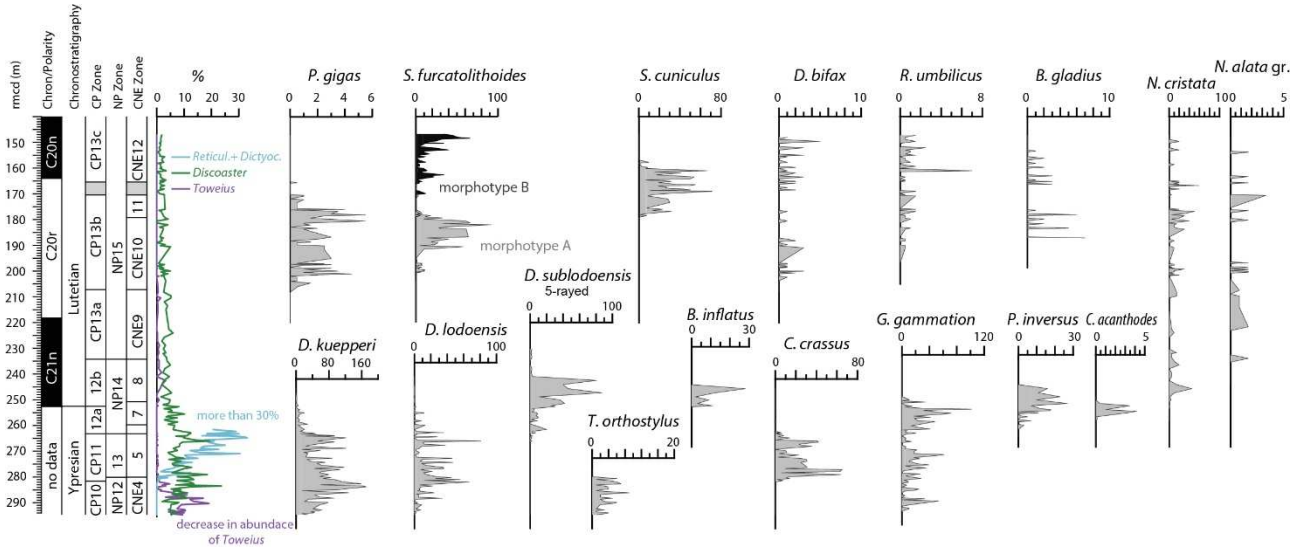

Figure 2.4*:* Semi-quantitative abundance patterns of selected calcareous nannofossil taxa (Nmm^{-2}). To the left magnetostratography (Yamamoto et al., 2018) and calcareous nannofossil biostratigraphy: CP zone (Okada and Bukry, 1980), NP Zone (Martini, 1971); CNE Zone (Agnini et al., 2014).

-The Top of *Tribrachiatus orthostylus*

The extinction of *T. orthostylus* is used to the mark the base of Zone CNE6 (Agnini et al., 2014) or Zone NP13 (Martini, 1971). This taxon is consistently rare at Site U1410 and goes extinct at 280.09 rmcd (Figure 2.7). The reliability of this event has been questioned by some authors (Wei and Wise, 1989; Tori and Monechi, 2013), however, the comparison between the record from Site U1410 and other datasets worldwide (Agnini et al., 2006; Westerhold et al., 2017) indicates that this event is one of the more reliable biohorizons of the early-middle Eocene. It is worth to note that *T. orthostylus*, the last member of the *Rhomboaster-Tribrachiatus* plexus goes extinct at the end of the EECO while the first representatives of this group firstly appear at the PETM, suggesting a very specific adaptation of these two genera to the extreme climate conditions of the early Eocene.

-The Base and Base common of *Discoaster sublodoensis* (5-rayed morphotype)

The Base common of *D. sublodoensis* is the event used to denote the base of Zone CNE6 (Agnini et al., 2014), Subzone CP12a (Okada and Bukry, 1980) and Zone NP14 (Martini, 1971). Following Agnini et al. (2014), we decide to use the Base common of the 5-rayed morphotype to identify the base of these zones because the presence of *D. lodoensis/D.sublodoensis* transitional specimens makes the precise positioning of this event very difficult. Although this choice reduces the taxonomic

ambiguity of *D. sublodoensis,* this datum is still considered problematic in terms of correlation between different successions (Westerhold et al., 2017) because of its scattered abundance close to its evolutionary appearance (Backman et al., 1986; Agnini et al., 2006; Bernaola et al., 2006). At Site U1410, rare and scattered specimens of 5-rayed *D. sublodoensis* have been observed from 266.24 rmcd, but its occurrence becomes more continuous from only 263.22 rmcd upward, where we have tentatively placed the Bc of *D. sublodoensis* (Figure 2.7). Upward this species is consistently observed except for one sample at 258.61 rmcd.

-The Top *Coccolithus crassus*

At Site U1410, *C. crassus* goes extinct at 261.97 rmcd (Figure 2.7). This biohorozon lies approximately ~2 meters below the Tc of *D. lodoensis.* A similar biostratigraphic position was also observed at Possagno (Agnini, personal communication, 2018), Exmouth Plateaux (Shamrock and Watkins, 2012) and Demerara Rise (Westerhold et al., 2017). The distinctiveness of the species and its consistent ranking and spacing suggest that this biohorizon is promising and would help in refining this interval.

-The Base and Base common of *Pseudotriquetrorhabdulus inversus*

In the studied section, the first discontinuous entry of *P. inversus* observed at 260.77 rmcd and it is followed by a prominent increase at 254.29 rmcd (Figure 2.7). In agreement with previous data from South Atlantic, the Base common of *P. inversus* slightly predates the Top of *D. lodoensis* (Backman et al., 1986).

-**The Top of *Discoaster lodoensis***

The base of Zone CNE6 (Agnini et al., 2014) is defined by the Top of *D. lodoensis.* At Site U1410, the final range of *D. lodoensis* shows a tail of scattered abundance with isolate multiple pulses (Figure 2.7). This distribution prevents to identify confidently the Top of this taxon, which was tentatively placed at 259.74 rmcd. By contrast, this taxon shows a clear final decline over a short stratigraphic range both at Possagno (Agnini et al., 2006) and DSDP Site 527 (Backman, 1986), where the position of this biohorizon has been delineated confidently. More data are thus needed to further check the reliability of this event.

-The Base common *Chiphragmalithus* spp.

The first appearance of genus *Chiphragmalithus* has been usually observed close to the Base common of *D. lodoensis* (C24n, ~ 52 Ma, Perch-Nielsen, 1985), however the fact that the specimens observed

within Zone NP14 (~ 48 Ma) have no stratigraphic continuity with their putative ancestors calls into question their phylogenetical relationship and thus the appropriateness to ascribe these younger forms to genus *Chiphragmalithus*. For sake of simplicity we decide to continue to include these taxa in genus *Chiphragmalithus* but a more comprehensive taxonomic reassessment is strongly necessary.
At Site U1410, specimens of *Chiphragmalithus* spp. are found to occur close to the Top common of *D. lodoensis.* Forms belonging to this genus are sporadically observed from 257.45 rmcd but become relatively common and continuous from 256.83 rmcd upwards (Figure 2.7). A gradual increase of the wall/rim height and the progressive development of the original central structure progressively transform *Neococcolithes* into *Chiphragmalithus* (Bown and Newsam, 2017). The evolution of this lineage is eventually concluded when *Chiphragmalithus* intergrades into *Nannotetrina* by a progressive flattening and extension of the rim into a plate-like structure and the transformation of the central structure into a ridged cross. The recognition of forms ascribable to *Chiphragmalithus* can be thus used to approximate the appearance of *Nannotetrina* because of the short stratigraphic range of the former taxon and the phylogenetical relationship between these two genera.
The stratigraphic distribution of *C. acanthodes* and intergrading morphotypes occurs in a similar biostratigraphic position at DSDP Sites 527 and 528 (Backman et al., 1986), at ODP Site 1258 (Westerhold et al., 2017) and at IODP Sites U1407-1411 (Norris et al., 2012; Bown and Newsam, 2017).

- **The Base of *Blackites inflatus***

The Base of *B. inflatus* marks the base of Subzone one CP12b (Okada and Bukry, 1980) and it serves as primary marker to denote the Lutetian Global Stratotype Section and Point (GSSP) in the Gorrondaxte section (Basque Country, Northern Spain; Molina et al., 2011). At Site U1410, the entry of this taxon is recorded at 252.54 rmcd, just below the Base of *N. cristata* and very close C21r/C21n transition (252.53 rmcd) (Figure 2.7). This position is in agreement with available data from Atlantic oceans sites (Westerhold et al., 2017). The ranking and the spacing of Bases of *B. inflatus* and *N. cristata* are also consistent with data from Gorrondatxe, but their positions with respect to magnetostratigraphy are largely inconsistent. Indeed, at the GSSP section the Base of *B. inflatus* lies at the 60 % up of Chron C21r (Bernaola et al., 2006; Molina et al., 2011), which results in a ~ 0.5 Ma older calibration for this event. Our datum from Site U1410 further points out the urgent need to revaluate and discuss the Base of *B. inflatus* in order to harmonize the different data available, this is particularly important because this biohorizon defines the base of the Lutetian (Westerhold et al., 2017; Agnini et al., 2017). An additional limit of this taxon is that it is usually absent in frankly open ocean settings or in poorly preserved materials (Agnini et al., 2014; Westerhold et al., 2017).

-**The Base of *Nannoterina cristata***

The Base of *N. cristata* is used to mark the base of Zone CNE8 (Agnini et al., 2014) (Fig. 2.7). As stated above, the appearance of this taxon is preceded by the occurrence of transitional morphotypes that intergrade *Chiphragmalithus acanthodes* into *Nannotetrina cristata* (see Appendix II, Plate 2.6, fig. 19, 20, 21). At Site U1410, the Base of *N. cristata* occurs at 250.79 rmcd, just above the Base of *B. inflatus* (Figure 2.7). This result is in agreement with previous data (Bernaola et al., 2006; Agnini et al., 2014, Westerhold et al., 2017, Tori and Monechi, 2013). However, as discussed for the Base of *B. inflatus,* the position respect to magnetostratigraphy shows significant discrepancies between Atlantic deep-sea sections and the Tethyan Possagno section (Agnini et al., 2006 Westerhold et al., 2017, this study), and the Spanish land-based marine sections in the Tethys area (Molina et al., 2011; Tori and Monechi, 2013).

-The Top of *Girgisia gammation*

At Site U1410, the Top of *G. gammation* virtually coincides with the Base of *N. cristata* (Figure 2.7). This biohorizon has been observed in a similar biostratigraphic position in the Indian Ocean and Tethys domain (Shamrock and Watkins, 2012; Tori and Monechi, 2013). In the study succession, the abundance pattern of this species shows significant fluctuations in abundance and while it displays high abundances in Subzone CP12a (zones CNE6-CNE7) the final part of its stratigraphic range is characterized by a sharp decline in abundance followed by a scattered tail of distribution that could inhibit the precise recognition of the position of this biohorizon.

-The Top *Discoaster kuepperi*

The Top of *D. kuepperi* is detected within Subone CP12b, consistent with previous data (Shamrock and Watkins, 2012; Tori and Monechi, 2013). At Site U1410, this taxon is the dominant component within *Discoaster* throughout the Ypresian. Its abundance pattern shows two distinctive peaks in abundance: the first coincides with the *Toweius/ Dictyococcites-Reticulofenestra* turnover, while the second is observed close to the Base of 5-rayed *D. sublodoensis.* Shortly above this interval, the abundance pattern of *D. kuepperi* shows a rapid decline and low abundances persist until its disappearance at 248.11 rmcd (Figure 2.7).

-The Top of *Blackites inflatus*

This event together with the Base of *Nannotetrina alata* gr. (sensu Agnini et al., 2014) was indicated as a marker to define the base of Zone CP13a (Bukry, 1973; Okada & Bukry, 1980). At Site U1410, the stratigraphic range of *B. inflatus* is unusually short and this taxon shows a sharp final decline in

the middle part of Zone CNE8 (or Subzone CP12b), significantly below the Base of *N. alata* gr. (Figure 2.7). Available data from literature indicate that these two biohorizons are closely spaced so that the result from Site U1410 represents an anticipated exit (Shamrock and Watkins, 2012; Tori and Monechi, 2013).

-**The Top of *Pseudotriquetrorhabdulus inversus***

At Site U1410, this species disappears in the upper part of Zone NP14 (or middle part of Subzones CP12b or Zone CNE8). Previous studies (Backman et al. 1986; Shamrock and Watkins, 2012; Tori and Monechi, 2013) indicated that *P. inversus* ranges higher into the middle Eocene, but this is not observed in this study.

-The Top Common of 5-rayed *Discoaster sublodoensis*

Discoaster sublodensis (5-rayed) shows significant fluctuations in abundance throughout the study section. Between 253.10 and 241.76 rmcd, of *D. sublodoensis* displays high abundances that are followed by a sharp drop in abundance and eventually by a relatively long tail of discontinuous abundance (Figure 2.7). We tentatively define the Top common of this form at 241.76 rmcd. A similar sharp decline in abundance is reported also at DSDP Site 527 (Backman, 1986) and at Possagno (Agnini et al., 2014), but in the last succession *D. sublodoensis* shows a continuous occurrence through the final part of its range.

-The B of *Nannotetrina alata* gr.

The Base of *Nannotetrina alata* gr., which includes *Nannotetrina alata* and *Nannotetrina fulgens* (Agnini et al., 2014), defines the base of Zone CNE9 (Agnini et al., 2014), Zone NP15 (Martini, 1971) and Subzone CP13a (Okada and Bukry, 1980). At Site U1410, *Nannotetrina alata* gr. is rare and the low abundance makes the delineation of this biohorizon difficult. *Nannotetrina alata* gr. first appears at 234.26 rmcd, in upper part of the stratigraphic range of *D. sublodoensis*, which lies in the middle part of Chron 21n (Figure 2.7). This datum is in agreement with the datum from Possagno (Agnini et al., 2006, 2014) (Fig. 2.8). A similar position respect to magnetostratigraphy is reported also in the Gorrondatxe section (Bernaola et al., 2006), whereas it was observed in the lower part of C20r in the Agost section (Tori and Monechi, 2013). Though the general scarcity of this taxon, the extension of counts to 2 mm^2 have produced a sufficiently well-resolved abundance pattern that allowed for a recognize the position of the biorihorizon quite confidently.

Event	Species	Sample Top	Sample Base	Top depth (rmcd)	Base depth (rmcd)	Mean depth	Chron	Age Ma GTS2012	Position from Top Chron
T	*Pletolithus gigas*	1410B-19X-3W-0	1410B-19X-3W-40	165.22	165.62	165.42	C20r	43.50	1.56
Bc	*S. furcatolithoides* morph. B	1410B-19X-3W-40	1410A-17X-2W-80	165.62	165.89	165.76	C20r	43.51	1.89
B	*S. furcatolithoides* morph. B	1410B-19X-3W-0	1410A-19X-3W-40	165.22	165.62	165.42	C20r	43.50	1.56
Tc	*Pletolithus gigas*	1410B-19X-6W-60	1410B-19X-6W- 80	170.32	170.52	170.42	C20r	43.71	6.56
B	*Sphenolithus cuniculus*	1410C-18X-5W-20	1410C-18X-6W-60	179.01	179.41	179.21	C20r	44.08	15.35
Bc	*S. furcatolithoides* morph. A	1410B-21X-3W-7	1410C-20X-3W-27	197.74	198.07	197.91	C20r	44.86	34.05
B	*S. furcatolithoides* morph. A	1410C-20X-5W-67	1410B-21X-5W-87	201.47	201.54	201.51	C20r	45.01	37.65
B	*Pletolithus gigas*	1410A-20X-CC	1410C-21X-5W- 7	206.21	208.19	207.20	C20r	45.25	43.34
B	*Pletolithus giganteus*	1410B-23X-5W-5	1410A-21X-5W-75	214.95	216.13	215.54	C20r	45.60	51.68
B	*Nannotetrina alata* gr.	1410B-25X-3W-85	1410C-23X-2W- 87	233.53	234.99	234.26	C21n	46.48	15.86
Tc	*Discoaster sublodoensis* (5-rayed)	1410C-23X-6W-87	1410A-23X-1W-7	240.99	242.52	241.76	C21n	46.84	23.36
T	*Pseudotriquetrorhabdulus inversus*	1410A-23X-1W-7	1410A-23X-2W-17	242.52	244.12	243.32	C21n	46.91	24.92
T	*Blackites inflatus*	1410A-23X-2W-17	1410A-23X-3W-26	244.12	245.71	244.92	C21n	46.99	26.52
T	*Discoaster kuepperi*	1410A-23X-4W-39	1410A-23X-5V43	247.34	248.88	248.11	C21n	47.14	29.71
T	*Girgisia gammation*	1410A-23X-6W-13	1410C-24X-3W-130	250.08	251.49	250.79	C21n	47.27	32.39
B	*Nannotetrina cristata*	1410A-23X-6W-13	1410C-24X-3W- 130	250.08	251.49	250.79	C21n	47.27	32.39
B	*Blackites inflatus*	1410A-24X-4W-66	1410C-24X-4W-103	252.35	252.72	252.54	—	*47.35	*0.00
Bc	*Chiphragmalithus*	1410B-26X-3W-119	1410B-26X-4W- 5	256.65	257.01	256.83	—	*47.84	*4.30
Tc	*Discoaster lodoensis*	1410B-26X-5W-107	1410B-26X-5W-148	259.53	259.94	259.74	—	*48.17	*7.21
B	*Pseudotriquetrorhabdulus inversus*	1410B-26X-5W-148	1410C-25X-3W-90	259.94	261.59	260.77	—	*48.29	*8.23
T	*Coccolithus crassus*	1410C-25X-3W-90	1410C-25X-4W-15	261.59	262.34	261.97	—	*48.43	*9.43
Bc	*Discoaster sublodoensis* (5-rayed)	1410B-27X-2W-8	1410C-25X-4W-103	263.21	263.22	263.22	—	*48.57	*10.69
B	*Discoaster sublodoensis* (5-rayed)	1410B-27X-3W-139	1410C-27X-4W-32	266.02	266.45	266.24	—	*48.91	*13.71
T	*Tribrachiathus orthostylus*	1410A-26X-5W-93	1410A-26X-5W-132	279.89	280.28	280.09	—	*50.49	—
B	*Coccolithus crassus*	1410A-26X-6W-92	1410A-26X-CCW-25	281.38	281.91	281.65	—	**50.67	**1.56
turnover	*Toweius/ Dictyococcites* *Reticulofenestra*	1410A-26X-5W-132 1410A-26X-6W-16	1410A-27X-2W-96 1410A-27X-2W-133	280.29 280.62	285.02 285.39	280.45 285.20	—	**47.39 **47.93	**5.12 **0.37

Table 2.1: Position of the principal biohorozons at Site U1410. Biostratigraphic data are tired to magnetostratigraphy (Yamamoto et al., 2018) and calibrated using Geological Time Scale calibration ages (GTS12, Gradstein et al., 2012). Datum ties points used are available Chron boundaries (C21n/C20r; C20r/C20n). Symbol (*) indicates events calibrated using C21r/C21n and symbol (**) events calibrated using the Top of *T. orthostylus* at 50.49 Ma (Agnini et al., 2014 converted to GTS12). Sedimentation rates were assumed to remain constant between ties points.

-The Base of *Pletolithus gigas*

This biohorizon marks the base of Zone CNE10 (Agnini et al., 2014) and Subzone CP13b (Okada and Bukry, 1980). At Site U1410, this event is recorded at 207.20 rmcd, ~20% up in Chron C20r (Figure 2.7). In this study we consistently separate *Pletolithus gigas* (new combination, Chapter 3) from morphotypes with a rotated cross in the central area (*Pletolithus giganteus,* Chapter 3). The presence of *P. giganteus* and intergrading forms below the range of *P. gigas* could make the positioning of the base Subone CP13b or Zone CNE10 potentially problematic (Agnini et al., 2014). Despite the fact that *P. gigas* is usually rare, the biostratigraphic position of this biohorizon is consistent if compared with previous datasets from different settings (Backman, 1986; Agnini et al., 2006; Bernaola et al., 2006; Shamrock et al., 2012; Tori and Monechi, 2013; Agnini et al., 2014). Though, the possible taxonomic issue and the low abundance this biohorizon has a good reliability.

-The Base and Base common of *Sphenolithus furcatolithoides* morphotype A

Here we follow the taxonomic concept of Agnini et al. (2014) who distinguished two morphotype (A and B) within *S. furcatolithoides* based on the different optical behaviour (for details see the original paper). At Site U1410, *S. furcatolithoides* morphotype A shows a stratigraphic distribution within

Subzone CP13b. Specifically, very rare and scattered specimens were observed from 201.51 rmcd (B), but its occurrence becomes more common and continuous only from 197.91 rmcd (Bc) (Figure 2.7). The abundance pattern of *S. furcatholithoides* morphotype A nicely correlates with that observed at Blake Nose, Exmouth Plateau and Agost section suggesting that this is good additional biohorizon.

-The Base of *Sphenolithus cuniculus*

The Base common of *S. cuniculus* is used to define the base of Zone CNE11 (Agnini et al., 2014). At Site U1410, the first occurrence (B) of this species, occurring at 179.21 rmcd, is immediately followed by an increase in abundance (Bc) (178.76 rmcd) so that the B and the Bc of this species are virtually coincident at Site 1410 (Figure 2.7). Conversely, at Site 1051B the B and Bc are found to be spaced but one possible explanation for this apparent incongruency is the presence of transitional forms between these two taxa which suggests a phylogenetical relationship between *S. furcatolithoides* morphotype A e *S. cuniculus* and could have resulted in a different positioning of the biohorizon depending on the taxonomic concept adopted (Agnini et al., 2014; Cappelli et al., in prep)

-**The Base common of *S. furcatolithoides* morphotype B**

At Site 1410, the Base common of *S. furcatolithoides* morphotype B was observed at 165.42 rmcd (Figure 2.7). Below its presence is rare and spotty throughout the middle part of the range of *S. cuniculus.* Though there is only one datum available for the abundance pattern of *S. furcatolithoides* morphotype B from Site 1051 (Agnini et al., 2014), these data are very consistent and suggest that the Base common of *S. furcatolithoides* morphotype B could be used as additional biohorizon.

-**The Top of *Pletolithus gigas***

This biohorizon marks the base of Zone CNE12 (Agnini et al., 2014) and Subzone CP13b (Okada and Bukry, 1980). At Site U1410, the position of this zonal boundary is difficult to recognise because the index species displayed a very sporadic distribution in the final part of its stratigraphic distribution from 170.42 rmcd to 165.42 rmcd where the last specimen has been observed (Figure 2.7). Compared with the abundance pattern of *Pletolithus gigas* at Site 1051 (Agnini et al., 2014), the two datasets display a very similar trend but different absolute abundances, in particular *P. gigas* is exceedingly rare at Site U1410 so that the Top common of *P. gigas* at Site 1051 may correlate with the Top of this taxon at Site U1410 (Figure 2.7). However, it should be noted that at Site 527 *P. gigas* displays a different pattern with sharper decline in abundance (Backman, 1986).

With respect to magnetostratigraphy, the Top of *P. gigas* is consistently observed in the upper part of Chron C20r in open ocean sites (Site 527, Site 1051; Backman, 1986; Agnini et al 2014), the only

exception is the datum from Agost (Spain) where it lies in the middle part of Chron C20n. A possible explanation for this inconsistency, especially considering the different depositional setting, is that the tail of distribution of this taxon is not reliable for the presence of reworked specimens that have moved the biohorizon higher up. All this considered, the Top of *P. gigas* is not recognised as an ideal biohorizon, however the presence of additional biohorizons such as (Top of *S. cuniculus* and Base common of *S. furcatolithoides* morphotype B) may represent important additional data in order to provide the best biostratigraphic framework.

-The Top of *Blackites gladius*

The Top of *B. gladius* defines the base of Zone NP15 (Martini et al., 1971). Traditionally, the position of this biohorizon was approximated by the Top of *N. alata* gr. (Martini et al., 1971), as a consequence the base on Zone NP15 should correlates with the base of Subzone CP13c (Okada and Bukry, 1980; Perch-Nilesen, 1985; Martini and Müller, 1986). However, it is now well documented that the range of *B. gladius* extends significantly above the base of Subzone CP13c (Berggren and Aubry, 1984; Wei and Wise, 1989), up into Zones NP16 and NP17 (Bown, 2005a). Problems related to the position of this biohorizon are likely due to the fact that this taxon is very rare or absent in multiple settings (Martini and Müller, 1986; Shamrock and Watkins, 2012). At Site U1410, the sporadic presence of this taxon prevents any reliable recognition of this biohorizon (Figure 2.7).

-The Base and Base common of *Reticulofenstra umbilicus*

The Base of *R. umbilicus* marks the base of Subzone CP14a (Okada and Bukry, 1980). At Site U1410, we documented the sporadic occurrence of *R. umbilicus* throughout the range of *P. gigas* (Figure 2.7). This observation is consistent with a number of other datasets in which the simultaneous presence of *R. umbilicus* and *P. gigas* was reported (Applegate and Wise, 1987; Wei and Wise, 1989; Fornaciari et al., 2010; Shamrock and Watkins, 2012; Agnini et al., 2014). The co-existence of these two taxa represents an important drawback but the absence of alternative biohorizons in this interval has obligated biostratigraphers to use this event anyway. This choice was eventually made also taking into account that in almost all of the study cases the presence of *R. umbilicus* is discontinuous in the lower part of its range. This is not the case for the abundance of *R. umbilicus* higher up when this taxon becomes common. The Bc of *R. umbilicus* defines the base of Zone CNE13 (Agnini et al., 2014) but we have only documented a sporadic occurrence of this taxon with simultaneous presence of *P. gigas.* This indicates that the top of the section belongs to Zone CNE12.

-The Base of *Discoaster bifax*

In the CP zonal scheme, the Base of *D. bifax* and the Base of *R. umbilicus* are used to mark the base of Subzone CP14a (Okada and Bukry, 1980). At Site U1410 as well as in other areas (Shamrock and Watkins, 2012; Tori and Monechi, 2013; Agnini et al., 2014), rare specimens of *D. bifax* occurs significantly below the Top of *P. gigas*, suggesting that this biohorizon is problematic and, if used, it will invalidate the biozonal scheme (Figure 2.7).

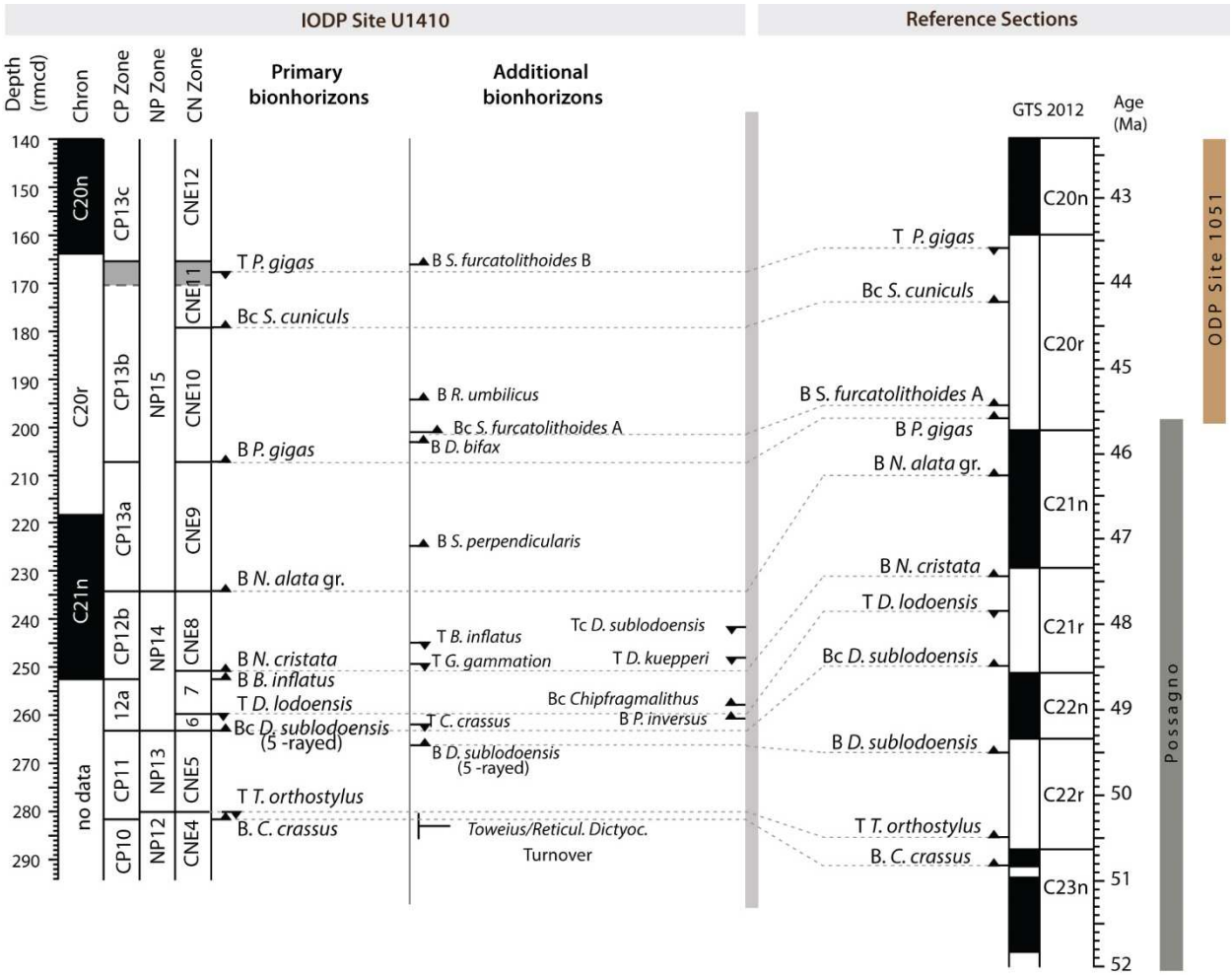

Figure 2.5*:* Principal calcareous nannofossil events from Site U140 reported against ages of primary events recognized in the reference sections of Possagno and ODP Site 1051 (Agnini et al., 2014). Ages of events have been converted to GTS 2012. To the left magnetostratigraphy (Yamamoto, 2018) and calcareous nannofossil biostratigraphy: NP Zone (Martini; 1971) CP Zone (Okada and Bukry, 1980); CNE Zone (Agnini et al., 2014).

2.5 DISCUSSION

2.5.1 Major changes in the calcareous nannofossil record

The study interval represents the time of the onset of an irreversible readjustment of nannoplankton assemblages. The appearance and expansion of the very successful *Noelaerhabdaceae* through the early-middle Eocene is the first step on the way to the dominance of this family in the modern ocean

(*Gephyrocapsa* and *Emiliana*). Calcareous nannofossil data from Site U1410 allow us to analyse in detail the dynamics of the assemblages during the initial phase in the evolution of *Noelaerhabdaceae*. The PCA performed on assemblage data highlighted the main role played by the entry of this taxonomic group in shaping the assemblages. Indeed, *Reticulofenestra* and *Dictyococcites* have the most meaningful loading taxa on PC1 and PC2 factors, respectively.

The PC1 loadings on assemblage data grouped together taxa that show similar trends during the early-middle Eocene transition. PC1 loadings are positive for those taxa that decrease markedly or goes extinct (*Zygrhablithus, Discoaster, Sphenolithus, Toweius)*, whereas taxa with negative loadings increase significantly *(Reticulofenestra)* (Figure 2.9). The pattern of the PC1 curve is broadly mirrored by the abundance trend of *Reticulofenestra* and, by lesser extent, of *Zygrhablithus.* Two abrupt negative shifts mark the decreasing long-term trend of PC1.

The first one occurs just above the climax of the EECO and coincides with the continuous and common entry of the genus *Reticulofestra*. After this first step, *Reticulofenestra* continues to progressively increase up to the early middle Eocene boundary where this group displays a second shift toward higher abundances. From this step upward, the assemblage remains relatively constant and a new "steady state" was reached, which lasted for the rest of the study interval and is characterized by very high and relatively constant percentages of *Reticulofenestra*. At the same level where the reticulofenestrids reached their new steady state, the abundance of the holococcolith *Zygrhablithus* underwent a significant drop in abundance and never recovered to the abundance of the early Eocene. The abundance of *Zygrhablithus* in the fossil record is generally thought to be strongly affected by preservation. The delicate structure of holococcoliths, which consist of minute and equidimensional calcite crystallites, in principal makes *Zygrhablithus* vulnerable to dissolution, but in sediments rich in $CaCO_3$ their crystalline structure is prone to serve as centres for calcite overgrowth (Wind and Wise, 1978; Bown et al., 2008; Jang and Wise, 2009).

At Site U1410, it is likely that there is no systematic alteration of *Zygrhablithus* abundance; either in nannofossil chalk, where early calcite overgrowth protects specimens of *Zygrhablithus*, or in clay-rich sediments, where the effects of dissolution are minimal.

The general shift in the relative abundance of the two major components of the assemblage largely explains the PC1 trend, but the statistical analysis does not highlight the main factor that controls these variations through time. Indeed, the PC1 factors does not show correlation with stable isotope values, which are considered as proxies for environmental changes. This is not unexpected since the variations in the general assemblage composition are considerable, whereas the isotope values show only minor fluctuations.

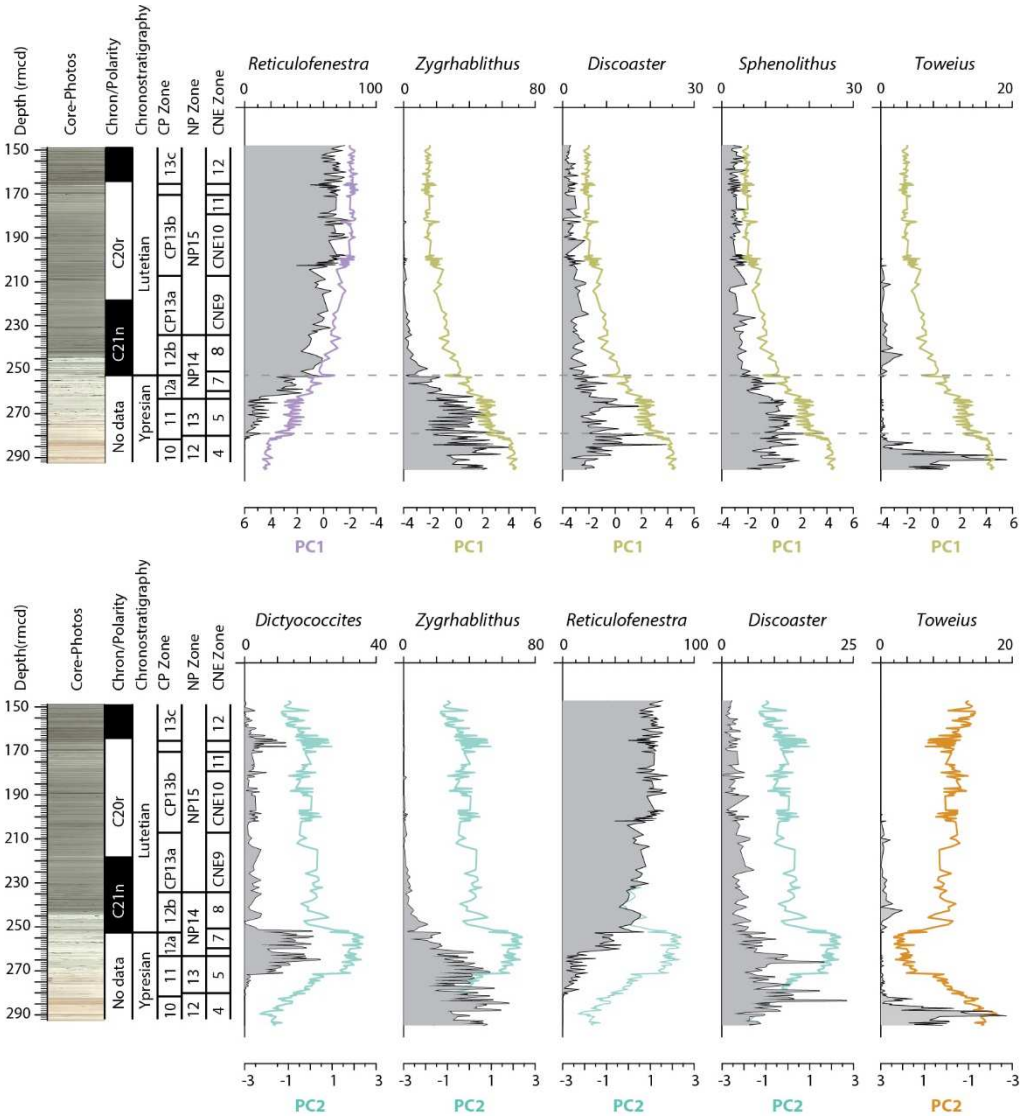

Figure 2.6*:* Comparison of PC1 and PC2 with the relative abundance trends of the strongest loadings taxa. Dashed lines highlight two shifts in the PC1 trend. To the left Core images, chronostratigraphy, magnetostratigraphy (Yamamoto et al., 2018) and calcareous nannofossil biostratigraphy: NP Zone (Martini; 1971), CP Zone (Okada and Bukry, 1980), CNE Zone (Agnini et al., 2014).

The PC2 mostly represents fluctuations of *Dictyococcites.* This genus shows a distinctive abundance trend, showing relatively high abundance in the early Eocene, but it is rare throughout the middle Eocene. *Reticulofenestra* and *Dictyococcites* are strictly morphologically related and therefore it could be hypothesized that they shared similar ecological preferences or thrived in the same ecological niche. The abrupt decline of *Dictyococcites* at the Ypresian- Lutetian boundary may reflect an ecological competition with the more opportunistic *Reticulofenestra,* which was probably able to tolerate easily the abiotic changes taking place in the surface water structure. The drop of *Dictyococcites* may have provided a further competitive advantage for *Reticulofenestra,* which eventually dominates the assemblages of the middle Eocene.

2.5.2 Calcareous nannofossil assemblages and the paleoecological evolution

Studies of modern coccolithophore populations suggest that changes in the assemblage composition is mainly controlled by the thermal and nutrient structure of surface waters (Okada and Honjo, 1973; Winter et al., 1994; Gibbs et al., 2006). In general, highly eutrophic environments favor low diversity assemblages with meso/eutrophic taxa that usually thrive under extreme competition. On the contrary, stable and oligotrophic environments facilitate the spreading of species that are able to outcompete other taxa either with high speciation or habitat partitioning. Pioneering studies on the biogeography of Paleogene nannofossil assemblages have highlighted that numerous taxa displayed a clear preference for specific temperature and fertility conditions (Haq and Lohmann, 1976, Wei and Wise, 1990; Aubry, 1992; 1998). Calcareous nannofossil assemblage data have been commonly used in the past to provide clues of surface waters environmental conditions, this potential has proved to be useful especially during dramatic climate events occurred during the Paleogene. In the last decades, the paleoecological affinities of the different taxa have tested comparing nannofossil data with other biotic and geochemical proxies. This approach has allowed to improve our understanding of the paleoecological behaviour of the single taxa, their ecological affinity and response to changes in paleoenviromental conditions (Bralower, 2002; Agnini et al., 2007; Villa et al., 2008).

Although the potential of nannofossils in paleoecological reconstructions has been largely recognized by the scientific community, there is still a bit of uncertainty especially when considering extinct taxa. The main limit possibly affecting the Paleogene calcareous nannofossils is that many taxa are extinct so that very little is known about their life strategies. From the literature, we know that life cycles of modern coccolithophores are extremely complicated, being characterized by two phases in which the organism secretes different platelets (coccoliths, holococcoliths, nannoliths, etc) that seems to be produced under different ecological conditions (Billard and Innouye, 2004; Young and Henriksen, 2003; Young et al., 2005). Unfortunately, direct evidences that this was the case also in the past does not exist so that the hypothesis of analogous life cycles is something that we can just infer (Agnini et al., 2016). A second important factor to take into account is the sensitivity of nannoplankton to changes in environmental parameters. In general, calcareous nannoplankton seems to be more resilient to surface water perturbations so that their response to changes is subdued compared to other plankton groups (Newsam et al., 2017). Even more difficult to explain is that some taxa apparently show similar behaviours in different paleoenvironmental situations (Villa et al., 2008; Bown and Pearson, 2009; Schneider et al., 2013). Even if we would able to exclude all the biases related to the above mentioned issues a doubt still would remain on the influence that the different factors have on species behaviour, which may be controlled by ecological (disease, predation, and competition) but also environmental factors (Bralower et al., 2002). Even considering the possible limits, calcareous

nannoplankton still remain one of the most important tool for paleoclimatic/paleoceanographic reconstructions.

Over the past years, numerous studies have been focused on calcareous nannofossil response to rapid and extreme climate changes. Calcareous nannofossils showed modifications in the relative abundance of taxa but little or no significant evolutionary changes during some of the minor events occurred during the early Paleogene such as the early Eocene hyperthermals ETM2 or ETM3 (Agnini et al, 2009; Gibbs et al., 2012). However, more prominent events (,e.g., PETM, EECO, MECO and EOT) are associated with significant changes in the assemblage composition, with the appearance of short-lived excursion taxa and/or high evolutionary rates (e.g., Agnini et al., 2007, Bralower, 2002, Gibbs et al., 2006). Few high-resolution studies have focused on the effect of the long-term component of Eocene climate on nannoplankton assemblages (Agnini et al., 2006; Gibbs et al., 2012; Schneider et al., 2011; Shamrock and Watkins 2012, Villa et al., 2018, 2014). Agnini et al. (2006) proposed that either the decrease in temperature or the sharp increase in nutrient availability or the two together are the ecological parameters controlling the nannoplankton evolution during the early-middle Eocene. More recently, Schneider et al. (2011) also suggested that water-column destratification and increased nutrient supply to surface waters in the aftermath of the EECO were the main factors influencing the global expansion of *Reticulofenestra.*

The long-term changes occurred during the early-middle Eocene are documented in the highly resolved dataset from Site U1410, which integrates geochemical proxies with nannofossil data. The bulk isotope composition of carbonates analysed at Site U1410 records the evolution of the sea surface conditions as documented by calcareous nannofossils and thus the comparison of the two datasets are of particular interest if we want shed light on the relationship between the organic evolution and the changes in the abiotic environment. In the study interval, the $\delta^{18}O$ data is used as a proxy of sea surface water temperatures, whereas the $\delta^{13}C$ record is a more complicated proxy being controlled by the global carbon cycle and in particular by many processes/mechanisms such as for instance the exchanges among different carbon reservoirs, the enhancement or decrease of the intensity of the biological pump and the red/ox conditions at the sea floor.

Based on trends and changes observed in PaleoEnvironmental Index, the study succession can be subdivided in three distinctive intervals: 1) a lower part of the succession where warm / oligotropchic taxa prevail, 2) a middle part with transitional characters and 3) the upper part with temperate/ mesotrophic taxa dominate the assemblages (Figure 2.5).

The early Eocene instability phase (from the base to 266.45rmcd)

During this interval, the PEI evidences for a general sustained warm-water and oligotrophic conditions, although significant fluctuations, documented by the high standard deviation, suggest a large instability of the environmental. This is confirmed by the $\delta^{18}O$ profile that shows relatively high values across this interval, which is characterized by multiple short-term high amplitude fluctuations (Figure 2.5). In the same interval, several transient negative excursions that might relate to global CIEs (Sexton et al., 2011; Turner et al., 2014; Slotnick et al. 2012, 2015a, b; Luciani et al., 2016, 2018; Westerhold et al., 2017, 2018) punctuate the long-term $\delta^{13}C$ trend. Comparing the two datasets, the most prominent feature of this interval is an extreme variability of both the biotic and geochemical records, with the background warm-oligotrophic conditions interrupted by relatively more temperate and eutrophic intervals. During this first interval, the pattern of the PEI is shaped by the abundance of *Discoaster* and mainly by *D. kuepperi,* which flourished during the climax of the EECO. Assemblage data from Site U1410 indicate that warm/ oligotrophic conditions persist up to the upper part of Zone CNE5 (Figure 2.5), which perfectly fits with the position recently proposed for the end of EECO (Luciani et al., 2016); although the mode and tempo of the transition from the extreme conditions of the EECO and the onset of the long-term cooling trend are still poorly constrained.

The late early Eocene transitional phase (from 266.45rmcd to 252.54rmcd)

In this interval, the PEI significantly increases and this is the result of a permanent change in the assemblage composition, in fact the warm/ oligotrophic taxa undergo a progressive decline, whereas the temperate/mesotrophic group increases in its relative abundance (Figure 2.5). From the geochemical point of view, the base of this interval is marked by a positive step in $\delta^{18}O$, whereas $\delta^{13}C$ displays relatively high values. The relatively small magnitude of isotope shift in $\delta^{18}O$ corresponds to a shift in the PEI, which corroborates the idea that calcareous nannofossil data and geochemical proxies are interconnected (Figure 2.5). The unexpected high sensitivity shown by nannoplankton to changes in abiotic parameters is likely related the fact that the extreme background conditions of the EECO were close to a threshold in the climate dynamics that was suddenly passed and results in significant changes in the calcareous nannofossil assemblages. This is especially true for those taxa that are better adapted to the extreme warm and oligotrophic and warm conditions characterizing the EECO. *Discoaster, Sphenolithus, Zygrhablithus* are indeed interpreted as *K*-specialist taxa (Haq and Lohmann, 1976; Backman, 1986; Wei and Wise, 1990; Bralower, 2002; Gibbs et al., 2006; Agnini et al., 2007a) with low tolerance to changes in ecological and environmental conditions. However, small but prolonged changes in thermal structure and, to lesser degree in nutrient distribution of water column, might have affected this very specialized ecological niches, causing a contraction of the

vulnerable *K*-specialist communities and simultaneous expansion of the more opportunist *Reticulofenestra*.

The middle Eocene stability phase (from 252.54rmcd to the top of the study interval)
At Site U1410 highly temperate and mesotrophic assemblages were already established by the late Ypresian, with warm water-oligotrophic taxa representing less than 20% of the assemblages (Figure 2.5). The plot showing the semi-quantitative abundances indicates that the decline of warm waters oligotrophic favouring group progressively continues through this interval. Both $\delta^{18}O$ and $\delta^{13}C$ patterns suggest a general trend towards cooler and more eutrophic conditions. However, the stability observed in the PEI values is not completely reflected in the stable isotope trends that shows in the basal part of this interval distinctive perturbations, although of small magnitudes. A simple explanation for this observation is that the presumed environmental perturbation did not pass the threshold required to determine a significant signal in the general composition of nannofossil assemblages.

2.5.3 The record of Site U1410 in a global paleoclimatic perspective

Based on high-resolution stable isotope benthic records from Atlantic and Pacific ODP Sites (1258, 1262, 1209), recent studies covering the late Ypresian-early Lutetian interval have highlighted a number of critical steps in the climate evolution: the prolonged phase of low$\delta^{18}O$ values lying within the Chron C23n, the onset of the global cooling close to C22n/C22r boundary and two warming reversals within Chron C21n (Figure 2.10) (Westerhold et al., 2018). Overall, the stable isotope records documented at Site U1410 show a trend that well correlates with the most recent global deep-sea sites compilation (Westerhold et al., 2017, 2018). At Site U1410, one of the most distinctive feature of the stable isotope records is represented by the decline of the $\delta^{13}C$ associated with a negative trend in $\delta^{18}O$ values just above the Ypresian-Lutetian boundary (253.49-241.98rmcd). This interval coincides with prominent variations in the $CaCO_3$ curve suggesting that significant changes in the sediment compositions occurred before the onset of the drift sedimentation and can be tentatively correlated with the warming event observed in a consistent position at Site 1209 (Westerhold et al., 2018). During this relatively short-lived event the nannofossil assemblages does not exhibit any significant variation, the only exception is the peak in abundance of *D. subolodoensis* which can be interpreted as a potential response to enhanced warm / oligotrophic conditions occurred during this interval (Figure 2.10).
Interestingly, previous data from the Gorrondatxe section, which host the GGSP for the base of Lutetian, reported the presence of a possible hyperthermal event close to the Ypresian-Lutetian

boundary (Payros et al., 2012; Intxauspe-Zubiaurre et al., 2017a, b). At Gorrondatxe, diagnostic features for this event are the decline in both bulk and benthic foraminiferal $\delta^{13}C$ values, a distinct deterioration in foraminiferal preservation and high abundances of warm planktonic foraminiferal taxa and opportunist benthic foraminifera (Payros et al., 2012). Calcareous nannofossils were also be analysed but no significant changes have been observed in the composition of autochthonous calcareous nannofossil assemblages (Intxauspe-Zubiaurre et al., 2017a, b). Although the isotope excursions occur above the Bases of *B. inflatus* and *N. cristata* both at Site U1410 and at Gorrondatxe (Figure 2.9), inconsistence in the position of this event with respect to bio-magnetostratigraphy call into question that they represent the same global event. Previous studies have suggested a correlation between the event observed at Gorrondatxe and last transient CIE recognized in the long series of early Eocene hyperthermal events (C21RH6 in Sexton et al., 2011 or in C21rH5 Tuner et al., 2014 and Westerhold et al. 2017, 2018), but also this interpretation is not supported by new bio-magnetostratigraphic data from deep-sea Atlantic sites (Westerhold et al., 2017).

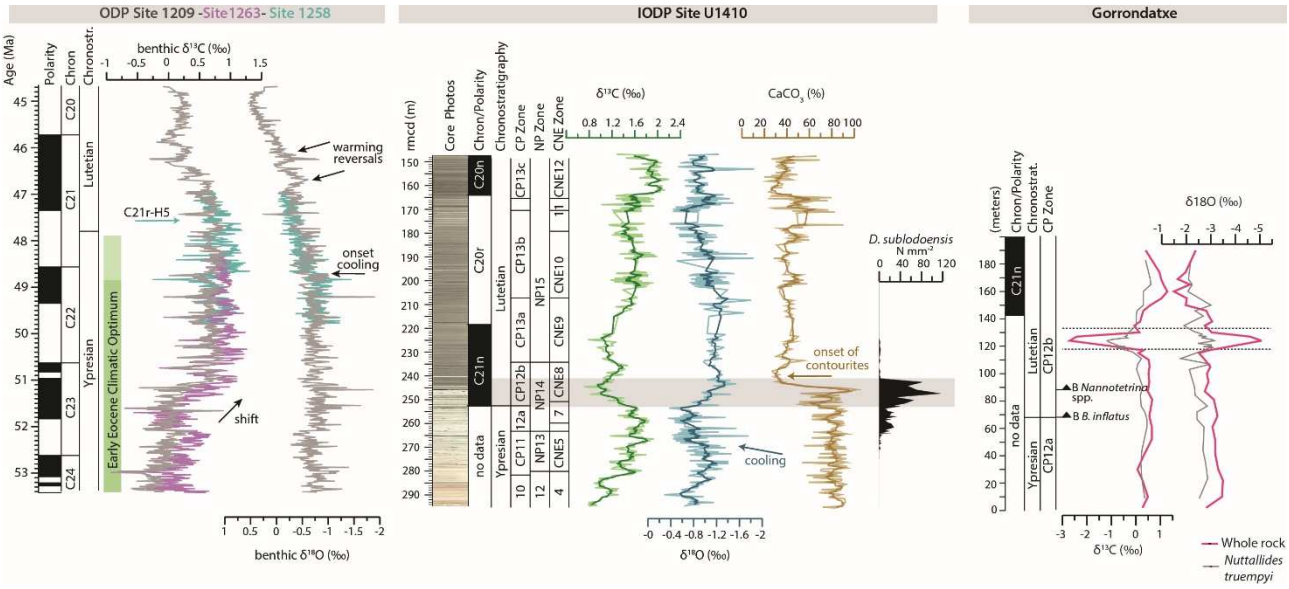

Figure 2.7*:* Overview of geochemical data spanning from the late early Eocene to the early middle Eocene. From the left to the right: Atlantic and Pacific benthic stable isotope composite from 44.68 to 53.4 Ma (Westerhold et al., 2018, converted to GTS 2012), IODP SiteU1410 stable isotope and carbonate records from bulk sediments are plotted against magnetostratigraphy and biostratigraphy. The grey band indicates the interval that might correspond to the warming reversal observed in the benthic isotope records at Site 1209 (Westerhold et al., 2018). The abundance pattern of *Discoaster sublodoensis*, which shows a peak in abundance across this interval is also shown. To the right the carbon and oxygen isotope perturbation at the C21r/C21n transition observed at Gorrondatxe (Payros et al., 2012). The onset of this isotope excursion was correlated with the C21r-H5 event, which was originally described at Site 1258 (Sexton et al., 2011).

2.6 SUMMARY AND CONCLUSION

Site U1410 (Southeast Newfoundland Ridge) represents the first continuous sedimentary record in the North Atlantic basin across the early-middle Eocene transition, which is marked at this location by a prominent change in the sedimentary regime related to the onset of drift sedimentation. This study is focused on calcareous nannofossil biostratigraphy and assemblage fluctuations over ~7 million year interval, spanning from the last part of the EECO to the following early phase of global cooling. Quantitative evaluation of abundance patterns of selected species, which include both standard markers and promising additional taxa, allow us to generate a detailed biostratigraphic framework on this time interval. Our results confirm the complex picture of the early-middle Eocene biostratigraphy (Agnini et al., 2014). Several taxa show a tail of strongly reduced presence below-above their first-last consistent occurrence (*D. lodoensis, D. sublodoensis, P. gigas, R. umbilicus*) or are consistently rare or absent in specific settings *(B. inflatus, N. cristata, N. alata* gr.*, P. gigas*). A further complication is related to the ambiguous taxonomy of some taxa that could affect indirectly the reliability some biohorizons. Finally, the virtual lack of highly resolved datasets during this time interval makes biostratigraphic correlations between different sections highly inaccurate.

Assemblage data indicate that early Eocene nannoplankton assemblages substantially differ from middle Eocene assemblages. This difference is mainly related to the gradual expansion of *Reticulofenestra* associated with a progressive decline of the taxa (*Toweius, Zyghrablithus, Discoaster* and *Sphenolithus)* that dominate during the Early Eocene Climatic Optimum. Changes in assemblage composition from Site U140 have been interpreted also in terms of paleoecological changes and compared with the bulk $\delta^{13}C$ and $\delta^{18}O$ stable isotope records. The decline of warm-oligotrophic *Zyghrablithus, Discoaster, Sphenolithus* coincides with a shift towards slightly cooler and progressively more eutrophic conditions. This important change in the assemblage is though to reflect a reduction of the optimal habitat space for warm/oligotrophic that have eventually favoured the expansion of the cosmopolitan *Reticulofenestra.* In middle Eocene the composition of the assemblages remain, consistently dominated by *Reticulofenestra* but the stable isotope profile indicates the occurrence of a transient reversal in the long-term cooling trend that is possibly testify by the sharp peak in abundance of *D. sublodoensis*. Recent dataset have evidence for the the existence of a transient warming episode close the early-middle Eocene boundary (Payros et al., 2012, Intxauspe-Zubiaurre et al., 2017a,b; Westerhold et al., 2018), but its correlation worldwide is still a matter of debate. In fact, it is becoming incresinglly clear that climate and carbon cycle dynamics during the initial phase of the post-EECO long-term cooling might have been more complicated than originally thought, and further datasets are thus required to better constrain this crucial time interval.

REFERENCES

Agnini, C., Muttoni, G., Kent, D. V., & Rio, D. (2006). Eocene biostratigraphy and magnetic stratigraphy from Possagno, Italy: The calcareous nannofossil response to climate variability. *Earth and Planetary Science Letters*, 241(3-4), 815-830. https://doi.org/10.1016/j.epsl.2005.11.00

Agnini, C., Fornaciari, E., Rio, D., Tateo, F., Backman, J., & Giusberti, L. (2007). Responses of calcareous nannofossil assemblages, mineralogy and geochemistry to the environmental perturbations across the Paleocene/Eocene boundary in the Venetian pre-alps. *Marine Micropaleontology,* 63(1-2), 19-38. https://doi.org/10.1016/j.marmicro.2006.10.002

Agnini, C., Macri, P., Backman, J., Brinkhuis, H., Fornaciari, E., Giusberti, L., Speranza, F. (2009). An early Eocene carbon cycle perturbation at ~52.5 ma in the Southern Alps: Chronology and biotic response. *Paleoceanography*, 24(2) https://doi.org/10.1029/2008PA001649

Agnini, C., Fornaciari, E., Raffi, I., Catanzariti, R., Pälike, H., Backman, J., & Rio, D. (2014). Biozonation and biochronology of Paleogene calcareous nannofossils from low and middle latitudes. *Newsletters on Stratigraphy,* 47(2), 131-181. https://doi.org/10.1127/0078-0421/2014/004

Agnini, C., Spofforth, D. J. A., Dickens, G. R., Rio, D., Pälike, H., Backman, J., Muttoni, G., Dallanave, E. (2016). Stable isotope and calcareous nannofossil assemblage record of the late Paleocene and early Eocene (Cicogna Section). *Climate of the Past, 12*(4), 883-909. https://doi.org/10.5194/cp-12-883-2016

Agnini, C., Monechi, S., & Raffi, I. (2017). Calcareous nannofossil biostratigraphy: Historical background and application in Cenozoic chronostratigraphy. *Lethaia,* 50(3), 447-463. https://doi.org/10.1111/let.12218

Anagnostou, E., John, E. H., Edgar, K. M., Foster, G. L., Ridgwell, A., Inglis, G. N., Pearson, P. N. (2016). Changing atmospheric CO_2 concentration was the primary driver of early Cenozoic climate. *Nature, 533*, 380-384. https://doi.org/10.1038/nature17423

Applegate, J.L., and Wise, S.W., Jr., (1987). Eocene calcareous nannofossils, Deep Sea Drilling Project Site 605, upper continental rise off New Jersey U.S.A. *In* van Hinte, J.E., Wise, S.W., Jr., et al., *Init. Repts. DSDP,* 93: Washington (U.S. Govt. Printing Office), 685-698

Aubry, M.-P. (1984). Handbook of Cenozoic Calcareous Nannoplankton, book 1, Ortholithae (Discoaster). *Am. Mus. Nat. Hist. Micropaleontol. Press*, New York, 1–263.

Aubry, M.-P. (1988). Handbook of Cenozoic Calcareous Nannoplankton book 2, Ortholithae (Holococcoliths, Ceratoliths, Ortholiths and Other. *Am. Mus. Nat. Hist. Micropaleontol. Press*, New York, 1–279.

Aubry, M.P. (1988). Handbook of Cenozoic Calcareous Nannoplankton, book 3, Ortholithae (Pentaliths and Other), Heliolithae (Fasciculiths, Sphenoliths and Other (1989) *Am. Mus. Nat. Hist. Micropaleontol. Press*, New York, 1–279.

Aubry, M.P. (1990). Handbook of Cenozoic Calcareous Nannoplankton, book 4, Heliolithae (Helicoliths, Cribriliths, Lopadoliths and Other. Am. Mus. Nat. Hist. Micropaleontol. Press, New York, 1–381.

Aubry, M.-P. (1992). Late Paleogene calcareous nannoplankton evolution: a tale of climatic deterioration, in: Prothero, D.R., Berggren, W.A. (Eds.), Eocene- Oligocene Climatic and Biotic Evolution. Princeton *University Press, Princeton*, pp. 272–309

Aubry, M.P.(1999). Handbook of Cenozoic Calcareous Nannoplankton, book 5, Heliolithae (Zygoliths and Rhabdoliths, *Am. Mus. Nat. Hist. Micropaleontol. Press*, *New York*, 1–368.

Aubry, M.P. (1998). Early Paleogene calcareous nannoplankton evolution: a tale of climatic amelioration, in: Late Paleocene–early Eocene Biotic and Climatic Events in the Marine and Terrestrial Records, *Columbia University Press, New York*, 158–201.

Aubry, M.P. (1995). From chronology to stratigraphy: interpreting the Lower and Middle Eocene stratigraphic record in the Atlantic Ocean. *SEPM Spec. Publ*. 54, 213–274.

Backman, J., & Shackleton, N. J. (1983). Quantitative biochronology of Pliocene and early Pleistocene calcareous nannofossils from the Atlantic, Indian and Pacific Oceans. Marine *Micropaleontology*, 8(2), 141-170. https://doi.org/10.1016/0377-8398(83)90009-9

Backman, J. (1986). Late Paleocene to middle Eocene calcareous nannofossil biochronology from the Shatsky Rise, Walvis Ridge and Italy. *Palaeogeography, Palaeoclimatology, Palaeoecology, 57*(1), 43-59. https://doi.org/10.1016/0031-0182(86)90005-2

Backman, J., Raffi, I., Rio, D., Fornaciari, E., & Pälike, H. (2012). Biozonation and biochronology of Miocene through Pleistocene calcareous nannofossils from low and middle latitudes. *Newsletters on Stratigraphy*, 45(3), 221-244. https://doi.org/10.1127/0078-0421/2012/0022

Beerling, D. J., & Royer, D. L. (2011). Convergent Cenozoic CO_2 history. *Nature Geoscience, 4*(7), 418-420. https://doi.org/10.1038/ngeo118

Bernaola, G., Orue-Etxebarria, X., Payros, A., Dinarès-Turell, J., Tosquella, J., Apellaniz, E., & Caballero, F. (2006). Biomagnetostratigraphic analysis of the Gorrondatxe section (Basque Country, Western Pyrenees): Its significance for the definition of the Ypresian/Lutetian boundary stratotype. *Neues Jahrbuch Fur Geologie Und Palaontologie - Abhandlungen, 241*(1), 67-109

Bijl, P. K., Schouten, S., Sluijs, A., Reichart, G. -.J, Zachos, J. C., & Brinkhuis, H. (2009). Early Palaeogene temperature evolution of the southwest Pacific Ocean. *Nature*, 461(7265), 776-779. https://doi.org/10.1038/nature08399

Bijl, P. K., Bendle, J. A. P., Bohaty, S. M., Pross, J., Schouten, S., Tauxe, L., Brinkhuis, H. (2013). Eocene cooling linked to early flow across the Tasmanian gateway. *Proceedings of the National Academy of Sciences of the United States of America*, 110(24), 9645-9650. https://doi.org/10.1073/pnas.1220872110

Billard, C. and Innouye, I. (2004). What is new in coccolithophore biology? in: *Coccolithophores – From Molecular Processes to Global Impact*, Springer, Berlin, 1–29, 2004

Boulila, S., Vahlenkamp, M., De Vleeschouwer, D., Laskar, J., Yamamoto, Y., Pälike, H., Röhl, U. (2018). Towards a robust and consistent middle Eocene astronomical timescale. *Earth and Planetary Science Letters,* 486, 94-107. https://doi.org/10.1016/j.epsl.2018.01.00

Boyle, P. R., Romans, B. W., Tucholke, B. E., Norris, R. D., Swift, S. A., & Sexton, P. F. (2017). Cenozoic North Atlantic deep circulation history recorded in contourite drifts, offshore Newfoundland, Canada. *Marine Geology*, 385, 185-203. https://doi.org/10.1016/j.margeo.2016.12.01

Bown, P. R., Young, J. R. (1998). Techniques. In: Bown, P. R., (Ed.), Calcareous Nannofossil Biostratigraphy. Kluwer Academic Publishers, p. 16–28

Bown, P.R., Lees, J.A., Young, J.R., (2004). Calcareous nannofossil evolution and diversity through time, in: Thierstein, H.R., Young, J.R. (Eds.), *Coccolithophores: From Molecular Processes to Global Impact*. Springer-Verlag, pp. 481–508.

Bown, P.R. (2005a): Palaeogene calcareous nannofossils from the Kilwa and Lindi areas of coastal Tanzania (Tanzania Drilling Project 2003-4). *Journal of Nannoplankton Research*, 27(1), 21-95.

Bown, P. R. (2005b). Calcareous nannoplankton evolution: A tale of two oceans. *Micropaleontology, 51*(4), 299-308. https://doi.org/10.2113/gsmicropal.51.4.299

Bown, P.R. & Dunkley Jones, T. (2006). New Palaeogene calcareous nannofossil taxa from coastal Tanzania: Tanzania Drilling Project Sites 11 to 14. *Journal of Nannoplankton Research*, 28(1), 17-34

Bown, P. R., Jones, T. D., Lees, J. A., Randell, R. D., Mizzi, J. A., Pearson, P. N., Wade, B. S. (2008). A Paleogene calcareous microfossil Konservat-Lagerstätte from the Kilwa Group of coastal Tanzania. *Bulletin of the Geological Society of America*, 120(1-2), 3-12. https://doi.org/10.1130/B26261

Bown, P., & Pearson, P. (2009). Calcareous plankton evolution and the Paleocene-Eocene thermal maximum event: New evidence from Tanzania. *Marine Micropaleontology,* 71(1-2), 60-70. https://doi.org/10.1016/j.marmicro.2009.01.005

Bown, P.R. & Dunkley Jones, T. (2012). Calcareous nannofossils from the Paleogene equatorial Pacific (IODP Expedition 320 Sites U1331-1334). *Journal of Nannoplankton Research*, 32(2), 3-51.

Bown, P.R. & Newsam, C. (2017). Calcareous nannofossils from the Eocene North Atlantic Ocean (IODP Expedition 342 Sites U1403–1411). *Journal of Nannoplankton Research*,37(1), 25-60.

Bralower, T. J. (2002). Evidence of surface water oligotrophy during the Paleocene-Eocene Thermal Maximum: Nannofossil assemblage data from Ocean Drilling Program Site 690, Maud Rise, Weddell Sea. *Paleoceanography*, 17(2), 13-1

Coxall, H.K., Pearson, P.N. (2007). The Eocene-Oligocene transition, in: Williams, M., Hayward, A., Gregory, J., Schmidt, D.N. (Eds.), Deep Time Perspectives on Climate Change: Marrying the Signal from Computer Models and Biological Proxies. *Geological Society Special Publication*, pp. 351–387.

Coxall, H. K., Huck, C. E., Huber, M., Lear, C. H., Legarda-Lisarri, A., O'Regan, M., Backman, J. (2018). Export of nutrient rich northern component water preceded early Oligocene Antarctic glaciation. *Nature Geoscienc*e, 11(3), 190-196. https://doi.org/10.1038/s41561-018-0069-9

Cramer, B. S., Wright, J. D., Kent, D. V., & Aubry, M.P. (2003). Orbital climate forcing of $\delta^{13}C$ excursions in the late Paleocene-early Eocene (Chrons C24n-C25n). *Paleoceanography*, 18(4) https://doi.org/10.1029/2003PA000909

Cramwinckel, M. J., Huber, M., Kocken, I. J., Agnini, C., Bijl, P. K., Bohaty, S. M., Sluijs, A. (2018). Synchronous tropical and polar temperature evolution in the Eocene letter. *Nature,* 559(7714), 382-386. https://doi.org/10.1038/s41586-018-0272-2

Dallanave, E., Bachtadse, V., Crouch, E. M., Tauxe, L., Shepherd, C. L., Morgans, H. E. G., Sugisaki, S. (2016). Constraining early to middle Eocene climate evolution of the Southwest Pacific and Southern Ocean. *Earth and Planetary Science Letters,* 433, 380-392. https://doi.org/10.1016/j.epsl.2015.11.010

Dickens, G. R. (2011). Down the rabbit hole: Toward appropriate discussion of methane release from gas hydrate systems during the Paleocene-Eocene Thermal Maximum and other past hyperthermal events. *Climate of the Past, 7*(3), 831-846. https://doi.org/10.5194/cp-7-831-2011

Erbacher, J., Mosher, D.C., Malone, M.J., Shipboard Scientific Party, 2004b. Proceedings of the ocean drilling program, initial reports, 207 [CD-ROM]. Available from: ocean drilling program, Texas A&M University, College Station TX 77845-9547, USA https://doi.org/10.2973/odp.proc.ir.207.2004

Erbacher, J., Mosher, D.C., Malone, M.J., et al., 2004. *Proc. ODP, Init. Repts.,* 207: College Station, TX (Ocean Drilling Program). https://doi.org/10.2973/odp.proc.ir.207.2004

Fornaciari, E., Agnini, C., Catanzariti, R., Rio, D., Bolla, E. M., & Valvasoni, E. (2010). Mid-latitude calcareous nannofossil biostratigraphy and biochronology across the middle to late Eocene transition. *Stratigraphy,* 7(4), 229-264.

Galeotti, S., Krishnan, S., Pagani, M., Lanci, L., Gaudio, A., Zachos, J. C., Lourens, L. (2010). Orbital chronology of early Eocene hyperthermals from the Contessa road section, central Italy. *Earth and Planetary Science Letters, 290*(1-2), 192-200. https://doi.org/10.1016/j.epsl.2009.12.021

Galeotti, S., Moretti, M., Sabatino, N., Sprovieri, M., Ceccatelli, M., Francescone, F., Monechi, S. (2017). Cyclochronology of the early Eocene carbon isotope record from a composite Contessa Road-Bottaccione section (Gubbio, central Italy). *Newsletters on Stratigraphy,* 50(3), 231-244. https://doi.org/10.1127/nos/2017/0347

Gibbs, S. J., Bralower, T. J., Bown, P. R., Zachos, J. C., & Bybell, L. M. (2006). Shelf and open-ocean calcareous phytoplankton assemblages across the Paleocene-Eocene Thermal Maximum: Implications for global productivity gradients. Geology, 34(4), 233-236. https://doi.org/10.1130/G22381.1

Gibbs, S. J., Bown, P. R., Murphy, B. H., Sluijs, A., Edgar, K. M., Pälike, H., Zachos, J. C. (2012). Scaled biotic disruption during early Eocene global warming events. *Biogeosciences,* 9(11), 4679-4688. https://doi.org/10.5194/bg-9-4679-2012

Greenwood, D. R., & Wing, S. L. (1995). Eocene continental climates and latitudinal temperature gradients. *Geology*, 23(11), 1044-1048. https://doi.org/10.1130/0091-7613(1995)023<1044:ECCALT>2.3.CO;2

Haq, B. U., & Lohmann, G. P. (1976). Early Cenozoic calcareous nannoplankton biogeography of the Atlantic Ocean. *Marine Micropaleontology,* 1(C), 119-194. https://doi.org/10.1016/0377-8398(76)90008-6

Hollis, C. J., Handley, L., Crouch, E. M., Morgans, H. E. G., Baker, J. A., Creech, J., Pancost, R. D. (2009). Tropical sea temperatures in the high-latitude South Pacific during the Eocene. *Geology, 37*(2), 99-102. https://doi.org/10.1130/G25200A.1

Hollis, C. J., Taylor, K. W. R., Handley, L., Pancost, R. D., Huber, M., Creech, J. B., Zachos, J. C. (2012). Early Paleogene temperature history of the Southwest Pacific Ocean: Reconciling proxies and models. *Earth and Planetary Science Letters*, 349-350, 53-66. https://doi.org/10.1016/j.epsl.2012.06.024

Intxauspe-Zubiaurre, B., Flores, J., Payros, A. (2017a). Variations to calcareous nannofossil $CaCO_3$ content during the middle Eocene C21r-H6 Hyperthermal Event (~ 47.4 ma) in the Gorrondatxe section (Bay of Biscay, Western Pyrenees). *Palaeogeography, Palaeoclimatology, Palaeoecology,* 487, 296-306. https://doi.org/10.1016/j.palaeo.2017.09.015

Intxauspe-Zubiaurre, B., Payros, A., Flores, J., & Apellaniz, E. (2017b). Changes to sea-surface characteristics during the middle Eocene (47.4 ma) C21r-H6 Event: Evidence from calcareous nannofossil assemblages of the Gorrondatxe section (Western Pyrenees). *Newsletters on Stratigraphy*, 50(3), 245-267. https://doi.org/10.1127/nos/2017/0305

Jiang, S., & Wise Jr., S. W. (2009). Distinguishing the influence of diagenesis on the paleoecological reconstruction of nannoplankton across the Paleocene/Eocene Thermal Maximum: An example from the Kerguelen Plateau, Southern Indian Ocean. *Marine Micropaleontology, 72*(1-2), 49-59. https://doi.org/10.1016/j.marmicro.2009.03.003

Jones, T. D., Bown, P. R., Pearson, P. N., Wade, B. S., Coxall, H. K., & Lear, C. H. (2008). Major shifts in calcareous phytoplankton assemblages through the Eocene-Oligocene transition of Tanzania and their implications for low-latitude primary production. *Paleoceanography*, 23(4) https://doi.org/10.1029/2008PA001640

Kennett, J. P. (1977). Cenozoic evolution of Antarctic glaciation, the circum-Antarctic Ocean, and their impact on global paleoceanography. *J. Geophys. Res*. 82, 3843–3860.

Lauretano, V., Littler, K., Polling, M., Zachos, J. C., & Lourens, L. J. (2015). Frequency, magnitude and character of hyperthermal events at the onset of the Early Eocene Climatic Optimum. *Climate of the Past, 11*(10), 1313-1324. https://doi.org/10.5194/cp-11-1313-2015

Lourens, L. J., Sluijs, A., Kroon, D., Zachos, J. C., Thomas, E., Röhl, U., Raffi, I. (2005). Astronomical pacing of late Palaeocene to early Eocene global warming events. *Nature, 435*(7045), 1083-1087. https://doi.org/10.1038/nature03814

Luciani, V., Dickens, R. G., Backman, J., Fornaciari, E., Giusberti, L., Agnini, C., & D'Onofrio, R. (2016). Major perturbations in the global carbon cycle and photosymbiont-bearing planktic foraminifera during the early Eocene. *Climate of the Past*, 12(4), 981-1007. https://doi.org/10.5194/cp-12-981-2016

Luciani, V., D'Onofrio, R., Dickens, G. R., & Wade, B. S. (2017). Planktic foraminiferal response to Early Eocene carbon cycle perturbations in the Southeast Atlantic Ocean (ODP Site 1263). *Global and Planetary Change, 158*, 119-133. https://doi.org/10.1016/j.gloplacha.2017.09.007

Lunt, D. J., Ridgwell, A., Sluijs, A., Zachos, J., Hunter, S., & Haywood, A. (2011). A model for orbital pacing of methane hydrate destabilization during the Palaeogene. *Nature Geoscience, 4*(11), 775-778. https://doi.org/10.1038/ngeo1266

Martini, E. (1971). Standard Tertiary and Quaternary calcareous nannoplankton zonation, in: Proceedings of the 2nd Planktonic Conference, 2, Tecnoscienza, Roma, 739–785, 1971.

Molina, E., Alegret, L., Apellaniz, E., Bernaola, G., Caballero, F., Dinarès-Turell, J., Uchman, A. (2011). The Global Stratotype Section and Point (GSSP) for the base of the Lutetian Stage at the Gorrondatxe section, Spain. *Episodes, 34*(2), 86-108

Monechi, S., Buccianti, A., & Gardin, S. (2000). Biotic signals from nannoflora across the iridium anomaly in the upper Eocene of the Massignano section: Evidence from statistical analysis. *Marine Micropaleontology*, 39(1-4), 219-237. https://doi.org/10.1016/S0377-8398(00)00022-0

Muttoni, G., & Kent, D. V. (2007). Widespread formation of cherts during the Early Eocene Climate Optimum. *Palaeogeography, Palaeoclimatology, Palaeoecology, 253*(3-4), 348-362. https://doi.org/10.1016/j.palaeo.2007.06.008

Newsam, C., Bown, P. R., Bridget, S., & Jones, H. L. (2017). Muted calcareous nannoplankton response at the Middle-Late Eocene Turnover event in the Western North Atlantic Ocean. *Newsletters on Stratigraphy,* 50(3), 297-309. https://doi.org/10.1127/nos/2016/0306

Nicolo, M. J., Dickens, G. R., Hollis, C. J., & Zachos, J. C. (2007). Multiple early Eocene hyperthermals: Their sedimentary expression on the New Zealand continental margin and in the deep sea. Geology, 35(8), 699-702. https://doi.org/10.1130/G23648A.1

Norris, R. D., Klaus, A., & Kroon, D. (2001). Mid-Eocene deep water, the late Palaeocene thermal maximum and continental slope mass wasting during the Cretaceous-Palaeogene impact. *Geol. Soc. Spec. Publ.* 183, 23-48. https://doi.org/10.1144/GSL.SP.2001.183.01.02

Norris, R.D., Kroon, D., Klaus, A., et al. (1998). Blake Nose paleoceanographic transect,Western North Atlantic. In: Norris, R.D., Kroon, D., Klaus, A. (Eds.), Proceedings of the Ocean Drilling ProgramInitial Reports 171B. Ocean Drilling Program, College Station, TX, pp. 1–749

Norris, R. D., Kroon, D., Huber, B. T., & Erbacher, J. (2001). Cretaceous-Palaeogene ocean and climate change in the subtropical North Atlantic. *Geol. Soc. Spec. Publ*. 183, 1-22. https://doi.org/10.1144/GSL.SP.2001.183.01.01

Norris, R.D., Wilson, P.A., Blum, P., Scientists, E. 342, (2014). Paleogene Newfoundland Sediment Drifts and MDHDS Test, in: Proceedings of the Integrated Ocean Drilling Program, 342: College Station, TX (Integrated Ocean Drilling Program). https://doi.org/10.2204/iodp.proc.342.2014

Okada, H., & Honjo, S. (1973). The distribution of oceanic coccolithophorids in the Pacific. *Deep-Sea Research and Oceanographic Abstracts,* 20(4), 355-364, IN3-IN4,365-374. https://doi.org/10.1016/0011-7471(73)90059-4

Okada, H., & Bukry, D. (1980). Supplementary modification and introduction of code numbers to the low-latitude coccolith biostratigraphic zonation (Bukry, 1973; 1975). *Marine Micropaleontology*, 5(C), 321-325. https://doi.org/10.1016/0377-8398(80)90016-X

Oreshkina, T. V. (2012). Evidence of late Paleocene - early Eocene hyperthermal events in biosiliceous sediments of Western Siberia and adjacent areas. *Austrian Journal of Earth Sciences,* 105(1), 145-153

Pagani, M., Zachos, J. C., Freeman, K. H., Tipple, B., & Bohaty, S. (2005). Atmospheric science: Marked decline in atmospheric carbon dioxide concentrations during the Paleogene. *Science*, 309(5734), 600-603. https://doi.org/10.1126/science.1110063

Payros, A., Ortiz, S., Alegret, L., Orue-Etxebarria, X., Apellaniz, E., & Molina, E. (2012). An early Lutetian carbon-cycle perturbation: Insights from the Gorrondatxe section (Western Pyrenees, Bay of Biscay). *Paleoceanography*, 27(2) https://doi.org/10.1029/2012PA002300

Perch-Nielsen, K. (1985). Cenozoic calcareous nannofossils, in: Bolli, H.M., Saunders, J.B., Perch-Nielsen, K. (Eds.), Plankton Stratigraphy. Cambridge University Press, Cambridge, pp. 427–554

Persico, D., Villa, G. (2004). Eocene-Oligocene calcareous nannofossils from Maud Rise and Kerguelen Plateau (Antarctica): Paleoecological and paleoceanographic implications. *Marine Micropaleontology*, 52(1-4), 153-179. https://doi.org/10.1016/j.marmicro.2004.05.002

Pross, J., Contreras, L., Bijl, P. K., Greenwood, D. R., Bohaty, S. M., Schouten, S., Yamane, M. (2012). Persistent near–tropical warmth on the Antarctic continent during the early Eocene epoch. *Nature,* 488(7409), 73-77. https://doi.org/10.1038/nature1130

Quillévéré, F., Norris, R. D., Kroon, D., & Wilson, P. A. (2008). Transient ocean warming and shifts in carbon reservoirs during the early danian. *Earth and Planetary Science Letters, 265*(3-4), 600-615. https://doi.org/10.1016/j.epsl.2007.10.040

Schneider, L. J., Bralower, T. J., & Kump, L. R. (2011). Response of nannoplankton to early Eocene ocean destratification. *Palaeogeography, Palaeoclimatology, Palaeoecology,* 310(3-4), 152-162. https://doi.org/10.1016/j.palaeo.2011.06.018

Sexton, P. F., Norris, R. D., Wilson, P. A., Pälike, H., Westerhold, T., Röhl, U., Gibbs, S. (2011). Eocene global warming events driven by ventilation of oceanic dissolved organic carbon. *Nature*, 471(7338), 349-353. https://doi.org/10.1038/nature09826

Shamrock, J.L. (2010). A new calcareous nannofossil species of the genus *Sphenolithus* from the Middle Eocene (Lutetian) and its biostratigraphic significance. *Journal of Nannoplankton Research*, 31(1): 5-10

Shamrock, J. L., & Watkins, D. K. (2012). Eocene calcareous nannofossil biostratigraphy and community structure from Exmouth Plateau, Eastern Indian Ocean (ODP Site 762). *Stratigraphy*, 9(1), 1-54.

Slotnick, B. S., Dickens, G. R., Nicolo, M. J., Hollis, C. J., Crampton, J. S., Zachos, J. C., & Sluijs, A. (2012). Large-amplitude variations in carbon cycling and terrestrial weathering during the latest Paleocene and earliest Eocene: The record at Mead Stream, New Zealand. *Journal of Geology, 120*(5), 487-505. https://doi.org/10.1086/666743

Slotnick, B. S., Lauretano, V., Backman, J., Dickens, G. R., Sluijs, A., & Lourens, L. (2015a). Early Paleogene variations in the calcite compensation depth: New constraints using old borehole sediments from across Ninetyeast Ridge, Central Indian 0cean. *Climate of the Past, 11*(3), 473-493. https://doi.org/10.5194/cp-11-473-201

Slotnick, B. S., Dickens, G. R., Hollis, C. J., Crampton, J. S., Percy Strong, C., & Phillips, A. (2015b). The onset of the Early Eocene Climatic Optimum at Branch Stream, Clarence River Valley, New Zealand. *New Zealand Journal of Geology and Geophysics,* 58(3), 262-280. https://doi.org/10.1080/00288306.2015.1063514

Spofforth, D. J. A., Agnini, C., Pälike, H., Rio, D., Fornaciari, E., Giusberti, L., Muttoni, G. (2010). Organic carbon burial following the Middle Eocene Climatic Optimum in the central western Tethys. *Paleoceanography,* 25(3) https://doi.org/10.1029/2009PA001738

Thomas, E., & Zachos, J. C. (2000). Was the late paleocene thermal maximum a unique event? *GFF, 122*(1), 169-170. https://doi.org/10.1080/11035890001221169

Toffanin, F., Agnini, C., Fornaciari, E., Rio, D., Giusberti, L., Luciani, V., Spofforth, D.J.A., Pälike, H. (2011). Changes in calcareous nannofossil assemblages during the Middle Eocene Climatic Optimum: Clues from the central-western Tethys (Alano section, NE Italy). *Marine Micropaleontology* 81, 22–31. https://doi.org/10.1016/j.marmicro.2011.07.002

Tori, F., & Monechi, S. (2013). Lutetian calcareous nannofossil events in the Agost section (Spain): Implications toward a revision of the middle Eocene biomagnetostratigraphy. *Lethaia*, 46(3), 293-307. https://doi.org/10.1111/let.12008

Turner, S. K., Sexton, P. F., Charles, C. D., & Norris, R. D. (2014). Persistence of carbon release events through the peak of early Eocene global warmth. *Nature Geoscience*, 7(10), 748-751. https://doi.org/10.1038/NGEO2240

Vahlenkamp, M., Niezgodzki, I., De Vleeschouwer, D., Bickert, T., Harper, D., Kirtland Turner, S., Pälike, H. (2018). Astronomically paced changes in deep-water circulation in the western North Atlantic during the middle Eocene. *Earth and Planetary Science Letters*, 484, 329-340. https://doi.org/10.1016/j.epsl.2017.12.016

Villa, G., Fioroni, C., Pea, L., Bohaty, S., & Persico, D. (2008). Middle Eocene-late Oligocene climate variability: Calcareous nannofossil response at Kerguelen Plateau, Site 748. *Marine Micropaleontology*, 69(2), 173-192. https://doi.org/10.1016/j.marmicro.2008.07.00

Villa, G., Fioroni, C., Persico, D., Roberts, A. P., & Florindo, F. (2014). Middle Eocene to late Oligocene Antarctic glaciation/deglaciation and Southern Ocean productivity. *Paleoceanography*, 29(3), 223-237. https://doi.org/10.1002/2013PA002518

Wei, W., & Wise Jr., S. W. (1989). Paleogene calcareous nannofossil magnetobiochronology: Results from South Atlantic DSDP Site 516. *Marine Micropaleontology*, 14(1-3), 119-152. https://doi.org/10.1016/0377-8398(89)90034-0

Wei, W., & Wise Jr., S. W. (1990). Biogeographic gradients of middle Eocene-Oligocene calcareous nannoplankton in the South Atlantic Ocean. *Palaeogeography, Palaeoclimatology, Palaeoecology*, 79(1-2), 29-61. https://doi.org/10.1016/0031-0182(90)90104-F

Westerhold, T., Röhl, U., Frederichs, T., Agnini, C., Raffi, I., Zachos, J. C., & Wilkens, R. H. (2017). Astronomical calibration of the Ypresian timescale: Implications for seafloor spreading rates and the chaotic behavior of the solar system? *Climate of the Past,* 13(9), 1129-1152. https://doi.org/10.5194/cp-13-1129-201

Westerhold, T., Röhl, U., Donner, B., & Zachos, J. C. (2018). Global extent of early Eocene hyperthermal events: A new Pacific benthic foraminiferal isotope record from Shatsky Rise (ODP Site 1209).*Paleoceanography and Paleoclimatology,* 33(6), 626-642. https://doi.org/10.1029/2017PA003306

Wind, F. H., & Wise, S. W. (1978). Mesozoic holococcoliths. *Geology, 6*(3), 140-142. https://doi.org/10.1130/0091-7613(1978)6<140:MH>2.0.CO;2

Winter, A., Jordan, R.W., Roth, P.H. (1994). Biogeography of living coccolithophores in ocean waters, in: Winter, A., Siesser, W.G. (Eds.), Coccolithophores. *Cambridge University Press*, Cambridge, pp. 161–178.

Yamamoto, Y., Fukami, H., Taniguchi, W., and Lippert, P.C. (2018). Data report: updated magnetostratigraphy for IODP Sites U1403, U1408, U1409, and U1410. In Norris, R.D., Wilson, P.A., Blum, P., and the Expedition 342 Scientists, Proceedings of the Integrated Ocean Drilling Program, 342: College Station, TX (Integrated Ocean Drilling Program). https://doi.org/10.2204/iodp.proc.342.207.2018

Young, J. R. and Henriksen K. (2003). Biomineralization within vesicles: the calcite of coccoliths. In: Dove P.M., De Yoreo J. J., Weiner S., Eds., Biomineralisation. *Reviews in Mineralogy and Geochemistry,* 54, 189-215.

Young, J. R., Geisen, M., & Probert, I. (2005). A review of selected aspects of coccolithophore biology with implications for paleobiodiversity estimation. *Micropaleontology,* 51(4), 267-288. https://doi.org/10.1649/772

Zachos, J., Pagani, H., Sloan, L., Thomas, E., & Billups, K. (2001). Trends, rhythms, and aberrations in global climate 65 Ma to present. *Science*, 292(5517), 686-693. https://doi.org/10.1126/science.1059412

Zachos, J. C., Kroon, D., & Blum, P. (2004). ODP leg 208: The early cenozoic extreme climates transect along walvis ridge. *JOIDES Journal, 30*(1), 8-13.

Zachos, J. C., Dickens, G. R., & Zeebe, R. E. (2008). An early Cenozoic perspective on greenhouse warming and carbon cycle dynamics. *Nature*, 451(7176), 279-283. https://doi.org/10.1038/nature06588

Appendix I

Taxonomic list: Taxa cited in the text are reported in alphabetical order by genric hepithet.

Blackites Hay and Towe 1962
Blackites inflatus (Bramlette and Sullivan 1961)
Blackites gladius (Locker 1967) Varol 1989

Campylosphaera Kamptner 1963

Chiasmolithus Hay et al. 1966

Chiphragmalithus Bramlette and Sullivan 1961
Chiphragmalithus acanthoides Bramlette and Sullivan 1961

Cyclicargolithus Bukry, 1971
Cyclicargolithus luminis (Sullivan, 1965) Bukry 1971

Clausicoccus Prins 1979
Clausicoccus subdistichus (Roth and Hay in Hay et al. 1967) Prins 1979
Clausicoccus fenestratus (Deflandre and Fert 1954) Prins 1979
Clausicoccus obrutus (Perch-Nielsen 1971) Prins 1979
Clausicoccus vanheckiae (Perch-Nielsen 1986)

Coccolithus Schwartz 1894
Coccolithus crassus Bramlette and Sullivan 1961
Coccolithus pelagicus (Wallich 1877) Schiller 1930

Dictyococcites Black 1967

Discoaster Tan 1927
Discoaster bifax Bukry 1971
Discoaster kuepperi Stradner 1959
Discoaster lodoensis Bramlette and Sullivan 1961
Discoaster sublodoensis Bramlette and Sullivan 1961

Ellipsolithus Sullivan 1964

Ericsonia Black (1964)

Girgisia Varol 1989
*Girgisia gammation (*Bramlette and Sullivan 1961) Varol 1989

Helicosphaera Kamptner 1954

Nannotetrina Achuthan and Stradner 1969
Nannotetrina alata (Martini in Martini and Stradner 1960) Haq and Lohmann 1976
Nannotetrina cristata (Martini 1958) Perch-Nielsen 1971
Nannotetrina fulgens (Stradner in Martini and Stradner 1960) Achuthan and Stradner 1969

Pontosphaera Lohmann, 1902

Pletolithus Cappelli et al. in preparation
Pletolithus gigas (Bramelette and Sullivan) Cappelli et al. (in preparation)
Pletolithis giganteus Cappelli et al. (in preparation)

Pseudotriquetrorhabdulus Wise in Wise and Constans 1976
Pseudotriquetrorhabdulus inversus (Bukry and Bramlette 1969) Wise in Wise and Constans 1976

Reticulofenestra Hay et al. 1966
Reticulofenestra umbilicus (Levin 1965) Martini and Ritzkowski 1968

Rhomboaster Bramlette and Sullivan 1961

Sphenolithus Deflandre in Grasse, 1952
Sphenolithus cuniculus Bown 2005
Sphenolithus furcatolithoides Locker 1967

Toweius Hay and Mohler 1967

Tribrachiatus Shamrai 1963
*Tribrachiatus orthostylus (*Bramlette and Riedel 1954) Shamrai 1963

Zygrhablithus Deflandre, 1959

Appendix II

Plates

Plate 2.1. LM images of selected calcareous nannofossil taxa from Site IODP U1410. All photos are in crossed nicols. Scale bar 10 µm **1-2**. *Toweius callosus.* Samples 1410A-28X-2W-29; 1410A-26X-6-52 **3.** *Toweius* sp**.** Sample 1410A-27X-1W- 94 **4-6.** *Toweius magnicrassus.* Samples 1410A-26X-6W-52, 1410A-26X-6- 103; 1410B-27X-1W-118 **7.** *Girgisia gammation.* Sample 1410A 26X-CC **8.** *Dictyococcites* sp.1. Sample 1410B-25X-2W-87 **9.** *Dictyococcites hesslandi.* Sample 1410B-27X-6W-18 **10.** *Dictyococcites* cf. *D. bisectus* (<10 µm). Sample 1410A-19X-CC **11.** *Cyclicargolithus floridanus.,* Sample 1410A-23X-4W-39 **12.** *Reticulofenestra dictyoda.* Sample 1410C-23X-5W-87 **13.** *Reticulofenestra wadae.* Sample 1410C-23X-2W- 87 **14-15.** *Reticulofenestra umbilicus.* Samples 1410C-19X-4W-67, 1410B-20X-5W-40 **16.** *Ericsonia formosa.* Sample 1410A-17X-6W- 80 **17-18:** *Coccolithus pelagicus* Samples 1410C-18X-5W-100, 1410C-18X-3W-100 **18-21.** *Coccolithus crassus.* Samples 1410B-27X-5W-4, 1410B-27X-5W-4, 1410B-27-1W-118 **22.** *Coccolithus sheri.* Sample 1410B-21X-5W-127 **23-24.** *Coccolithus biparteoperculatus.* Samples 1410B-17X-4W-110, 1410B-17X-2-30 **25-26.** *Coccolithus* cf. *C. hulliae.* Samples 1410B-23X-5W-5, 1410B-22-CC, **27.** *Clausicoccus subdistichus*. Sample 1410A-22X-5W-127**. 28-30.** *Clausicoccus fenestratus*. Samples 1410A-15X-3W-60, 1410B-21X-2W-127, 1410C-20X-2W-67.

Plate 2.2: LM images of selected calcareous nannofossil taxa from Site IODP U1410. All photos are in crossed nicols. Scale bar 10 µm **1,5.** *Pletolithus mutatus* (n. comb.). Sample 1410A-19X-7W-22, 1410A-17X-6-80 **2.** *Pletolithus opdykei* (n. comb.). Sample 1410A-17X-6W-80 **3.** *Pletolithus staurion* (n. comb.). 1410A-22X-CC **4.** *Pletolithus giganteus* (n. sp.). Sample 1410A-19X-7W-22 **6-8.** *Pletolithus gigas* (n. comb.) Samples 1410C-18X-4W- 80. 1410A-19X-7W-22, 1410C-18X-4W-80 **9.** *Chiasmolithus solitus.* Sample 1410A-15X-4W-70 **10-13.** *Chiasmolithus consuetus.* Samples 1410C-20X-4W-67, 1410A-19X-CC, 1410A-22X-3W-127, 1410B-27X-6W-18 **14-15.** *Helicosphaera lophota.* Samples 1410C-18X-5W-100, 1410C-19X-2W-67 **16.** *Helicosphaera seminulum.* Sample 1410A-22X-4W-127 **17.** *Helicosphaera* cf. *H. bramlettei.* Sample 1410B-28X-2W-145 **18.** *Helicosphaera bramlettei.* Sample 1410C-21X-6W- 7 **19.** *Pontosphaera exilis.* Sample 1410C-23X-5W-87 **20.** *Pontosphaera pectinata.* Sample 1410C-23X-5W-87 **21.** *Pontosphaera punctosa.* Sample 1410B-20X-4W-20 **22.** *Pontosphaera multipora.* Sample 1410C-23X-4W-85 **23.** *Pontosphaera plana.* Sample 1410A-20X-CC.

Plate 2.3: LM images of selected calcareous nannofossil taxa from IODP Site U1410. All photos are in crossed nicols. Scale bar 10 µm. **1.** *Blackites inflatus.* Sample1410A-23X-3W-26 **2.** *Blackites subtilis.* Sample 1410B-20X-4W- 20 **3.** *Blackites* cf. *B. spinosus***.** Sample 1410C-23X-3W- 87 **4.** *Blackites tenuis.* Sample 1410C-23X-3W- 87 **5.6.** *Blackites stilus.* Samples 1410C-18X-5W-20, 1410C-19X-2W- 67 **7.** *Blackites* base. Sample 1410B-25X-2W-87 **8.** *Blackites virgatus.* Sample 1410C-18X-4W-80 **9.** *Pseudotriquetrorhabdulus inversus.* Sample 1410C-23X-5W-43 **10.** *Blackites pseudomorionum*. Sample 1410B-21X-2W-127 **11.** *Blackites fustis*. Sample 1410C-18X-5W-100 **12-14.** *Blackites globulus.* Samples 1410B-21X-4W-127, 1410C-20X-4W- 67, 1410C-20X-5W-67 **15.** *Blackites creber*. Sample 1410C-19X-4W- 67 16 **16.** *Blackites* cf. *B. gladius.* Sample 1410C-19X-2W- 67 **17,18.** *Blackites gladius,* Samples 1410B-20X-4W-20. 1410B-20X-5W- 40 **19.** *Blackites rotundus*, Sample 1410A-16X-5W-100 **20-22.** *Zygrhablithus bijugatus* Samples 1410B-27X-5W-4, 1410B-27X-1-118, 1410C-20X-4W-67 **23,24.** *Zygrhablithus* bases. Samples 1410A-28X-2W- 29, 1410B-27X-6W-18.

Plate 2.4: LM images of selected calcareous nannofossil taxa from IODP Site U1410. All photos are in crossed nicols. Scale bar 10 µm **1.** *Sphenolithus radians,* a. 0°, b. 45° Sample 1410B 27X-1W-118 **2.** *Sphenolithus spiniger,* a. 0°, b. 45° Sample 1410A-15X-4W-70 **3, 4.** *Sphenolithus* with "processes" (see Chapter 4). a. 0°, b. 45° Samples 1410A-22X-3W-127, 1410A-19X-7- 22 **5,6.** *Sphenolithus furcatolithoides* morphotype A (see Chapter 4). a. 0°, b. 45°Samples 1410C-19X-3W-65, 1410C-19X-4- 67 **7,8.** *Sphenolithus cuniculus*. a. 0°, b. 45°Samples 1410B-17X- 3W-140, 1410B -19X-6W- 60 **9,10.** *Sphenolithus furcatolithoides* morphotype B (see chapter 4) . a. 0°, b. 45°Samples 1410B-17X-3W-100, 1410B-17X-W2-30 **11,12.** *Sphenolithus strigosus*, a. 0°, b. 45°Samples 1410B-17X-5W-12, 1410B-17X -3W-100 **13.** *Umbilicosphaera bramlettei*. Sample 1410C-23X-2- 87 **14.** *Ellipsolithus* sp. 1410C-23X-5W-87 **15.** *Neocrepidolithus grandiculus.* Sample 1410B-27X-2W-127 **16.** *Campilosphaera dela*. Sample1410B-20X-5W-40 **17.** *Markalius inversus.* Sample 1410B -20X-5W- 40 **18.** *Lophodolithus mochlophorus.* Sample 1410C-19X-4W- 67.

Plate 2.5: LM images of selected calcareous nannofossil taxa from IODP Site U1410. All photos are in parallel light. Scale bar 10 µm. **1,2.** *Discoaster lodoensis.* Samples 1410A -27X-4W-121, 1410A -26X-6W- 52, **3.** *Discoaster lodoensis* 7 rays. Sample 1410A-26X-5W-132. **4-8.** *Discoaster sublodoensis.* Samples 1410A-23X-1W-7, 1410B-24X-1W-87, 1410A-23X-6W- 13, 1410B-27X-1W-118, 1410B-27X-1W-118 **9, 11.** *Disocaster barbadiensis* 8 rays. Samples 1410A-22X-4W- 127, 1410B-21X-2W- 127, 1410A-22X-2W-127 **12.** *Discoaster sublodoensis* 7 rays, Sample 1410A-22X-4W- 127 **13, 17-19.** *Discoaster gemmifer.* Samples 1410C-19X-3-65, 1410A-23X-1W- 7, 1410B-17X-4W-110, 1410A-16X-4W- 90 **14.** *Discoaster martinii.* Sample 1410B-17X-2W- 30 **15, 16.** *Discoaster saipanensis* 7 rays. Samples 1410B-20X-5W- 40, 1410A-22X-2W-127 **20.** *Discoaster nodifer.* Sample 1410A-16X-4W-90.

Plate 2.6: LM Images of selected calcareous nannofossil taxa from IODP Site U1410. All photos are in parallel light. Scale bar 10 µm. **1.** *Disocaster kuepperi.* Sample 1410B-27X-2W-127 **2,3.** *Disocaster kuepperi,* same specimen. Sample 1410A-27X-6W-70 **4.** *Discoaster praebifax.* Sample 1410A 22X-3W- 127 **5-7.** *Discoaster wemmelensis.* Samples 1410B 17X-2W- 30, 1410A-22X-4W-127, 1410B-21X-2W-127 **8.** *Discoaster distinctus.* Sample 1410B-18X-3W- 40 **9.** *Discoaster* sp.. Sample 1410B-19X-5W- 40 **10.** *Discoaster bifax.* Sample 1410A-16X-5- 100 **11.** *Discoaster barbadiensis* 8 rays. Sample 1410C-20X-4-67 **12.** *Discoaster barbadiensis.* Sample 1410B-17X-4W-110 **13.** *Discoaster nodifer.* Sample 1410B-20X-4W-20 **14.** *Tribrachiathus orthostylus.* Sample 1410A-26X-6-52 **15.** *Chiphragmalithus calathus.* Sample 1410A-28X-CC **16-18.** *Chiphragmalithus acanthodes.* Samples 1410B-26X-

2W-115, 1410C-24X-4W-143, 1410A-24X-2W-93 **19-21.** *Chiphragmalithus* sp.1. Samples 1410B-26X-3-119, 1410B-26X-2-53, 1410B-26X-2W- 53 **22-24.** *Nannotetrina cristata.* Samples 1410B-21X-4W-127, 1410C-24X-4W-66, 1410C-24X-4W-143 **25.** *Nannotetrina spinosa.* Sample 1410B-21X-2W-127 **26.** *Nannotetrina pappii.* Sample 1410A-22X-2W-127 **27.** *Nannotetrina alata* group.

Plate 2.7:LM iImages of selected calcareous nannofossil taxa from IODP Site U1410. All photos are in parallel light. Scale bar 10 µm. **1-3.** *Nannotetrina alata* group. Samples 1410A-22X-2W-127, 1410B-24X-1W- 87, 1410B-23X-5W- 5 **4,5.** *Nannotetrina cristata.* Samples 1410A-23X-5W- 43, 1410B-24X-2W- 87 **6,7,9-11.** *Nannotetrina alata* goup. Samples 1410B-19X-4W- 20, 1410C-18X-3-60W, 1410B-19X-5W- 40, 1410B-19X-5W- 40, 1410B-21X-4W- 127 **8.** *Nannotetrina pappii.* Sample 1410B-19X-3W- 20 **12-14.** *Nannotetrina cristata.* Samples 1410C-18X-4W-80, 1410C-18X-4W- 80, 1410C-19X-4W- 67 **15,16.** *Nannotetrina pappii.* Samples 1410B-19X-3W- 20, 1410B-18X-4W- 50.

Plate 2.8: SEM mages of selected calcareous nannofossil taxa from IODP Site U1410. Scale bar 5 µm. **1, 2.** *Coccolithus pelagicus.* Samples 1410B-21X-3W-127, 1410A-18X-CC **3.** *Coccolithus* cf. *C. hulliae* (distal view). Sample 1410B-21X-3W-127 **4.** *Coccolithus* cf. *C. hulliae* (proximal view). 1410B-21X-3W-127 **5-8.** *Ericsonia formosa.* Samples 1410B-21X-3W-127, 1410A-17X-2W- 120, 1410A-17X-2W-120, 1410C -19X-2- 67 **9-11.** *Clausicoccus subdistichus.* Samples 1410C -19X-2- 67, 1410B-18X-3W- 40, 1410B-20X-4W- 20 **12.** *Clausicoccus vanheckiae.* Sample 1410B-21X-3W-127 **13.** *Pletolithus gigas* (new comb.). Sample 1410B-21X-3W-127 **14.** *Chiasmolithus grandis.* Sample 1410B-21X-3W-127 **15.** *Chiasmolithus consuetus.* Sample 1410B-21X-3W-127 **15.** *Chiasmolithus* sp. Coccosphere. Sample 1410A-17X-2-120.

Plate 2.9: SEM mages of selected calcareous nannofossil taxa from IODP Site U1410. Scale bar 5 µm. **1.** *Helicosphaera bramlettei.* Sample 1410B-21X-3W-127 **2.** *Helicosphaera seminulum.* Sample 1410A-17X-2W- 120 **3,4.** *Helicosphaera lophota.* Samples 1410C-18X-5W-100, 1410B-21X-3-127 **5.** *Helicosphaera papillata.* Sample 1410A-17X-2W-120 **6.** *Pontosphaera multipora,* Sample 1410B-21X-3W-127 **7.** *Pontosphaera perforomarginata.* Sample 1410B-21X-3W-27 **8.** *Pontosphaera plana?* Sample1410C-20X-2W-67 **9.** *Pontosphaera formosa.* Sample 1410A-17X-2W-120 **10.** *Pontosphaera clinosulcata.* Sample 1410C19X-3W-65 **11.** *Umbilicosphaera* sp. Sample 1410C -19X-3W-65 **12.** *Neococcolithes* sp. Sample 1410A-17X-2W-120 **13.** *Lophodolithus nascens.* Sample 1410A-17X-2W-120 **14.** *Lophodolithud mochlophorus.* Sample 1410B-21X-3W-127 **15.** *Scyphosphaera expansa.* Sample 1410A-17X-2W-120.

Plate 2.10: SEM mages of selected calcareous nannofossil taxa from IODP Site U1410. Scale bar 5 µm. **1,2.** *Reticulofenstra daviesii.* Sample 1410C-20X-2W-120, 1410C-20X-2W-57 **3.** *Reticulofenstra dictyoda.* Sample 1410C-20X-2W-57 **4.** *Dictyococcites* sp. 1. Sample 1410B-21X-3W-127 **5.** *Cyclicargolithus luminis.* Sample 1410B-23X-4W-7. **6.** *Reticulofenesta* sp. Coccosphere. Sample 1410B-21X-3W-127 **7.** *Blackites spinosus.* Sample 1410B-21X-3W-127 **8.** *Blackites tenuis.* Sample 1410B-21X-3W-127 **9.** *Blackites subtilis* Sample 1410B-24X-1W-87 **10.** *Pseudotriquetrorhabdulus inversus.* Sample 1410B-21X-3W-127 **11.** *Blackites* bases. Sample 1410B-21X-3W-127 **12,13.** *Blackites rotundus.* Samples 1410B-21X-3W-127, 1410C-20X-4W-4 **14,15.** *Blackites gladius.* Sample 1410B-21X-3W-127. Sample 1410A-17X-2W-120.

Plate 2.11: SEM mages of selected calcareous nannofossil taxa from IODP Site U1410. Scale bar 5 µm. **1.** *Discoaster saipanensis.* Sample 1410C-19X-2W-67 **2.** *Discoaster barbadiensis* 8 rays. Sample 1410C-19X-2W-67 **3.** *Discoaster barbadiensis.* Sample 1410C-19X-2W-67 **4.** *Discoaster wemmelensis.* Sample 1410C-19X-2W-67 **5.** *Discoaster barbadiensis.* Samples 1410C-19X-2W-67, 1410C-19X-2W-67 **7.** *Discoaster* cf. *D. barbadiensis.* Sample 1410C-18X-CC **8.** *Discoaster praebifax.* Sample 1410B-23X-4W-7 **9.** *Discoaster bifax.* Sample 1410C-19X-2W-67 **10.** *Discoaster* sp.. Sample 1410C-19X-2W-67 **11.** *Discoaster lodoensis* (reworked). Sample 1410C-21X-3W-127 **12.** *Discoaster nodifer.* Sample 1410C-21X-3W-127 **13.** *Campilosphaera dela.* Sample 1410B-21X-CC **14.** *Zygrhablithus bijugathus*. Sample 1410B-21X-3W-127.

Plate 2.1

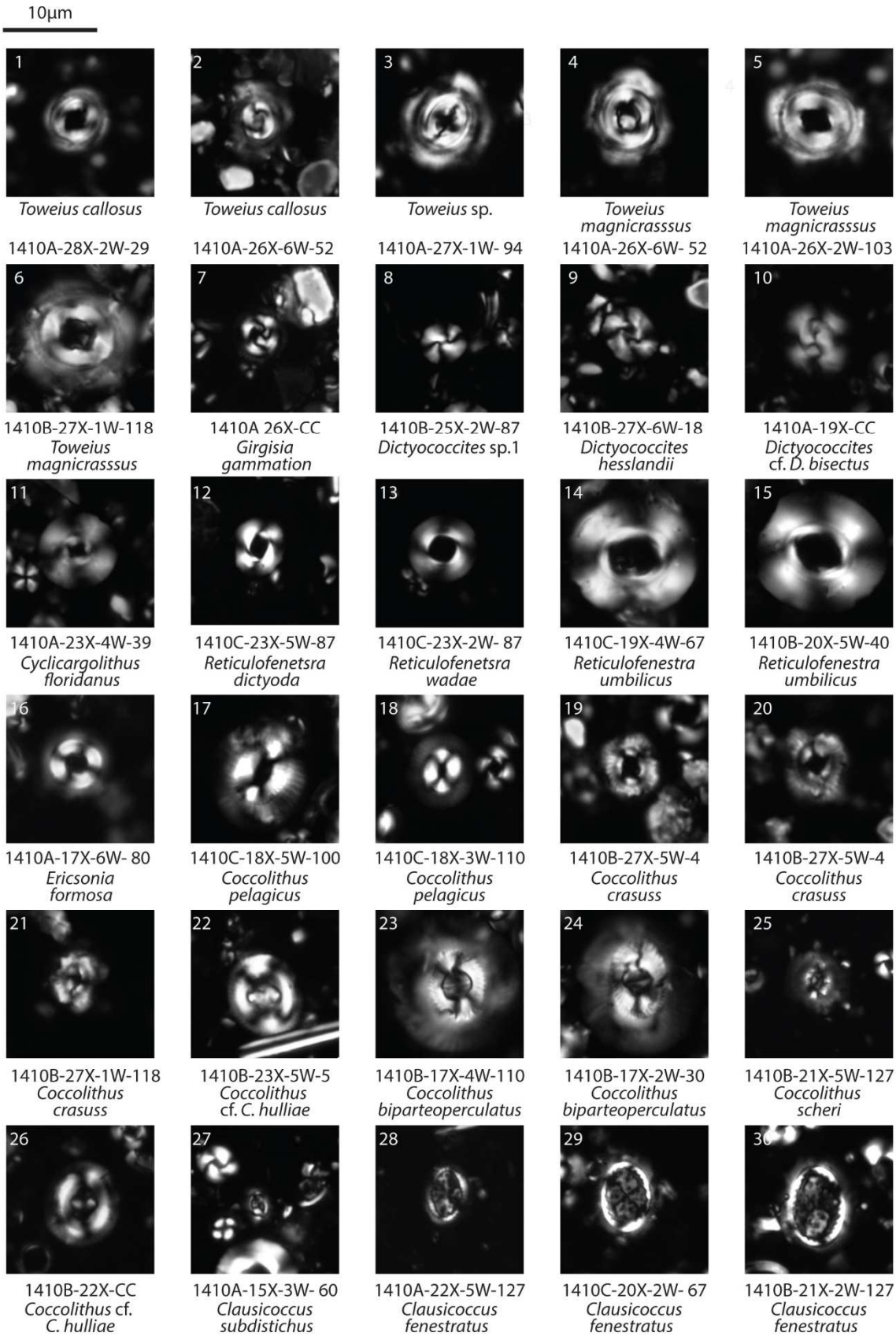
10µm
1
Toweius callosus
1410A-28X-2W-29
2
Toweius callosus
1410A-26X-6W-52
3
Toweius sp.
1410A-27X-1W- 94
4
Toweius magnicrasssus
1410A-26X-6W- 52
5
Toweius magnicrasssus
1410A-26X-2W-103
6
1410B-27X-1W-118
Toweius magnicrasssus
7
1410A 26X-CC
Girgisia gammation
8
1410B-25X-2W-87
Dictyococcites sp.1
9
1410B-27X-6W-18
Dictyococcites hesslandii
10
1410A-19X-CC
Dictyococcites cf. D. bisectus
11
1410A-23X-4W-39
Cyclicargolithus floridanus
12
1410C-23X-5W-87
Reticulofenetsra dictyoda
13
1410C-23X-2W- 87
Reticulofenetsra wadae
14
1410C-19X-4W-67
Reticulofenestra umbilicus
15
1410B-20X-5W-40
Reticulofenestra umbilicus
16
1410A-17X-6W- 80
Ericsonia formosa
17
1410C-18X-5W-100
Coccolithus pelagicus
18
1410C-18X-3W-110
Coccolithus pelagicus
19
1410B-27X-5W-4
Coccolithus crasuss
20
1410B-27X-5W-4
Coccolithus crasuss
21
1410B-27X-1W-118
Coccolithus crasuss
22
1410B-23X-5W-5
Coccolithus cf. C. hulliae
23
1410B-17X-4W-110
Coccolithus biparteoperculatus
24
1410B-17X-2W-30
Coccolithus biparteoperculatus
25
1410B-21X-5W-127
Coccolithus scheri
26
1410B-22X-CC
Coccolithus cf. C. hulliae
27
1410A-15X-3W- 60
Clausicoccus subdistichus
28
1410A-22X-5W-127
Clausicoccus fenestratus
29
1410C-20X-2W- 67
Clausicoccus fenestratus
30
1410B-21X-2W-127
Clausicoccus fenestratus

Plate 2.2

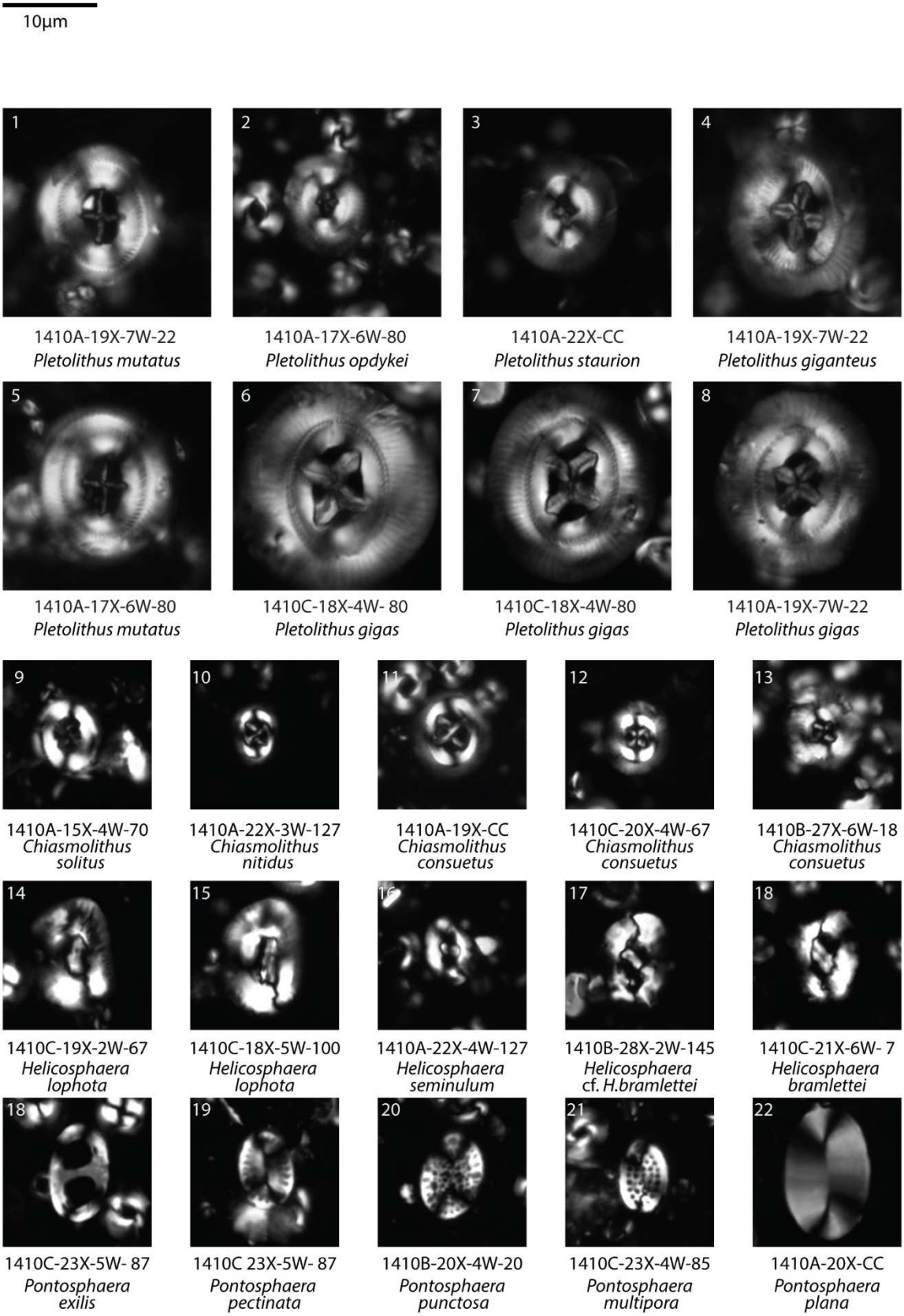
10µm
1
1410A-19X-7W-22
Pletolithus mutatus
2
1410A-17X-6W-80
Pletolithus opdykei
3
1410A-22X-CC
Pletolithus staurion
4
1410A-19X-7W-22
Pletolithus giganteus
5
1410A-17X-6W-80
Pletolithus mutatus
6
1410C-18X-4W- 80
Pletolithus gigas
7
1410C-18X-4W-80
Pletolithus gigas
8
1410A-19X-7W-22
Pletolithus gigas
9
1410A-15X-4W-70
Chiasmolithus solitus
10
1410A-22X-3W-127
Chiasmolithus nitidus
11
1410A-19X-CC
Chiasmolithus consuetus
12
1410C-20X-4W-67
Chiasmolithus consuetus
13
1410B-27X-6W-18
Chiasmolithus consuetus
14
1410C-19X-2W-67
Helicosphaera lophota
15
1410C-18X-5W-100
Helicosphaera lophota
16
1410A-22X-4W-127
Helicosphaera seminulum
17
1410B-28X-2W-145
Helicosphaera cf. H.bramlettei
18
1410C-21X-6W- 7
Helicosphaera bramlettei
18
1410C-23X-5W- 87
Pontosphaera exilis
19
1410C 23X-5W- 87
Pontosphaera pectinata
20
1410B-20X-4W-20
Pontosphaera punctosa
21
1410C-23X-4W-85
Pontosphaera multipora
22
1410A-20X-CC
Pontosphaera plana

Plate 2.3

10µm

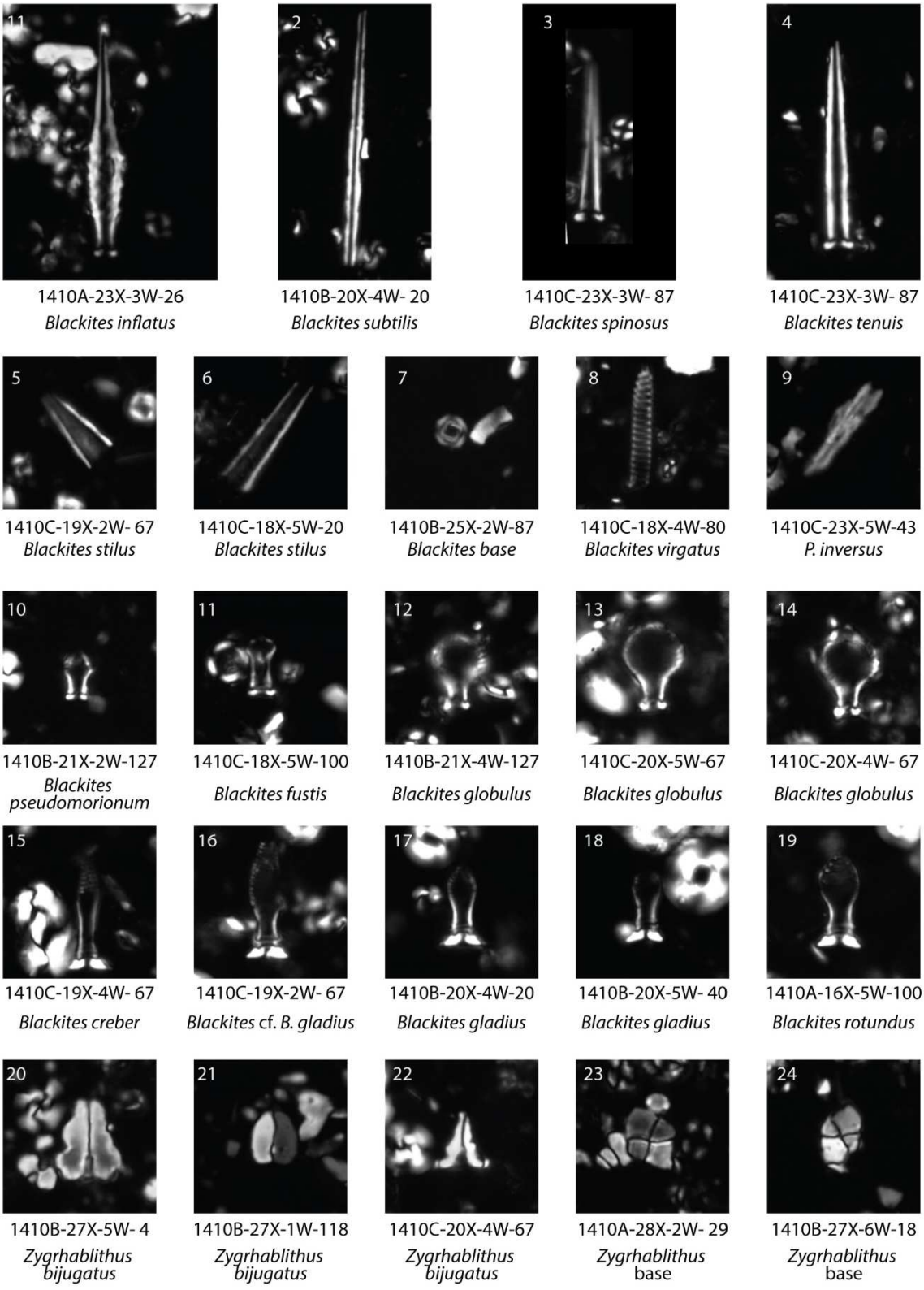

Plate 2.4


10µm
1a
1b
2a
2b
3a
5µm
1410B 27X-1W-118
Sphenolithus radians
1410A-15X-4W- 70
Sphenolithus spiniger
1410A-22X-3W-127
Spenoliths with processes
3b
4a
4b
5a
5b
1410A-19X-7W- 22
Spenoliths with processes
1410C-19X-4W- 67
Spenolithus furcatolithoides morphotype A
6a
6b
7a
7b
8a
1410C-19X-3W-65
Spenolithus furcatolithoides morphotype A
1410B -19X-6W- 60
Spenolithus cuniculus
1410B-17X- 3W-140
Spenolithus cuniculus
8b
9a
9b
10a
10b
1410B-17X-3W-100
Spenolithus furcatolithoides morphotype B
1410B-17X-2W-30
Spenolithus furcatolithoides morphotype B
11a
11b
12a
12b
13
1410B-17X-5W-120
Spenolithus strigosus
1410B-17X -3W-100
Spenolithus strigosus
1410C-23X-2W- 87
Umbilicosphaera bramlettei
14
15
16
17
18
1410C-23X-5W- 87
Ellipsolithus sp.
1410B 27-2W-127
Neocrepidolithus grandiculus
1410B-20X-5W-40
Campilosphaera
1410B -20X-5W- 40
Markalius inversus
1410C-19X-4W- 67
Lophodolithus mochlophorus

Plate 2.5

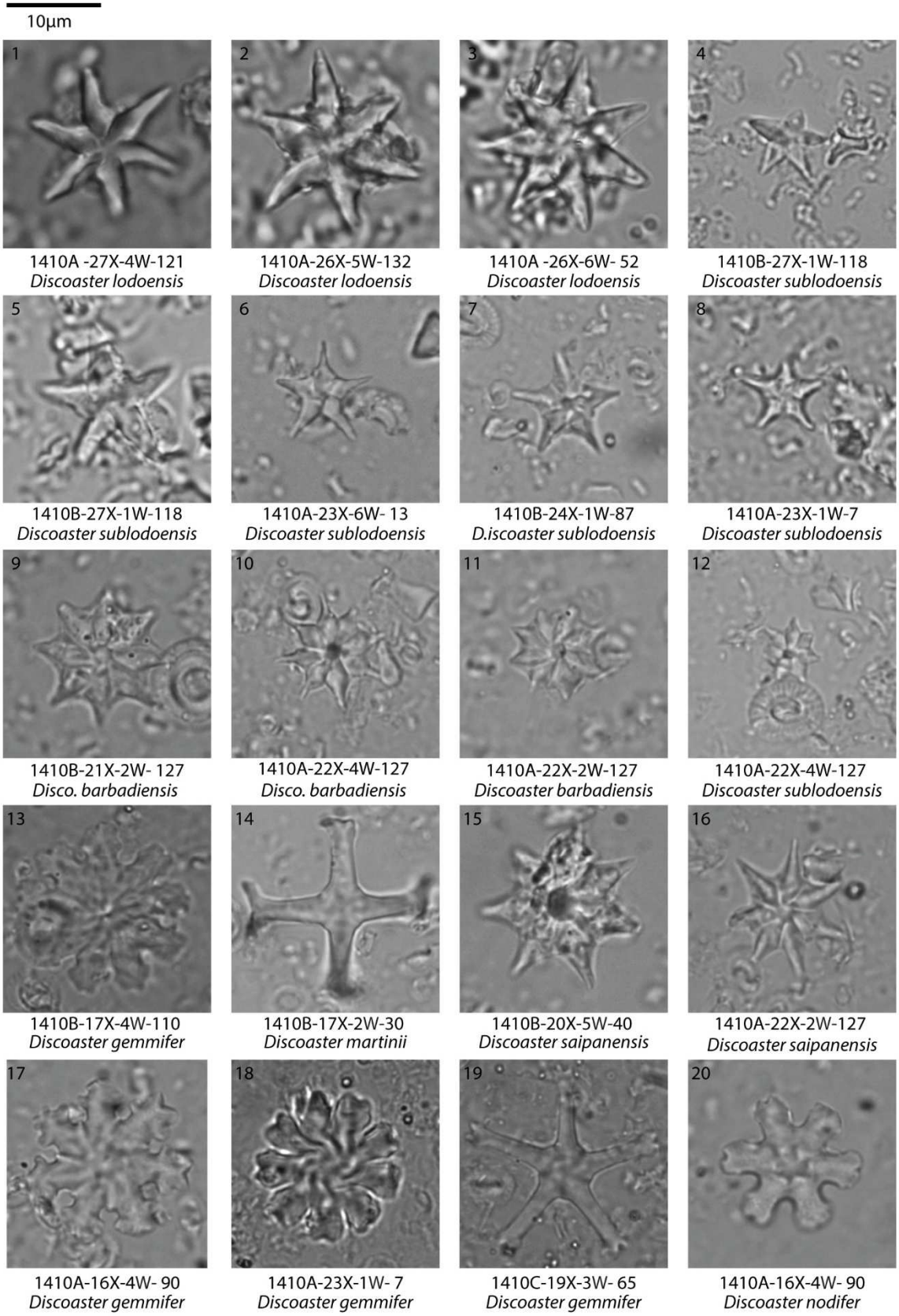
10µm
1
1410A -27X-4W-121
Discoaster lodoensis
2
1410A-26X-5W-132
Discoaster lodoensis
3
1410A -26X-6W- 52
Discoaster lodoensis
4
1410B-27X-1W-118
Discoaster sublodoensis
5
1410B-27X-1W-118
Discoaster sublodoensis
6
1410A-23X-6W- 13
Discoaster sublodoensis
7
1410B-24X-1W-87
D.iscoaster sublodoensis
8
1410A-23X-1W-7
Discoaster sublodoensis
9
1410B-21X-2W- 127
Disco. barbadiensis
10
1410A-22X-4W-127
Disco. barbadiensis
11
1410A-22X-2W-127
Discoaster barbadiensis
12
1410A-22X-4W-127
Discoaster sublodoensis
13
1410B-17X-4W-110
Discoaster gemmifer
14
1410B-17X-2W-30
Discoaster martinii
15
1410B-20X-5W-40
Discoaster saipanensis
16
1410A-22X-2W-127
Discoaster saipanensis
17
1410A-16X-4W- 90
Discoaster gemmifer
18
1410A-23X-1W- 7
Discoaster gemmifer
19
1410C-19X-3W- 65
Discoaster gemmifer
20
1410A-16X-4W- 90
Discoaster nodifer

Plate 2.6

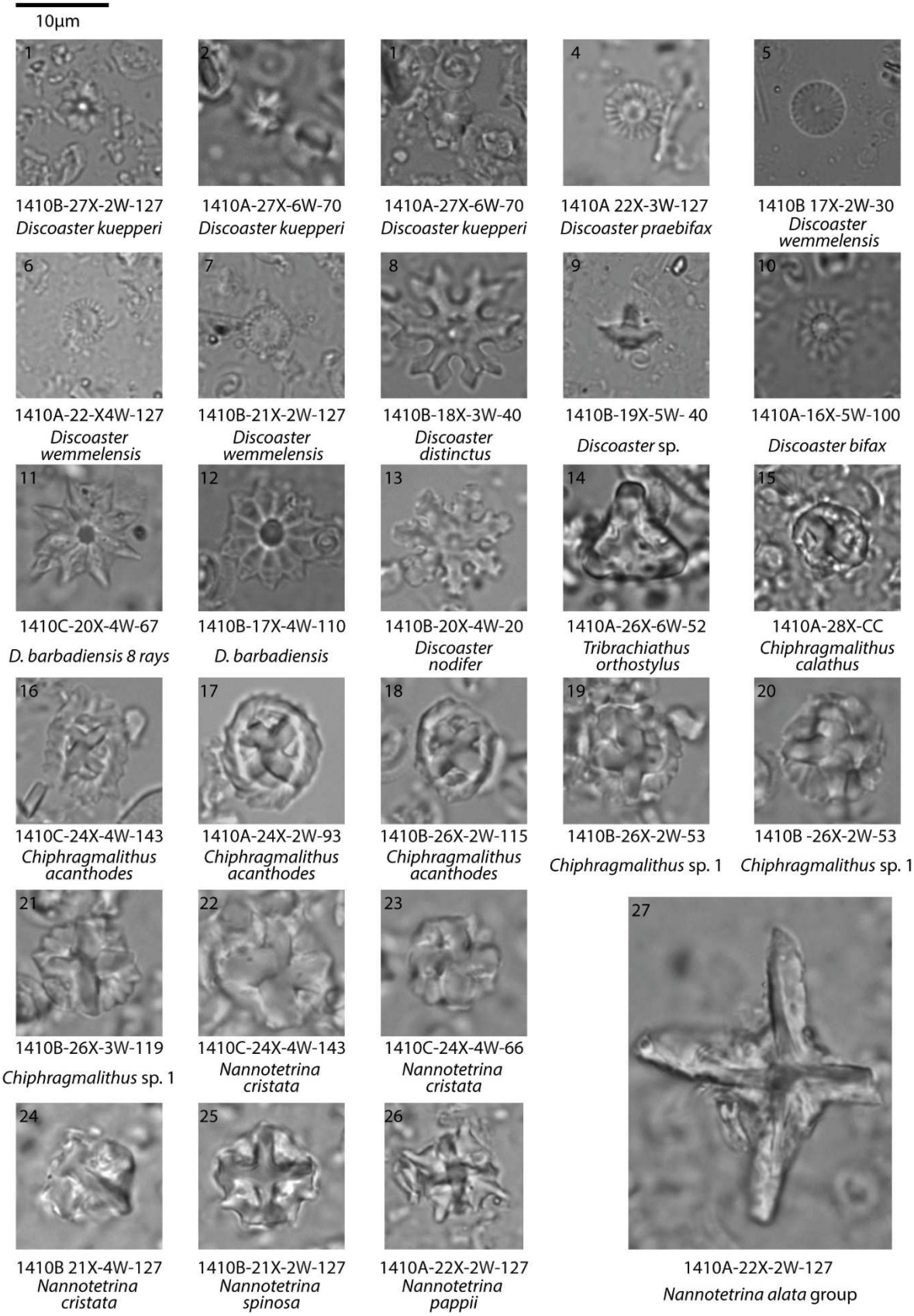
10µm
1
1410B-27X-2W-127
Discoaster kuepperi
2
1410A-27X-6W-70
Discoaster kuepperi
1
1410A-27X-6W-70
Discoaster kuepperi
4
1410A 22X-3W-127
Discoaster praebifax
5
1410B 17X-2W-30
Discoaster wemmelensis
6
1410A-22-X4W-127
Discoaster wemmelensis
7
1410B-21X-2W-127
Discoaster wemmelensis
8
1410B-18X-3W-40
Discoaster distinctus
9
1410B-19X-5W- 40
Discoaster sp.
10
1410A-16X-5W-100
Discoaster bifax
11
1410C-20X-4W-67
D. barbadiensis 8 rays
12
1410B-17X-4W-110
D. barbadiensis
13
1410B-20X-4W-20
Discoaster nodifer
14
1410A-26X-6W-52
Tribrachiathus orthostylus
15
1410A-28X-CC
Chiphragmalithus calathus
16
1410C-24X-4W-143
Chiphragmalithus acanthodes
17
1410A-24X-2W-93
Chiphragmalithus acanthodes
18
1410B-26X-2W-115
Chiphragmalithus acanthodes
19
1410B-26X-2W-53
Chiphragmalithus sp. 1
20
1410B -26X-2W-53
Chiphragmalithus sp. 1
21
1410B-26X-3W-119
Chiphragmalithus sp. 1
22
1410C-24X-4W-143
Nannotetrina cristata
23
1410C-24X-4W-66
Nannotetrina cristata
24
1410B 21X-4W-127
Nannotetrina cristata
25
1410B-21X-2W-127
Nannotetrina spinosa
26
1410A-22X-2W-127
Nannotetrina pappii
27
1410A-22X-2W-127
Nannotetrina alata group

Plate 2.7

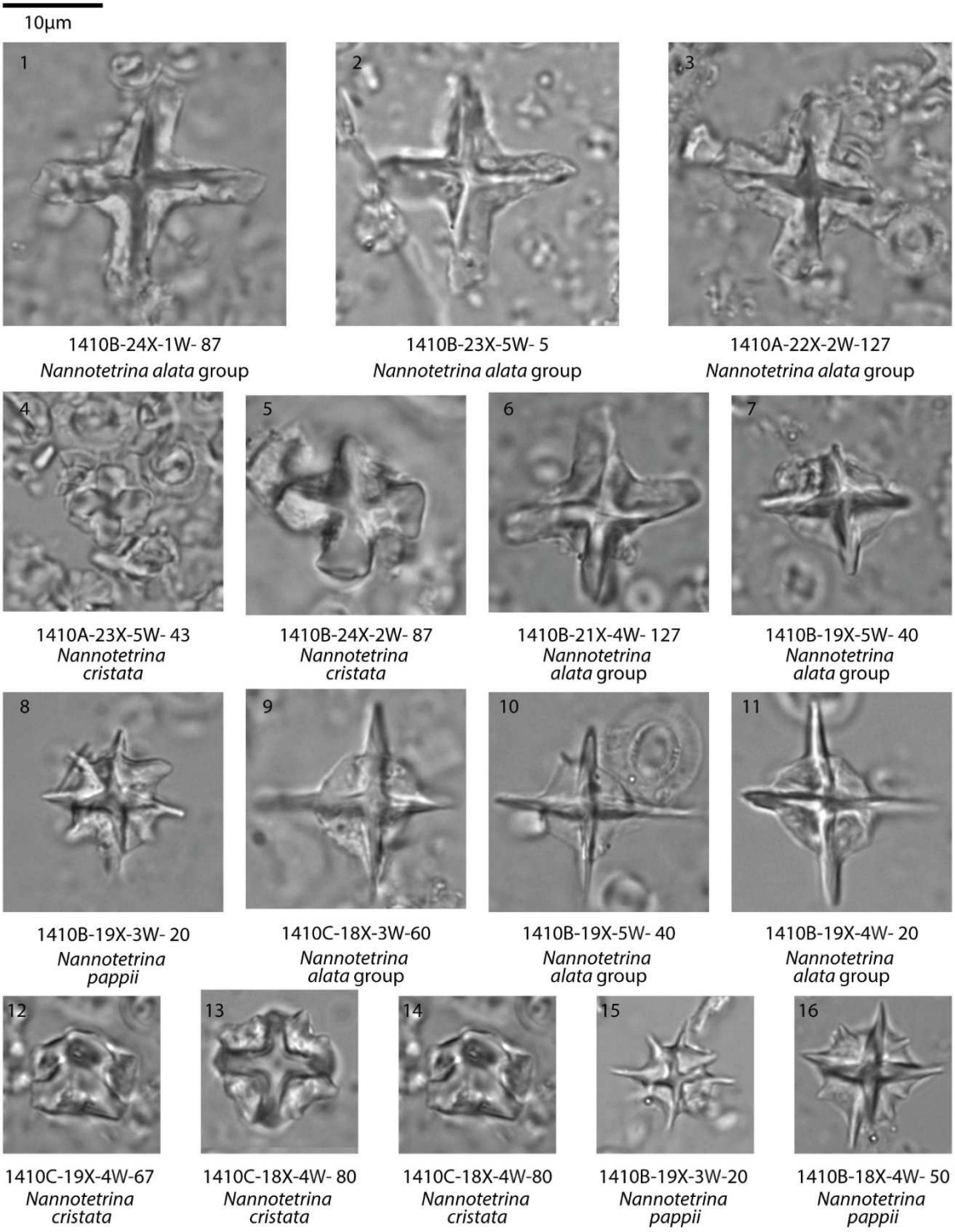
10µm
1
1410B-24X-1W- 87
Nannotetrina alata group
2
1410B-23X-5W- 5
Nannotetrina alata group
3
1410A-22X-2W-127
Nannotetrina alata group
4
1410A-23X-5W- 43
Nannotetrina cristata
5
1410B-24X-2W- 87
Nannotetrina cristata
6
1410B-21X-4W- 127
Nannotetrina alata group
7
1410B-19X-5W- 40
Nannotetrina alata group
8
1410B-19X-3W- 20
Nannotetrina pappii
9
1410C-18X-3W-60
Nannotetrina alata group
10
1410B-19X-5W- 40
Nannotetrina alata group
11
1410B-19X-4W- 20
Nannotetrina alata group
12
1410C-19X-4W-67
Nannotetrina cristata
13
1410C-18X-4W- 80
Nannotetrina cristata
14
1410C-18X-4W-80
Nannotetrina cristata
15
1410B-19X-3W-20
Nannotetrina pappii
16
1410B-18X-4W- 50
Nannotetrina pappii

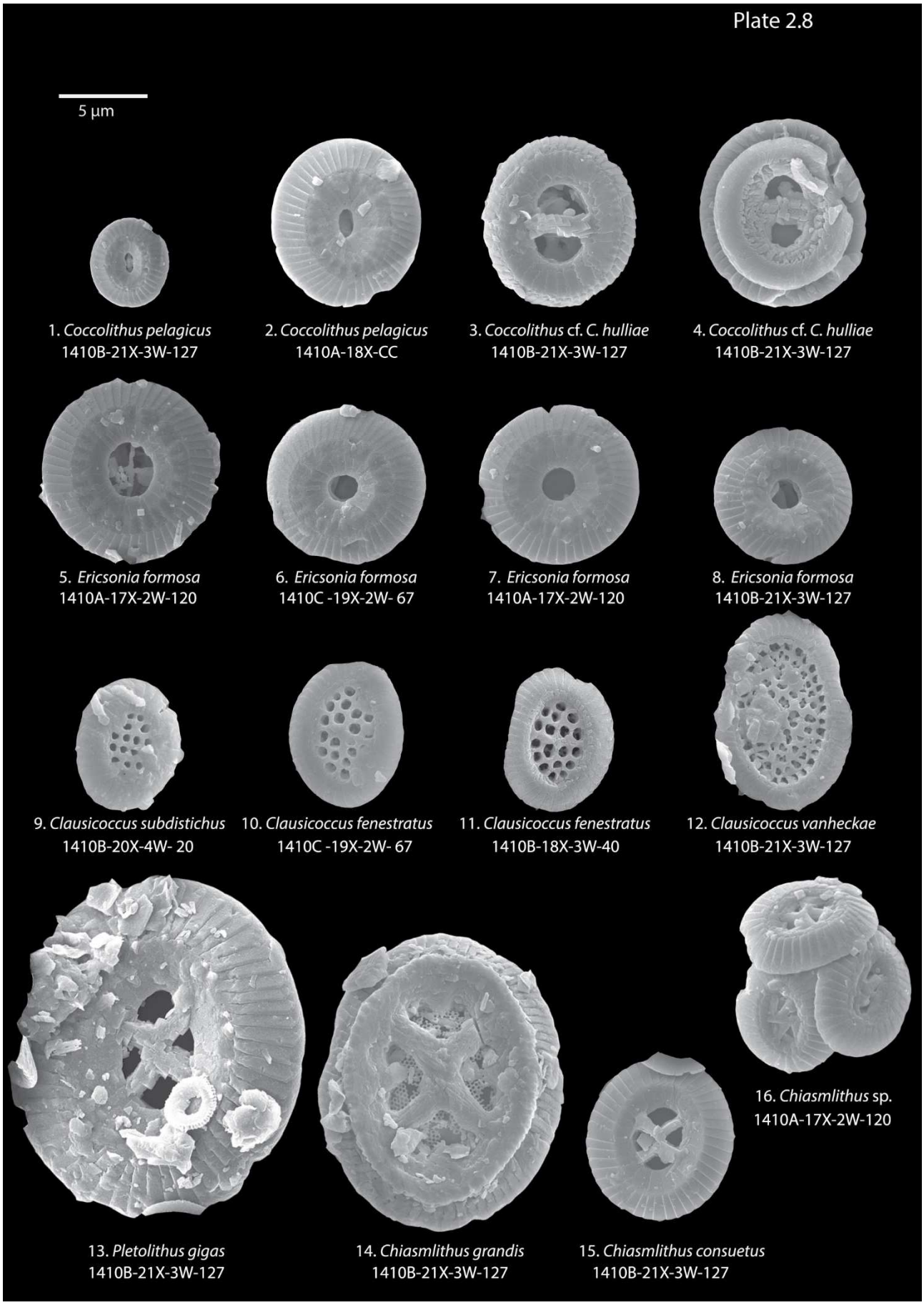
Plate 2.8
5 µm
1. Coccolithus pelagicus
1410B-21X-3W-127
2. Coccolithus pelagicus
1410A-18X-CC
3. Coccolithus cf. C. hulliae
1410B-21X-3W-127
4. Coccolithus cf. C. hulliae
1410B-21X-3W-127
5. Ericsonia formosa
1410A-17X-2W-120
6. Ericsonia formosa
1410C -19X-2W- 67
7. Ericsonia formosa
1410A-17X-2W-120
8. Ericsonia formosa
1410B-21X-3W-127
9. Clausicoccus subdistichus
1410B-20X-4W- 20
10. Clausicoccus fenestratus
1410C -19X-2W- 67
11. Clausicoccus fenestratus
1410B-18X-3W-40
12. Clausicoccus vanheckae
1410B-21X-3W-127
16. Chiasmlithus sp.
1410A-17X-2W-120
13. Pletolithus gigas
1410B-21X-3W-127
14. Chiasmlithus grandis
1410B-21X-3W-127
15. Chiasmlithus consuetus
1410B-21X-3W-127

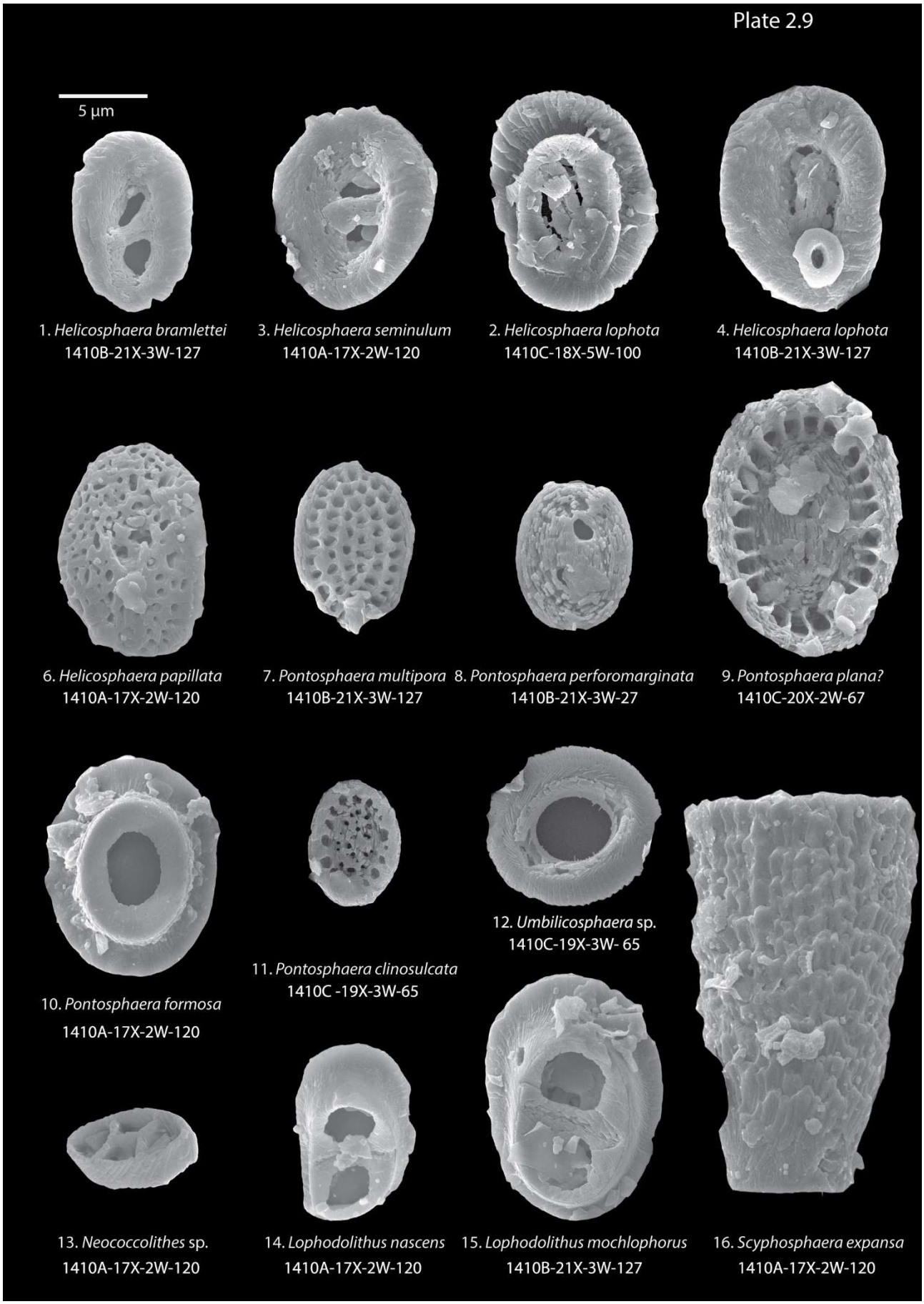
Plate 2.9
5 µm
1. Helicosphaera bramlettei
1410B-21X-3W-127
3. Helicosphaera seminulum
1410A-17X-2W-120
2. Helicosphaera lophota
1410C-18X-5W-100
4. Helicosphaera lophota
1410B-21X-3W-127
6. Helicosphaera papillata
1410A-17X-2W-120
7. Pontosphaera multipora
1410B-21X-3W-127
8. Pontosphaera perforomarginata
1410B-21X-3W-27
9. Pontosphaera plana?
1410C-20X-2W-67
10. Pontosphaera formosa
1410A-17X-2W-120
11. Pontosphaera clinosulcata
1410C -19X-3W-65
12. Umbilicosphaera sp.
1410C-19X-3W- 65
13. Neococcolithes sp.
1410A-17X-2W-120
14. Lophodolithus nascens
1410A-17X-2W-120
15. Lophodolithus mochlophorus
1410B-21X-3W-127
16. Scyphosphaera expansa
1410A-17X-2W-120

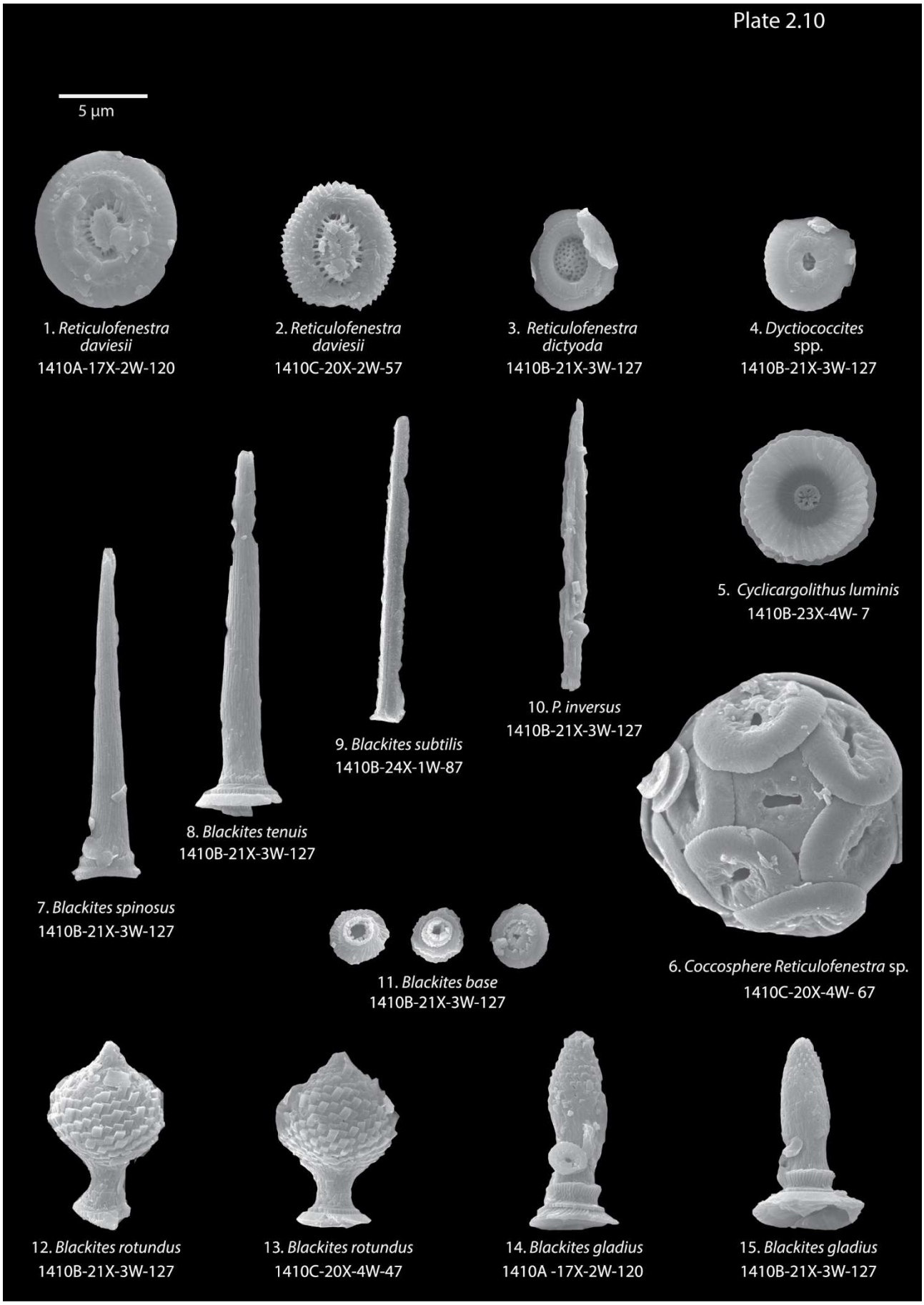
Plate 2.10
5 µm
1. Reticulofenestra daviesii
1410A-17X-2W-120
2. Reticulofenestra daviesii
1410C-20X-2W-57
3. Reticulofenestra dictyoda
1410B-21X-3W-127
4. Dyctiococcites spp.
1410B-21X-3W-127
5. Cyclicargolithus luminis
1410B-23X-4W- 7
6. Coccosphere Reticulofenestra sp.
1410C-20X-4W- 67
7. Blackites spinosus
1410B-21X-3W-127
8. Blackites tenuis
1410B-21X-3W-127
9. Blackites subtilis
1410B-24X-1W-87
10. P. inversus
1410B-21X-3W-127
11. Blackites base
1410B-21X-3W-127
12. Blackites rotundus
1410B-21X-3W-127
13. Blackites rotundus
1410C-20X-4W-47
14. Blackites gladius
1410A -17X-2W-120
15. Blackites gladius
1410B-21X-3W-127

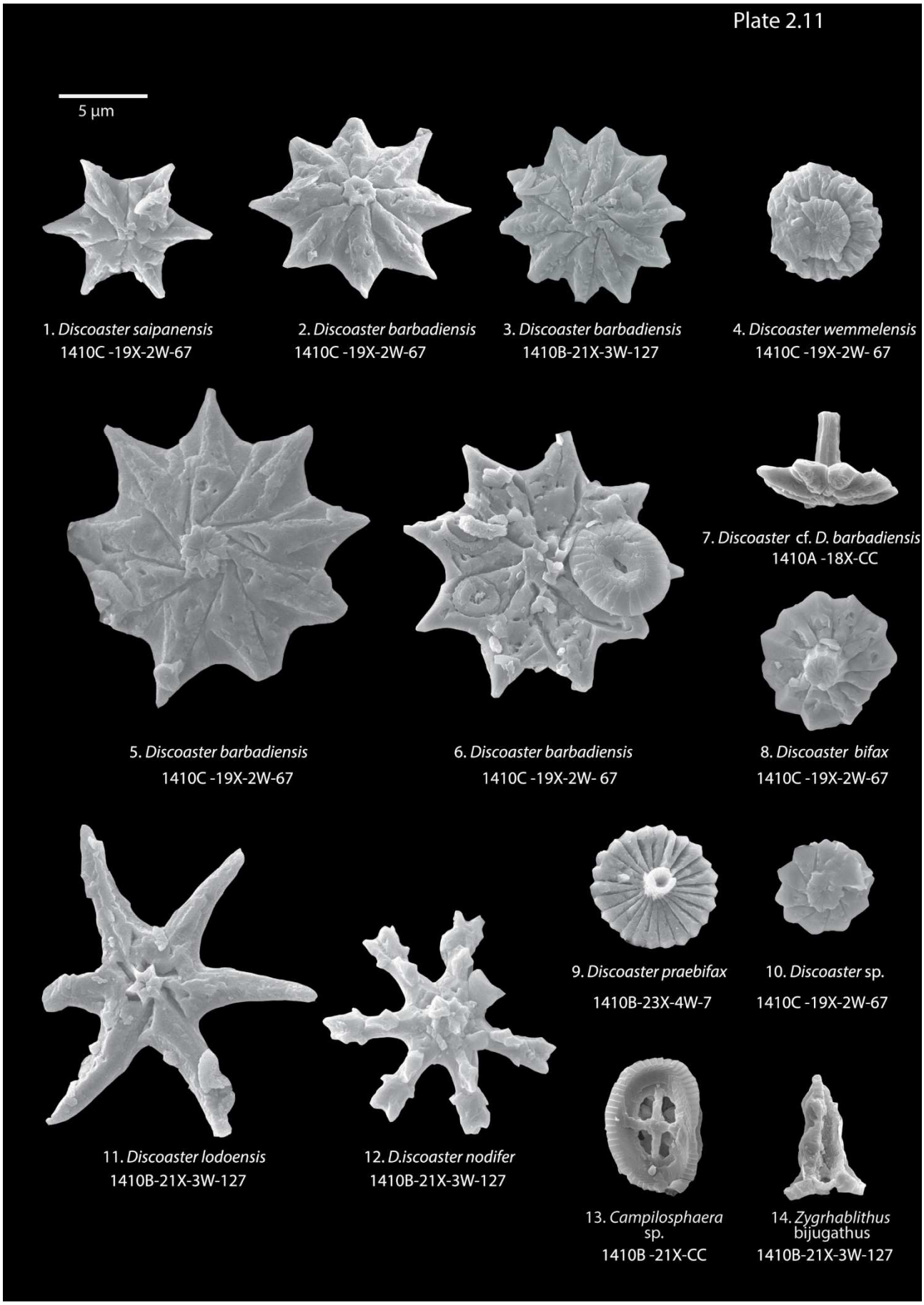
Plate 2.11
5 µm
1. Discoaster saipanensis
1410C -19X-2W-67
2. Discoaster barbadiensis
1410C -19X-2W-67
3. Discoaster barbadiensis
1410B-21X-3W-127
4. Discoaster wemmelensis
1410C -19X-2W- 67
7. Discoaster cf. D. barbadiensis
1410A -18X-CC
5. Discoaster barbadiensis
1410C -19X-2W-67
6. Discoaster barbadiensis
1410C -19X-2W- 67
8. Discoaster bifax
1410C -19X-2W-67
9. Discoaster praebifax
1410B-23X-4W-7
10. Discoaster sp.
1410C -19X-2W-67
11. Discoaster lodoensis
1410B-21X-3W-127
12. D.iscoaster nodifer
1410B-21X-3W-127
13. Campilosphaera sp.
1410B -21X-CC
14. Zygrhablithus bijugathus
1410B-21X-3W-127

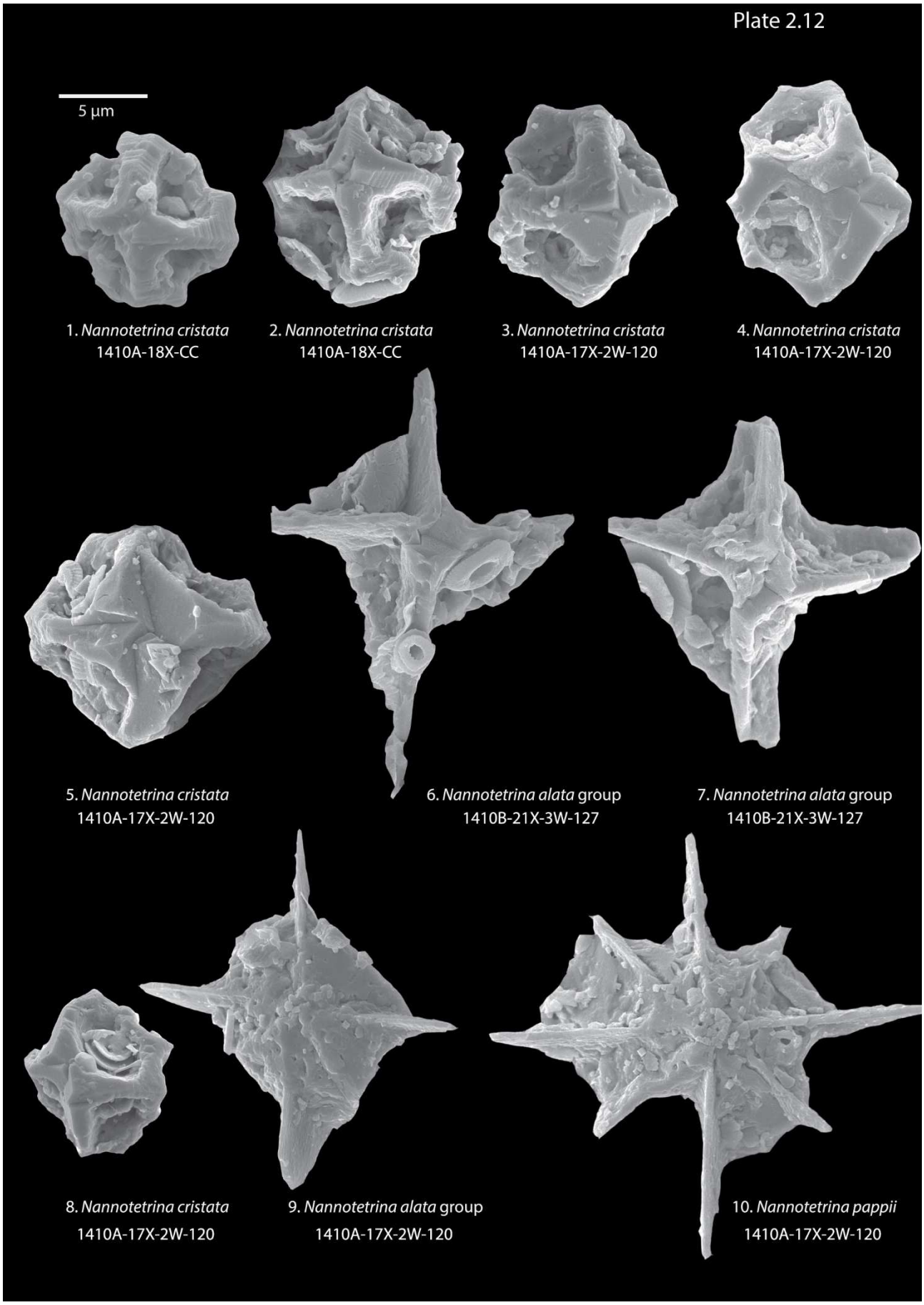
Plate 2.12
5 µm
1. Nannotetrina cristata
1410A-18X-CC
2. Nannotetrina cristata
1410A-18X-CC
3. Nannotetrina cristata
1410A-17X-2W-120
4. Nannotetrina cristata
1410A-17X-2W-120
5. Nannotetrina cristata
1410A-17X-2W-120
6. Nannotetrina alata group
1410B-21X-3W-127
7. Nannotetrina alata group
1410B-21X-3W-127
8. Nannotetrina cristata
1410A-17X-2W-120
9. Nannotetrina alata group
1410A-17X-2W-120
10. Nannotetrina pappii
1410A-17X-2W-120

Chapter 3

A reassessment of middle Eocene large coccolithaceans: biostratigraphic implications and paleoclimatic clues

Abstract

The combined light microscope-scanning electron microscope (SEM) study of exceptionally well preserved calcareous nannofossil assemblages from clay-rich middle Eocene sediments recovered at Site U1410 (NW Atlantic Ocean) has enabled us to document a new evolutionary lineage among Coccolithus-like placoliths with a well-developed cross or x-shaped structure in the central area. Based on our observations, we describe a new genus *Pletolithus*, a new species *Pletolithus giganteus* and four new combinations (*Pletolithus opdykei, Pletolithus staurion, Pletolithus mutatus* and *Pletolithus gigas*). The distinctive ultra-structures of different morphotypes and the presence of transitional morphologies suggest that *Pletolithus* evolved from a morphological variant of Coccolithus. Intriguingly this lineage appeared during an interval of remarkable change in the deep current activities in the North Atlantic as well as of carbon isotope shifts. The gradual morphologic evolution among coccolithaceans is initially characterized by the appearance of a fine and delicate structure in the central area which is followed by an increase in size of the primitive structure that also becomes more massive. Morphometric measurements on *P. gigas* and on the morphologically related *P. giganteus*, provides evidence for the presence of two distinct populations allowing for an objective differentiation of these two species, which in turn provides unambiguous taxonomic definition for the marker species *P. gigas*. These data improve the stability of middle Eocene biostratigraphy and show the iterative nature of the development of these peculiar structures in the central area that have occurred repeatedly in the early Paleogene and Mesozoic.

3.1 INTRODUCTION

The early-middle Eocene transition represents a major shift in the Earth's climate evolution. The long-term warming phase of the Paleocene – early Eocene peaked during the Early Eocene Climatic Optimum (EECO; ~52-50 Ma) and was followed by the middle-late Eocene cooling phase, which eventually led to the onset of large scale glaciations in Antarctica by the earliest Oligocene. Our knowledge of these Paleogene temperature trends is principally based on multi-site benthic foraminifera ($\delta^{18}O$) records (Zachos et al., 2001, 2008; Cramer et al., 2009). The post-EECO temperature decline is a prominent feature recorded as an increase (+3 ‰) in the deep-sea foraminiferal stable oxygen ($\delta^{18}O$) values, but it is also suggested by other proxies such as the benthic foraminiferal Mg/Ca ratio (Lear et al., 2000)) and for surface ocean by TEX_{86} (Bijl et al., 2009, 2013; Hollis et al., 2012; Inglis et al., 2015). This trend is associated with a decline in atmospheric greenhouse gases (Pagani et al., 2005; Zachos et al., 2008; Cramwinckel et al., 2018) and tectonic changes in the southern hemisphere (Lawver and Gahan, 2003; Lagabriellle et al., 2009). The long-term cooling was accompanied by notable ecological changes in marine biota, with a significant

diversity loss in calcareous nannoplankton assemblages from the middle Eocene (Bown et al., 2004, Bown, 2005b).

Calcareous nannoplankton are particularly relevant when trying to understand the marine dynamics because this group together with diatoms has been the main primary producer lying at the basis of trophic levels and has played a fundamental role in the organic (biomass) and inorganic ($CaCO_3$ test) carbon cycle as well as in albedo feedbacks (Tyrrell and Young, 2008). Their abundance, wide biogeographic distribution and rapid evolutionary rates make them the perfect tool to investigate short- and long-term modifications of the plankton community but also of the Earth's evolution through time.

This is important if considering that there is still the need to acquire more data of the Eocene interval to reconstruct a consistent scenario especially when considering that while the benthic foraminifera data suggest a global post-EECO cooling, planktic foraminifera records indicate, at least at some sites, that the cooling of sea surface waters might not be a worldwide feature. Cooling is well documented at mid to high latitudes in the Southern hemisphere but the post-EECO surface water temperature decline seems to be less evident at the low latitudes and in the northern hemisphere (Bornemann et al., 2016). However, this proposed scenario remains unresolved if recent data from the tropical Atlantic Ocean are compared with other available records from low latitudes (Cramwinckel et al., 2018).

IODP Site U1410 in the northwest Atlantic Ocean (Norris et al., 2014) provides a complete post-EECO record through to the early middle Eocene. In the North Atlantic, this interval was characterized by a major change in the sedimentary regime related to the onset of drift sedimentation (Norris et al., 2014; Bornemann et al., 2016; Boyle et al., 2017; Coxall et al., 2018). This site is also well placed to acquire more data that can provide evidence for either a global sea surface cooling or a patchy characterization of the long-term cooling trend. Reviews of Paleogene calcareous nannofossil evolution (Aubry, 1992; 1998; Bown et al, 2004) have highlighted a remarkable decrease of species richness through the middle to late Eocene in the calcareous phytoplankton assemblages but the multimillion year scale resolution adopted does not capture the detailed pattern of these important changes, as well as the possible cause-effect relationships between evolutionary patterns and climate. The understanding of the modifications occurred during the early-middle Eocene is really crucial to propose a global scenario of this still little known and under studied interval, that lies exactly in between two major climate extremes, the Paleocene Eocene Thermal Maximum and the Oligocene Antarctic glaciation. For this reason, it is important to produce very highly-resolved datasets that give an overview of the changes in the assemblages but, more importantly will provide detailed patterns of the major evolutionary lineages among calcareous nannofossils.

Calcareous nannofossil data, coupled with records of stable isotopes and carbonate content from Site U1410, can be used to investigate the early phase of the long-term climatic disruption and test whether this was a trigger for evolutionary response in calcareous nannofossil assemblages. Here we specifically focus on the development of a new lineage among large middle Eocene coccolithaceans, preceding the appearance of the zonal species *Coccolithus gigas* (Bown & Newsam, 2017). Over the past years, a very broad interpretation of the original description of this species and the rare availability of material containing morphologically-related middle Eocene coccolithaceans have increased the uncertainty of this the species identification but also, and more importantly, on the evolution of a plexus of large *Coccolithus*-like species across the early-middle Eocene. The expanded middle Eocene succession of clay rich sediments from Site U1410 with exceptionally well-preserved calcareous nannofossils is thus the ideal archive to document the evolutionary history of this important lineage, which emerged concurrently with the onset of drift sedimentation in the North Atlantic.

Reassessment of the *C. gigas* group will provide a more rigorous and, hopefully, more stable taxonomy but will also improve and stabilise the current biozonation schemes based on calcareous nannofossils (Martini, 1971, Okada and Bukry, 1980; Agnini et al., 2014). In addition, it will improve our understanding of the overall evolution of this group and its relationship with climate changes. In this regard, the middle Eocene is a relatively poorly-known interval of Earth history, lacking identifiable extreme events and so detailed palaeontological records. The bonus of this work is that this is the first high-resolution quantitative dataset that covers this interval of time that represents a transition phase as the Earth system switched from greenhouse to icehouse climate mode.

3.2 MATERIALS AND METHODS

3.2.1 IODP Site U1410-Geological Setting

Integrated Ocean Drilling Program (IODP) Site U1410 is located in the Northwest Atlantic on the Southeast Newfoundland Ridge (Latitude: 41°19.6987 N; Longitude: 49°10.1995 W; Figure 3.1). During the Eocene, sediments were deposited at an estimated paleo-water depth of 2950 m, well above the average CCD for the interval. The lower Eocene sediments consists of pinkish-white nannofossil chalk (Unit IV, Norris et al., 2014), whereas middle Eocene successions were deposited as clay-rich drift sediments. This unit is primarily composed of greenish-gray nannofossil ooze with some bands (10-25 cm) of light gray to white nannofossil ooze (Unit III, Norris et al., 2014). These sequences are characterized by high accumulation rates across the middle Eocene (~2.2 cm/k.y.) and contain exceptionally well preserved calcareous nannofossils (Norris et al., 2014).

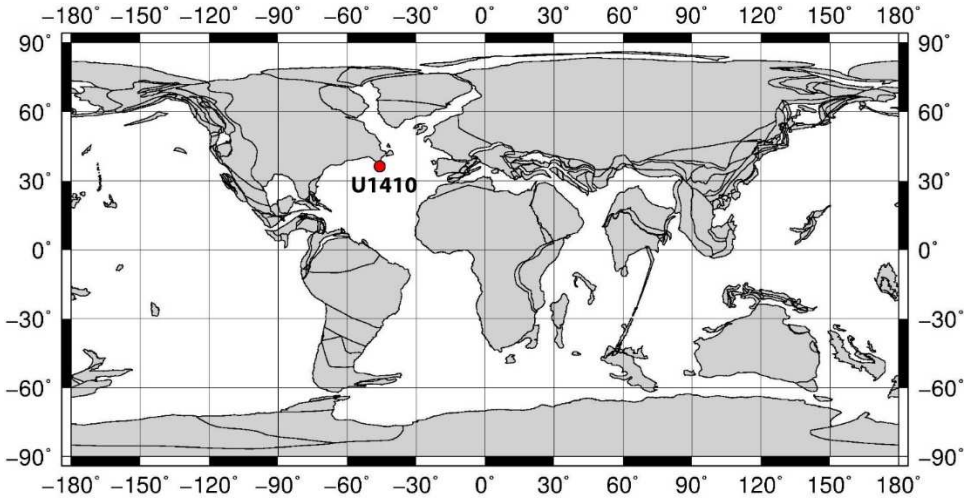

Figure 3.1: Paleo-geographic map of the middle Eocene (45 Ma) showing the location of IODP Site U1410 (www.odsn.de).

3.2.2 Light microscope samples preparation and observations techniques

The composite section for Site U1410, modified after Vahlenkamp et al. (2018) was studied from 294.69 to 147.23 revised meter composite depth (rmcd). 226 samples were prepared as smear slides with standard methods (Bown & Young, 1998) for calcareous nannofossils analysis using transmitted-light microscopy (x1250 magnification).

The position of calcareous nannofossil biohorizons are from Cappelli et al. (in prep). The biostratigraphic events and assemblage patterns of taxa of interest of this study are based on standard counting method (modified after Backman and Shackleton, 1983; Agnini et al., 2014), which is counting the number of specimens of selected taxa in a pre-fixed area of 1or 2 mm^2 (normalized to 1 mm^2). Following Agnini et al. (2014), biostratigraphic events are termed as Base (B), Top (T), Bc (Base Common) to describe stratigraphic lowest, highest and lowest continuous/ common occurrence, respectively. The biostratigraphic schemes adopted are the traditional biozonations of Martini (1971), Okada and Bukry (1980) and the one recently proposed by Agnini et al. (2014). Calcareous nannofossils were identified to species level following taxonomic concepts of various authors (Perch-Nielsen, 1985; Bown, 2005a; Bown & Dunkley Jones et al. 2006; Agnini et al., 2014; Bown & Newsam, 2017) but detailed taxonomic descriptions of forms belonging to the *Coccolithus gigas* group are given in order to provide an unambiguous taxonomy.

Morphometric measurements of specimens belonging to the species *Pletolithus gigas* and *Pletolithus giganteus* (see taxonomic notes) were performed on a total of 23 samples. Well-preserved specimens (80) were digitally acquired using an Invenio 5D II digital camera and measured using the DeltaPix InSight software. Different biometric parameters were determined for each specimen: size (i.e., placolith length, placolith width and placolith area), geometry of the central area (i.e., central-opening

length, central opening width and central opening area) and length of the central area crossbars. Morphometric data were then analyzed using PAST software (Hammer et al., 2001).

3.2.3 Sample preparation and observation techniques for scanning electron microscope (SEM) analysis

Selected samples were studied by scanning electron microscopy using a JEOL Digital JSM-6480LV SEM at University College of London (UCL). In order to observe the same specimens in both light microscope (LM) and SEM, several samples were prepared following the technique proposed by Gallagher (1988). This technique was implemented by printing a mesh (Figure 3.2) on round cover slips (12 mm diameter). A few drops of sample solution are put on the circular cover slip and are allowed to dry on a hot plate. For the LM analysis, the cover slip with the sediment is placed on a rectangular slide (size) and a few drops of distilled water are added in order to allow the penetration of transmitted light. Distilled water was used instead of methanol, as originally suggested by Gallagher (1988), because the use of the latter one is now discouraged for health reasons. Finally, we covered the circular cover slip with a rectangular cover slip (24X24 mm), immobilized with an adhesive (e.g., tape or blue-tack). In LM, the positions of selected specimens were recorded with reference to the mesh notation. Images of the mesh with different magnifications were taken and used to identify the exact position of the study specimen. After LM analysis, the rectangular cover slip is carefully removed and the circular cover slip is placed on the hot plate where it is allowed to dry at low temperature. For SEM study the circular cover slip is mounted on a SEM Stub using a carbon adhesive and coated with a layer of gold. In SEM, the ink of the mesh is still visible and the specimen analysed at LM can be identified and then photographed.

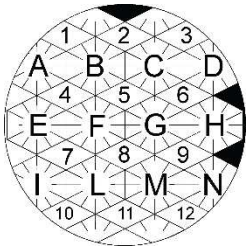

Figure 3.2: Example of the mesh printed in ink on 12mm diameter cover slip.

3.3 TAXONOMIC BACKGROUND

Recently, the coccolithacean coccoliths were divided into three informal groups by Bown and Dunkley Jones (2012,): *Coccolithus pelagicus* Group, *Chiasmolithus-Cruciplacolithus* Group and *Clausicoccus* Group. The first two groups are the focus of this work. Most Paleogene coccolithacean placoliths with crossbars in the central area are traditionally ascribed to the genera *Cruciplacolithus, Chiasmolithus* and *Sullivania*, although the latter is not widely used. A number of previous studies

have analyzed the evolution of these genera, suggesting ancestor-descendant relationships between *Cruciplacolithus* and *Chiasmolithus*, and different phylogentic relationships among the different species (e.g., Gartner, 1970; Romein, 1979; Perch-Nielsen, 1985; Varol, 1992). The original descriptions of the genera *Cruciplacolithus* (Hay and Mohler, 1967) and *Chiasmolithus* (Hay, Mohler and Wade, 1966) used the orientation of the crossbars with respect to the placolith axes. *Cruciplacolithus* includes all species that have a central cross aligned with the axes of the placolith and *Chiasmolithus* includes species with a X-shaped structure, composed by two bars in the central area.

In 1970, Gartner performed the first detailed descriptive study on species ascribable to *Chiasmolithus* and based on ultrastructure of the central area crossbars observed in LM and SEM he separated *Chiasmolithus* species into two informal subgroups. Similarly, Varol (1992) used both rim and crossbar structure to formally separate different species of *Chiasmolithus* and erected a new genus, *Sullivania.* According to the original definition, *Sullivania* differs from *Chiasmolithus* by having a single distally exposed tube cycle, simpler crossbar construction, and no central mesh. In addition, *Sullivania* differs from *Cruciplacolithus* by having an X-shaped structure instead of a cross. Over the past years, the idea that species with a cross structure in the central area and belonging to the coccolithaceans can be subdivided in two different subgroups (i.e., *Chiasmolithus/Sulliviana* and *Cruciplacolithus*) solely based on orientation of the bars present in the central area has been largely applied in the Paleocene but also for "morphotypes" that appeared during the middle Eocene. Recently, several middle Eocene coccolithaceans, traditionally ascribed to genera *Chiasmolithus* or *Cruciplacolithus*, were reassigned to genus *Coccolithus* (Bown, 2005a; Bown & Newsam, 2017) and included in the sub-generic informal group of *Coccolithus gigas* (e.g., *C. gigas, C. staurion, C. mutatus).*

A broad interpretation of the original description of these middle Eocene species (e.g. *C. gigas*), their relatively rare occurrence in the fossil record (e.g., C. *staurion* and C. *mutatus*) and morphological modification produced by diagenetic modifications has resulted in different species concepts among different authors. A brief overview on the taxonomy of these species is thus needed and reported in the following.

Coccolithus gigas was described by Bramlette & Sullivan (1961) as "unusually large placoliths (19-25 µm) with a central area transversely spanned by an X-shaped structure". The description also mentioned the presence of fine teeth along the inner margin of the slope, however, this morphological character is not considered distinctive for the species. This species has been assigned to different genera by different authors. In particular, Hay et al. (1966) ascribed the species *gigas* to the genus *Chiasmolithus* based on the presence of the X-shaped structure in the central area, while Varol (1992)

placed it in the genus *Sulliviana.* Bown and Newsam (2017) recently reassigned this species to the genus *Coccolithus.* The latter authors also emended the species concept of *C. gigas* by placing limit of at least 30 ° on the angle made by the long bar with the longitudinal axis of the placolith. Different ancestors have been proposed for this species: *Chiasmolithus solitus* by Romein (1979), *Chiasmolithus californicus* by Perch-Nielsen (1985) and *Sulliviana minima* by Varol (1992).

The presence of *C. gigas*-like specimens with asymmetric crossbars was first described in Tanzanian material by Pearson et al., (2004) and Bown (2005) and subsequently in the North Atlantic by Bown and Newsam (2017). These latter authors described *Coccolithus* cf. *C. gigas* as having robust structure in the central area and it differs from *C. gigas s.s.* by having a rotated (up to 29 °) to axial crossbars instead of a nearly diagonal X shaped structure.

At the same time as Bramlette & Sulllivan (1961) first described *C. gigas*, they also proposed a species called *Coccolithus staurion.* This taxon was described as a large placolith (usually 12-15 µm in length, which means that there is no overlap in size with *C. gigas*) with a small central area spanned by a very small central cross that can be obscure in some specimens. This species has been ascribed to several different genera: *Birkelundia* by Perch-Nilsen (1971) based on the structure of the proximal shield; *Cruciplacolithus* by Varol (1992) because of the central axial cross structure; and *Coccolithus* by Bown (2005a) because of the *Coccolithus*-type rim.

Coccolithus opdykei was recently described by Bown and Newsam (2017) from sediments retrieved during IODP Exp. 342 (North Atlantic Ocean). According to these authors, this taxon is very similar to *C. staurion* but smaller, ranging from 7 to12 µm in length. The central area is nearly filled by the central cross. *Coccolithus opdykei* and *C. staurion* are thus very similar to each other but are distinguished on size. In addition, *Ericsonia insolita* Perch-Nielsen (1971), is considered as synonym of the species *C. staurion* (Bown, 2005a).

Cruciplacolithus mutatus was firstly formalized by Perch-Nielsen (1971) and described as an elliptical to sub-circular placolith with an axial central cross structure. The author differentiates this species from *C. staurion* because of the wider central area, the shape of the cross is less regular and the structure of the distal shield is different. In the original description, the author refers to a sort of "seam" present in the distal shield of the placolith. Varol (1992) ascribed this species to the genus *Cruciplacolithus* and suggested a phylogentic link with the Paleocene species *Cruciplacolithus intermedius*. Lately, Bown (2005a) assigned this species to the genus *Coccolithus* because it has a Coccolithus-type rim structure, and in any case the extant species *Coccolithus pelagicus* is also know to form central area and transverse crossbars.

As an aside, when preservation is very good or exceptional, it appears from SEM observations that many fossil *Coccolithus pelagicus* coccoliths have very narrow, fragile axial crossbars that are not

visible in LM (Bown, 2010). These cross-bearing forms of *Coccolithus pelagicus* have been reported from the upper Paleocene/lower Eocene sediments of Tanzania (Bown, 2008) and from Oligocene and Miocene epochs (e.g., *C. tenuiforatus* Clocchiatti and Jerkovic, 1970). The uneven distribution of these morphotypes could thus be explained either as due to the rarity of the taxon or to the reiteration of the same morphotype occurring several times at different stratigraphic levels (iterative evolution).

3.4 RESULTS

3.4.1 Distribution patterns and taxonomy

Calcareous nannofossils are abundant throughout the study interval at Site 1410 and their preservation ranges from good to excellent, with small coccoliths and delicate structures (e.g., central area grills) usually present and well preserved. The extraordinary quality of preservation is explained by the clay-rich nature of the sediments, with the clay acting as a protection that prevents recrystallization and overgrowth, which commonly affect specimens in carbonate-rich deep sea oozes. The study interval ranges from Zone CP10 to Subzone CP13c of Okada & Bukry (1980) and from Zone CNE4 to Zone CNE12 of Agnini et al. (2014) (Cappelli et al., in prep.), based on the Base of *Discoaster lodoensis*, Top of *C. gigas*, and absence of common *Reticulofenestra umbilicus*. One important point to better understand the possible relationships among all the species belonging to the so-called *C. gigas* group is to precisely define their distribution patterns in order to reconstruct the relative stratigraphic relationships among the different taxa and hypothesize possible evolutionary lineages (Figure 3.3).

At Site U1410 the relatively large coccolithaceans, *Pletolithu mutatus, Pletolithus staurion* and the smaller variant *Pletolithus opdykei* (see taxonomic notes), first appear in the middle part of Zone CNE8. Specimens characterized by a wide central area spanned by delicate crossbars are ascribed to the species *P. mutatus.* The cross-shaped central structure can be aligned with the placolith axes or slightly rotated (Plate 3.1). These forms are very distinctive under light microscope, especially the thick tube-cyle margin that appears as a narrow orange ring in XPL. The bars forming the cross are delicately constructed and, despite the exceptional preservation, specimens with a broken or missing crossbars were observed. At SiteU140, *Pletolithus mutatus* displays a rare but nearly continuous presence throughout its stratigraphic range (Figure 3.4).

Pletolithus staurion is a species possibly related to *Pletolithus. gigas* (see taxonomic note), but is very rare and characterized by a sporadic distribution at Site U1410. This species has a narrow central area that is almost completely filled by robust crossbars (Plate 3.1). The same morphological features characterize *P. opdykei*, which by definition is characterized by a smaller size (Plate 3.1). For both

these taxa, the bars in the central area can be sometimes hard to recognize because of the small size of the crossbars and of the central area.

The new taxon, *Pletolithus giganteus* (see taxonomic note) was encountered from 215.54 rmcd. It comprises very large coccoliths (>16 µm) with robust asymmetric crossbars and a relatively wide central area. Bown & Newsam (2017), described a similar morphotype, referred to as *C.* cf. *gigas*, with central area crossbars rotated with respect to the placolith axes. The ultrastructure of the bars produces an axial extinction line along the bars (Plate 3.2). This is distinct from *Pletolithus gigas* which is characterized by robust diagonal cross bars (X-shaped) with the two bars set at an angle of less of 90°. The cross bars of *P. gigas* have an axial extinction lines, which appears as a roof-like structure in XPL, this peculiar feature is due to the arrangement of the tiny single elements of the bars (Plate. 3.2).

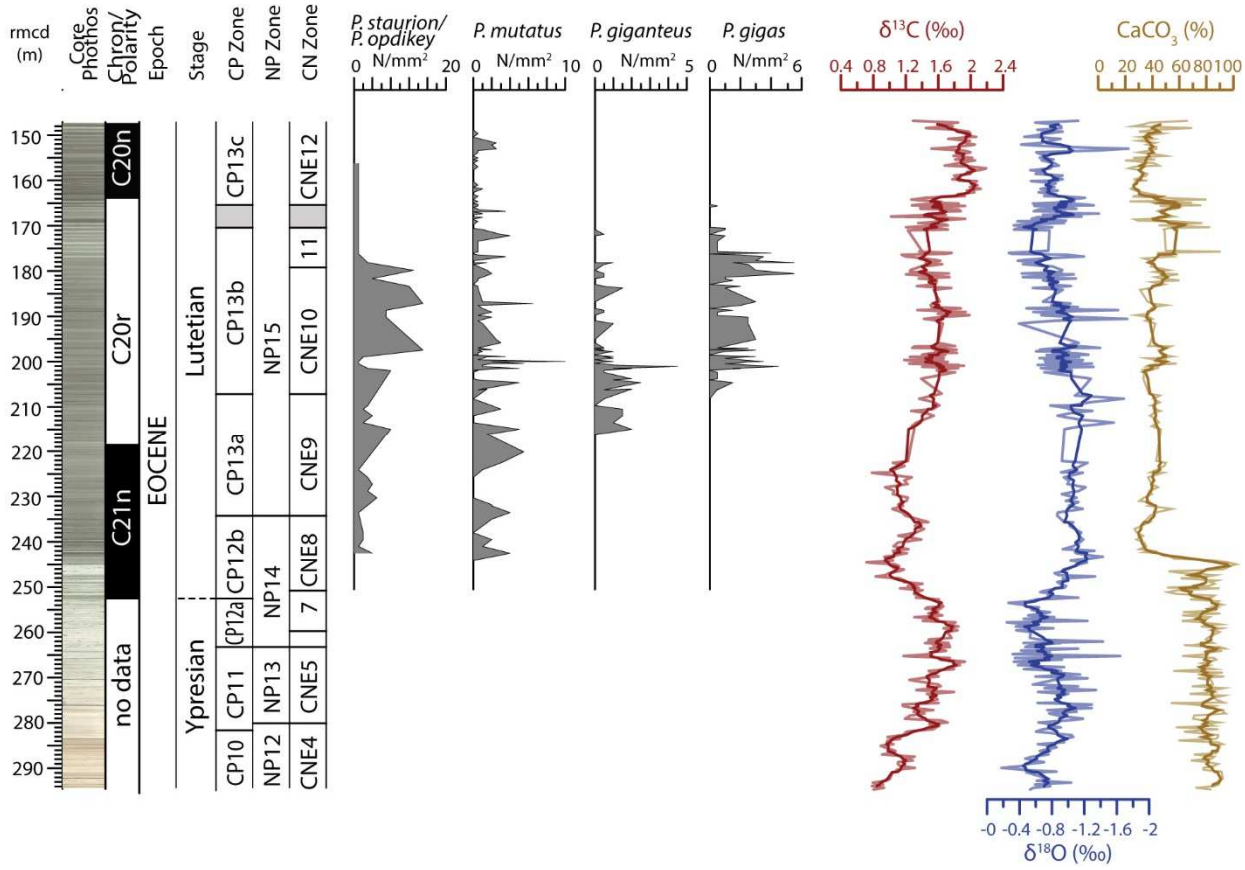

Figure 3.3: Calcareous nannofossil biostratigraphy (A, Okada & Bukry 1980; B, Martini 1970; C, Agnini et al., 2014), abundance pattern of species belonging to the studied lineage and records of bulk carbonate $\delta^{13}C$, $\delta^{18}O$ and $CaCO_3$ content. On the left are reported the informal intervals used for the description of the geochemical data. Lithostratigraphy and magnetostratigraphic data are from Norris et al (2014) and Yamamoto et al. (2018).

The appearance of *P. gigateus* predates the first entry of *P. gigas* by 7.90 m (~35 thousand years). *Pletolithus gigas* is general rare with a sharp decline in abundance towards its Top, which is also correlative with the Base common of *Sphenolithus cuniculus. Pletolithis opdykei, P. staurion* and *P.*

mutatus persist significantly above *P. gigas*, although they become extremely rare and sporadic in their distribution.

The morphological and morphometric analyses highlight that the rotated crossbars of *P. giganteus* gradually transform into a X-shaped structure and this supports a phylogenetic relationship between these two taxa that is confirmed by intermediate morphotypes and overlapping stratigraphic ranges. In order to develop a taxonomic definition that is more objective and easy to apply, twenty-seven samples with morphotypes possibly ascribed to *P. giganteus* and *P. gigas* were analyzed and morphometric measurements were performed on all the 80 specimens encountered in the study samples. The morphological features measured in this study are: (1) the maximum length and width of the placolith, (2) the length and width of the central area, (3) the area of the central area and entire placolith, and 4) the length of the short and long crossbar. Once measured, these values were displayed as scatter plots (Figure 3.4A). These plots show that the specimens display a wide spread of values for most of the morphometric parameters, except for the bar length ratio. This is best illustrated by the frequency histograms (Fig. 3.4 B), which show that the bar ratio (i.e., the ratio between the length of the long and short crossbar), displays a clear bimodal distribution pattern, with 1.3 representing the ratio value that separates two distinct populations.

If other morphological features are also taken into account, for instance, the orientation of the crossbars, it becomes apparent that the population with smaller crossbar ratio (average = 1.17) coincides with the *P. gigas* species concept, while the forms with values >1.3 (average = 1.38) represent a separate taxon, which we formally describe here as *P. giganteus.* Moreover, there is overlap between surface area of the placoliths but *P. gigas* has higher values, and the average values are significantly different, specifically 294.50 and 251.61 respectively.

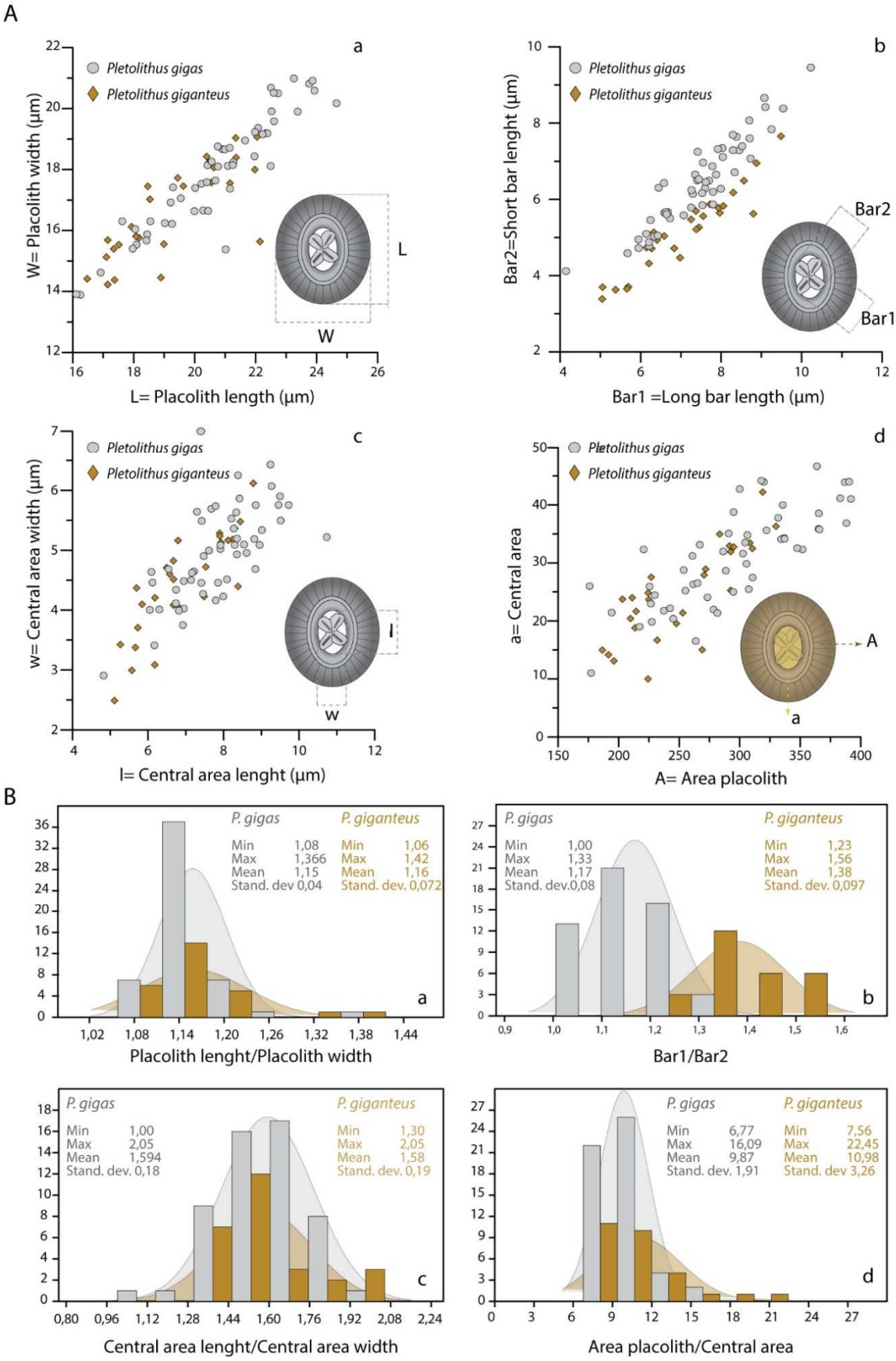

Figure 3.4 A. Scatter plots of (a) placolith length versus placolith width, (b) long bar length versus short bar length, (c) central area length versus central area width, (d) area placolith versus central area. **B.** Frequency histograms of (a) placolith length versus placolith width, (b) long bar length versus short bar length, (c) central area length versus central area width, (d) area placolith versus central area.

3.4.2 SEM observations

The exquisite preservation of the study material indicated by LM observations is fully confirmed by the SEM analysis, which reveals the presence of the most fragile and delicate original features. This includes the common presence of minute structures, such as central area nets in reticulofenestrids and delicate central area crossbars in small and medium size placoliths. This kind of preservation allows us to provide detail descriptions of the arrangement of single elements forming the central area structures, which typically result in distinctive features, such as extinction figures in XPL.

Our SEM observations confirm that the species we have studied possess typical *Coccolithus*-like shield structure (coccolithacean type) but also possess central crossbars structures that are in some cases small and fragile. The forms with robust axial crossbars are here assigned to *P. opdykei/P. staurion* group. SEM images show that each bar consists of one set of staggered plates arranged in a single row, both on the distal and proximal sides.These elements are roughly wedge-shaped and interfinger one to each other (Plate 3.3, figs. 6,8).

By contrast, *Coccolithus mutatus* has very narrow crossbars but the ultrastructure is also formed by a single row of elements (Plate 3.4). On the proximal side, these show a complex construction because wedge-shaped elements interlock with each other. The central area is generally wider than in the smaller forms and the tube is raised with respect to the distal shield (Plate 3.4).

In SEM *Pletolithus giganteus* and *P. gigas* show a broad and low tube cycle with robust crossbars (Plate 3.5). On the proximal side, the bars consist of interfingering wedge-shaped elements that are transversely oriented with respect to the bars axes. There is also a slight depression along the axes (Plate 3.5, fgs. 3b, 6b). On the distal side, overlapping rectangular plates are nearly aligned with the bar axes (Plate 3.5, fgs. 1b, 2b).

Finally, specimens included within *Chiasmolithus* and/ or *Sulliviana* show significant differences in the ultrastructure of the bars especially when comparing these taxa with *P. gigas, P. giganteus* and *P. opdykei/P. staurion* (Plate 3.6). Our observations are in agreement with the detailed descriptions given by Gartner (1970) who subdivided these taxa into two groups: the *Chiasmolithus grandis* group and *Chiasmolithus consuetus* group.

Species belonging to *Chiasmolithus grandis* group (*Chiasmolithus bidens, Chiasmolithus expansus, Chiasmolithus oamaruensis* and *Chiasmolithus solitus*) are typically characterized by a relatively complex bar construction with the distal side of the x-shaped structure formed by a number of axially aligned calcite laths; whereas the proximal side consists of transversely aligned laths. This arrangement results in an axial dark suture that is clearly visible at light microscope (XPL).

The *Chiasmolithus consuetus* group is characterized by bars whose ultrastructure consists of overlapping tabular calcite plates stacked one on the other and closely appressed, both on the distal and proximal sides, as clearly shown by *Chiasmolithus consuetus* (Plate 3.6).

3.5. DISCUSSION

3.5.1 Evolutionary trends

Calcareous nannofossil evolutionary lineages and the possible relationships between different taxa are based on morphological criteria and stratigraphic data because molecular data are not available for these fossil and mostly extinct forms. Together with morphological features, stratigraphic ranges and the presence of forms with intermediate morphological features among different species are essential in order to reconstruct an evolutionary plexus.

Our observations from Site U1410 suggest that during the middle Eocene a group of taxonomically related forms likely evolved from a common ancestor most likely within the genus *Coccolithus*. This group includes the species *P. opdykei, P. staurion, P. mutatus, P. giganteus* and *P. gigas* and these taxa likely originated from an ancestral form having a coccolithacean rim structure with delicate crossbars in the central area. The presence of forms with this feature are reported from different stratigraphic levels and their distribution pattern may suggest that similar morphotypes could have appeared iteratively and not only during the middle Eocene, where they evolved and produce quite distinctive taxa that gave rise to a new lineage among the coccolithaceans. In agreement with previous authors (Gartner, 1970; Varol, 1992), we consider the structure of the crossbars to be an important feature which helps to reconstruct the phylogenetic relationships among different species. In particular, SEM observations have allowed to describe different bar ultrastructures that have been used to recognize differences and affinities among the various taxa.

The virtually coincident first appearances of *P. staurion* and *P. mutatus* in the lower-middle part of Chron C21n mark the onset of the increase in size of the central area crossbars (Figure 3.4). *Pletolithus mutatus* has delicate cross-shaped structure in the central opening, which is only partially filled in by the bars of the cross that is usually large. In contrast, *P. opdykei* and *P. staurion* are characterized by more robust crossbars, which usually almost fill the central area. These two species have the same morphologic features and are differentiated by size, with *P. opdykei* smaller than *P. staurion* (Bown and Newsam, 2017). However, their stratigraphic distribution is the same and so there may be little justification for their separation. We refer to them here as the *P. staurion* group.

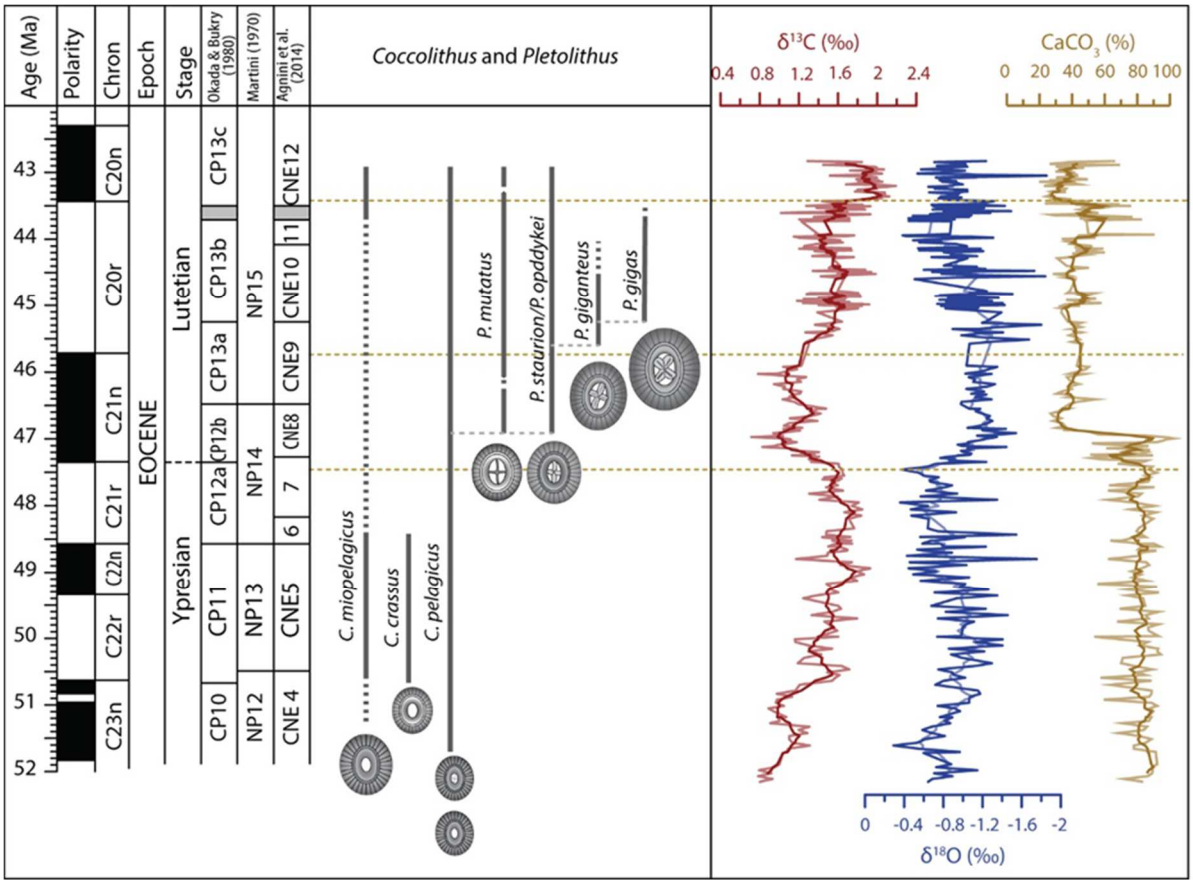

Figure 3.5: Records of bulk carbonate $\delta^{13}C$, $\delta^{18}O$ and $CaCO_3$ content, biostratigraphy and range chart of species belonging to the discussed lineage are plotted against age. Shipboard magnetostratigraphy (Norris et al., 2014, Yamamoto et al., 2018) and biostratigraphic data have been integrated to construct an age model. The Geological Time Scale 2012 is adopted (GTS12; Gradstein et al., 2012). Datum ties points used are available Chron boundaries (C21r/C21n, C21n/C20r; C20r/C20n) and the Top of *T. orthostylus* (NP12-NP13 and CNE4-CNE5 boundaries) at 50.49 Ma (Agnini et al., 2014 converted to GTS12). Sedimentation rates were assumed to remain constant between ties points. According to Gradstein et al. (2012), the position of Ypresian-Lutetian boundary is placed at 47.8 Ma. Note that in the studied succession this age does not coincide with the lowest occurrence *B. inflatus* (CP12a-CP12b boundary) that defines the base of Lutetian.

The appearance of *P. giganteus* marks a notable morphological change within the group with a significant change in orientation of the crossbars (Figure 3.5). This initiated an evolutionary trend that led to the diagonal cross bar seen in *C. gigas.* The structure of the bars of these two species is similar and supports the close affinity between the two and, at the same time, excludes *C. californicus* or *C. consuetus* as possible ancestors.

The progressive rotation of the crossbars has also been observed in several different nannofossil groups at different stratigraphic levels, for example, in the Cretaceous *Eiffelithus* lineage (Watkins & Bergen, 2003, Shamrock and Watkins, 2009) and the early Paleocene *Cruciplacolithus-Chiasmolithus* plexus (Romein, 1979; Van Heck & Prins, 1987). One possible explanation is that the *P. staurion – P.giganteus – P gigas* lineage represents another example of iterative evolution where the appearance and development of a central structure associated to its rotation is one of the morphologic characters that reiterate through time. Morphometric data collected for *P. giganteus* and *P. gigas* suggest a continuous morphologic gradient related to the progressive rotation of the bars

between these two species. This gradual transition makes the determination of these taxa largely subjective. To minimize this subjectivity, Bown & Newsam (2017) proposed that the angle formed between the long axis of the placolith and the central structure should be used as the main criterion to distinguish *P. giganteus* from *P. gigas*, but this parameter is quite difficult to measure if the preservation is not exceptional because recrystallization could hide the central structure and, more importantly, the precise identification of the long axis in these large placoliths is sometime very challenging. Alternatively, we instead propose to use a bar length ratio of 1.3 to differentiate the specimens, with *P. gigas* <1.3 and *P. giganteus* >1.3. This parameter is easier to apply and displays a direct correlation with the parameter previously suggested by Bown & Newsam (2017), in fact the larger the bar length ratio, the smaller the angle between the central structure and the long axis of the placolith. More importantly, the length bar ratio is able to subdivide specimens having a crossbar from specimens with a x-shaped structure in the central opening most of the time.

3.5.2 Taxonomic considerations

The taxonomy of middle Eocene coccolithaceans is complicated by the iterative nature of their evolutionary lineages. As crossbar orientation has often been used as a higher taxonomic level (genus) criterion this may result in generic groups being polyphyletic, grouping superficially similar morphologies which are nevertheless not closely related because of the iterative re-evolution of structures such as diagonal crossbars. This is the case for *P. gigas*, which has usually been ascribed to *Chiasmolithus* based on its diagonally-orientated crossbars but as we shown here, this species is more closely related to the genus *Coccolithus* having evolved from ancestral forms with axial crossbars (Fig. 3.5). Similarly, *P. mutatus* and *P. staurion* group have previously been considered part of the genus *Cruciplacolithus* based on the presence of axial crossbars, but their rim morphology and stratigraphic distribution suggests they are phylogenetically distant from Paleocene *Cruciplacolithus* but close to *Coccolithus*.

Our interpretation of the middle Eocene group of large coccolithacenas raises questions concerning the generic classification of these forms. Following the original definition of *Cruciplacolithus* and *Chiasmolithus* species belonging to this informal group should be classified based on the orientation (axial or diagonal) of central area structure. However, our observation show that this middle Eocene group does not have a close phylogenetic links with the *Cruciplacolithus* or *Chiasmolithus* lineages but rather is more closely affiliated with *Coccolithus*, which includes species with simple bars or narrow axial crossbars (http://www.mikrotax.org).

Here we propose a new genus to include these large *Coccolithus*-like forms with relatively robust central area crossbars with varying orientation. Both the morphological and stratigraphic evidence

support the grouping of these forms and preserves the phylogentic integrity of the genera *Cruciplacolithus* and *Chiasmolithus*. We concede that Coccolithus does show a great deal of morphological variability and that modern representatives of this genus may have transverse and axial crossbars, but we believe that the size, robustness and distinctiveness of these central structures supports the creation of a new genus.

One argument in favor to this hypothesis is the stability of early Paleogene taxonomy because if we accept the idea that the structure in the central area are not an appropriate morphological character this could result in the invalidation of genera *Chiasmolithus* and *Cruciplacolithus* which in turn could produce heavy repercussions on the calcareous nannofossil taxonomy. A second reason to introduce a new genus is based on the consideration that the generic assignment for Paleogene nannofossils is often based on its practical use. The introduction of a new genus surely represent an additional formal subdivision but it may be applied relatively easily for practical purposes.

3.5.3 Large middle Eocene coccolithaceans and their use in biostratigraphy

Pletolithus gigas is a well established marker species in middle Eocene calcareous nannofossil biostratigraphy. The Base and the Top of *P. gigas* are the primary marker events defining the base of nannofossil subzones CP13b and CP13c of Okada & Bukry (1980) and the base of zones CNE10 and CNE12 of Agnini et al. (2014). *Pletolithus gigas* possesses some of the prerequisites for a good biostratigraphic marker: 1) it is a large and distinctive form; 2) it is heavily-calcified and thus particularly resistant to dissolution and 3) it is has a widespread biogeographic distribution. However, one of its main drawbacks is that its abundance is generally very low, and this can result in uneven stratigraphic distribution patterns. As a result, despite the longevity of the use of this species in middle Eocene biostratigraphy, the reliability of its related biohorizons remain poorly tested.

At Site U1410, the base of *P. gigas* lies in the lower part of Chron C20r, providing an estimated age calibration of 45.31 Ma using Geological Time Scale 2012 (GTS; 2012; Gradstein et al., 2012) (Figure 3.5). This calibration is in fair agreement with that of Agnini et al. (2014), which is ca. 270 kyr older. Though these estimates are close, two main arguments may explain this discrepancy and help to minimize the observed differences. The first is related to the presence of transitional morphotypes between *P. giganteus* and *P. gigas*. Since, at present, there is not a commonly accepted taxonomy of *P. gigas,* previous studies may have adopted a broader or stricter concept of this taxon leading producing to diachronous results, reflecting the the different stratigraphic ranges of the two species rather than representing real diachroneity in one species. If specimens of *P. giganteus* have been ascribed to *P. gigas*, this would result in an older age estimation for the base of the subzone because the first appearance of *P. giganteus* predates that of *P. gigas*. The second argument is related

to the depositional setting and the methodology used to calibrate biohorizons. In order to provide age estimates of biohorizons we use magnetostratigraphic data, and in particular the ages of the bases and tops of the chron where the biohorizon lies, with the important assumption that sediment accumulation rates throughout the chron remains constant. In this particular case, Chron C20r has a long duration (~2.3 Myr), so this assumption could not be easily verified, especially considering that the section is characterized alternations of clay and carbonate-rich sediments, reflecting varying terrigenous input in a drift sedimentation regime. If sedimentation rate is not constant this may affect age calibration and so it is preferable to have more highly-resolved datasets, ideally astronomically rather than magnetostratigraphically tuned, to provide more reliable age estimations.

To summarize, the use of a morphometric approach has provided more objective criteria with which to define and identify *P. gigas.* This should improve taxonomic consistency and subsequent biostratigraphic and biochronologic results. Inconsistences introduced by depositional settings however can only be minimized by seeking new astrocyclostratigraphic-based data, which are currently not available. A final important requirement for a good biohorizon is that the marker species displays a continuous, and hopefully common, abundance. This is clearly not the case for *P. gigas*, which displays sporadic and rare occurrences in its upper range, preceding its final extinction (Agnini et al., 2014). The Top of P. gigas has been age calibrated at Site 1051 (North Atlantic Ocean) as 43.6 Ma (age recalibrated to GTS12; Agnini et al., 2014) in fairly good agreement with our Site U1410 data, at 43.71 Ma (170.42 rmcd). However, Site U1410 an isolated specimen was also found at 43.50 Ma (165.42rmcd). The combined effect of several factors (i.e., rarity, sample preparation and study area) may account for the differences observed between our data and that from Site 1051, with rarity at Site U1410 the most likely explanation. The reliability of the Top of *P. gigas* is therefore questionable because the abundance pattern of this species is not easily reproducible in its upper range, though variable accumulation rates at IODP Site U1410 could also have exacerbated the observed discrepancy. Despite the fact that we have add new lines of evidence that the Top of *P. gigas* is a poorly reliable biohorizon, unfortunately no alterative options are available. In this situation, it is convenient to know that some issues are related to this biohorizon. The use of other species within this group, such as *P. mutatus*, may provide useful secondary biostratigraphic information in support of the primary marker species *P. gigas*.

3.5.4 Middle Eocene coccolithacenas evolutionary lineage in the geochemical framework

The interplay between biotic and abiotic factors is a major control on the changes observed in calcareous nannofossil assemblages. This is shown in the fossil record by shifts in relative abundance and appearances and disappearances of taxa, which coincide with proxies of environmental change, such as carbon isotope excursions. Though these biosphere -geosphere interactions are widely accepted, the exact timing between the biotic response and paleoenvironmental changes are variable and not completely understood. Here we compare the calcareous nannofossil and stable isotope records to test for potential links between environmental changes and the evolution observed among the middle Eocene coccolithaceans.

Very few high-resolution stable isotope records are available for the late Ypresian – early Lutetian interval and most of them do not cover the entire interval of our study (e.g., Sexton et al., 2006; 2011; Coccioni et al., 2012; Payros et al., 2012; Luciani et al., 2016; Westerhold et al., 2017). Our data indicate that the EECO was followed by a phase of long term rise in $\delta^{13}C$ values interrupted by several low amplitude CIEs (Figure 3.6), and this is consistent with the isotope records from the Tethyan Possagno section (NE Italy) and Pacific DSDP Site 577 (Luciani et al., 2016; Dickens & Backman, 2013). At the base of Chron C21n, this trend peaks with a relatively prominent negative coupled excursions in the carbon isotopes. This event is not correlative with the Ypresian – Lutetian event of Payros et al. (2012) but rather coincides with a negative peak in the amplitude modulation of astronomic parameters (Sexton et al., 2011; Boulila et al., 2018). This level corresponds to the first appearance of the middle Eocene large coccolithaceans group and the species *P. staurion/P. opdykei* and *P. mutatus*. At Site U1410 this change is also coincident with a significant change in lithology, which shifts from white nannofossil chalk to greenish-grey nannofossil clay (Fig.3). This change marks a transition from pelagic ooze to more clay-rich deposition, related to the initial stages of drift sedimentation (see Boyle et al., 2017). The shift is sedimentation is a significant Atlantic event but may not reflect global drivers, and so it is hard to hypothesize that this triggered the onset of this lineage, unless these species originated in the Atlantic before colonizing other oceans.

The next step in the evolution of the *P. staurion – P. gigas* lineage, is the appearance of *P. giganteus*, which occurs where $\delta^{13}C$ isotope values shift toward more positive values (Figure 3.6). The transition between the appearance of *P. giganteus* and the first appearance of *P. gigas* has an estimated duration of ca. 350 kyr and corresponds to a phase of gradual increase in the stable carbon isotope values, and remain relatively stable for the rest of Chron C20r. There is therefore some correlation between changes observed in the $\delta^{13}C$ curve and the appearances of the different taxa. This dataset is intriguing because it suggests that in some way evolution is related to changes in the physical environment but more data are needed to confirm that the same relationship occurs more widely.

3.6 CONCLUSION

The sedimentary succession recovered at Site U1410 reveals the emergence of a new lineage of large coccolithaceans. We observed a series morphological changes (crossbars rotation) that enabled us to reconstruct the evolutionary history of species *Pletolithus gigas* (Bown & Newsam, 2017). Based on detailed morphological observation in both LM and SEM we propose a new genus, *Pletolithus,* and a new species, *Pletolithus giganteus*.

Biostratigraphic and biometric data have allowed us to improve the definition and identification of *P. gigas*, and to distinguish the new species *P. giganteus,* which is characterized by the presence of a rotated crossbars in the central area. The overlap of biometric data between these species suggests a gradual evolutionary transition that include the progressive rotation of the axial crossbars of *P. giganteus* into the X-shaped structure of *P. gigas.* The use of the bar length ratio allows for on objective and easily applicable identification of these two species.

We have shown that *P. gigas and P. giganteus* are not the ancestral forms in this lineage but that a species of *Coccolithus* was the most likely progenitor. The presence of a well-developed x- or cross-shaped structure in the central area is the diagnostic character of the new genus *Pletolithus.* The appearance of this kind of structure in the central area is interpreted as an example of iterative evolution since calcareous nannofossils have experienced exactly the same trend in morphologic evolution multiple times, the last is when the *Cruciplacolithus-Chiasmolithus* plexus emerged in the Paleocene.

Comparing the $\delta^{13}C$ data with the various steps (appearances / disappearances) that occurred within this lineage, a correlation is evident because at each change in the carbon isotope profile corresponds an appearance of a taxon. More speculatively but also very intriguingly the entry of this forms corresponds to a local but remarkable change in the paleoceanography related to the onset of deep water circulation in the North Atlantic.

Systematic Paleontology

Order COCCOLITHALES Haeckel, 1894 emend. Young & Bown, 1997

Family COCCOLITHACEAE Poche, 1913 emend. Young & Bown, 1997

***Pletolithus* n.gen.**

Type species: *Coccolithus gigas* Bramlette & Sullivan, 1961

Derivatio nominis: From latin *pletum,* meaning filled, and referring to the crossbars that often fill the central area.

Type locality: IODP Exp. 342 Site U1410, Southeast Newfoundland Ridge, northwest Atlantic.

Type level: Lutetian

Diagnosis: Placolith with *Coccolithus*-type shields and tube, the central area is spanned by a well-developed x- or cross-shaped structure. The central structure may be rotated with respect to the main axes of the placolith. The distal shield is wider than the proximal one. The size of the central area is highly variable, ranging from very small to very large.

Remarks: This genus has many features in common with *Coccolithus* from which it most likely derives. The diagnostic feature is the presence of a large or conspicuous central structure that partially fills in the central opening.

Species: The following species can be tentatively assigned to this genus: *Cruciplacolithus mutatus* Perch-Nielsen, 1971*, Coccolithus staurion* Bramlette & Sullivan, 1961*, Coccolithus opdykei* Bown & Newsam 2017*, Coccolithus gigas* Bramlette & Sullivan, 1961.

Pletolithus opdykei (Bown and Newsam, 2017) comb. nov.

Diagnosis: Large placoliths (< 12 µm) with a narrow central area that is filled by broad, axial to near-axial crossbars.

Pletolithus staurion (Bramlette & Sullivan, 1961) comb. nov.

Diagnosis: According to the original definition this species includes very large placoliths (> 12 µm) with a narrow central area and a robust central cross aligned in the axes of the placolith ellipse (Bown and Newsam, 2017).

Differentiation: Distinguished from *Pletolithus opdykei* by its larger size.

Pletolithus mutatus (Perch-Nielsen , 1971) comb. nov.

Diagnosis: Very large placolith (>14 µm) with wide and raised tube cycle and broad central area that is spanned by delicate crossbars. The central cross may be axial or slightly rotated respect to the longitudinal axis of the coccolith.

Description: The distal shield consists of 50-60 slightly overlapping elements that give rise to low angle oblique sutures. The outline may be normally or broadly elliptical. The tube cycle is raised and consists of 55-65 elements with complex sutures that partially cover the distal shield. The smaller proximal shield consists of elements that show a slightly dextral obliquity in proximal view. Thin crossbars occupies the central area. On the distal side the cross-bars consist of 10-25 rectangular interlocking laths, while on the proximal side they consist of 15-25 wedge shaped elements. The elements on the proximal side are alternatively oriented and forms a unique row that slightly extends into the proximal shield. The cross may be slightly asymmetrical relative to the placolith axes and bars may be straight or curved. The complex ultrastructure of central cross is observable in well preserved specimens under light microscope. The tube cycle is highly birefringent under cross-polarized light. This species is commonly preserved as broken specimens due to the delicate bars.

Differentiation: *Pletolithus mutatus* can be differentiated from species ascribable to *Coccolithus* by the thin axial or slightly rotated crossbars spanning the central area and by the raised tube cycle. The central cross of *P. staurion* is also axial but specimens of this species have more robust crossbars that almost fill the central area.

Pletolithus giganteus **sp. nov.**

Derivatio nomis: From latin *giganteus,* meaning large, referring to the very large size of this species.

Diagnosis: Very large (> 16 µm) elliptical placolith with narrow to large central area spanned by robust bars that form an asymmetric diagonal cross.

Description: Very large coccolithacean with a distal shield consisting of 60-70 elements with an elliptical outline. The tube connecting the two shields is broad and consists of flat elements with complex sutures. The smaller proximal shield is composed of elements with dextral obliquity in proximal view. Specimens belonging to this species show a high variability in the dimension of the central area, which can occupy from 7% to 13% of the total placolith area. An asymmetrical diagonal cross spans the central area. On the distal side, bars consist of rectangular plates stacked one on others, whose axes are roughly aligned with the long axes of the bars. On the proximal side, bars are composed of one row of robust wedge shaped elements (roughly triangular), normally oriented to bars axes. These elements partially interfinger, but do not interfinger along the full length of the

wedge. Thickening at the base of the triangular plate is common and it gives rise to a poorly developed depression along the bars axes. Under cross-polarized light, small extinction lines run parallel to the bars axes.

Differentation: Pletolithus giganteus can be distinguished by the intermediate orientation of the crossbars. *Pletolithus giganteus* can be differentiated from *P. staurion* by the generally smaller size, smaller central area and by axial oriented cross of the latter. *Pletolithus giganteus* can be distinguished from *P. gigas* by the diagonally oriented (X-shaped) cross-bars of the latter form. The best diagnostic feature in distinguishing consistently between these species is represented by the bar length ratio. This value is generally >1.3 in *P. giganteus* and <1.3 in *P. gigas. Pletolithus giganteus* can be distinguished from *P. mutatus* by the more robust bars, their different construction and the raised tube cycle.

Size: 16-22 µm

Holotype: Plate 3.2, Fig. 7

Holotype size: 21 µm

Paratype: Plate 3.2, Fig. 1

Paratype size: 18 µm

Type locality: IODP EXP. 342 Site U1410, Southeast Newfoundland Ridge, northwest Atlantic.

Type level: SubZone CP13b (Okada & Bukry, 1980) or Zone CNE10 (Agnini et al., 2014), middle Eocene, sample Site U1410-20X-3W-067.

Range: Restricted to upper subzone CP13a-CP13b (Okada & Bukry, 1980) or upper Zone CNE9-Zone CNE10 (Agnini et al., 2014).

Remarks: The Base of *Pletolithus giganteus* slightly predates the Base of *Pletolithus gigas,* which is used to mark both of the base of subzone of CP13b (Okada & Bukry, 1980) and the base of Zone CNE10 (Agnini et al., 2014).

Occurrence: The species occurs, with low frequency, in the lower part of Chron 20r.

Repository: Holotype and paratypes are deposited in the permanent collection of the Museo di Geologia e Paleontologia dell'Università di Padova (MGPD), Padova, Italy (protocol XXXX).

Pletolithus gigas (Bramlette & Sullivan, 1961) comb. nov.

(Note: this contribution emphasizes the original description, to clarify the morphological criteria of the species and to constrain the differentiation from *P. mutatus* and *P. gigas*).

Diagnosis: Very large, normally elliptical coccolithacean, with a robust X-shaped structure spanning the central area. Bars show a complex construction and the tube cycle do not overlap the distal shield.

Description: The distal shield is composed of 60-70 elements radially oriented or may display a slight dextral obliquity in distal view. On the distal side, the broad tube cycle is composed of 40-50 interlocking elements that gently inclined towards the central area. The proximal side consists of 55-65 elements with dextral obliquity in proximal view. In the central area, robust diagonal crossbars form a X-shaped structure. Bars have a complex construction: on the distal side they consists of axially arranged elements while on the proximal side they are composed of one row of wedge shaped elements transversely oriented. The triangular elements of the proximal side point alternatively in opposite directions and interfinger with each others for almost their entire length. A central depression run along bars axes. Under cross-polarized light, this construction gives rise to two dark extinction lines along the bar axes. Specimens with two straight and sigmoid bars may be observed. In contrast to the original description, specimens with fine "teeth" along the margin have never been observed.
Differentation: Pletolithus gigas can be differentiated from the others species of *Pletolithus* by the robust X-shaped structure in the central area. *Pletolithus gigas* can be distinguished by *P. giganteus* by the shape of the central structure, which has bar length ratio <1.3. *Pletolithus gigas* differs from the species belonging to *Chiasmolithus* by the ultrastructure of the bars and for the flat tube.

Plates

Plate 3.1: LM images of *Pletolithus* from IODP Site U1410. Scale bar 10 µm **1.** *Pletolithus opdykei,* Sample 1410B-20X-5W-40 a. Crossed nicols b. Parallel nicols **2.** *Pletolithus opdykei,* Sample 1410B-21X-3W-127 a. Crossed nicols b. Parallel nicols **3.** *Pletolithus staurion*, Sample 1410B 21X-3W-127, a. Crossed nicols b. Parallel nicols **4.** *Pletolithus staurion,* Sample 1410C-20X-6W-67 a. Crossed nicols b. Parallel nicols **5.** *Pletolithus staurion,* Sample 1410C-20X-4, 67 a. Crossed nicols b. Parallel nicols **6.** *Pletolithus mutatus,* Sample 1410B-23X-2W-7 a. Crossed nicols b. Parallel nicols **7.** *Pletolithus mutatus,* Sample 1410C-20X-5W-67 a. Crossed nicols b. Parallel nicols **8.** *Pletolithus mutatus,* 1410B 21X-4W-127 a. Crossed nicols b. Parallel nicols **9.** *Pletolithus mutatus,* Sample 1410C-18X-5W-20 a. Crossed nicols b. Parallel nicols **10**. *Pletolithus mutatus,* Sample 1410C-18X-5W-20 a. Crossed nicols b. Parallel nicols.

Plate 3.2: LM images of *Pletolithus* from IODP Site U1410. Scale bar 10 µm**. 1.***Pletolithus giganteus.* Sample 1410C-20X-6W-67 a. Crossed nicols b. Parallel nicols **2.** *Pletolithus giganteus.* Sample 1410C-20X-6W-67 a. Crossed nicols b. Parallel nicols **3.** *Pletolithus giganteus*. 1410C 20X-4W-67 a. Crossed nicols b. Parallel nicols **4.** *Pletolithus giganteus,* Sample 1410C-20X-3W-67 a. Crossed nicols b. Parallel nicols **5.** *Pletolithus mutatus.* Sample 1410C-20X-3W-67 a. Crossed nicols b. Parallel nicols **6.** *Pletolithus mutatus.* Sample 1410B-20X-5W-40 a. Crossed nicols b. Parallel nicols **7.** *Pletolithus gigas,* Sample 1410C-19X-2W-67 a. Crossed nicols b. Parallel nicols **8.** *Pletolithus gigas.* 1410B 20X-5W-40 a. Crossed nicols b. Parallel nicols **9.** *Pletolithus gigas,* Sample 1410C-18X-3W-60 a. Crossed nicols b. Parallel nicols **10**. *Pletolithus gigas.* Sample 1410C-18X-4W-80 a. Crossed nicols b. Parallel nicols.

Plate 3.3: SEM images from Site IODP Site U1410. Scale bar 5 µm unless otherwise noted**. 1.** *Coccolithus pelagicus,* Sample 1410A-18X-CC **2.** *Coccolithus pelagicus.* Sample 1410B-21X-3W-127 **3.** *Pletolithus pelagicus*. 1410B-21X-3W-127 a. Complete placolith in distal view b. Detail of central area crossbars **4.** *Coccolithus pelagicus.* Sample 1410C-20X-4W-67 **5.** *Coccolithus pelagicus.* Sample 1410C-19X-2W-67 a. Complete placolith in proximal view b. Detail of central area crossbars **6.** *Pletolithus opdyke.* Sample 1410B-21X-3W-127 a. Complete placolith in proximal view b. Detail of central area crossbars **7.** *Coccolithus pelagicus,* Sample 1410B-21X-CC **8.** *Pletolithus staurion.* 1410B-21X-3W-127 a. Complete placolith in proximal view b. Detail of central area crossbars.

Plate 3.4: SEM images from Site IODP Site U1410. Scale bar 5 µm unless otherwise noted**. 1.** *Pletolithus opdykei.* Sample 1410B 21X-3W-127 **2.** *Pletolithus mutatus.* Sample 1410C 19X-2W-67 a. Complete placolith in distal view b. Detail of central area crossbars **3.** *Pletolithus mutatus*. 1410B-21X-3W-127 a. Complete placolith in distal view b. Detail of central area crossbars **4.** *Pletolithus mutatus.* Sample 1410B-23X-4W-7 a. Complete placolith in proximal view b. Detail of central area crossbars **5.** *Pletolithus mutatus.* Sample 1410B-21X-3W-127 **6.** *Coccolithus pelagicus,* coccosphere. Sample 1410C-19X-2W-67.

Plate 3.5: SEM images from IODP Site U1410. Scale bar 5 µm unless otherwise noted. **1.** *Pletolithus giganteus.* Sample 1410B-21X-3W-127 a. Complete placolith in distal vieX b. Detail of central area crossbars **2.** *Pletolithus giganteus.* Sample 1410C-19X-3, 65 a. Complete placolith in distal view b. Detail of central area crossbars **3.** *Pletolithus giganteus.* 1410B-21X-3W-127 a. Complete placolith in distal view b. Detail of central area crossbars **4.** *Pletolithus gigas.* Sample 1410C-19X-2W-67 a **5.** *Pletolithus gigas,* Sample 1410C-18X-CC **6.** *Pletolithus gigas.* Sample 1410B-21X-3W-127 a. Complete placolith in proximal view b. Detail of central area crossbars.

Plate 3.6: SEM images from IODP Site U1410. Scale bar 5 µm unless otherwise noted. **1.** *Chiasmolithus consuetus* (proximal view). Sample 1410B-21X-3W-127 **2.** *Chiasmolithus consuetus* (proximal view). Sample 1410B-21X-3W-127 a. **3.** *Chiasmolithus consuetus* (proximal view).1410B-21X-3W-127 **4.** *Chiasmolithus*

consuetus (distal view). Sample 1410C-19X-2W-67 a **5.** *Chiasmolithus consuetus.* Sample 1410B-21X-3W-127 a. Complete placolith in distal view b. Detail of central area crossbars. **6.** *Chiasmolithus consuetus.* Sample 1410B-21X-3W-127 a. Complete placolith in proximal view b. Detail of central area crossbars. **7.** *Chiasmolithus solithus* (proximal view). Sample 1410B-21X-3W-127 **8.** *Chiasmolithus solithus* (distal view). Sample 1410B-21X-3W-127 **9.** *Chiasmolithus solithus* (distal view). Sample 1410B-17X-2W-120 **7.** *Chiasmolithus solithus* (proximal view). Sample 1410A-21X-3W-127 **8.** *Chiasmolithus solithus* (proximal view). Sample 1410A-21X-3W-127 **9.** *Chiasmolithus solithus* (distal view). Sample 1410C-19X-2W-67 **8.** *Chiasmolithus expansus* (proximal view). Sample 1410A-21X-3W-127 **9.** *Chiasmolithus expansus* (distal view). Sample 1410A-21X-3W-127

10 µm

Plate 3.1

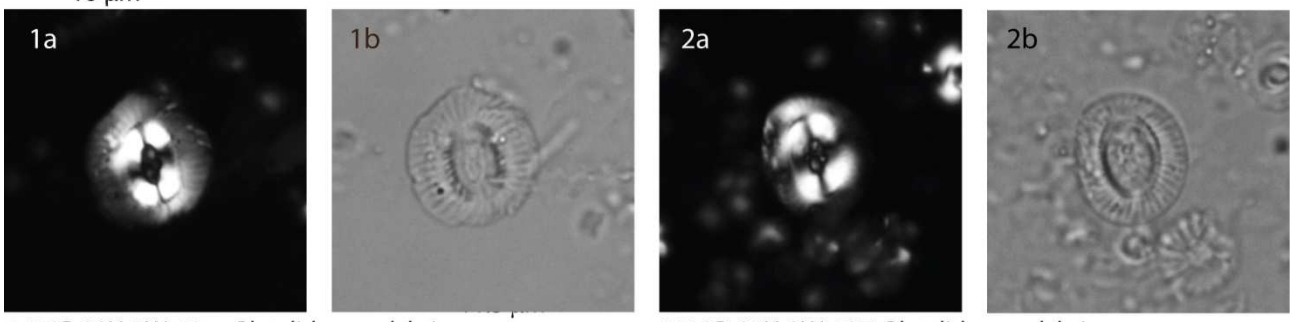

1410B 20X-5W-40 *Pletolithus opdykei*

1410B-21X-3W-127 *Pletolithus opdykei*

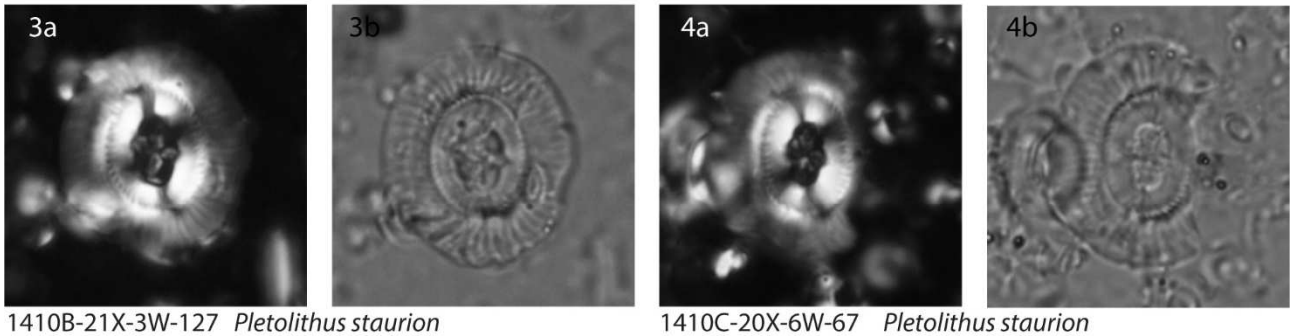

1410B-21X-3W-127 *Pletolithus staurion*

1410C-20X-6W-67 *Pletolithus staurion*

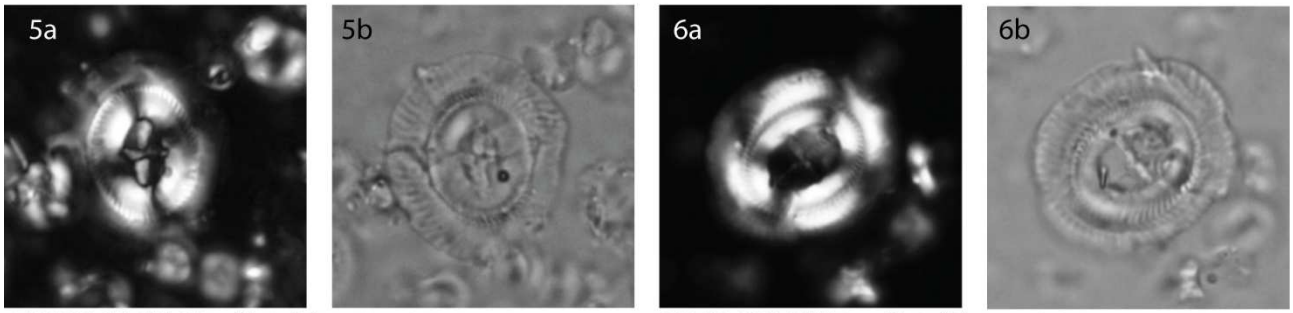

1410C-20X-4W-67 *Pletolithus staurion*

1410B-23X-2W-7 *Pletolithus mutatus*

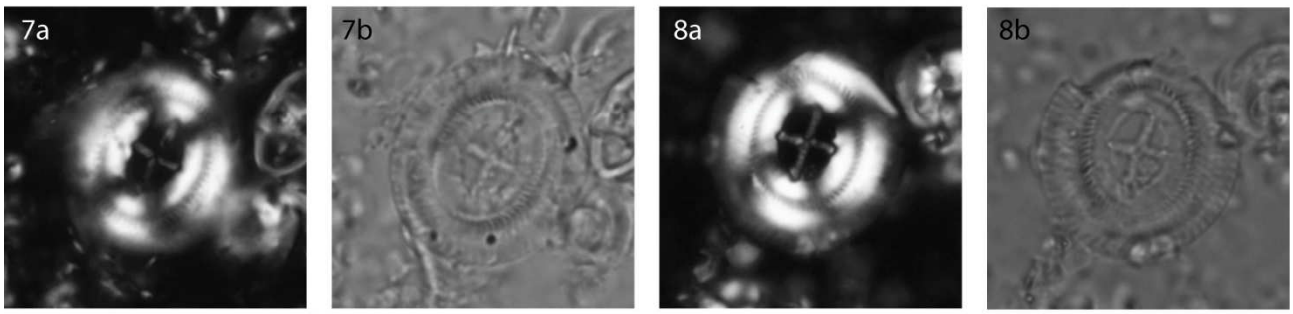

1410C-20X-5W-67 *Pletolithus mutatus*

1410B-21X-4W-127 *Pletolithus mutatus*

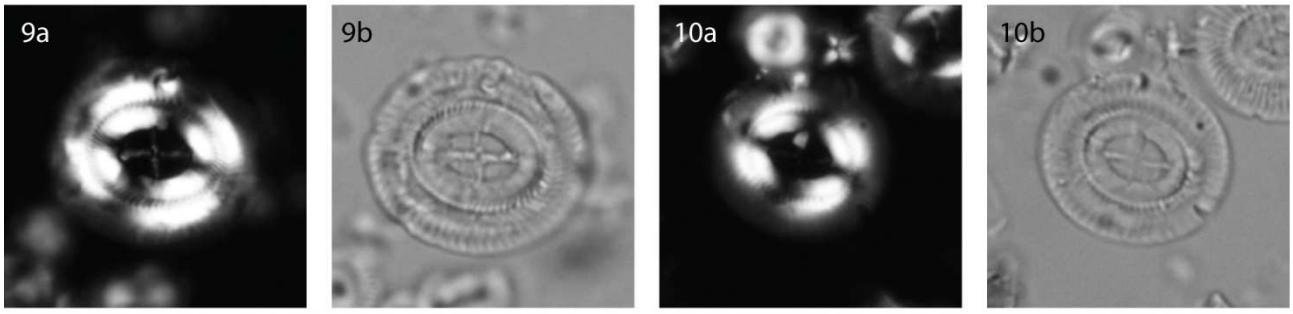

1410C-18X-5W-20 *Pletolithus mutatus*

1410C-18X-5W-20 *Pletolithus mutatus*

10 µm

Plate 3.2

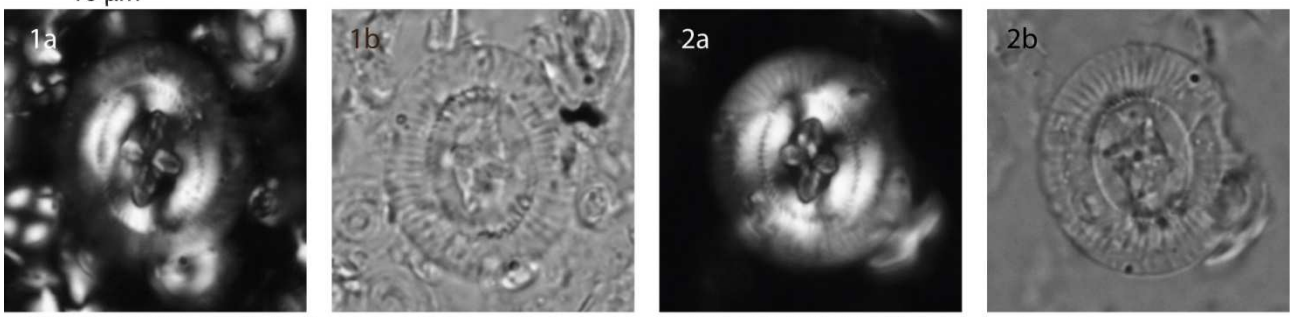

1410C-20X-6W-67 *Pletolithus giganteus*

1410C-20X-6W-67 *Pletolithus giganteus*

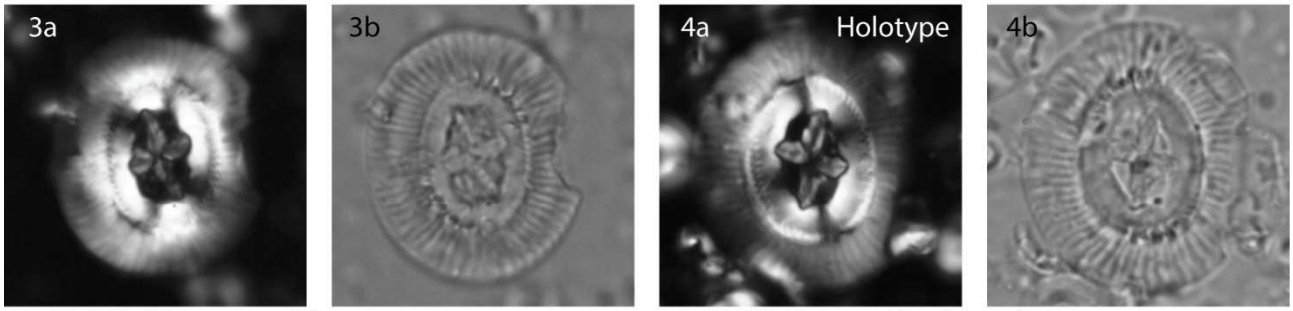

1410C-20X-4W-67 *Pletolithus giganteus*

1410C-20X-3W-67 *Pletolithus giganteus*

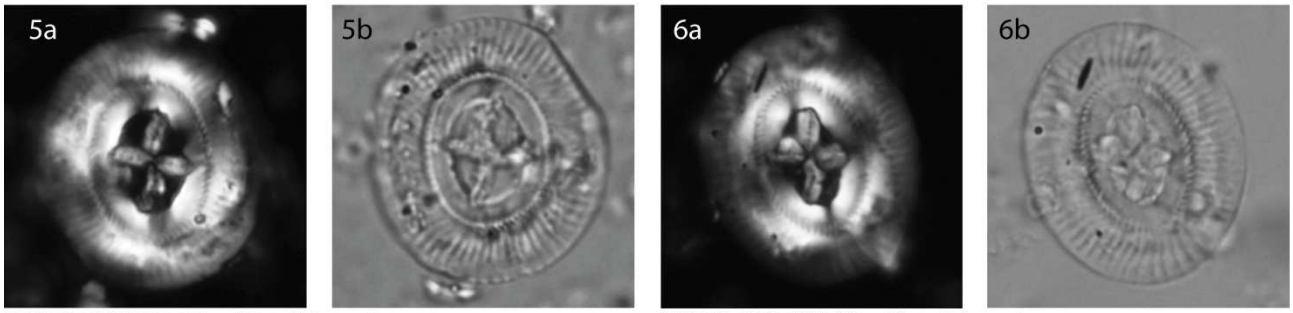

1410C-20X-3W-67 *Pletolithus giganteus*

1410B-20X-5W-40 *Pletolithus giganteus*

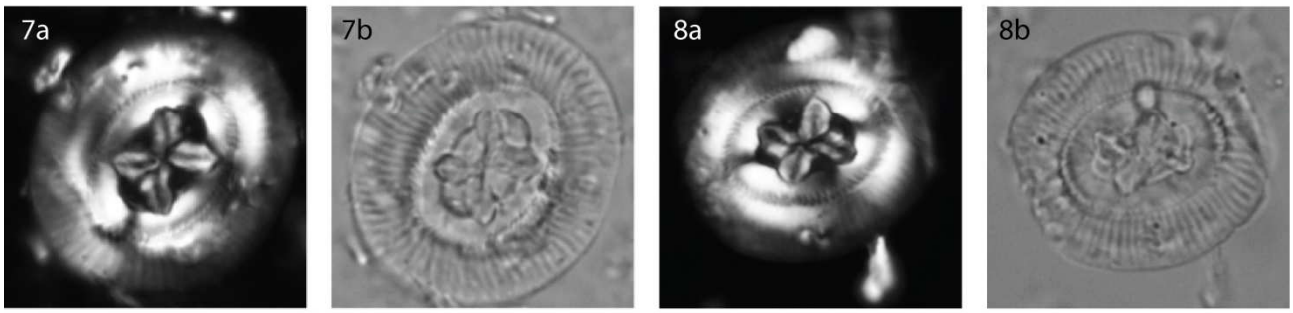

1410C-19X-2W-67 *Pletolithus gigas*

1410B-20X-5W-40 *Pletolithus gigas*

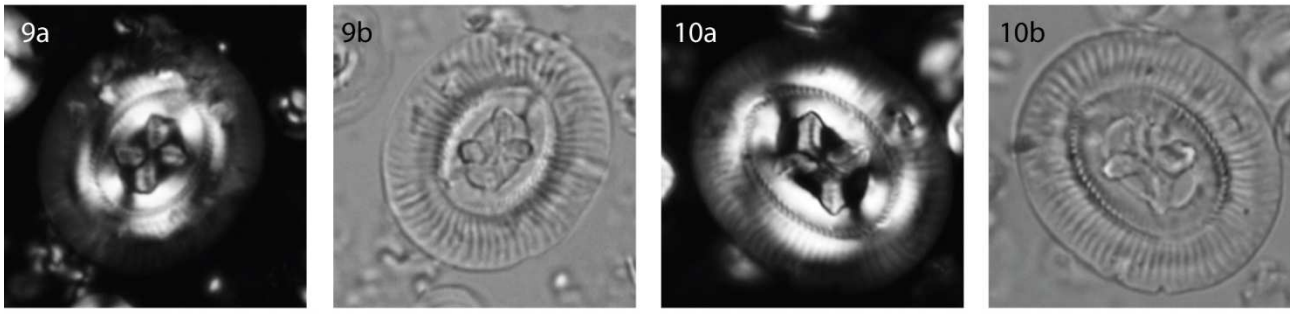

1410C-18X-3W-60 *Pletolithus gigas*

1410C-18X-4W-80 *Pletolithus gigas*

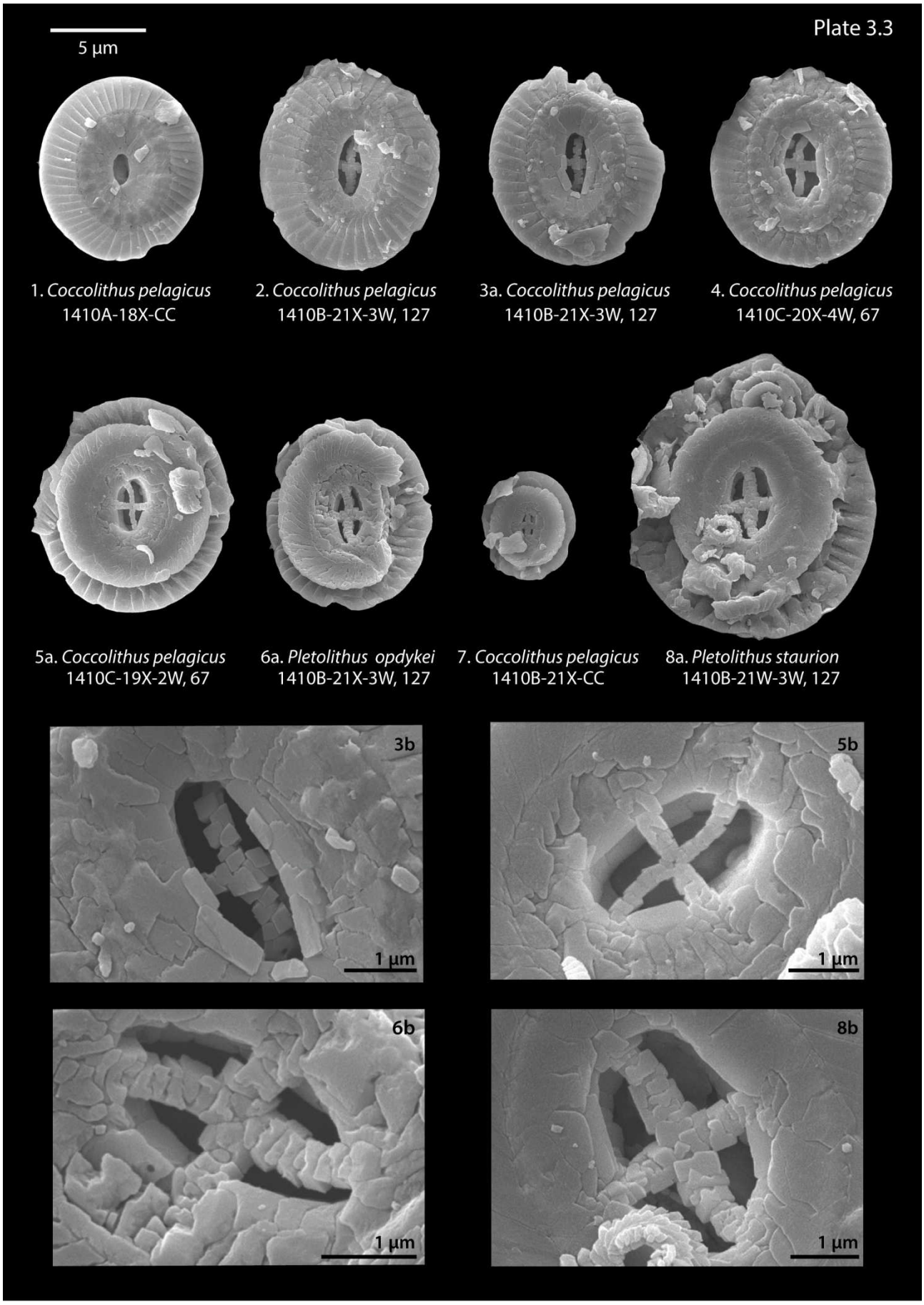
Plate 3.3
5 µm
1. Coccolithus pelagicus
1410A-18X-CC
2. Coccolithus pelagicus
1410B-21X-3W, 127
3a. Coccolithus pelagicus
1410B-21X-3W, 127
4. Coccolithus pelagicus
1410C-20X-4W, 67
5a. Coccolithus pelagicus
1410C-19X-2W, 67
6a. Pletolithus opdykei
1410B-21X-3W, 127
7. Coccolithus pelagicus
1410B-21X-CC
8a. Pletolithus staurion
1410B-21W-3W, 127
3b
1 µm
5b
1 µm
6b
1 µm
8b
1 µm

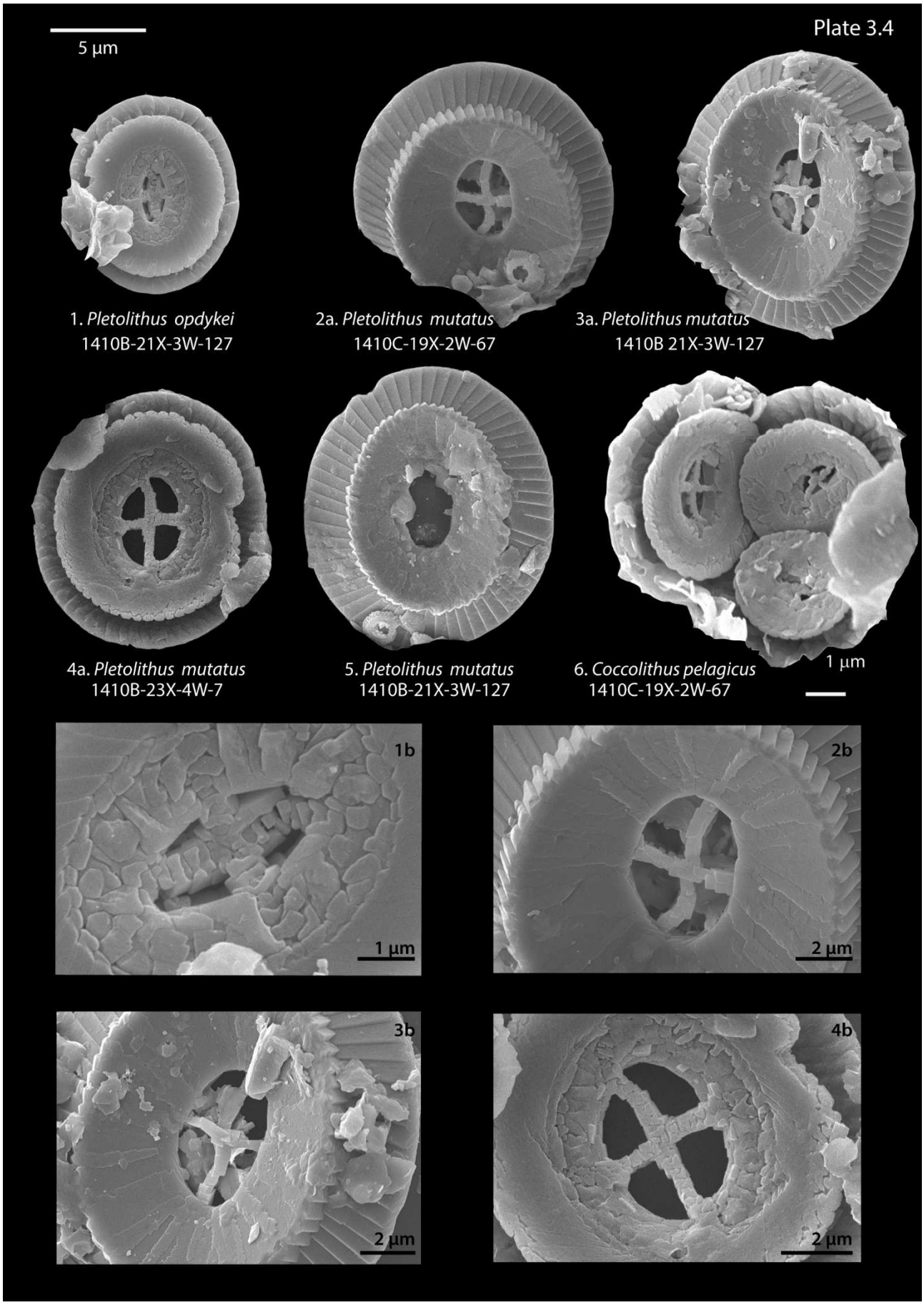
Plate 3.4
5 µm
1. Pletolithus opdykei
1410B-21X-3W-127
2a. Pletolithus mutatus
1410C-19X-2W-67
3a. Pletolithus mutatus
1410B 21X-3W-127
4a. Pletolithus mutatus
1410B-23X-4W-7
5. Pletolithus mutatus
1410B-21X-3W-127
6. Coccolithus pelagicus
1410C-19X-2W-67
1 µm
1b
1 µm
2b
2 µm
3b
2 µm
4b
2 µm

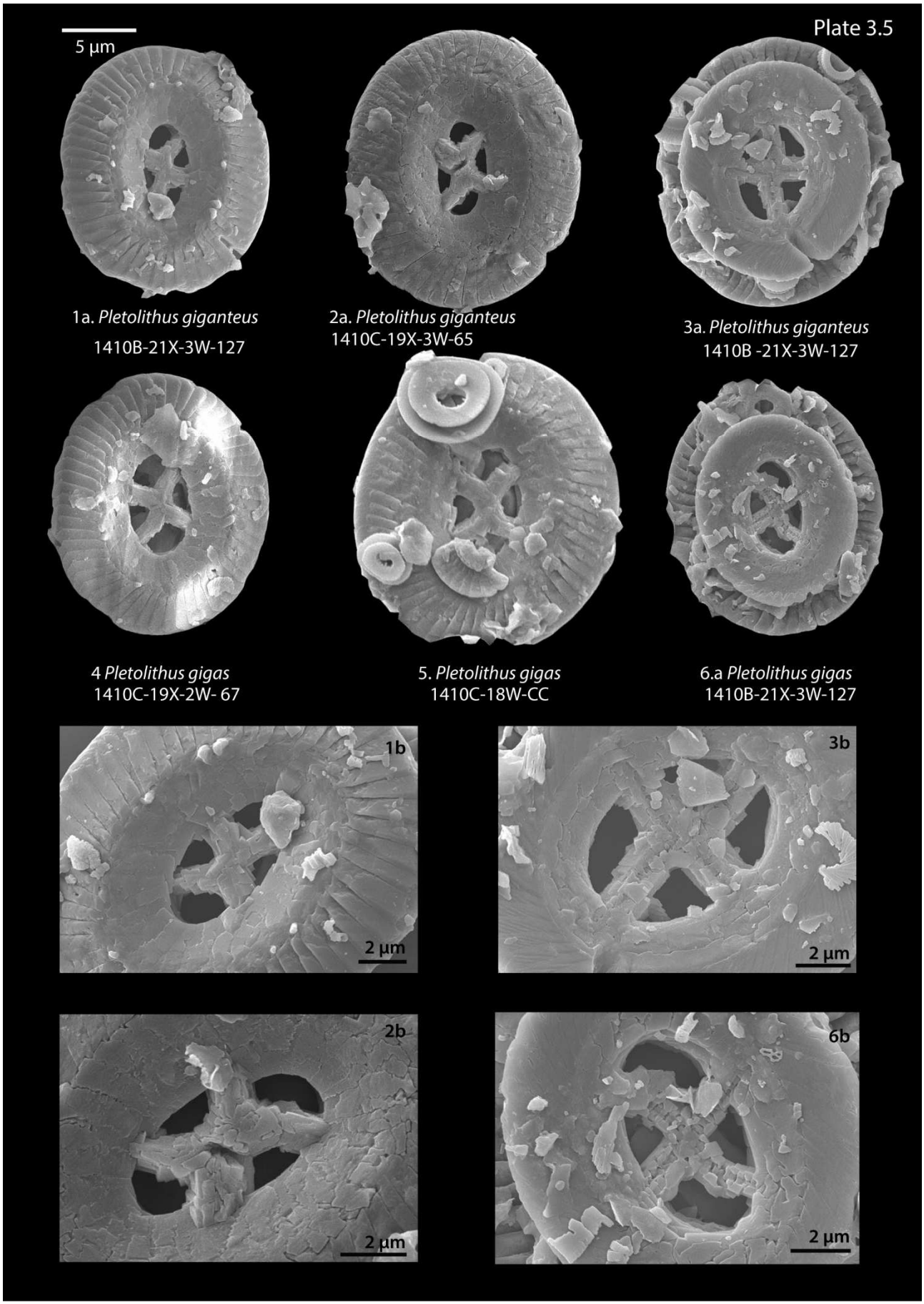
Plate 3.5
5 µm
1a. Pletolithus giganteus
1410B-21X-3W-127
2a. Pletolithus giganteus
1410C-19X-3W-65
3a. Pletolithus giganteus
1410B -21X-3W-127
4 Pletolithus gigas
1410C-19X-2W- 67
5. Pletolithus gigas
1410C-18W-CC
6.a Pletolithus gigas
1410B-21X-3W-127
1b
2 µm
3b
2 µm
2b
2 µm
6b
2 µm

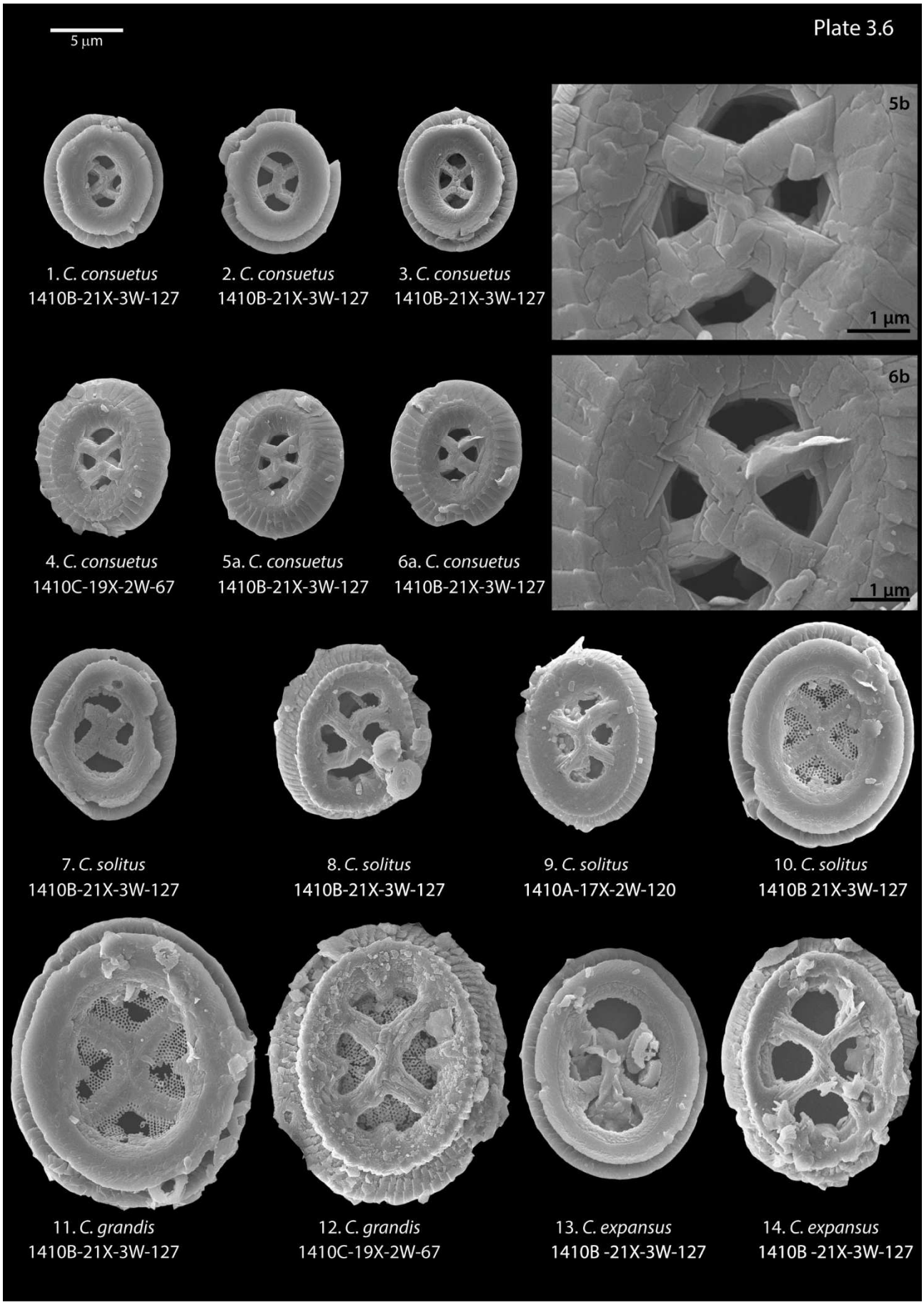
Plate 3.6
5 µm
1. C. consuetus
1410B-21X-3W-127
2. C. consuetus
1410B-21X-3W-127
3. C. consuetus
1410B-21X-3W-127
5b
1 µm
4. C. consuetus
1410C-19X-2W-67
5a. C. consuetus
1410B-21X-3W-127
6a. C. consuetus
1410B-21X-3W-127
6b
1 µm
7. C. solitus
1410B-21X-3W-127
8. C. solitus
1410B-21X-3W-127
9. C. solitus
1410A-17X-2W-120
10. C. solitus
1410B 21X-3W-127
11. C. grandis
1410B-21X-3W-127
12. C. grandis
1410C-19X-2W-67
13. C. expansus
1410B -21X-3W-127
14. C. expansus
1410B -21X-3W-127

REFERENCES

Agnini, C., Fornaciari, E., Raffi, I., Catanzariti, R., Pälike, H., Backman, J., & Rio, D. (2014). Biozonation and biochronology of Paleogene calcareous nannofossils from low and middle latitudes. *Newsletters on Stratigraphy,*47(2), 131-181. https://doi.org/10.1127/0078-0421/2014/004

Aubry, M.-P. (1992). Late Paleogene calcareous nannoplankton evolution: a tale of climatic deterioration, in: Prothero, D.R., Berggren, W.A. (Eds.), Eocene- Oligocene Climatic and Biotic Evolution. Princeton *University Press, Princeton*, pp. 272–309

Aubry, M.-P. (1998): Early Paleogene calcareous nannoplankton evolution: a tale of climatic amelioration, in: Late Paleocene–early Eocene Biotic and Climatic Events in the Marine and Terrestrial Records, Columbia University Press, New York, 158–201.

Bijl, P. K., Schouten, S., Sluijs, A., Reichart, G. -J, Zachos, J. C., & Brinkhuis, H. (2009). Early Palaeogene temperature evolution of the Southwest Pacific Ocean. Nature, 461(7265), 776-779. https://doi.org/10.1038/nature08399

Bijl, P. K., Bendle, J. A. P., Bohaty, S. M., Pross, J., Schouten, S., Tauxe, L., Brinkhuis, H. (2013). Eocene cooling linked to early flow across the Tasmanian gateway. *Proceedings of the National Academy of Sciences of the United States of America*, 110(24), 9645-9650. https://doi.org/10.1073/pnas.1220872110

Bornemann, A., D'haenens, S., Norris, R. D., & Speijer, R. P. (2016). The demise of the early Eocene greenhouse – Decoupled deep and surface water cooling in the eastern North Atlantic. *Global and Planetary Change*, 145, 130-140. https://doi.org/10.1016/j.gloplacha.2016.08.010

Boulila, S., Vahlenkamp, M., De Vleeschouwer, D., Laskar, J., Yamamoto, Y., Pälike, H., Röhl, U. (2018). Towards a robust and consistent middle Eocene astronomical timescale. *Earth and Planetary Science Letters, 486*, 94-107. https://doi.org/10.1016/j.epsl.2018.01.00

Boyle, P. R., Romans, B. W., Tucholke, B. E., Norris, R. D., Swift, S. A., & Sexton, P. F. (2017). Cenozoic north Atlantic deep circulation history recorded in contourite drifts, offshore Newfoundland, Canada. *Marine Geology*, 385, 185-203. https://doi.org/10.1016/j.margeo.2016.12.01

Bown, P. R., Young, J. R. (1998). Techniques. In: Bown, P. R., (Ed.), Calcareous Nannofossil Biostratigraphy. *Kluwer Academic Publishers*, p. 16–28

Bown, P.R., Lees, J.A., Young, J.R., (2004). Calcareous nannofossil evolution and diversity through time, in: Thierstein, H.R., Young, J.R. (Eds.), Coccolithophores: From Molecular Processes to Global Impact. Springer-Verlag, pp. 481–508.

Bown, P.R. (2005a): Palaeogene calcareous nannofossils from the Kilwa and Lindi areas of coastal Tanzania (Tanzania Drilling Project 2003-4). *Journal of Nannoplankton Research*, 27(1), 21-95.

Bown, P. R. (2005b). Calcareous nannoplankton evolution: A tale of two oceans. *Micropaleontology, 51*(4), 299-308. https://doi.org/10.2113/gsmicropal.51.4.299

Bown, P.R. & Dunkley Jones, T. (2006). New Palaeogene calcareous nannofossil taxa from coastal Tanzania: Tanzania Drilling Project Sites 11 to 14. *Journal of Nannoplankton Research*, 28(1), 17-34

Bown, P.R (2010). Calcareous nannofossils fom the Paleocene/Eocene Thermal Maximum interval of southern Tanzania (TDP Site 14). *Journal of Nannoplankton Research*. 31 (1), 11-38.

Bown, P.R. & Dunkley Jones, T. (2012). Calcareous nannofossils from the Paleogene equatorial Pacific (IODP Expedition 320 Sites U1331-1334). *Journal of Nannoplankton Research*. 32 (2), 3-51.

Bown, P.R. & Newsam, C. (2017). Calcareous nannofossils from the Eocene North Atlantic Ocean (IODP Expedition 342 Sites U1403–1411). *Journal of Nannoplankton Research*, 37(1), 25-60

Bramlette, M.N. & Sullivan, F.R., (1961). Coccolithophorids and related nannoplankton of the Early Tertiary in California. *Micropaleontology*, **7**(129-188).

Coccioni, R., Bancalà, G., Catanzariti, R., Fornaciari, E., Frontalini, F., Giusberti, L., Jovane, L., Luciani, V., Savian, J., Sprovieri, M. (2012). An integrated stratigraphic record of the Palaeocene-lower Eocene at Gubbio (Italy), new insights into the early Palaeogene hyperthermals and carbon isotope excursions*, Terra Nova*, 24, 380–386. http://dx.doi.org/10.1111/j.1365-3121.2012.01076.x .

Coplen, T. B., Brand, W. A., Gehre, M., Gröning, M., Meijer, H. A. J., Toman, B., & Verkouteren, R. M. (2006). New guidelines for $\delta^{13}C$ measurements. *Analytical Chemistry*, 78(7), 2439-2441. https://doi.org/10.1021/ac052027c

Coxall, H. K., Huck, C. E., Huber, M., Lear, C. H., Legarda-Lisarri, A., O'Regan, M., Backman, J. (2018). Export of nutrient rich northern component water preceded early Oligocene Antarctic glaciation. *Nature Geoscienc*e, 11(3), 190-196. https://doi.org/10.1038/s41561-018-0069-9

Cramer, B. S., Toggweiler, J. R., Wright, J. D., Katz, M. E., & Miller, K. G. (2009). Ocean overturning since the late Cretaceous: Inferences from a new benthic foraminiferal isotope compilation. *Paleoceanography*, 24(4) https://doi.org/10.1029/2008PA001683

Cramwinckel, M. J., Huber, M., Kocken, I. J., Agnini, C., Bijl, P. K., Bohaty, S. M., Sluijs, A. (2018). Synchronous tropical and polar temperature evolution in the Eocene letter. *Nature,* 559(7714), 382-386. https://doi.org/10.1038/s41586-018-0272-2

Gartner, S. (1970). Phylogenetic lineages in the lower Tertiary coccolith genus *Chiasmolithus.* Proceedings of the North American Paleontological Convention. Part G, 930-957.

Gallagher, L. T. (1988). A technique for viewing the same nannofossil specimen in light microscope and scanning electron microscope using standard preparation materials. *Journal of Micropalaeontology*, 7(1), 53-57. https://doi.org/10.1144/jm.7.1.53

Gradstein, F.M., Ogg, J.G., Schmitz, M.D., Ogg, G.M. (Eds.), 2012. The Geologic Time Scale 2012. Elsevier, Amsterdam pp. 1144. https://doi.org/10.1016/B978-0-444-59425-9.01001-5

Hammer, Ø, Harper, D. A. T., and Ryan, P. D. (2001). PAST: Paleontological statistics software package for education and data analysis, Palaeontol. Electron., 4, 9.

Hay, W.W., Mohler, H.P. & Wade, M.E. (1966). Calcareous nannofossil from Nal'chik (northwest Caucasus). *Eclogae Geologicae. Helvetiae*, 59, 379-399.

Hay, W.W., Mohler, H.P., Roth, P.H., Schmidt, R.R. & Boudreaux, J.E. (1967). Calcareous nannoplankton zonation of the Cenozoic of the Gulf Coast and Caribbean-Antillean area, and transoceanic correlation. *Transactions of the Gulf Coast Association of Geological Societies*, 17, 428-480.

Hollis, C. J., Taylor, K. W. R., Handley, L., Pancost, R. D., Huber, M., Creech, J. B., Zachos, J. C. (2012). Early Paleogene temperature history of the southwest Pacific Ocean: Reconciling proxies and models. *Earth and Planetary Science Letters*, 349-350, 53-66. https://doi.org/10.1016/j.epsl.2012.06.024

Inglis, G. N., Farnsworth, A., Lunt, D., Foster, G. L., Hollis, C. J., Pagani, M., Pancost, R. D. (2015). Descent toward the icehouse: Eocene sea surface cooling inferred from GDGT distributions. *Paleoceanography*, 30(7), 1000-1020. https://doi.org/10.1002/2014PA002723

Lagabrielle, Y., Goddéris, Y., Donnadieu, Y., Malavieille, J., & Suarez, M. (2009). The tectonic history of Drake Passage and its possible impacts on global climate. *Earth and Planetary Science Letters*, 279(3-4), 197-211. https://doi.org/10.1016/j.epsl.2008.12.03

Lawver, L. A., & Gahagan, L. M. (2003). Evolution of Cenozoic seaways in the circum-Antarctic region. *Palaeogeography, Palaeoclimatology, Palaeoecology*, 198(1-2), 11-37. https://doi.org/10.1016/S0031-0182(03)00392-4

Lear, C. H., Elderfield, H., & Wilson, P. A. (2000). Cenozoic deep-sea temperatures and global ice volumes from Mg/Ca in benthic foraminiferal calcite. *Science*, 287(5451), 269-272. https://doi.org/10.1126/science.287.5451.269

Luciani, V., Dickens, R. G., Backman, J., Fornaciari, E., Giusberti, L., Agnini, C., & D'Onofrio, R. (2016). Major perturbations in the global carbon cycle and photosymbiont-bearing planktic foraminifera during the early Eocene. *Climate of the Past*, 12(4), 981-1007. https://doi.org/10.5194/cp-12-981-2016

Martini, E. (1971). Standard Tertiary and Quaternary calcareous nannoplankton zonation, in: Proceedings of the 2nd Planktonic Conference, 2, Tecnoscienza, Roma, 739–785, 1971.

Norris, R.D., Wilson, P.A., Blum, P., Scientists, E. 342, (2014). Paleogene Newfoundland Sediment Drifts and MDHDS Test, in: *Proceedings of the Integrated Ocean Drilling Program*, 342: College Station, TX (Integrated Ocean Drilling Program). https://doi.org/10.2204/iodp.proc.342.2014

Okada, H., & Bukry, D. (1980). Supplementary modification and introduction of code numbers to the low-latitude coccolith biostratigraphic zonation (Bukry, 1973; 1975). *Marine Micropaleontology*, 5(C), 321-325. https://doi.org/10.1016/0377-8398(80)90016-X

Pearson, P. N., Nicholas, C. J., Singano, J. M., Bown, P. R., Coxall, H. K., van Dongen, B. E., Huber, B.T., Karega, A., Less, J.L., Msaky, E., Pancost, R.D., Perason, M., Roberts, A. P. (2004). Paleogene and cretaceous sediment cores from the Kilwa and Lindi areas of coastal Tanzania: Tanzania drilling project sites 1-5. *Journal of African Earth Sciences, 39*(1-2), 25-62. https://doi.org/10.1016/j.jafrearsci.2004.05.001

Pagani, M., Zachos, J. C., Freeman, K. H., Tipple, B., & Bohaty, S. (2005). Atmospheric science: Marked decline in atmospheric carbon dioxide concentrations during the Paleogene. *Science*, 309(5734), 600-603. https://doi.org/10.1126/science.1110063

Payros, A., Ortiz, S., Alegret, L., Orue-Etxebarria, X., Apellaniz, E., & Molina, E. (2012). An early Lutetian carbon-cycle perturbation: Insights from the Gorrondatxe section (Western Pyrenees, Bay of Biscay). *Paleoceanography*, 27(2) https://doi.org/10.1029/2012PA002300

Perch-Nielsen, K., (1971). Elektronenmikroskopische untersuchungen an Coccolithen und verwandten Formen aus dem Eozan von Danemark. *Biologiske Skrifter. Kongelige Danske Videnskabernes Selskab*, 18(3), 1-76.

Perch-Nielsen, K. (1985). Cenozoic calcareous nannofossils, in: Bolli, H.M., Saunders, J.B., Perch-Nielsen, K. (Eds.), Plankton Stratigraphy. Cambridge University Press, Cambridge, pp. 427–554.

Romein, A.J.T. (1979). Lineages in Early Paleogene calcareous nannoplankton. *Utrecht Micropaleontological Bulletins*, 22, 1-231.

Sexton, P. F., Wilson, P. A., & Norris, R. D. (2006). Testing the Cenozoic multisite composite $\delta^{18}O$ and $\delta^{13}C$ curves: New monospecific Eocene records from a single locality, Demerara Rise (Ocean Drilling Program leg 207). *Paleoceanography,* 21(2) https://doi.org/10.1029/2005PA001253

Sexton, P. F., Norris, R. D., Wilson, P. A., Pälike, H., Westerhold, T., Röhl, U., Gibbs, S. (2011). Eocene global warming events driven by ventilation of oceanic dissolved organic carbon. *Nature,* 471(7338), 349-353. https://doi.org/10.1038/nature09826

Shamrock, J. L., & Watkins, D. K. (2009). Evolution of the cretaceous calcareous nannofossil genus *Eiffellithus* and its biostratigraphic significance.*Cretaceous Research,30*(5), 1083-1102. https://doi.org/10.1016/j.cretres.2009.03.009

Spofforth, D. J. A., Agnini, C., Pälike, H., Rio, D., Fornaciari, E., Giusberti, L., Muttoni, G. (2010). Organic carbon burial following the Middle Eocene Climatic Optimum in the central western Tethys. *Paleoceanography, 25*(3) https://doi.org/10.1029/2009PA001738

Tyrrell, T. and Young, J. R. (2008). Coccolithophores. In Steele, J. H., Thorpe, S. A and Turekian, K. K., (2nd Edition.). Encyclopedia of Ocean Sciences. Academic Press, San Diego, US, pp. 606–614.

van Heck, S.E. & Prins, B. (1987). A refined nannoplankton zonation for the Danian of the Central North Sea. *Abhandlungen der Geologischen Bundesanstalt*, 39, 285-303.

Vahlenkamp, M., Niezgodzki, I., De Vleeschouwer, D., Bickert, T., Harper, D., Kirtland Turner, S., Pälike, H. (2018). Astronomically paced changes in deep-water circulation in the western North Atlantic during the middle Eocene. *Earth and Planetary Science Letters*, 484, 329-340. https://doi.org/10.1016/j.epsl.2017.12.016

Varol, O. (1992). *Sullivania* a new genus of Palaeogene coccoliths. *Journal of Micropalaeontology*, 11(2), 141-149. https://doi.org/10.1144/jm.11.2.14

Watkins, D. K., & Bergen, J. A. (2003). Late Albian adaptive radiation in the calcareous nannofossil genus *Eiffellithus*. *Micropaleontology*, 49 (3), 231-250. https://doi.org/10.2113/49.3.231

Westerhold, T., Röhl, U., Frederichs, T., Agnini, C., Raffi, I., Zachos, J. C., & Wilkens, R. H. (2017). Astronomical calibration of the Ypresian timescale: Implications for seafloor spreading rates and the chaotic behavior of the solar system? *Climate of the Past,* 13(9), 1129-1152. https://doi.org/10.5194/cp-13-1129-201

Yamamoto, Y., Fukami, H., Taniguchi, W., and Lippert, P.C. (2018). Data report: updated magnetostratigraphy for IODP Sites U1403, U1408, U1409, and U1410. In Norris, R.D., Wilson, P.A., Blum, P., and the Expedition 342 Scientists, Proceedings of the Integrated Ocean Drilling Program, 342: College Station, TX (Integrated Ocean Drilling Program). https://doi.org/10.2204/iodp.proc.342.207.2018

Young, J.R. & Bown, P.R. (1997). Cenozoic calcareous nannoplankton classification. *Journal of Nannoplankton Research*, 19, 36–47.

Zachos, J., Pagani, H., Sloan, L., Thomas, E., & Billups, K. (2001). Trends, rhythms, and aberrations in global climate 65 Ma to present. *Science*, 292(5517), 686-693. https://doi.org/10.1126/science.1059412

Zachos, J. C., Dickens, G. R., & Zeebe, R. E. (2008). An early Cenozoic perspective on greenhouse warming and carbon cycle dynamics. *Nature*, 451(7176), 279-283. https://doi.org/10.1038/nature06588

Chapter 4

The evolution of early middle Eocene sphenoliths: a record from Southeast Newfoundland Ridge (Site U1410)

Abstract

In this study, we document the evolution of early-middle Eocene sphenoliths as recorded at IODP Site U1410 (Southeast Newfoundland Ridge). This sequence is the most complete and expanded of the North Atlantic and is characterized by an exquisite preservation of microfossils. Quantitative analyses among sphenoliths indicate that the early-middle Eocene transition was marked by an important rearrangement within the principal components of sphenolith assemblages with the prominent decrease of *Sphenolithus radians* and *Sphenolithus moriformis* coinciding with the onset of *Sphenolithus spiniger* dominance. This turnover fascinating corresponds with a distinctive perturbation in the stable isotope records documented slightly above the Ypresian-Lutetian boundary. This first evolutionary step was followed by a remarkable episode of diversification during which we document the emergence of a number of morphotypes which eventually led to the appearance and development of the *Sphenolithus furcatolithoides* lineage. This lineage likely evolved from a sphenolith without any apical structure and likely ascribable to *Sphenolithus moriformis* group but characterized by a different optical behaviour. This ancestral form is gradually substituted by forms bearing fine processes that later evolved in morphotypes with well-developed bifurcating apical spines. The peculiarity of middle Eocene *Sphenolithus furcatolithoides* gr. is the extraordinary variability of the spine morphology but the real innovation of this lineage is related to its ultrastructure which results in unique and distinctive extinction figures. The highly resolved record from IODP Site U1410 allows a detailed reconstruction of all the evolutionary steps occurred in the early-middle Eocene among sphenoliths and of the possible relationships with changes in the geosphere (i.e., physical environment and climate). As it is often the case, evolutionary lineages provide good biohorizons that in this case could serve as additional events to improve the available biostratigraphic framework.

4.1 INTRODUCTION

The early-middle Eocene transition is a crucial interval in the Cenozoic climate. This interval encompasses the decline of the sustained greenhouse conditions of the Early Eocene Climatic Optimum (EECO) and the initial phase of the long-term middle-late Eocene cooling (Zachos et al., 2001; 2008). The decline in temperature during the middle-late Eocene is evident from the multiple oceanic benthic foraminifera $\delta^{18}O$ records (Cramer et al., 2009; Zachos et al., 2001, 2008) but also documented in the benthic foraminifera Mg/Ca ratio (Lear et al., 2000; Dutton et al., 2005; Hollis et al., 2012) and TEX86 compilations (Bijl et al., 2009; Hollis et al., 2012; Inglis et al., 2015; Cramwinkel at al., 2018). Previous studies have proposed that the post-EECO global cooling was primary driven by the decline of atmospheric pCO_2 (Pagani et al., 2005; Zachos et al., 2008) but other

authors suggested a link with the tectonic changes occurred in the southern hemisphere that may have favored the thermal isolation of Antarctica (Lawver and Gahan, 2003; Lagabrielle et al., 2009).

The EECO was an interval of exceptional warming during which the Earth experienced the highest deep-sea temperatures over the last 80 million years. The absolute estimation of these temperatures suggested that they were more than 14°C warmer if compared to the present day (Zachos et al., 2008; Bijl et al., 2009; Huber and Caballero, 2011; Hollis et al., 2012; Pross et al., 2012; Inglis et al., 2015; Cramwinkel et al., 2018). Defining the onset and the duration of the EECO is still a matter of discussion (Luciani et al., 2016; Westerhold et al., 2008). Though the original definition of the EECO is based on the $\delta^{18}O$ record (Zachos et al., 2001), recent works (Luciani et al., 2016) have instead proposed to use the $\delta^{13}C$ profile to define the onset of this climatic phase, which then coincides with the carbon cycle perturbation termed "J event" (after Cramer et al., 2003). The end of the EECO was suggested to be correlative with the onset of the long cooling trend, which some authors have tentatively placed in correspondence with the first occurrence of the calcareous nannofossil *Discoaster sublodoensis,* close to the Chor 22n/C21r transition (Luciani et al., 2016, 2017; Westerhold et al., 2018). According to this emended definition, the EECO lasted ~ 4 million years (49-53 Ma) if the GTS2012 is adopted (Vandenberghe et al., 2012). Overall the climate evolution of early-middle Eocene displayed a high variability especially during the EECO, when benthic isotope records from Atlantic Ocean (Cramer et al., 2003, 2009; Sexton et al., 2011; Kirtland Tuner et al., 2014; Lauretano et al., 2016; Luciani et al., 2017; Westerhold et al., 2017), Pacific Ocean (Westerhold et al,. 2018) and from multiple land-based marine sections (Coccioni et al., 2012; Slotnik et al., 2015; Luciani et al., 2016) showed that the EECO and its aftermath are punctuated by numerous negative carbon isotope excursions (CIEs), associated with warming events (hyperthermals). Strong evidences support the idea that these hypertyhermals were orbitally forced. A recent stable isotope dataset from the Pacific Ocean indicates that conditions of environmental instability may have lasted up to the early Lutetian, where two warming episodes seem to have interrupted the onset of the global cooling (Westerhold et al., 2018).

Calcareous nannofossils were the dominant phytoplankton group in the early Paleogene but they declined in diversity from the middle Eocene with a general trend that mirrors the global cooling pattern (Figure 4.1) (Bown et al., 2004, Dunkley Jones et al., 2008; Villa et al. 2008). During the extreme greenhouse conditions across the EECO nannoplankton community underwent a profound regeneration with the appearance and expansion of the very successful genus *Reticulofenestra* (Agnini et al., 2006; Schneider et al., 2011; Shamrock et al., 2012) and the successive increase in nannofossill diversity, which culminated in the middle Eocene diversity maximum (Figure 4.1; Bown et al., 2004; 2008). Across this interval, the calcareous nannofossil genus *Sphenolithus,* a common

component of low-middle latitudes assemblages, experienced an important phase of diversification. This genus is thought to be extremely responsive to environmental forcing showing different species-specific preferences to changes in trophic/thermal conditions (Dunkley jones et al., 2008; Toffanin et al., 2011). Despite their great potential as biostratigraphic tool and paleoenvironmental proxy, the detailed dynamics of this group across the early-middle Eocene transition still remain poorly constrained. The sedimentary sequence at IODP Site U1410, which hosts exceptionally well preserved middle Eocene calcareous nannofossils (Norris et al., 2014), provided a unique case study to investigate the evolutionary pattern of this group during a relatively stable climate conditions. In this study, we present the semiquantitative data of sphenolith assemblages and discuss the evolutionary steps that gave rise to the emergence of *Sphenolithus furcatolithoides*. Semiquantitative data served also to evaluate the role of sphenoliths in the middle Eocene biostratigraphic framework and to highlight possible relationship between changes documented among middle Eocene sphenoliths and trends observed in environmental parameters (e.g., temperature, nutrients, etc.).

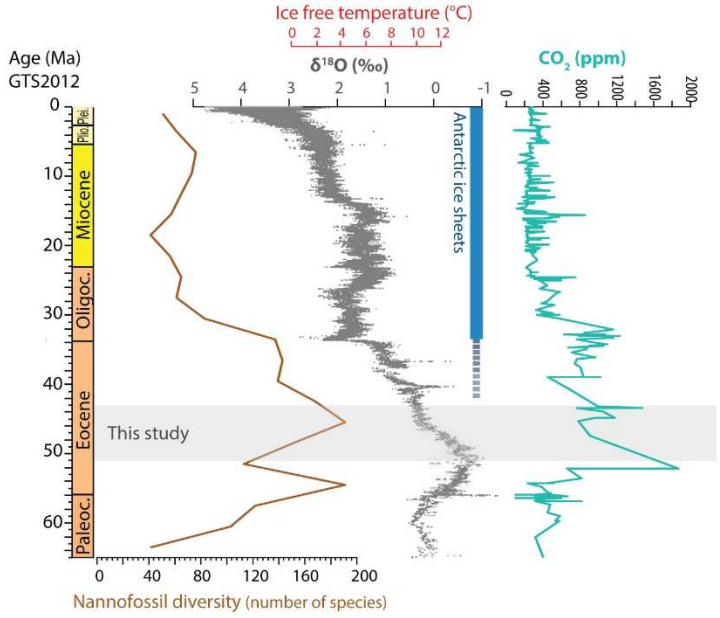

Figure 4.1: Nannofossil diversity trend (Bown et al., 2004), global composite $\delta^{18}O$ (Cramer et al., 2009) and CO_2 reconstruction (Beerling & Royer, 2011).

4.2. MATERIAL AND METHODS

4.2.1 Site description

IODP Site U1410 (41°19.6993′N, 49°10.1847′W) was retrieved during Exp. 342 and is located in the Northwest Atlantic on the Southeast Newfoundland Ridge, a positive bathymetric feature extending southeast from the Grand Banks (Figure 4.2). This is a mid-depth site (~ 2950 mbsf at 50 Ma) that was well above the carbonate compensation depth (CCD) during the Eocene (Norris et al., 2014). At Site U1410, three holes (A-C), which spans from the lower Eocene to Pleistocene (Norris et al., 2014),

were drilled. The initial Site U1410 shipboard spliced composite sequence was recently revised based on onshore-acquired XRF data (Vahlenkamp et al., 2018) and therefore some samples used in this study are not incorporated in the latest version of the splice. We updated the depth scale of our samples by using the new splice and all the depths are expressed as revised meter composite depth (rmcd) (Vahlenkamp et al., 2018). The studied section encompasses the interval between 294.69 rmcd and 146.83 rmcd, which corresponds to the lower middle Eocene transition. The position of chron boundaries are placed as follows: 163.86 rmcd for C20n/C20r, 218.40 rmcd for C20r/C21n; 252.53 rmcd for C21n/C21r (Vahlenkamp et al., 2018, Yamamoto et al., 2018). Magnetostratigraphic data are not available for the lower part of the succession.

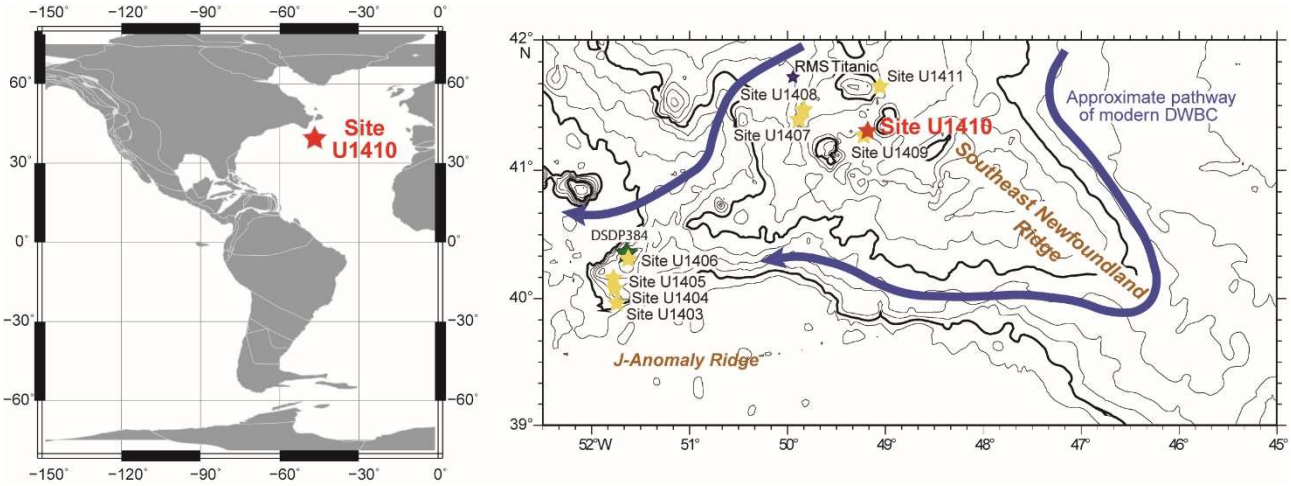

Figure 4.2: To the left, location map of IODP Site U1410 (base map provided by the Ocean Drilling Stratigraphic Network; http://www.odsn.de/odsn/index.html). To the right, a bathymetric map showing the area drilled during IODP Exp. 342 and the modern pathways of Deep Western Boundary Current (DWBC). Modified from Norris et al. (2014).

Across the studied interval, a tremendous change in sediments composition occurred close to the early-middle Eocene boundary, where carbonate content of sediments decreases from an average of 90% wt in (Unit IV) to an average of 50% wt in (Unit III) (Figure 4.3). In detail, the pinkish white carbonate-rich nannofossil chalk with cherts of Unit IV is substituted by gray and white nannofossil clay and ooze of Unit III (Norris et al., 2012). The clay rich sediments of Unit III represent contourite drift deposits (Norris et al., 2014), which resulted from the formation of a persistent deep current that transported the terrigenous component from a supposed source area located along the northeast Canadian continental margin to the Newfoundland Ridge (Boyle et al., 2017). The position of Site U1410 is on the pathway of the modern Deep Western Boundary Current (DWBC) (Figure 4.2) but the evidence of a progenitor of this current, termed as Northern Component Water (NCW), is documented since the middle Eocene (Boyle et al., 2017; Coxall et al., 2018;Valenkamp et al., 2018). At Site U1410 the new sedimentary regime, related to the contourite phase, led to a significant

increase in the sedimentation rate, which passed from an estimated value of ~ 0.6 cm/ky in the early Eocene to 1.3-2.6 cm/ky in middle Eocene (Norris et al., 2014). The activity of NCW was strongly influenced by astronomical forcing as testified by the striking rhythmic alternations of greenish nannofossil-rich clay and whitish nannofossil ooze of Unit III (Valhenkamp et al., 2018).

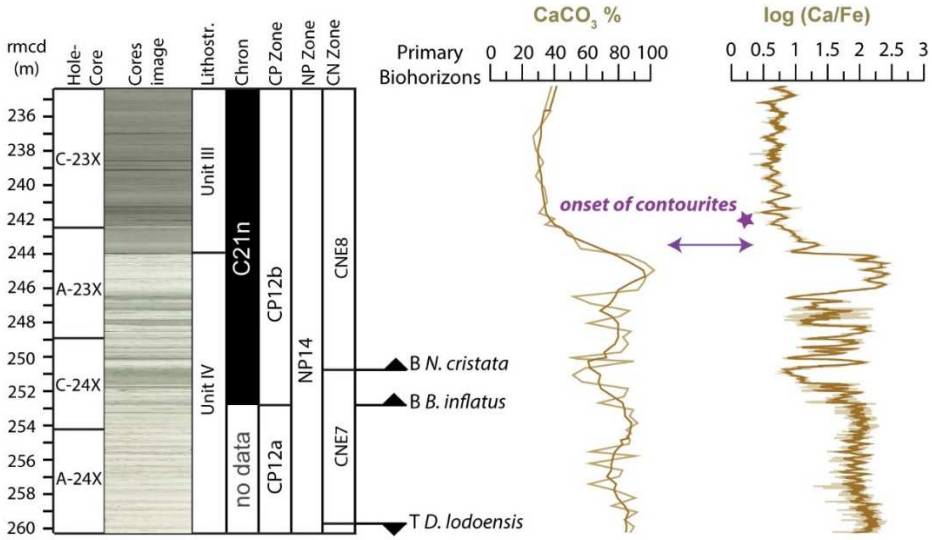

Figure 4.3: Core images showing the transition from white to pinkish white nannofossil chalk (lithostratigraphic Subunit IVa, Norris et al., 2014) to greenish grey nannofossil ooze (lithostratigraphic Unit III, Norris et al., 2014). $CaCO_3$ content (Cappelli et al., in prep.) and log (Ca/Fe) records (Boulila et al., 2018) are plotted against magnetostratigraphy (Yamamoto et al., 2018) and primary calcareous nannofossil data (Cappelli et al., in prep.) and biozones (CP Zone, Okada and Bukry, 1980; CN Zone, Agnini et al., 2014). The significant drop in the log (Ca/Fe) values at the Unit IV-Unit III boundary corresponds to the decrease in carbonate content related to the onset of drift sedimentation.

4.2.2 Calcareous nannofossil analysis

The calcareous nannofossil dataset is based on the study of 220 smear slides, which were prepared using standard methods (Bown & Young, 1998) and analyzed under a Zeiss light microscope (LM) at a magnification of 1250x. The position of calcareous nannofossil biohorizons and semiquantitative assemblage data are from Cappelli et al. (in prep) and are based on standard counting methods (modified after Backman and Shackleton, 1983; Agnini et al., 2014). In order to constrain biostratigraphic events based on sphenolith biohorozons and assemblage pattern, we performed an additional analysis by counting a total of 100 specimens belonging to the genus *Sphenolithus* (modified Rio et al., 1990). This datum was used to obtain the percentage of each species within the genus, but it served also to calculate the number of specimens present in a specific area ($1mm^2$). The number of specimens of a taxon counted on a specific area provides abundance patterns that usually are more consistent and more reliable especially in case the taxon is very rare. However, this kind of datum is influenced by preparation technique and by dissolution and terrigenous dilution that could bias the final result (Rio et al., 1990).

Specimens were identified to species level, whenever possible, following the taxonomy of Perch-Nielsen (1985); Bown (2005); Bown and Dunkley Jones (2006, 2012); Bown and Newsam (2017)

Shamrock (2010), and Agnini et al. (2014). Following Agnini et al (2014), biostratigraphic events are defined as Base (B) and Top (T) to describe the lowest and highest occurrences of the taxa, and as Base Common (Bc) and Top Common (Tc), which are placed where the abundance of the species of interest becomes continuous/common and discontinuous/rare, respectively.

The descriptive terminology for *Sphenolithus* follows the guidelines proposed by Young et al. (1997). Respect to the terminology used by these authors we introduced the term "process" to indicate an elongate extension of the lateral cycle that is usually very delicate and fragile. At light microscope, discrimination of sphenoliths species is conventionally based on the extinction pattern that sphenoliths form when they are oriented at 0 ° and 45° to the polarization direction. The great variability of these figures provides the main criteria for distinguishing different taxa.

Selected samples were observed under a scanning electron microscope (SEM, JEOL Digital JSM-6480LV installed at UCL), using circular strew slides (Bown and Young, 1998) and freshly broken sediment surface (Lees et al., 2004). In addition, SEM preparation included the use of circular slides with a printed grid, (Cappelli et al., in prep.), this method allowed for the recognition of the same specimen both under LM and SEM. Minor changes respect to the technique of Gallagher (1988) were applied, including the use of cover slip with a printed grid and the use of distilled water instead of methanol during the LM analysis. Specifically, samples were first observed under LM using different magnification in order to determine the position of the specimen of interest on the grid. After the LM analysis, the circular cover slips were dried on a hot plate, mounted on an aluminum stub and gold-coated for the SEM study (Bown & Young, 1998).

4.3. RESULTS

4.3.1 Sphenoliths abundance patterns

At Site U1410, calcareous nannofossils are abundant and the preservation ranges from moderate during the early Eocene to good in correspondence of the contourite active phase. In numerous samples, the high abundance of clay favors an exquisite preservation of microfossils that is better than in most of the early Paleogene deep-sea sediments.

Sphenolithus is a common component of nannofossil assemblages with highest abundances recorded in the early Eocene (~11 %) and lower abundance documented in the middle Eocene (~ 4 %). The decrease in abundance is recorded between 260 and 248 rmcd and it is associated with a significant increase of the genus *Reticulofenestra,* which becomes the dominant component of the nannofossil assemblages throughout the middle Eocene (Cappelli et al., in prep.)

At Site 1410, the early-middle Eocene sphenolith assemblages are characterized by a continuous and abundant presence of *Sphenolithus moriformis* gr., which accounts for ~ 47 % (on average) and

reaches a peak value of ~85 % in the early Eocene (Figure 4.4). Others important components of the sphenolith assembalges during the early Eocene are *Sphenolithus editus* and *Sphenolithus radians.* The former shows an average abundance of ~ 13 % up to 273.17 rmcd, then it declines gradually and finally displays a sporadic occurrence up to its extinction. The latter accounts for ~ 25 % (on average) of the entire assemblage in the early Eocene. This species shows a significant decrease just above the early-middle Eocene boundary, and then stabilizes around values of ~ 1% with sporadic and rare occurrence throughout the middle Eocene (Figure 4.4).

Very rare and scattered specimens of *S. spiniger* gr. have been observed from 273.17 rmcd but a sudden increase in abundance (up to 11 %) occurred at ~ 249 rmcd, where the Bc of *S. spiniger* gr. is positioned. Throughout its range, the abundance of *S. spiniger* gr. ranges around ~ 34 % though a high amplitude is visible around this average value and slight decrease occurs upward in the section (Figure 4.4). Following Toffanin et al. (2011), we adopted a broader definition for *S. spiniger* (Bukry, 1971), which includes specimens with a small apical spine (Plate 4.5, fig. 5-8).

Sphenoliths bearing delicate and fragile processes that diverge with different angles just above the base emerges in the middle Eocene. All these forms are grouped in an informal taxonomic unit termed "sphenoliths with processes". The high clay content of the study sediments has facilitated the preservation of these fine structures, which are probably not preserved in most of the other deep-sea successions. These amazing forms are characterized by a terrific morphological variability and they could be subdivided in three main groups:

- forms with a square base and a variable number (three or more) of processes (Plate 4.5, figs 10-12);
- forms with square base and two apical processes diverging with an angle lower or higher than 90° (Plate 4.1, figs. 2,3, 7,8,9; Plate 4.2 figs. 2-7; Plate 4.5 figs. 13,16);
- forms with a tapering base, a poorly developed lateral cycle and two fine high-angled lateral processes (Plate 4.2, figs. 17,18; Plate 4.4, fig. 10; Pl. 4.6, fig, 2-3).

These morphotypes are characterized by the same extinction figure at 45 °, where spines become dark and the base forms a bright cross-shaped figure. Similar forms have previously been observed in material retrieved during IODP Exp. 342 (Bown & Newsam, 2017) and they have been termed as *Sphenolithus* cf. *S. perpendicularis* or *S. perpendicularis.* Despite the morphologic similarities and the comparable extinction pattern, we tentatively separate *S. perpendicularis* (Shamrock, 2010) and *Sphenolithus kempii* (Bown and Dunkley Jones, 2012) from sphenoliths with processes. This is because in sphenoliths with processes spines are very fine and they appear to be an extension of the lateral cycle, rather than extension of a well-developed apical cycle (Plate 4.5, 4.6).

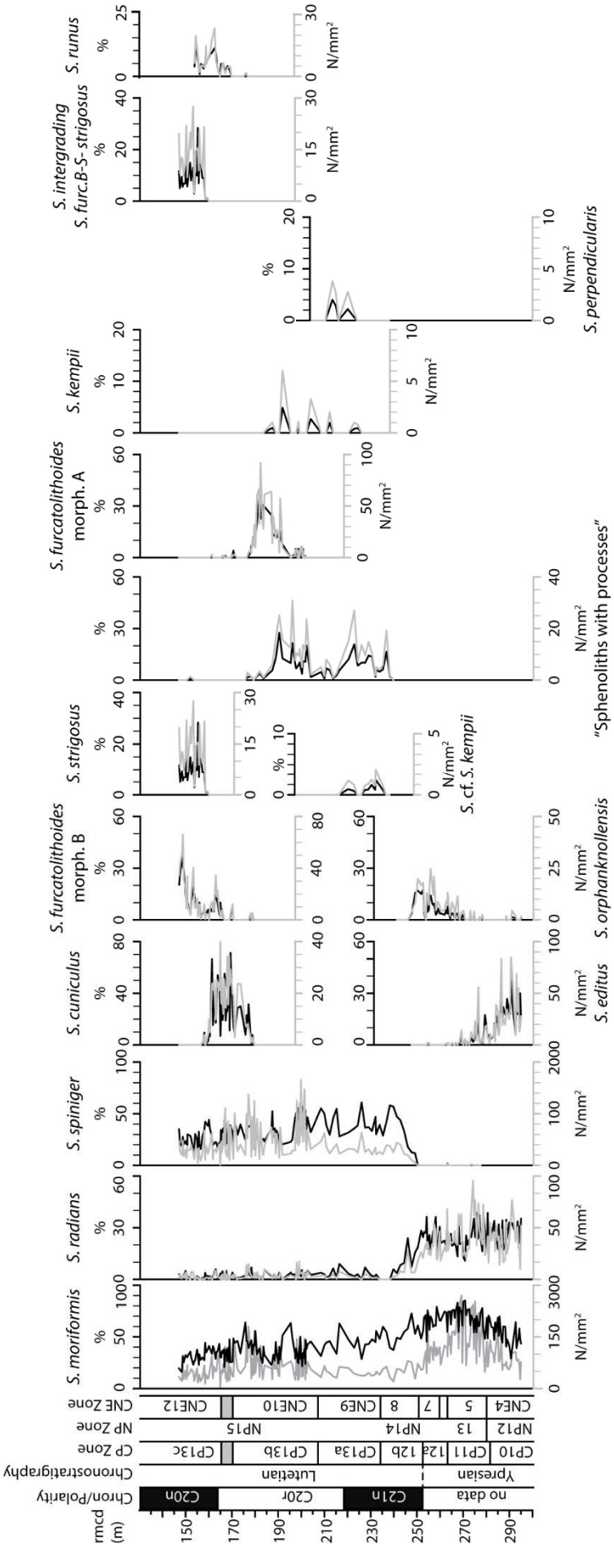
rmcd (m)
Chron/Polarity
Chronostratigraphy
CP Zone
NP Zone
CNE Zone
no data
C21n
C20r
C20n
Ypresian
Lutetian
CNE4
CNE9
CNE10
CNE12
NP12
NP14
NP15
CP10
CP11
CP12a
CP12b
CP13a
CP13b
CP13c
S. moriformis
S. radians
S. spiniger
S. cuniculus
S. furcatolithoides morph. B
S. strigosus
S. cf. S. kempii
S. furcatolithoides morph. A
S. kempii
S. intergrading S. furc.B-S. strigosus
S. runus
S. perpendicularis
S. editus
S. orphanknollensis
"Sphenoliths with processes"
%
N/mm²

Figure 4.4 (previous page)**:** Relative (%, in black) and semiquantitative (N/mm2, in grey) abundances of *Sphenolithus* at Site U1410. Also shown is the biostratigraphy (Cappelli et al., in prep.). To the left magnetostratigraphy (Yamamoto et al., 2018), chronostratigraphy, and calcareous nannofossil biostratigraphy (Cappelli et al., in prep.). Biostratigraphic schemes follow Okada & Bukry (1980, CP Zone), Martini (1971, NP Zone) and Agnini et al. (2014; CNE Zone).

The relative high abundance of sphenoliths at Site U1410 and their exceptional preservation is for sure related to the good preservation of the material but establishing whether the presence of spines in same species is related to overgrowth in the type material or to a presence of spines and processes is difficult to assess, even because the morphological variability and stratigraphic ranges of *S. perperdicularis* and *S. kempii* are poorly documented. At Site U1410, *S. perpendicularis* (Plate 4.1, 4.2; 4.6) and *S. kempii* (Plate 4.6, fig. 5) are consistently rare (~ 2 % and ~ 0.5 %), whereas sphenoliths with processes has a continuous occurrence from 238 to 180 rmcd and show an average value of ~ 8 % (Figure 4.4).

Somehow related to sphenoliths with processes, we recognized forms with a square base and 2 or 4 long, narrow lateral spines that diverge at a very low angle (Pl. 4.1). When these specimens are oriented at 45°, the spines become dark and cross-shaped figure appears. These forms have been ascribed to *S.* cf. *S. kempii* and they display a quite wide distribution ranging from the equatorial Pacific (Bown & Dunkley Jones, 2012, Sites U1331-1334), to Indian (Site 711; Fioroni et al., 2015) and to NW Atlantic oceans (Sites U1407 and U1409; Bown & Newsam, 2017).

When the sphenoliths with processes are still present, we recorded the first occurrence of *Sphenolithus furcatolithoides*. Following Agnini et al (2014), we distinguished two different morphotypes: *Sphenolithus furcatolithoides* morphotype A and *Sphenolithus furcatolithoides* morphotype B.

Sphenolithus furcatolithoides morphotype A has two tapering spines that bifurcate just above the base. The long spines are near-parallel in the lower part, whereas they may gently diverge from the long axis with different angles (< 90 °) in the upper part. *Sphenolithus furcatolithoides* morphotype A shows the same extinction patter of *S. perpendicularis*, with a bright cross-shaped and dark spines at 45° (Plates 4.2, 4.3, 4.6). At Site U1410, this morphotype is recorded from 201.5 rmcd and has a relatively short stratigraphic range throughout C20r (Figure 4.4). This taxon shows a rare and discontinuous occurrence in the initial part of its range, while upward it increases up to an average value of ~ 15 %. After a final peak in abundance (~ 32 %) at ca 18.341 rmcd, it declines to 1 % at 176.81 rmcd , showing a scattered occurrence until its extinction.

In correspondence of the progressive decline of *S. furcatolithoides* morphotype A*,* we recorded the first occurrence of *Sphenolithus cuniculus* (Figure 4.4). This species has been originally described in the Kilwa Masoko (Tanzania, Bown, 2005) and it has been reported also from Site 762C (Exmouth

Plateau, Shamrock, 2010) and Site 1051 (Blake Nose; Agnini et al., 2014). *Sphenolithus. cuniculus* is characterized by having very low proximal and lateral cycles. The original description of *S. cuniculus* includes ancestral specimens with poorly developed proximal cycles (Plate 4.3, figs. 2,5). These morphotypes evolve in forms in which the lateral cycle creates an open cone that encloses the low vertical elements of the proximal cycle (Plate 4.3 figs. 3,4,6-11; Plate 4.7). At 45° *S. cuniculus* shows a dark spine and dimly illuminated base. At Site U1410, this highly distinctive species is restricted to the upper part of C20r and to the lower part of C20n with an average abundance of 17 %. At 160 rmcd, *S. cuniculus* shows a sharp decreases up to 1 % and it eventually disappears at 156.66 rmcd (Figure 4.4).

Sphenolithus furcatolithoides morphotype B is recorded from 178.51 rmcd, but it is continuous and common just above 166.09 rmcd (Figure 4.4). Following Agnini et al. (2014) this morphotype differentiated from *S. furcatolithoides* morphotype A in having a different extinction figure at 45 °. In *S. furcatolithoides* morphotype B the base does not form a cross-shaped figure but a faintly illuminated bow-tie figure, where only two elements are clearly defined (Plate 4.3, fig. 18; Plate 4.4, figs. 3,4).

Sphenolithus strigosus appears at 159.94 rmcd (Figure 4.4). This species appears to be strictly related to *S. furcatolithoides* morphotype B, showing a similar morphology and the same extinction pattern (Plate 4.3, Plate 4.7). According to the original definition, the main difference between these two species is the height of the bifurcation on the spine. At Site U1410, we encountered numerous specimens that could not be confidently referred to either *S. furcatolithoides* morphotype B or to *S. strigosus* because terminal parts of the spines were often broken off. These forms have been merged into a single informal group, *Spenolithus* intergrading *S. furcatolithoides* morph.B-*strigosus. Sphenolithus furcatholithes* morphotype B, *S. strigosus* and specimens with uncertain affinities account for 10 %, 8 % and 9 %, respectively. Stratigraphic ranges of both *S. furcatolithoides* morphotype B and *S. strigousus* extends well above the observed interval.

4.4 DISCUSSION

4.4.1 Evolutionary lineages

The genus *Sphenolithus* first appeared in the lower Paleocene with the emergence of forms with a dome-shaped structure (*S. morifomis* gr.) (Plate 4.5, fig. 9). The Paleocene - early Eocene interval is marked by two major episodes of diversification (Agnini et al., 2007). The first radiation occurred during the late Paleocene with the origination of the first forms with an apical spine (i.e. *Sphenolithus anarrhopus),* whereas during the early Eocene, a second episode of radiation gave rise to the

appearance of several species with a well-developed apical spine (e.g., *Sphenolithus editus, Sphenilithus radians, Sphenolithus villae*) (Plate 4-5, figs. 1.3).

The middle Eocene documented the third phase of radiation within this genus. The first species evolved in the middle Eocene is *S. spiniger,* this taxon has a narrow triangular shape with a short compound apical cycle that may have an elongate extension (Plate 4.5, figs. 4-8). Identifying an ancestor for *S. spiniger* is tricky because our data do not show a clear stratigraphic overlap between *S. spiniger* gr. and *S. editus*, suggesting that both of them may have evolved from *S. moriformis* gr. Alternatively, *S. spiniger* may have evolved from the morphologically related *S. orphanknollensis* (Perch-Nielsen, 1985), which is always rare at Site U1410 but shows a stratigraphic overlap with *S. spiniger* gr.

The third phase of diversification within sphenoliths led also to the development of forms with an innovative construction, the duocrystaline spines. The type species for duocrystaline spine sphenoliths is *S. furcatolithoides.* To date, several theories have been proposed for the origin of this species. Perch-Nielsen (1985) suggested that *S. furcatolithoides* evolved from *S. spiniger*. Shamrock et al. (2010) indicated *S. perpendicularis* as the ancestor of *S. furcatolithoides* and agreed with Perch-Nielsen (1985) suggesting an evolutionary relationship with *S. spiniger.* On the other hand, Romein (1979) and Bown & Newsam (2017) proposed that *S. furcatolithoides* may have evolved from *S. radians*. Our observations indicate that the evolutionary history of *S. furcatholithoides* is quite complicated and it is a part of a new lineage that emerged from *S. moriformis* gr. In fact, we suggest that ancestral forms with fine processes evolved from *S. moriformis* gr.by developing fine processes as extension of the lateral cycle. More importantly, this phyletic relationship is based on the extinction figure at 45 ° which gradually passes from the typical pattern observed in *S. moriformis* to a bright cross-shaped figure in *Sphenolithus* sp.1 (Pl. 4.1).

As already mentioned, sphenoliths with processes include a wide range of morphologies which evolve through time. Primitive forms are generally characterized by a well-developed lateral cycle and two (or more) processes. The morphologic features associated to the stratigraphic ranges of these morphotypes suggest that *S. kempii* and *S. perpendicularis* represent the first adaptation attempt in evolution of this group. The morphological novelty is the passage from the presence of fragile processes to the development of robust spines through a progressively bulk up and decrease in number of the apical elements. Finally, the elongate extensions of the lateral cycle are transformed into a duo-crystalline apical cycle with the spine diverging just above the lateral cycle (Pl. 4.5 fig.15).

At Site U1410, there is no stratigraphic continuity between the range of *S. perpendicularis* and that of *S. furcatolithoides* morphotype A (Figure 4.5). This datum indicates that the emergence of *S. perpendicularis* is a first short-lived and unsuccessful tentative in this lineage. A second step in the

evolution of this group of sphenoliths coincides with the appearance of *S. furcatolithoides* morphotype A, the most likely ancestor of this species is a sphenolith with processes (Pl. 4.2, fig. 3) which then develops robust apical spines. This species is crucial in the evolution of this lineage because from this taxon both *S. cuniculus* and *S. furcatolithoides* morphotype B have possibly evolved (Figure 4.5).

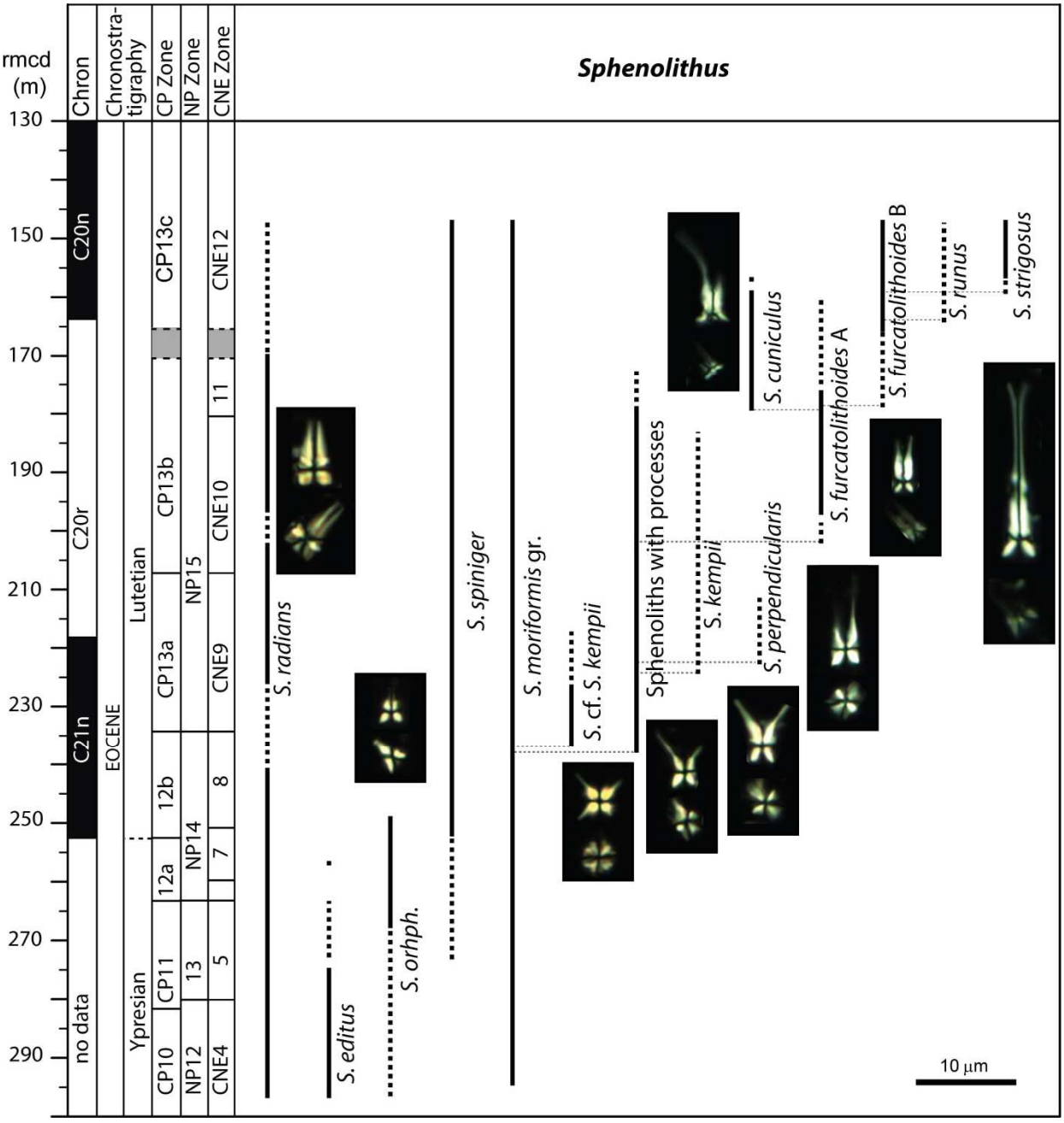

Figure 4.5: Stratigraphic distribution of *Sphenolithus* at Site U1410 plotted versus magnetostratigraphy (Yamamoto et al., 2018) biostratigraphy (CP Zone, Okada &Bukry, 1980; NP Zone, Martini, 1971; CNE Zone, Agnini et al., 2014). Positions of biohorizons are from Cappelli et al. (in prep). Dotted lines indicates interval with scattered occurrences.

Sphenolithus cuniculus is characterized by a progressive reduction of the base size and a substantial reorganisation of the entire base structure. In more evolved forms the base consists of an amorphous cycle completely incorporated in the lateral cycle (Pl. 4.7 fig. 1-4). The apical element of *S. cuniculus* is similar to that of *S. furcatolithoides* morphotype A but the spine tends to diverge more high on the apical cycle.

Although the stratigraphic ranges of these sphenoliths suggest that *S. cuniculus* should represent the connection between *S. furcatolithoides* morphotype A and *S. furcatolithoides* morphotype B, *S. cuniculus* is morphologically extremely different from the very similar *S. furcatolithoides* A and B and more likely represents a new branch departing from *S. furcatholitohides* Instead, *Sphenolithus furcatolithoides* A and *S. furcatolithoides* B are very similar but the former has a well-developed later cycle that is absent in the latter (Plate 4.6, 4.7). This distinction produces the different extinction pattern observed in these morphotypes at 45 °.

4.4.2 Possible improvements in biostratigraphy

The complicated Eocene biostratigraphic framework still needs a lot of work to be settled (Agnini et al., 2014). *Sphenolithus* are commonly used in Cenozoic calcareous nannofossil biostratigraphy because they are resistant to dissolution, they show moderately high abundance and rapid rates of evolution. This genus provides key events for the biostratigraphic subdivision of the Oligocene and their high potential is used also across the Oligocene-Miocene transition (Agnini et al., 2014). The importance of sphenoliths in the middle Eocene biostratigraphic framework has been first pointed out by Agnini et al. (2014), which introduced the Bc of *S. cuniculus* to define the base of Zone CNE11. Despite the significant biostratigraphic value of this genus, the middle Eocene sphenoliths still have poorly constrained stratigraphic ranges and as a consequence their potential as reliable biohorizons is still largely unknown.

The studied interval spans the traditional middle Eocene biozones NP12-NP15 Martini (1971), which correspond to Zone CP10- Subzone CP13c (Okada & Bukry, 1981). Estimating the value of bioevents related to sphenoliths throughout this interval is extremely important because biohorizons based on marker species, such as *B. inflatus* (base Subzone CP12b)*, Nannotetrina alata* (base Subzone CP13a) and *P. gigas* (base Subzone CP13b and Subzone CP13c) may be rare or absent in some depositional settings. In addition, *P. gigas* has an ambiguous taxonomic status and a scattered abundance pattern during the final part of its range, so that the T of *P. gigas* is considered one of the most problematic biohorizons of the entire Eocene (Agnini et al., 2014).

The appearance of *S. spiniger* has been documented in the upper part of Zone NP12 in several successions (Perch-Nielsen 1985; Bown and Dunkley Jones, 2012; Shamrock and Watkins, 2012).

At Site U1410, very rare and scattered specimens of *S. spiniger* have been observed from a 273.17 rmcd (Figure 4.6). A similar pattern was detected at Agost (Tori and Monechi, 2013). Even though this event requires additional calibrations, such scattered distribution would discourage the use of its first occurrence for biostratigraphic purposes.

An alternative is to use the Bc of *S. spiniger* or the cross-over in abundance (change in proportion of species abundance) between *S. radians* and *S. spiniger*. The cross-over in abundance between two species is an unconventional biohorizon that was first introduced by Thierstein et al. (1977) and it has been successfully used in the early Miocene (Backman et al., 2012). At Site U1410, both these biohorizons are recorded just above the B of *N. cristata,* which defines the base of CNE8 (Fig. 4.6).

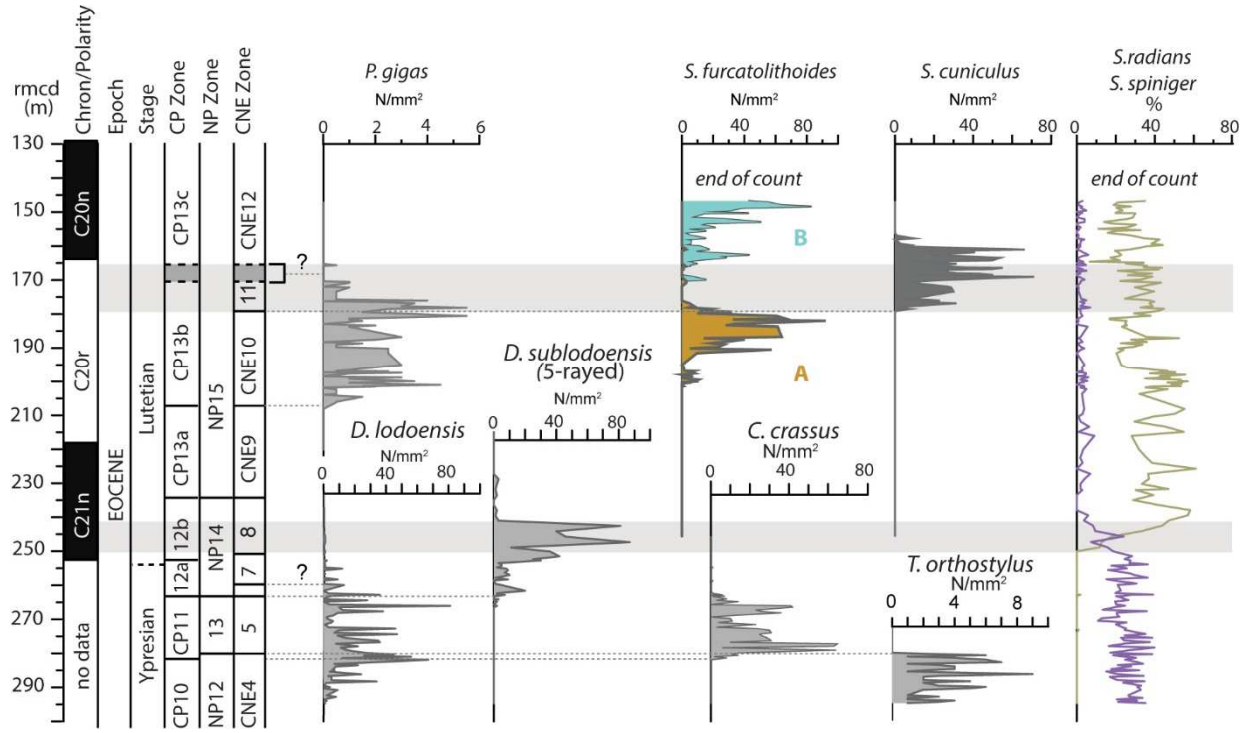

Figure 4.6: Selected calcareous nannofossil abundance patterns from IODP Site U1410. To the left magnetostratigraphy (Yamamoto et al., 2018), chronostratigraphy, and calcareous nannofossil biostratigraphy: NP Zone (Martini; 1971), CP Zone (Okada and Bukry, 1980), CNE Zone (Agnini et al., 2014). Abundace patterns of *P. gigas,D. lodoensis, D. sublodoensis, C. crassus* and *T. orthostylus* are from and calcareous nannofossil biostratiraphy are from Cappelli et al. (in prep.).

However, new high resolution semiquantitative data are essential to test the reliability of these events. The use of bioevent related to *Sphenolithus perpendicularis* was first suggested by Shamrock (2010) but even though this morphotype has a distinctive morphology, data from Site U1410 evidenced for scattered and rare abundance pattern.

Conversely, biostratigraphic events provided by *S. furcatolithoides* A -*S. cuniculus* -*S. furcatolithiudes* B plexus appear more reliable. The Bc of *S. cuniculus* is currently used as biostratigraphic biohorizon in CNE Zones (Agnini et al.; 2014), where it marks the base of Zone CNE11. At Site U1410 the B of *S. cuniculus* coincides with the Bc, but comparison of the abundance patterns from Site U1410 and Site 1051 (Agnini et al., 2014) indicates an good correlation between

the two datasets (Figure 4.7). This plexus evolved throughout the distribution range of *P gigas*, which displays a first decline in abundance just above the Bc of *S. cuniculus* in both at Site U1410 and Site 1051. At Site U1410, *P. gigas* is consistently rare/ frequent up to 170.42 rmcd. From this level upward, only one specimens of *P. gigas* was encountered ~15 meters above. A problematic interval, where *P. gigas* is present only as scattered specimens, was observed also at Site 1051. In terms of abundance patterns, the evolutionary sequence of sphenoliths is better constrained than those of *P. gigas*, and it appears very promising for biostratigraphic purposes.

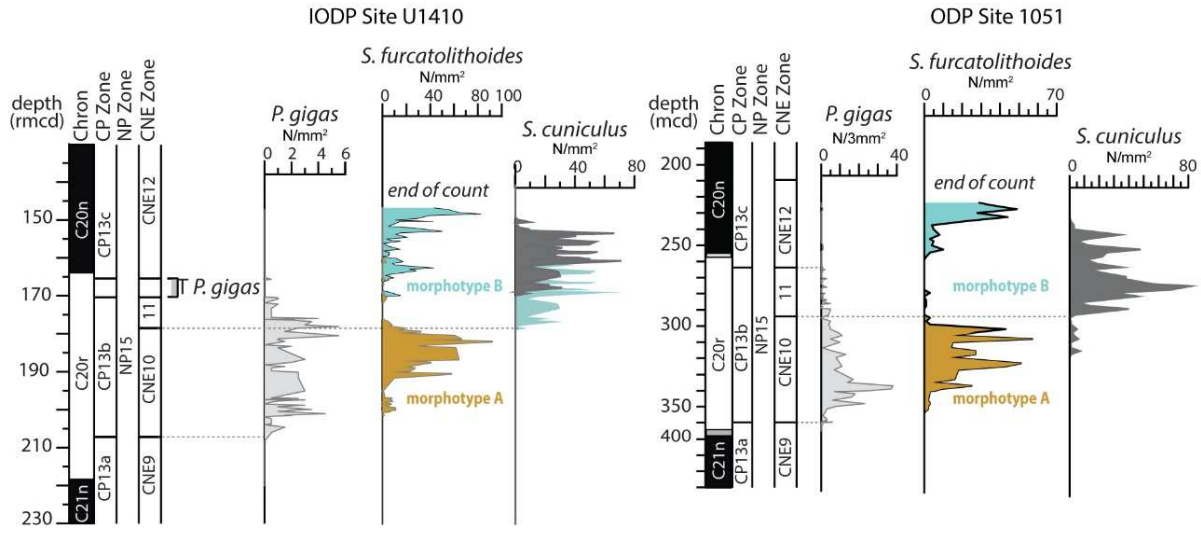

Figure 4.7: Comparison of distributions patterns of selected significant species for middle Eocene biostratigraphy from Site U1410 (this study and Cappelli et al., in prep.) and Site 1051(Agnini et al., 2014). To the left magnetostratigraphy (Yamamoto et al., 2018), chronostratigraphy, and calcareous nannofossil biostratigraphy: NP Zone (Martini; 1971), CP Zone (Okada and Bukry, 1980), CNE Zone (Agnini et al., 2014).

4.4.3 Geochemical and sphenolith data

Interpretations of the influence of biotic (i.e., predation/grazing and competition) and abiotic factors (i.e., changes in climate and ocean chemistry) in the development through evolutionary trends represent an interesting topic in calcareous nannofossil researches. Previous studies documented that the two major episodes of sphenolith diversification during Paleocene and early Eocene time are roughly associated with times of environmental changes, such as Early Late Paleocene Event (ELPE) and Early Eocene Layers of Mysterious Origin (ELMO) (Agnini et al., 2007). Nevertheless, a direct environmental forcing for these episodes of diversification cannot be determined.

Establishing the paleoenvironmental framework during which the middle Eocene diversification within sphenoliths occurred is challenging. Indeed, the climate evolution that characterizes the demise of the EECO and the onset of the global cooling is poorly resolved if compared to other intervals.

In order to assess whether environmental shifts may have influenced changes in the *Sphenolihus* assemblage, we compared our sphenolith data with stable isotope records (Fig. 4.8). Although the resolution of the geochemical dataset from Site U1410 prevents to confidently detect all the shifts related to already known hyperthermal-like events across the late early and middle Eocene, the $\delta^{13}C$ curve shows some trends that may indicate changes in environmental parameters.

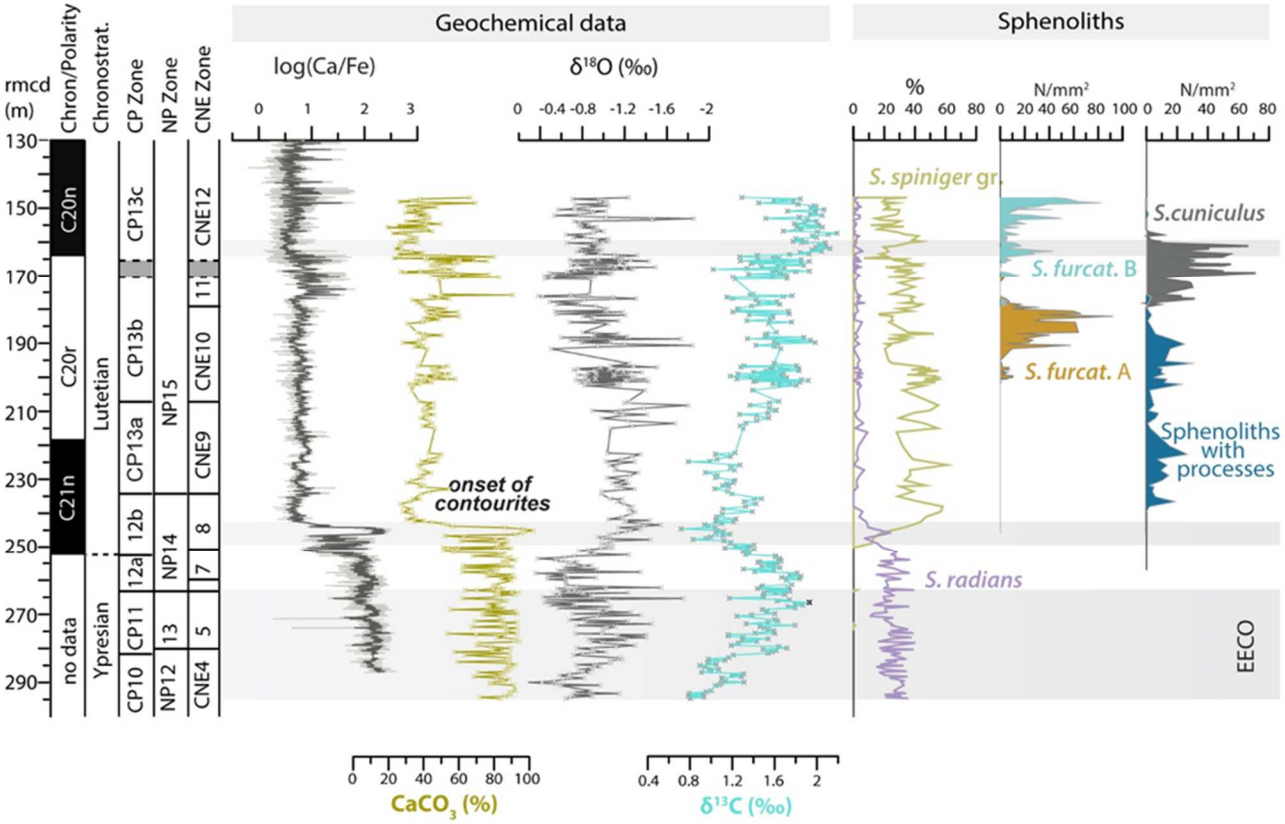

Figure 4.8: Geochemical proxies and abundance patterns of selected sphenolith taxa across the early-middle Eocene from IODP Site U1410. To the left magnetostratigraphy (Yamamoto et al., 2018), chronostratigraphy, and calcareous nannofossil biostratigraphy: NP Zone (Martini; 1971), CP Zone (Okada and Bukry, 1980), CNE Zone (Agnini et al., 2014). Log (Ca/Fe) is from Boulila et al. (2018); calcium carbonate content ($CaCO_3$, %); and bulk stable isotopes ($\delta^{18}O$ and $\delta^{13}C$) from Cappelli et al. (in prep.). The grey bars indicate the EECO (the end of ECCO is placed in correspondence of the Bc of *D. sublodoensis),* the $\delta^{13}C$ negative excursions in correspondence of the cross-over between *S. radians* and *S. spiniger,* and the step towards higher $\delta^{13}C$ values in correspondence of *S. cuniculus* demise.

During the late early-middle Eocene, the most significant shift in sphenoliths is the cross-over between *S. radians* and *S. spiniger*. In correspondence to this event, specifically from 249.28 to 242.58 rmcd, the $\delta^{13}C$ curve shows two negative shifts (~0.6‰ and ~ 0.7‰) that overlain on a general decreasing trend.

The genus *Sphenolithus* is typically considered a warm water oligotrophic taxon (Bralower, 2002; Gibbs et al., 2006; Schneider et al., 2011; Kalb & Bralower, 2012), but it sometimes behaves as a mesotrophic taxon during high productivity intervals (Wade & Bown, 2006, Dunkley Jones et al., 2008, Toffanin et al., 2011, Fioroni et al., 2015). Across key Eocene transient events, such as the

Middle Eocene Climatic Optimum (MECO) and the Eocene-Oligocene transition (EOT), the increase in abundance of *S. spiniger* (Toffanin et al., 2011) and *S. predistentus* (Dunkley Jones et al., 2008; Fioroni et al., 2015) have been interpreted as a positive response to increased eutrophic conditions. The species-specific response displayed by *Sphenolithus* across intervals of prominent environmental changes has been related to different specific adaptations within the genus (Dunkley Jones et al., 2008).

In this view, the early Lutetian may be tentatively interpreted as an environmentally relatively instable interval that favoured the proliferation of *S. spiniger* and the decline of *S. radians.* The first appearance of sphenoliths with processes occurred just above this interval. This group of sphenoliths evolved throughout a relatively stable interval with a minor negative $\delta^{13}C$ shifts of ~0.5‰ at 224.77 rmcd.

Sphenolithus fucatolithoides A and *S. cuniculus* evolved throughout an interval with ephemeral shifts in $\delta^{13}C$ overlaying on a general trend towards gradually higher values. A sudden shift at ~ 163 rmcd interrupted this stable condition. Interestingly, this step coincides with the decrease in *S. cuniculus* and the increase of long-lived *S. furcatolithoides* B. This correspondence suggests that the decline and the disappearance of *S. cuniculus* may be interpreted as a response to changes in environmental conditions. *Sphenolithus cuniculus* evolved after a long interval of stable conditions, which generally allow the evolution of highly specialized form. This species may has had strictly specific ecological preference making it more vulnerable even to minor environmental changes. It is possible that a sudden change in the environment had favoured the return of a morphostructure more similar to those of *S. furcatholithoides* A, which presumably had a less grade of specialization and a relatively wider range of tolerance to environmental parameters.

At Site U1410, the distribution range of *S. cuniculus* correlates with an interval characterized by relatively high log (Ca/Fe) ratio. This parameter has been interpreted as a proxy of the NCW strength, with high values correlated to a reduction in the strength of the deep current (Vahlenkamp et al; 2018). However, the relatively geographically restricted effect of changes in the deep current could not account for the widespread emergence and the proliferation of *S. cuniculus*.

4.5. CONCLUSION

This study is focused on the changes observed in the *Sphenolithus* assemblages across the early-late/ middle Eocene at Site U1410, a mid-depth site on the Southeast Newfoundland Ridge (Atlantic Ocean). At Site U1410, the middle Eocene interval contains exceptionally well-preserved nannofossils and provides new insights into evolutionary patterns among genus *Sphenolithus.* We documented the emergence of numerous mophotypes bearing delicate processes (sphenoliths with

processes) that most likely evolved from *S. moriformis* gr. Morphologies and distribution patterns of different morphotypes suggest that the evolution of this group gives rise to forms with a well-developed duocrystalline apical cycle, through two distinct episodes of diversifications. Specifically, a first phase of evolution results in the appearance of *S. perpendicularis*, while the second phase leads to the emergence of the similar but more successful *S. furcatolithoides* morphotype A. We suggest that both *S. cuniculus* and *S. furcatolothoides* morphotype B evolved from *S. furcatolithoides* morphotype A These three related taxa peak in abundance at different levels throughout subzones CP13b-CP13c, resulting in a highly distinctive distribution patterns. Comparison with semiquantitative data from ODP Site 1051 confirms that this plexus provides reliable primary (Bc of *S. cuniculus)* and additional biohorizons that improve the available biostratigraphic framework.

A comparison with of the carbon and oxygen stable isotope record evidences that the major changes among sphenoliths occur both during intervals of paleoenvironmental instability and stable phases. Interestingly, the cross-over between *S. radians* and *S. spiniger* occurred during a negative shift in the carbon isotope record in the lower part of C21n. Conversely, the appearance of *S. furcatolithoides* morphotype A and *S. cuniculus* occurs during a highly stable interval, which is interrupted by a positive shift in the isotope carbon values in correspondence of the increase of *S. furcatolithoides* morphotype B at the C20r/C20n transition.

Our results evidence that middle Eocene sphenoliths show very dynamic patterns but further work is needed both to strengthen the biostratigraphic potential of this genus throughout the middle Eocene and to investigate in more detail the relationship between the changes in sphenoliths and modification in environmental conditions.

A comprehensive taxonomic reasseassement of the middle Eocene sphenoliths taxonomy is essential in order to fully exploit the potential of this group both in biostratigraphy and paleoceanographic reconstructions.

Plates

Plate 4.1: Light microscope photographs (all photos are in crossed nicols). ***1.*** *Sphenolithus* sp. 1. Sample 1410C-23X-4W-85*;* ***2.*** Sphenoliths with processes. Sample 1410C-23X-3W-87 ***3.*** Sphenoliths with processes. Sample 1410B-23X-3W-5 ***4.*** *Sphenolithus* cf *S. kempii*. Sample 1410B-25X-2W-87 **5.** *Sphenolithus* cf *S. kempii*. Sample 1410A-22X-6W-127 **6.** *Sphenolithus* cf *S. kempii*, Sample 1410B-24X-1W-87 **7.** Sphenoliths with processes. Sample 1410A-22X-4W-127 **8.** Sphenoliths with processes. Sample 1410A-22X-4W-127 **9.** Sphenoliths with processes, Sample 1410A-22X-3X-127 **10.** *Sphenolithus* cf. *S. perpendicularis.* Sample 1410A-22X-4W-127 **11.** *Sphenolithus* cf. *S. perpendicularis*. Sample 1410B-24X-1X-87 **12.** *Sphenolithus* cf. *S. perpendicularis*, Sample 1410B-24X-2W-87 **13.** *Sphenolithus perpendicularis*. Sample 1410B-24X-1X-87 **14.** *Sphenolithus perpendicularis*. Sample 1410B-23-3W-**15.** *Sphenolithus perpendicularis*. Sample 1410B-23X-3W-5 **16.** *Sphenolithus perpendicularis*. Sample 1410B-23X-3W-5 **17.** *Sphenolithus perpendicularis*. Sample 1410B-23X-4W-7 **18.** *Sphenolithus perpendicularis*. Sample 1410B-23-4W- 7**.** a. 0°, b. 45°

Plate 4.2: Light microscope photographs (all photos are in crossed nicols). **1.** *Sphenolithus perpendicularis*. Sample 1410B-23X-3W-5 **2.** Sphenoliths with processes. Sample 1410C-20X-6W-67 **3.** Sphenoliths with processes. Sample 1410C-20X-6W-67 **4.** Sphenoliths with processes. Sample 1410C-20X-6W-67 **5.** Sphenoliths with processes. Sample 1410C-20X-5W-67 **6.** Sphenoliths with processes. Sample 1410C-20X-4W-147 **7.** Sphenoliths with processes. Sample 1410B-21-3W-127 **8.** *Sphenolithus furcatolithoides* morphotype A, Sample 1410C-20X-4W- 67 **9.** *Sphenolithus furcatolithoides* morphotype A, Sample 1410C-20X-4W-147 **10.** *Sphenolithus furcatolithoides* morphotype A. Sample 1410C-2X0-4W-147 **11.** *Sphenolithus furcatolithoides* morphotype A, Sample 1410C-20X-4W-67 **12.** *Sphenolithus furcatolithoides* morphotype A. Sample 1410C-20X-4W-67 **13.** *Sphenolithus furcatolithoides* morphotype A. Sample 1410B-21X-4W-127 **14.** *Sphenolithus furcatolithoides* morphotype A, Sample 1410C-19-3W-65 **15.** *Sphenolithus furcatolithoides* morphotype A. Sample 1410B-23X-3W-5 **16.** Sphenoliths with processes, Sample 1410C-19X-67W-67 **17.** Sphenoliths with processes. Sample 1410C-19X-3W-65 **18.** Sphenoliths with processes. Sample 1410A-19X-7W-22. a. 0°, b. 45°

Plate 4.3: Light microscope photographs (all photos are in crossed nicols). **1.** *Sphenolithus furcatolithoides* morphotype A. Sample 1410C-18X-4W-80 **2.** *Sphenolithus cuniculus* (primitive). Sample 1410C-18X-3W-60 **3.** *Sphenolithus cuniculus*. Sample 1410C-18X-3W-60 **4.** *Sphenolithus cuniculus*. Sample 1410C-18X-3W-60 **5.** *Sphenolithus cuniculus* (primitive). Sample 1410B-19-6W-60 **6.** *Sphenolithus cuniculus*, Sample 1410B-19-6W- 60 **7.** *Sphenolithus cuniculus*. Sample 1410B-19X-4W-20 **8.** *Sphenolithus cuniculus*. Sample 1410B-19X-4W-20 **9.** *Sphenolithus cuniculus*, Sample 1410B-19X-3W-0 **10.** *Sphenolithus cuniculus*. Sample 1410A-17X-3W-140 **11.** *Sphenolithus cuniculus*. Sample 1410A-17X-3W-140 **12.** *Sphenolithus strigosus*. Sample 1410A-16-4W- 90 **13.** *Sphenolithus strigosus*, Sample 1410B-17-5W-120 **14.** *Sphenolithus strigosus*. Sample 1410B-17X-4W-110 **15.** *Sphenolithus strigosus*. Sample 1410B-17X-4W-110 **16.** *Sphenolithus strigosus*. Sample 1410A-15X-3W-60 **17.** *Sphenolithus strigosus*. Sample 1410A-15X-3W-60 **18.** *Sphenolithus furcatolithoides* morphotype B. Sample 1410B-19X-3W-0. a. 0°, b. 45°

Plate 4.4: Light microscope photographs (all photos are in crossed nicols). **1.** *Sphenolithus furcatolithoides* morphotype B. Sample 1410A-15X-5W-80 **2.** *Sphenolithus furcatolithoides* morphotype B. Sample 1410B-18X-4W-50 **3.** *Sphenolithus furcatolithoides* morphotype B, Sample 1410B-17X-4W-110 **4.** *Sphenolithus* cf. *S. furcatolithoides* morphotype B. Sample 1410B-17-3X-100 **5.** *Sphenolithus* cf. *S. furcatolithoides* morphotype B. Sample 1410A-15X-5W- 80 **6.** *Sphenolithus* cf. *S. furcatolithoides* morphotype B, Sample 1410A-15-5W-80 **7.** *Sphenolithus* cf. *S. strigosus*. Sample 1410A 15X-5W-80 **8.** *Sphenolithus* cf. *S. strigosus*. Sample 1410A-15X-5W-80 **9.** *Sphenolithus runus*. Sample 1410A-15X-3W-60 **10.** Sphenoliths with processes. Sample 1410A-19X-7W-22 **11.** *Sphenolithus furcatolithoides* morphotype A. Sample 1410C-19X-2W- 67 **12.** *Sphenolithus cuniculus*. Sample 1410C-18X-3W-60 **13.** *Sphenolithus strigosus*. Sample 1410B-17X-2W- 30.

Plate 4.5: Light microscope (in XPL) and SEM photographs (scale bar 1µm). **1.** *Sphenolithus radians*. Sample 1410A-18X-CC **2.** *Sphenolithus radians*. Sample 1410B-21X-3W-127 **3.** *Sphenolithus radians*. Sample 1410B-21X-3-127 **4.** *Sphenolithus spiniger* group. Sample 1410B-23X-4-007 **5.** *Sphenolithus spiniger* group. Sample 1410B-21X-3-127 **6.** *Sphenolithus spiniger* gr. Sample 1410B-21X-3W-127 **7.** *Sphenolithus spiniger* gr. Sample 1410C-20X-4W-27 **8.** *Sphenolithus spiniger* group. Sample 1410C-19X-3W-65 **9.** *Sphenolithus moriformis*, Sample 1410B-23X-4W-7 **10.** Sphenoliths with processes Sample 1410B-23X-4W-7 **11.** Sphenoliths with processes. Sample 1410C-20X-6-67 **12.** Sphenoliths with processes. Sample 1410C-18X-3W-60 **13.** Sphenoliths with processes, SEM and LM (0° and 45°) photos of the same specimen. Sample 1410C-20X-6W-67 **14.** *Sphenolithus* cf. *S. perpendicularis,* SEM and LM (0° and 45°) photos of the same specimen. Sample 1410B-24X-1W-87 **15.** *Sphenolithus perpendicularis,* SEM and LM (0° and 45°) photos of the same specimen. Sample 1410B-23X-4W-7 **16.** *Sphenolithus* cf. *S. perpendicularis*, SEM and LM (0° and 45°) photos of the same specimen. Sample 1410B-23X-4W-7.

Plate 4.6: Light microscope (in crossed nicols) and SEM photographs (scale bar 1µm). **1.** *Sphenolithus* cf. *S. perpendicularis*. SEM and LM (0° and 45°) photos of the same specimen. Sample 1410C-20X-6W-67 **2.** Sphenoliths with processes. Sample 1410C-19X-3W-65 **3.** Sphenoliths with processes, SEM and LM (0° and 45°) photos of the same specimen. Sample 1410C-19X-3W-65 **4.** Sphenoliths with processes, SEM and LM (0° and 45°) photos of the same specimen. Sample 1410C-19X-3W-65 **5.** *Sphenolithus kempii*, SEM and LM (0° and 45°) photos of the same specimen. Sample 1410C-19X-3W-65 **6.** *Sphenolithus furcatolithoides* morphotype A, SEM and LM (0° and 45°) photos of the same specimen. Sample 1410C-19X-3W-65 **7.** *Sphenolithus furcatolithoides* morphotype A, SEM and LM (0° and 45°) photos of the same specimen. Sample 1410C-19X-3W-65 **8.** *Sphenolithus furcatolithoides* morphotype A, SEM and LM (0° and 45°) photos of the same specimen. Sample 1410C-19X-3W-65 **9.** *Sphenolithus furcatolithoides* morphotype A, SEM and LM (0° and 45°) photos of the same specimen. Sample 1410C-19X-3W-65 **10.** *Sphenolithus furcatolithoides* morphotype A Sample 1410A-18X-CC **11.** *Sphenolithus furcatolithoides* morphotype A. Sample 1410B-20X-4W-20 **12.** *Sphenolithus furcatolithoides* morphotype A. SEM and LM (0° and 45°) photos of the same specimen. Sample 1410B-20X-4W-20

Plate 4.7: Light microscope (in crossed nicols) and SEM photographs (scale bar 1µm). **1.** *Sphenolithus cuniculus*, SEM and LM (0° and 45°) photos of the same specimen. Sample 1410B-18X-3W-60 **2.** *Sphenolithus cuniculus*, SEM and LM (0° and 45°) photos of the same specimen. Sample 1410B-18X-3W-60 **3.** *Sphenolithus cuniculus*. Sample 1410A-17X-2W-120 **4.** *Sphenolithus cuniculus*. Sample 1410A-17X-2W-120 **5.** *Sphenolithus strigosus*, SEM and LM (0° and 45°) photos of the same specimen. Sample 1410B-17X-5W-120 **6.** *Sphenolithus strigosus*, SEM and LM (0° and 45°) photos of the same specimen. Sample 1410B-17X-5W-120 **7.** *Sphenolithus* cf. *S. furcatolithoides* morphotype B, SEM and LM (0° and 45°) photos of the same specimen. Sample 1410A-15X-4W-70 **8.** *Sphenolithus furcatolithoides* morphotype B, SEM and LM (0° and 45°) photos of the same specimen. Sample 1410A-15X-4W-70.

10µm

Plate 4.1

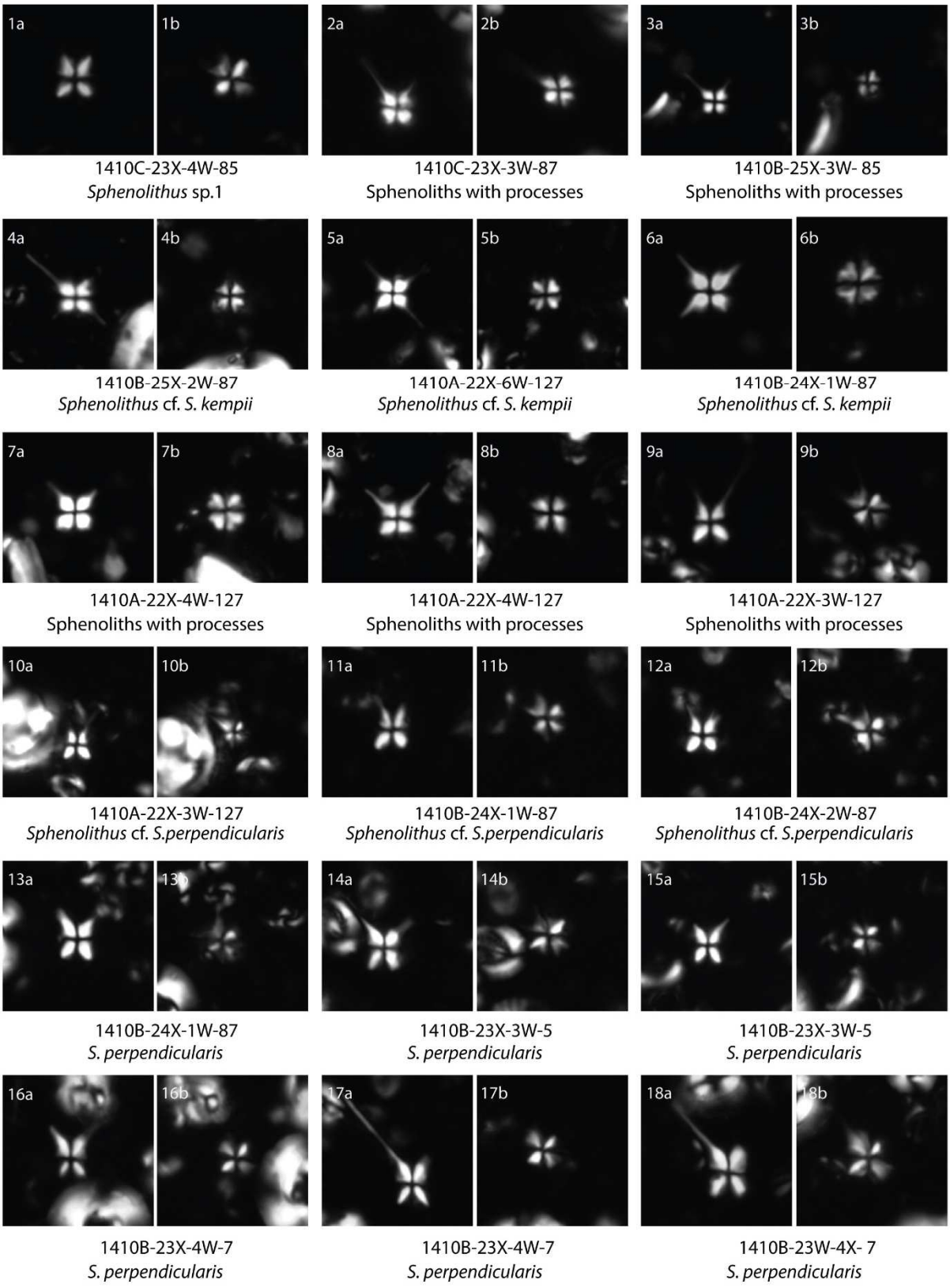

10µm

Plate 4.2

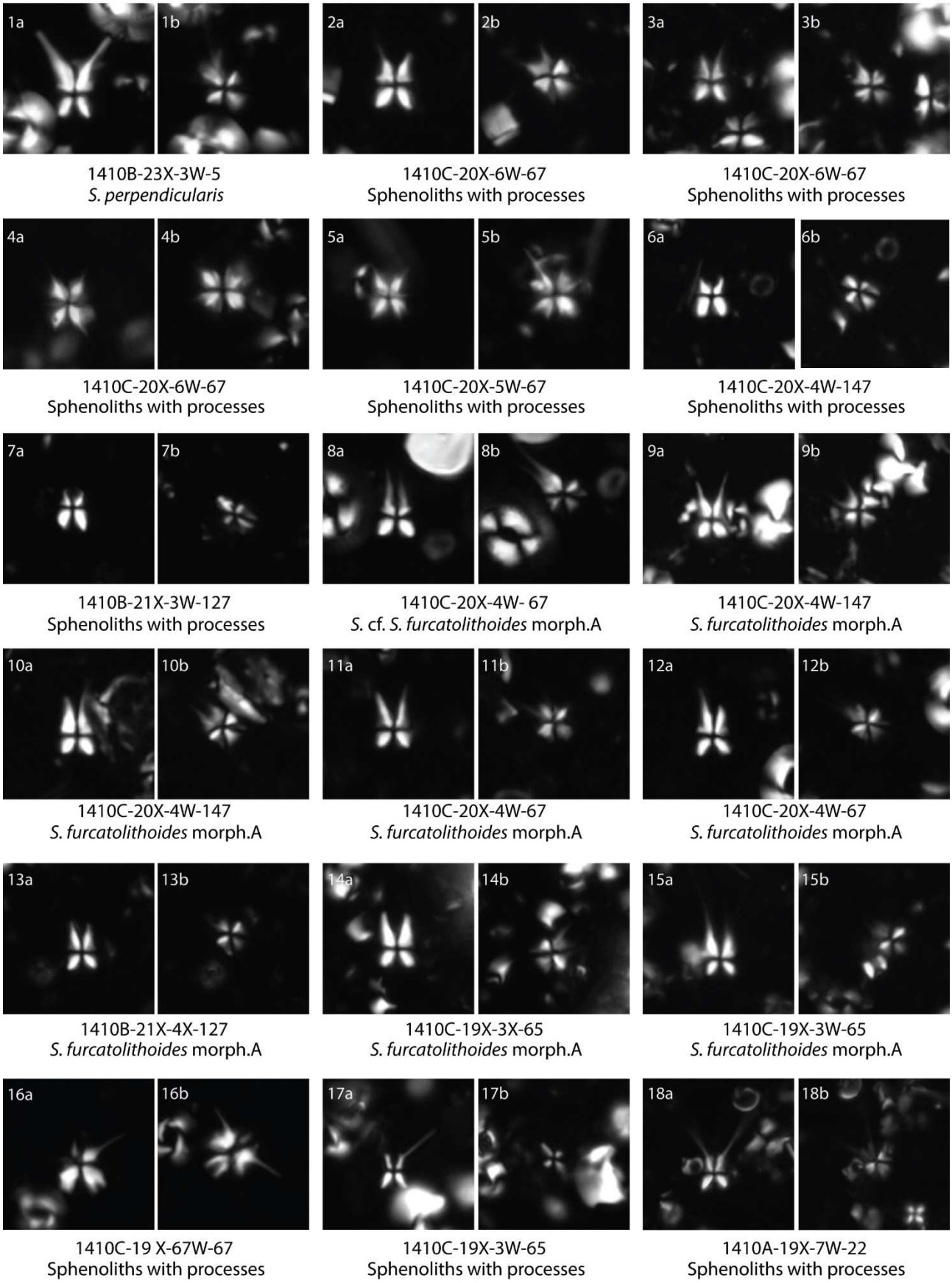

Plate 4.3

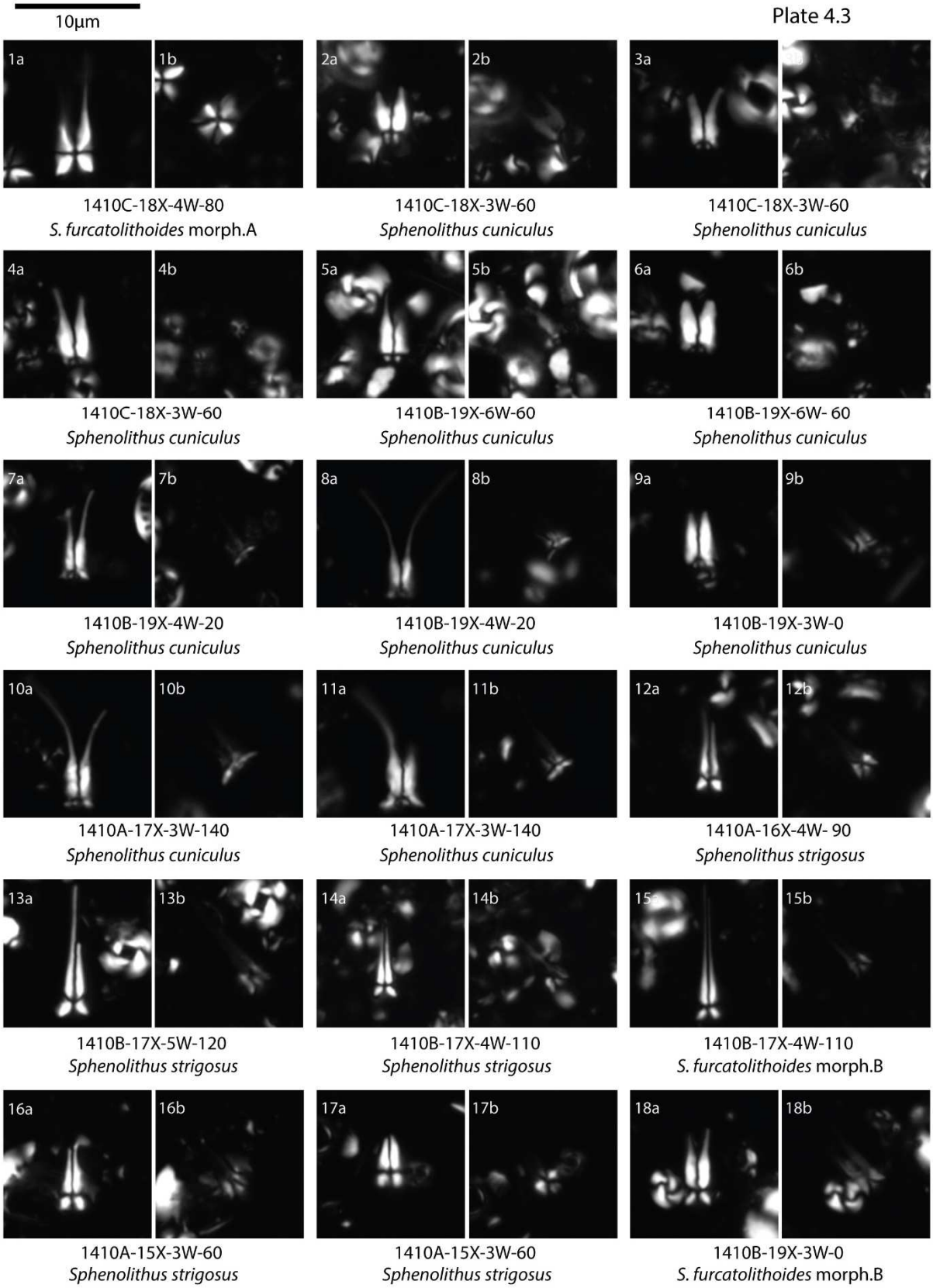
10µm
1a
1b
1410C-18X-4W-80
S. furcatolithoides morph.A
2a
2b
1410C-18X-3W-60
Sphenolithus cuniculus
3a
3b
1410C-18X-3W-60
Sphenolithus cuniculus
4a
4b
1410C-18X-3W-60
Sphenolithus cuniculus
5a
5b
1410B-19X-6W-60
Sphenolithus cuniculus
6a
6b
1410B-19X-6W- 60
Sphenolithus cuniculus
7a
7b
1410B-19X-4W-20
Sphenolithus cuniculus
8a
8b
1410B-19X-4W-20
Sphenolithus cuniculus
9a
9b
1410B-19X-3W-0
Sphenolithus cuniculus
10a
10b
1410A-17X-3W-140
Sphenolithus cuniculus
11a
11b
1410A-17X-3W-140
Sphenolithus cuniculus
12a
12b
1410A-16X-4W- 90
Sphenolithus strigosus
13a
13b
1410B-17X-5W-120
Sphenolithus strigosus
14a
14b
1410B-17X-4W-110
Sphenolithus strigosus
15a
15b
1410B-17X-4W-110
S. furcatolithoides morph.B
16a
16b
1410A-15X-3W-60
Sphenolithus strigosus
17a
17b
1410A-15X-3W-60
Sphenolithus strigosus
18a
18b
1410B-19X-3W-0
S. furcatolithoides morph.B

10µm

Plate 4.4

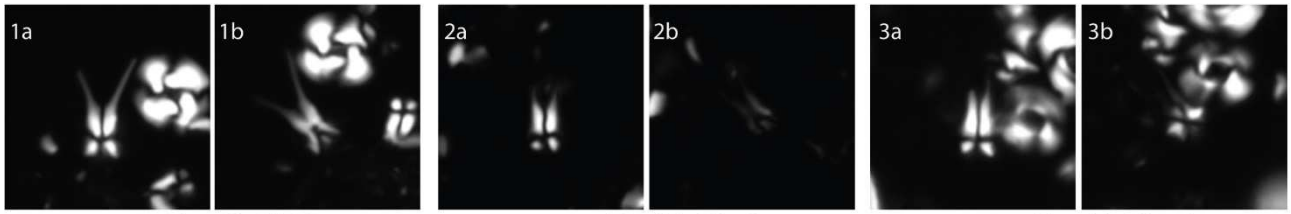

1410A-15X-5W-80
S. furcatolithoides morph.B

1410B-18X-4W-50
S. furcatolithoides morph.B

1410B-17X-4W-110
S. furcatolithoides morph.B

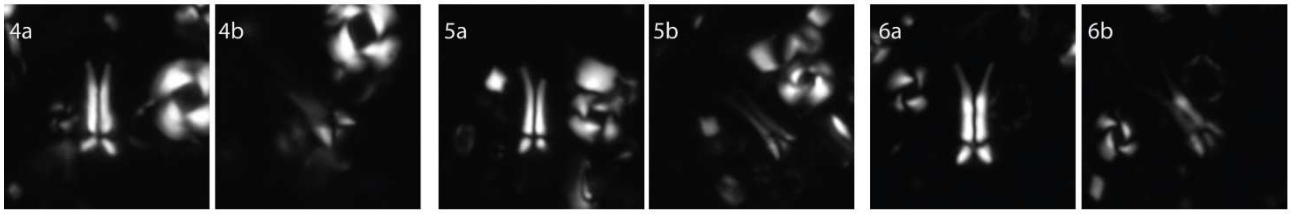

1410B-17X-3W-100
S. furcatolithoides B

1410A-15X-5W- 80
S. furcatolithoides B

1410A-15X-5W-80

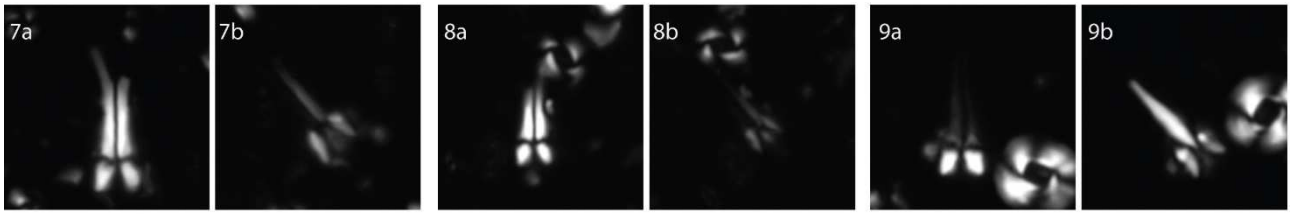

1410A-15X-5W-80
Sphenolithus intergading
S. furc. B-*S. strigosus*

1410A-15X-5W-80
Sphenolithus intergading
S. furc. B-*S. strigosus*

1410A-15X-3W-60
Sphenolithus runus

10µm

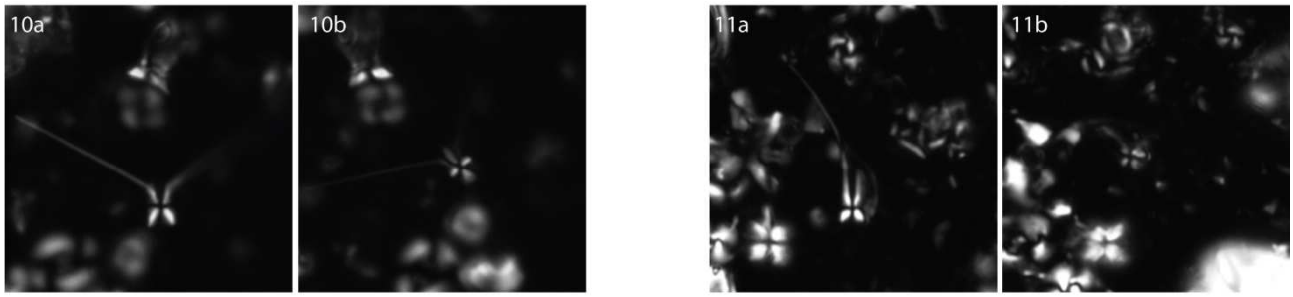

1410A-19X-7W-22
Sphenoliths with processes

1410C-19X-2W- 67
S. furcatolithoides morph. A

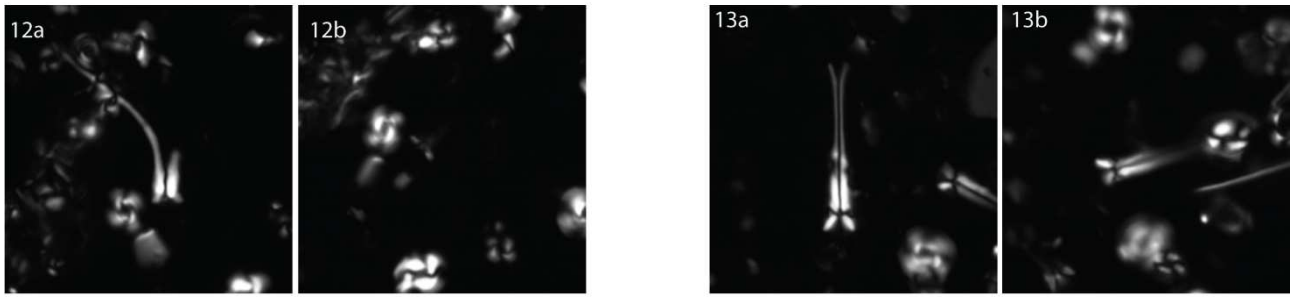

1410C-18X-3W-60
Sphenolithus cuniculus

1410B-17X-2W- 30
Sphenolithus strigosus

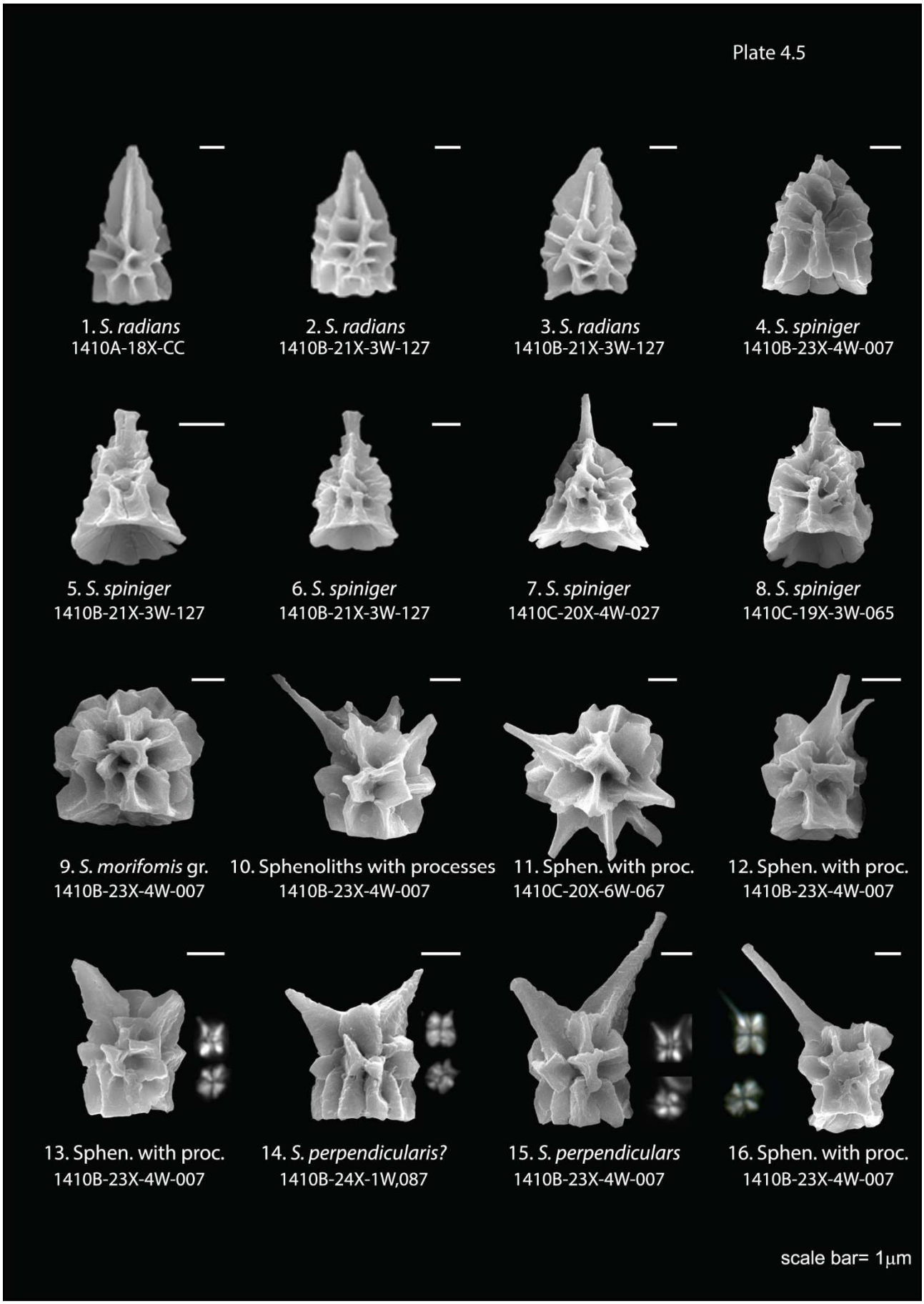
Plate 4.5
1. S. radians
1410A-18X-CC
2. S. radians
1410B-21X-3W-127
3. S. radians
1410B-21X-3W-127
4. S. spiniger
1410B-23X-4W-007
5. S. spiniger
1410B-21X-3W-127
6. S. spiniger
1410B-21X-3W-127
7. S. spiniger
1410C-20X-4W-027
8. S. spiniger
1410C-19X-3W-065
9. S. morifomis gr.
1410B-23X-4W-007
10. Sphenoliths with processes
1410B-23X-4W-007
11. Sphen. with proc.
1410C-20X-6W-067
12. Sphen. with proc.
1410B-23X-4W-007
13. Sphen. with proc.
1410B-23X-4W-007
14. S. perpendicularis?
1410B-24X-1W,087
15. S. perpendiculars
1410B-23X-4W-007
16. Sphen. with proc.
1410B-23X-4W-007
scale bar= 1μm

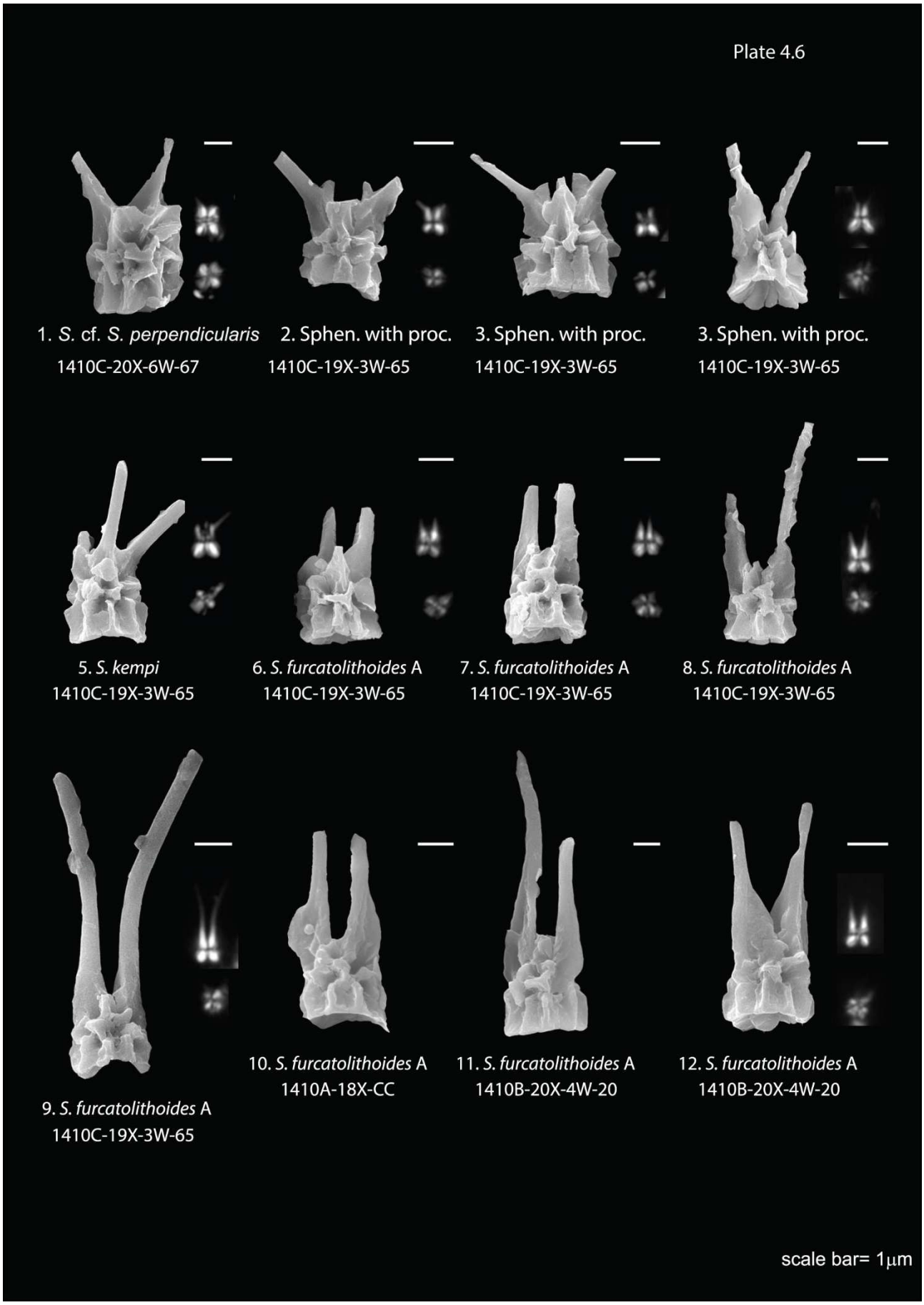
Plate 4.6
1. S. cf. S. perpendicularis
1410C-20X-6W-67
2. Sphen. with proc.
1410C-19X-3W-65
3. Sphen. with proc.
1410C-19X-3W-65
3. Sphen. with proc.
1410C-19X-3W-65
5. S. kempi
1410C-19X-3W-65
6. S. furcatolithoides A
1410C-19X-3W-65
7. S. furcatolithoides A
1410C-19X-3W-65
8. S. furcatolithoides A
1410C-19X-3W-65
9. S. furcatolithoides A
1410C-19X-3W-65
10. S. furcatolithoides A
1410A-18X-CC
11. S. furcatolithoides A
1410B-20X-4W-20
12. S. furcatolithoides A
1410B-20X-4W-20
scale bar= 1μm

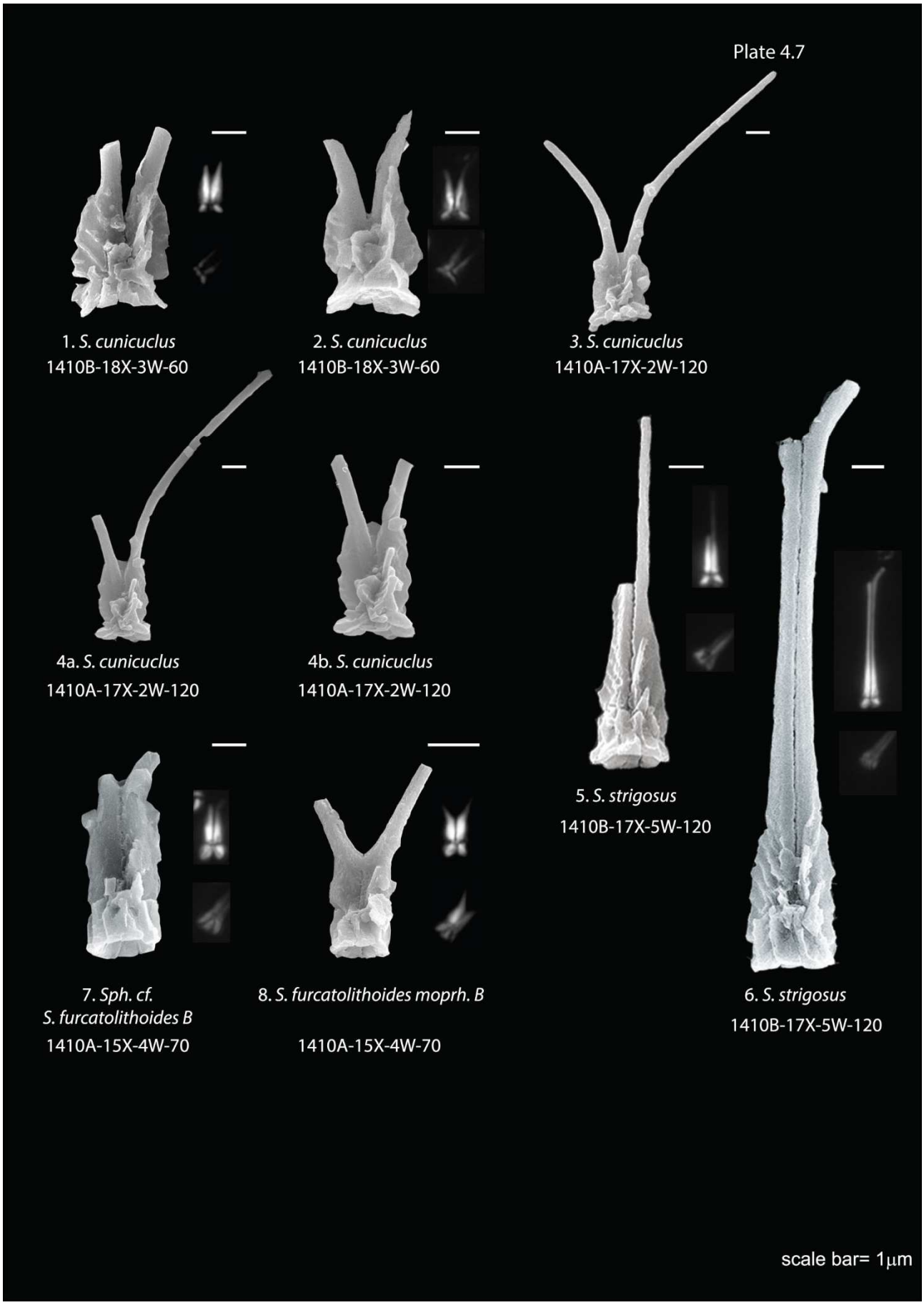
Plate 4.7
1. S. cunicuclus
1410B-18X-3W-60
2. S. cunicuclus
1410B-18X-3W-60
3. S. cunicuclus
1410A-17X-2W-120
4a. S. cunicuclus
1410A-17X-2W-120
4b. S. cunicuclus
1410A-17X-2W-120
5. S. strigosus
1410B-17X-5W-120
6. S. strigosus
1410B-17X-5W-120
7. Sph. cf.
S. furcatolithoides B
1410A-15X-4W-70
8. S. furcatolithoides moprh. B
1410A-15X-4W-70
scale bar= 1μm

REFEENCES

Agnini, C., Fornaciari, E., Raffi, I., Rio, D., Röhl, U., & Westerhold, T. (2007). High-resolution nannofossil biochronology of middle Paleocene to early Eocene at ODP Site 1262: Implications for calcareous nannoplankton evolution. *Marine Micropaleontology*,64(3-4),215-248. https://doi.org/10.1016/j.marmicro.2007.05.003

Agnini, C., Muttoni, G., Kent, D. V., & Rio, D. (2006). Eocene biostratigraphy and magnetic stratigraphy from Possagno, Italy: The calcareous nannofossil response to climate variability. *Earth and Planetary Science Letters*, 241(3-4), 815-830. https://doi.org/10.1016/j.epsl.2005.11.00

Agnini, C., Fornaciari, E., Raffi, I., Catanzariti, R., Pälike, H., Backman, J., & Rio, D. (2014). Biozonation and biochronology of Paleogene calcareous nannofossils from low and middle latitudes. *Newsletters on Stratigraphy,* 47(2), 131-181. https://doi.org/10.1127/0078-0421/2014/004

Backman, J., & Shackleton, N. J. (1983). Quantitative biochronology of Pliocene and early Pleistocene calcareous nannofossils from the Atlantic, Indian and Pacific Oceans. *Marine Micropaleontology*, 8(2), 141-170. https://doi.org/10.1016/0377-8398(83)90009-9

Backman, J., Raffi, I., Rio, D., Fornaciari, E., & Pälike, H. (2012). Biozonation and biochronology of Miocene through Pleistocene calcareous nannofossils from low and middle latitudes. *Newsletters on Stratigraphy*, 45(3), 221-244. https://doi.org/10.1127/0078-0421/2012/0022

Bijl, P. K., Schouten, S., Sluijs, A., Reichart, G. -.J, Zachos, J. C., & Brinkhuis, H. (2009). Early Palaeogene temperature evolution of the southwest Pacific Ocean. *Nature*, 461(7265), 776-779. https://doi.org/10.1038/nature08399

Boyle, P. R., Romans, B. W., Tucholke, B. E., Norris, R. D., Swift, S. A., & Sexton, P. F. (2017). Cenozoic north Atlantic deep circulation history recorded in contourite drifts, offshore Newfoundland, Canada. Marine *Geology*, 385, 185-203. https://doi.org/10.1016/j.margeo.2016.12.01

Bown, P. R., Young, J. R. (1998). Techniques. In: Bown, P. R., (Ed.), Calcareous Nannofossil Biostratigraphy. Kluwer Academic Publishers, p. 16–28

Bown, P.R., Lees, J.A., Young, J.R., (2004). Calcareous nannofossil evolution and diversity through time, in: Thierstein, H.R., Young, J.R. (Eds.), Coccolithophores: From Molecular Processes to Global Impact. Springer-Verlag, pp. 481–508.

Bown, P.R., (2005). Palaeogene calcareous nannofossils from the Kilwa and Lindi areas of coastal Tanzania (Tanzania Drilling Project 2003-4). Journal of Nannoplankton Research, 27(1): 21-95.

Bown, P.R. & Dunkley Jones, T. (2006). New Palaeogene calcareous nannofossil taxa from coastal Tanzania: Tanzania Drilling Project Sites 11 to 14. Journal of Nannoplankton Research, 28(1): 17-34

Bown, P. R., Jones, T. D., Lees, J. A., Randell, R. D., Mizzi, J. A., Pearson, P. N., Wade, B. S. (2008). A Paleogene calcareous microfossil Konservat-Lagerstätte from the Kilwa Group of coastal Tanzania. *Bulletin of the Geological Society of America*, 120(1-2), 3-12. https://doi.org/10.1130/B26261.

Bown, P.R. & Dunkley Jones, T., 2012. Calcareous nannofossils from the Paleogene equatorial Pacific (IODP Expedition 320 Sites U1331-1334). Journal of Nannoplankton Research, 32(2): 3-51

Bown, P.R. & Newsam, C., (2017). Calcareous nannofossils from the Eocene North Atlantic Ocean (IODP Expedition 342 Sites U1403–1411). *Journal of Nannoplankton Research*, 37(1): 25-60.

Bralower, T. J. (2002). Evidence of surface water oligotrophy during the Paleocene-Eocene Thermal Maximum: Nannofossil assemblage data from Ocean Drilling Program Site 690, Maud Rise, Weddell Sea. *Paleoceanography*, 17(2), 13-1

Coccioni, R., Bancalà, G., Catanzariti, R., Fornaciari, E., Frontalini, F., Giusberti, L., Jovane, L., Luciani, V., Savian, J., Sprovieri, M., 2012. An integrated stratigraphic record of the Palaeocene-lower Eocene at Gubbio (Italy), new insights into the early Palaeogene hyperthermals and carbon isotope excursions, *Terra Nova*, 24, 380−386. http://dx.doi.org/10.1111/j.1365-3121.2012.01076.x .

Coxall, H. K., Huck, C. E., Huber, M., Lear, C. H., Legarda-Lisarri, A., O'Regan, M., Backman, J. (2018). Export of nutrient rich northern component water preceded early oligocene antarctic glaciation. *Nature Geoscience*, 11(3), 190-196. https://doi.org/10.1038/s41561-018-0069-9

Cramer, B. S., Wright, J. D., Kent, D. V., & Aubry, M. (2003). Orbital climate forcing of $\delta^{13}C$ excursions in the late Paleocene-early Eocene (chrons C24n-C25n). *Paleoceanography*, 18(4) https://doi.org/10.1029/2003PA000909

Cramer, B. S., Toggweiler, J. R., Wright, J. D., Katz, M. E., & Miller, K. G. (2009). Ocean overturning since the late Cretaceous: Inferences from a new benthic foraminiferal isotope compilation. *Paleoceanography*, 24(4) https://doi.org/10.1029/2008PA00168

Cramwinckel, M. J., Huber, M., Kocken, I. J., Agnini, C., Bijl, P. K., Bohaty, S. M., Sluijs, A. (2018). Synchronous tropical and polar temperature evolution in the Eocene. *Nature,* 559(7714), 382-386. https://doi.org/10.1038/s41586-018-0272-2

Jones, T. D., Bown, P. R., Pearson, P. N., Wade, B. S., Coxall, H. K., & Lear, C. H. (2008). Major shifts in calcareous phytoplankton assemblages through the Eocene-Oligocene transition of Tanzania and their implications for low-latitude primary production. *Paleoceanography*, 23(4) https://doi.org/10.1029/2008PA001640

Dutton, A., Lohmann, K. C., & Leckie, R. M. (2005). Insights from the Paleogene tropical Pacific: Foraminiferal stable isotope and elemental results from Site 1209, Shatsky Rise. *Paleoceanography*, 20(3), 1-16. https://doi.org/10.1029/2004PA001098

Fioroni, C., Villa, G., Persico, D., & Jovane, L. (2015). Middle Eocene-lower Oligocene calcareous nannofossil biostratigraphy and paleoceanographic implications from Site 711 (equatorial Indian Ocean). *Marine Micropaleontology*, 118, 50-62. https://doi.org/10.1016/j.marmicro.2015.06.001

Gallagher, L. T. (1988). A technique for viewing the same nannofossil specimen in light microscope and scanning electron microscope using standard preparation materials. *Journal of Micropalaeontology*, 7(1), 53-57. https://doi.org/10.1144/jm.7.1.53

Gibbs, S. J., Bralower, T. J., Bown, P. R., Zachos, J. C., & Bybell, L. M. (2006). Shelf and open-ocean calcareous phytoplankton assemblages across the paleocene-eocene thermal maximum: Implications for global productivity gradients. *Geology*, 34(4), 233-236. https://doi.org/10.1130/G22381.1

Hollis, C. J., Taylor, K. W. R., Handley, L., Pancost, R. D., Huber, M., Creech, J. B., Zachos, J. C. (2012). Early Paleogene temperature history of the southwest Pacific Ocean: Reconciling proxies and models. *Earth and Planetary Science Letters*, 349-350, 53-66. https://doi.org/10.1016/j.epsl.2012.06.024

Huber, M., & Caballero, R. (2011). The early Eocene equable climate problem revisited. *Climate of the Past*, 7(2), 603-633. https://doi.org/10.5194/cp-7-603-201

Inglis, G. N., Farnsworth, A., Lunt, D., Foster, G. L., Hollis, C. J., Pagani, M., Pancost, R. D. (2015). Descent toward the icehouse: Eocene sea surface cooling inferred from GDGT distributions. *Paleoceanography*, 30(7), 1000-1020. https://doi.org/10.1002/2014PA002723

Kalb, A. L., & Bralower, T. J. (2012). Nannoplankton origination events and environmental changes in the late Paleocene and early Eocene. *Marine Micropaleontology*, 92-93, 1-15. https://doi.org/10.1016/j.marmicro.2012.03.00

Turner, S. K., Sexton, P. F., Charles, C. D., & Norris, R. D. (2014). Persistence of carbon release events through the peak of early Eocene global warmth. *Nature Geoscience*, 7(10), 748-751. https://doi.org/10.1038/NGEO2240

Lagabrielle, Y., Goddéris, Y., Donnadieu, Y., Malavieille, J., & Suarez, M. (2009). The tectonic history of Drake Passage and its possible impacts on global climate. *Earth and Planetary Science Letters*, 279(3-4), 197-211. https://doi.org/10.1016/j.epsl.2008.12.03

Lauretano, V., Hilgen, F. J., Zachos, J. C., & Lourens, L. J. (2016). Astronomically tuned age model for the early Eocene carbon isotope events: A new high-resolution δ^{13}Cbenthic record of ODP site 1263 between ~ 49 and ~ 54 Ma. *Newsletters on Stratigraphy*, 49(2), 383-400. https://doi.org/10.1127/nos/2016/0077

Lear, C. H., Elderfield, H., & Wilson, P. A. (2000). Cenozoic deep-sea temperatures and global ice volumes from Mg/Ca in benthic foraminiferal calcite. *Science*, 287(5451), 269-272. https://doi.org/10.1126/science.287.5451.26

Lees, J. A., Bown, P. R., Young, J. R., & Riding, J. B. (2004). Evidence for annual records of phytoplankton productivity in the Kimmeridge clay formation coccolith stone bands (upper Jurassic, Dorset, UK). *Marine Micropaleontology*, 52(1-4), 29-49. https://doi.org/10.1016/j.marmicro.2004.04.005

Luciani, V., Dickens, R. G., Backman, J., Fornaciari, E., Giusberti, L., Agnini, C., & D'Onofrio, R. (2016). Major perturbations in the global carbon cycle and photosymbiont-bearing planktic foraminifera during the early Eocene. *Climate of the Past*, 12(4), 981-1007. https://doi.org/10.5194/cp-12-981-2016

Martini, E. (1971). Standard Tertiary and Quaternary calcareous nannoplankton zonation, in: Proceedings of the 2nd Planktonic Conference, 2, Tecnoscienza, Roma, 739–785, 1971.

Norris, R.D., Wilson, P.A., Blum, P., Scientists, E. 342, 2014. Paleogene Newfoundland Sediment Drifts and MDHDS Test, in: Proceedings of the Integrated Ocean Drilling Program, 342: College Station, TX (Integrated Ocean Drilling Program). https://doi.org/10.2204/iodp.proc.342.2014

Okada, H., & Bukry, D. (1980). Supplementary modification and introduction of code numbers to the low-latitude coccolith biostratigraphic zonation (Bukry, 1973; 1975). *Marine Micropaleontology*, 5(C), 321-325. https://doi.org/10.1016/0377-8398(80)90016-X

Pagani, M., Zachos, J. C., Freeman, K. H., Tipple, B., & Bohaty, S. (2005). Atmospheric science: Marked decline in atmospheric carbon dioxide concentrations during the Paleogene. *Science*, 309(5734), 600-603. https://doi.org/10.1126/science.1110063

Perch-Nielsen, K. (1985). Cenozoic calcareous nannofossils, in: Bolli, H.M., Saunders, J.B., Perch-Nielsen, K. (Eds.), Plankton Stratigraphy. Cambridge University Press, Cambridge, pp. 427–554.

Pross, J., Contreras, L., Bijl, P. K., Greenwood, D. R., Bohaty, S. M., Schouten, S., Yamane, M. (2012). Persistent near–tropical warmth on the Antarctic continent during the early Eocene Epoch. *Nature*, 488(7409), 73-77. https://doi.org/10.1038/nature1130

Rio, D., Raffi, I., Villa., G. (1990). Pliocene-Pleistocene calcareous nannofossil distribution patterns in the Western Mediterranean. Proceedings of the Ocean Drilling Program, Scientific Results. Vol.17, 513-533.

Schneider, L. J., Bralower, T. J., & Kump, L. R. (2011). Response of nannoplankton to early Eocene ocean destratification. *Palaeogeography, Palaeoclimatology, Palaeoecology*, 310(3-4), 152-162. https://doi.org/10.1016/j.palaeo.2011.06.018

Sexton, P. F., Norris, R. D., Wilson, P. A., Pälike, H., Westerhold, T., Röhl, U., Gibbs, S. (2011). Eocene global warming events driven by ventilation of oceanic dissolved organic carbon. *Nature*, 471(7338), 349-353. https://doi.org/10.1038/nature09826

Toffanin, F., Agnini, C., Fornaciari, E., Rio, D., Giusberti, L., Luciani, V., Spofforth, D.J.A., Pälike, H. (2011). Changes in calcareous nannofossil assemblages during the Middle Eocene Climatic Optimum: Clues from the central-western Tethys (Alano section, NE Italy). *Marine Micropaleontology,* 81, 22–31. https://doi.org/10.1016/j.marmicro.2011.07.002

Shamrock, J.L. (2010). A new calcareous nannofossil species of the genus *Sphenolithus* from the Middle Eocene (Lutetian) and its biostratigraphic significance. Journal of Nannoplankton Research, 31(1): 5-10

Romein, A.J.T. (1979). Lineages in early Paleogene calcareous nannoplankton. Utrecht Micropaleontoleontological Bullettin. 22, 1-231.

Shamrock, J. L., & Watkins, D. K. (2012). Eocene calcareous nannofossil biostratigraphy and community structure from Exmouth Plateau, Eastern Indian Ocean (ODP site 762). *Stratigraphy*, 9(1), 1-54. Retrieved from www.scopus.com

Slotnick, B. S., Dickens, G. R., Hollis, C. J., Crampton, J. S., Strong, C. P., & Zachos, J. C. (2014). Extending lithologic and stable carbon isotope records at mead stream (New Zealand) through the middle Eocene. *Rendiconti Online Società Geologica Italiana*, 31, 201-202. https://doi.org/10.3301/ROL.2014.12

Tori, F., & Monechi, S. (2013). Lutetian calcareous nannofossil events in the Agost section (Spain): Implications toward a revision of the middle Eocene biomagnetostratigraphy. *Lethaia*, 46(3), 293-307. https://doi.org/10.1111/let.12008

Vahlenkamp, M., Niezgodzki, I., De Vleeschouwer, D., Bickert, T., Harper, D., Kirtland Turner, S., Pälike, H. (2018). Astronomically paced changes in deep-water circulation in the western North Atlantic during the middle Eocene. *Earth and Planetary Science Letters*, 484, 329-340. https://doi.org/10.1016/j.epsl.2017.12.016

Vandenberghe, N., F. J. Hilgen, R. P. Speijer, J. G. Ogg, F. M. Gradstein, O. Hammer, C. J. Hollis, and J. J. Hooker (2012), Chapter 28 - The Paleogene Period, in The Geologic Time Scale, edited by F. M. Gradstein, J. G. Ogg, M. D. Schmitz and G. M. Ogg, pp. 855-921, Elsevier, Boston, https://doi.org/10.1016/B978-0-444-59425-9.00028-7

Villa, G., Fioroni, C., Pea, L., Bohaty, S., & Persico, D. (2008). Middle Eocene-late Oligocene climate variability: Calcareous nannofossil response at Kerguelen Plateau, Site 748. *Marine Micropaleontology*, 69(2), 173-192. https://doi.org/10.1016/j.marmicro.2008.07.00

Wade, B. S., & Bown, P. R. (2006). Calcareous nannofossils in extreme environments: The Messinian Salinity Crisis, Polemi Basin, Cyprus. *Palaeogeography, Palaeoclimatology, Palaeoecology*, 233(3-4), 271-286. https://doi.org/10.1016/j.palaeo.2005.10.007

Westerhold, T., Röhl, U., Frederichs, T., Agnini, C., Raffi, I., Zachos, J. C., & Wilkens, R. H. (2017). Astronomical calibration of the Ypresian timescale: Implications for seafloor spreading rates and the chaotic behavior of the solar system? *Climate of the Past*, 13(9), 1129-1152. https://doi.org/10.5194/cp-13-1129-201

Westerhold, T., Röhl, U., Donner, B., & Zachos, J. C. (2018). Global extent of early Eocene hyperthermal events: A new Pacific benthic foraminiferal isotope record from Shatsky Rise (ODP Site 1209).*Paleoceanography and Paleoclimatology,* 33(6), 626-642. https://doi.org/10.1029/2017PA003306

Yamamoto, Y., Fukami, H., Taniguchi, W., and Lippert, P.C. (2018). Data report: updated magnetostratigraphy for IODP Sites U1403, U1408, U1409, and U1410. In Norris, R.D., Wilson, P.A., Blum, P., and the Expedition 342 Scientists, Proceedings of the Integrated Ocean Drilling Program, 342: College Station, TX (Integrated Ocean Drilling Program). https://doi.org/10.2204/iodp.proc.342.207.2018

Young, J. R., Bergen, J. A., Bown, P. R., Burnett, J. A., Fiorentino, A., Jordan, R. W., Von Salis, K. (1997). Guidelines for coccolith and calcareous nannofossil terminology. *Palaeontology*, 40(4), 875-912.

Zachos, J., Pagani, H., Sloan, L., Thomas, E., & Billups, K. (2001). Trends, rhythms, and aberrations in global climate 65 Ma to present. *Science*, 292(5517), 686-693. https://doi.org/10.1126/science.1059412

Zachos, J. C., & Kump, L. R. (2005). Carbon cycle feedbacks and the initiation of Antarctic glaciation in the earliest Oligocene. *Global and Planetary Change*, 47(1), 51-66. https://doi.org/10.1016/j.gloplacha.2005.01.001

Zachos, J. C., Dickens, G. R., & Zeebe, R. E. (2008). An early Cenozoic perspective on greenhouse warming and carbon-cycle dynamics. *Nature*, 451(7176), 279-283. https://doi.org/10.1038/nature06588

Chapter 5

Conclusion

The ~ 8 Myr time interval investigated in this PhD thesis is a relatively understudied interval of the Paleogene that encompasses the final stages of the extreme greenhouse conditions of the Early Eocene Climatic Optimum and the onset of the middle Eocene cooling. The aim of this study was to document the ecological and evolutionary dynamics of calcareous nannofossil assemblages across the early-middle Eocene transition and to improve the available Eocene biostratigraphic framework.

The case study is a sedimentary succession recovered at IODP Site U1410 on the Southeast Newfoundland Ridge, in the northwest Atlantic. At this Site, the lower Eocene sequence was characterized by pelagic sedimentation, but close to the Ypresian-Lutetian boundary expanded packages of clay-rich sediments dramatically change the sedimentation regime. The high abundance of clay has been related to the input of terrigenous material delivered by the progenitor of the North Atlantic Deep Western Boundary Current. Site U1410 provides the most complete record of the Ypresian-Lutetian transition in the North Atlantic and worldwide. In addition, the clay-rich drift sediments favoured the exquisite preservation of calcareous nannofossils and represents an extraordinary archive to document the profound reorganization after the EECO as well as the emergence and evolution of two biostratigraphically important evolutionary lineages among coccolithaceans and sphenoliths. In particular, the exceptional preservation of calcareous nannofossils enabled to document the delicate and fragile morphological features, such as central area crossbars and delicate spines of sphenoliths. The unique chance to study this amazing material has one more emphasized the importance of taxonomy to understand evolutionary processes and to provide reliable biostratigraphic data.

5.1 The long-term readjustment of calcareous nannofossil assemblages after the EECO

Calcareous nannoplankton has been one of the major phytoplankton group in ocean and understanding the tempo and mode of their evolution and their influence on the marine ecosystems is important but even more relevant during phase of the Earth's history that are characterized by dramatic changes in climate as for instance the switch from the EECO condition to the onset of the global cooling occurred at the early middle Eocene. During the EECO calcareous nannofossil assemblages is affected a major rearrangement towards a modern-like community structure, with the evolutionary turn-over between *Toweius* and *Reticulofenestra-Dictyoccocites*. At Site 1410, this turn-

over as well as the following proliferation of *Reticulofenestra,* which represented more than 50% of the assemblages by the early Lutetian, is particularly weel-documented (Chapter 2). On a long-term perspective, a broad parallelism has been observed between the paleoenvironmental signal inferred by nannoplankton assemblages and stable isotope records. The EECO interval has been interpreted as an unstable interval, where the warm-water and oligotrophic taxa (*Zygrhablithus, Discoaster* and *Sphenolithus)* are abundant but show significant fluctuations (principally driven by genus *Discoaster*). The latest Ypresian was characterized by a shift toward more temperate and eutrophic conditions that is proven by the decline of warm/r oligotrophic taxa and the simultaneous expansion of temperate/mesotrophic- *Reticulofenestra.* This change is coincident with a minor positive shift in the bulk oxygen isotope record that might indicate a variation in the thermal structure of the water column which could have reduced the optimal ecological niches of warm/oligotrophic taxa and favoured the dominance of the more opportunistic *Reticulofenestra.* From the base of the Lutetian calcareous nannofossil assemblages appears to have reached a new steady-state where *Reticulofenstra* dominated over the other taxa.

5.2 The Ypresian-Lutetian boundary: chronostratigraphic problems and possible short-term paleoenvironmental perturbation

The magnetostratigraphic and calcareous nannofossil records from Site U1410 have further highlighted some issues related to the use of the Base of *B. inflatus* as primary correlation criteria for the base of the Lutetian (Chapter 2). In the GSSP section of Gorrondatxe (Spain), this event has been found ca. 800 kyr above the base of Chron C21r, whereas in numerous section from the Atlantic Ocean as well as at Site U1410, this biohorizon lies at the C21r/C21n transition, which means that this event as well as the base of the Lutetian is ca. 45 kyr younger .

In addition, previous studies from Gorrondatxe section has suggested the occurrence of a hyperthermal event just above the Base of *B. inflatus.* At Site U1410, few meters above the Base of *B. inflatus*, the trend of $\delta^{13}C$ is characterized by a distinctive double-peak negative shift that is correlated with a clear decreasing trend of $\delta^{18}O$ values. These isotope trends and the concomitant increase in abundance of *D. sublodoensis* might be suggestive of a potential short-term warming episode. However, the possible correlation between the event recorded at Gorrondatxe and those at Site U1410 remains unresolved because they are in a different position respect to magnetostratigraphy.

5.3. The new evolutionary lineage among large middle Eocene coccolithaceans and the new described genus *Pletolithus*

At Site U1410, the expanded middle Eocene successions containing clay-rich nannofossil oozes with exceptionally well preserved nannofossils enabled to observe a number of structural features and progressive morphological changes that suggest that during the middle Eocene a new lineage among *Coccolithus*-like placoliths evolved with the formation of a well-developed cross or X-shaped structure in the central area (Chapter 3). Our findings have led to a taxonomic reassessment of middle Eocene large coccolithaceans, with the description of a new genus *(Pletolithus*) a new species *(Pletolithus giganteus)* and four new combinations (*Pletolithus opdykei, Pletolithus staurion, Pletolithus mutatus* and *Pletolithus gigas).* The new genus probably evolved from a morphological variant of *Coccolithus* characterized by having very delicate crossbars in the central area that become more distinctive and massive in the forms belonging to *Pletolithus*. The final step in the evolutionary trend is represented by the gradual rotation of the central area structure that evolved from a rotated cross in *P. giganteus* into an x-shaped structure in the marker species *P. gigas.* Morphometric measurements on *P. gigas* and on the strictly morphologically related *P. giganteus*, provide an unambiguous taxonomic concept of the marker species *P. gigas* and improve the stability of middle Eocene biostratigraphy. This lineage intriguingly emerged in correspondence of the onset of the drift-sedimentation while the appearance of related morphotypes coincided with changes in the $\delta^{13}C$. This study concludes that the evolutionary trend displayed by *Pletolithus* during the relatively stable condition of the Lutetian represents an example of iterative evolution where the appearance of robust central structures and their rotation are morphologic characters that reiterate trough time.

5.4 The *Sphenolithus furcatholithoides* lineage

Throughout the study interval, the composition of sphenolith assemblages underwent tosignificant changes (Chapter 4). Across the early-middle Eocene transition and in correspondence of distinctive excursions both in oxygen and carbon isotopes, we documented the decline of *S. radians* and the simultaneous increase of *S. spiniger.* This important change in the general composition of sphenolith assemblages was followed by an interval of morphostructural innovation that was marked by the appearance of morphotypes bearing a bifurcating apical spine (*Sphenolithus furcatolihoides* gr.). We proposed that these forms evolved from a *S. morifomis*-like ancestor through a progressive development of very delicate and fragile processes that eventually transformed into two or more robust spines diverging with different angles in the *S. kempii, S. perpendicularis, S. furcatolithoides, S. cuniculus, S. strigosus* plexus. Taxa belonging to this lineage include forms with a wide range of morphologies, but this study reveals that the extinction figure of the base at 45° is a crucial feature

in order to distinguish different morphotypes. Two different extinction figures have been observed: a bright cross-shaped figure in *S. kempii, S. perpendicularis, S. furcatolithoides* morphotype A and an almost dark bow tie-figure in *S. furcatolithoides* morphotype B, *S. cuniculus* and *S. strigosus.* These different patterns are related to a progressive reduction/ disappearance of the lateral cycle through time.

The detailed study of the successive evolutionary steps observed in this lineage allow torecognized or test biohorizons that could improve the biostratigraphic accuracy within the Lutetian stage.

5.5 The early middle Eocene biostratigraphic framework

The semiquantitative and relative abundance patterns of biostratigraphically important species allowed to test the recent biozonation proposed by Agnini et al., (2014). The spacing and the ranking of primary biohorizons recognized at Site U1410 are in agreement with the results from the reference sections of Possagno and Site 1051 (Chapter 2). However, the Base Common of *D. sublodoensis* 5-rayed morphotype, the Top of *D. lodoensis* and the Top of *P. gigas* are considered as problematic biohorizons due to their scattered abundance patterns especially close to their appearance or extinction levels.

A comparison with Site 1051 have evidenced that the Base common of *S. cuniculus* at Site U1410 is in good agreement t with the datum observed at Blake Nose site: This result is promising because it suggested that this biohorizon is (Chapter 4). Proposed additional biohorizons that are poorly documented but seems promising are the Top of *D. kuepperi* and the Top of *G. gammation.*

The detailed studies performed on *Pletolithus* (Chapter 3) and *Sphenolithus furcatolithoides* group (Chapter 4) provide comprehensive model of the evolution of these lineages and improve the taxonomy of the marker species *P. gigas.* The main value of these taxonomic studies is minimize the taxonomic effect and thus strengthening the available the middle Eocene biostratigraphic framework,.

5.6 Concluding remarks and future perspectives

One of the main task of this thesis was to assess the role of paleoenvironmental forcing on calcareous nannofossil evolutionary processes, including significant assemblages shifts and morphostructural innovations within specific groups. With regard to this task, calcareous nannofossil assemblages investigated at Site U1410 indicate that significant evolutionary events occur both during stressed environmental conditions and stable intervals. The turnover between *Toweius* and *Reticulofenestrids* took place during the extreme conditions characterizing the EECO , but the of the reorganization of the whole assemblage occurred over a longer time interval, during which relatively low amplitude changes in the physical and chemical parameters of surface waters are recorded. Similarly, the

appearance of reiterative characters among sphenoliths and coccolithaceans appears to have been associated with environmental stability, suggesting that the biotic factors might have played the main role in forcing the calcareous nannofossil evolution.

The initial phase of the Eocene long-term cooling has generally received less attention than other intervals. In order to fully understand marine ecosystem and paleoenvironmental evolution during this time interval, it is important to refine, expand and integrate the results presented in this study.

Further combined high-resolution calcareous nannofossil and geochemical records across the early-middle Eocene transition would allow a more comprehensive interpretation of the long and short-term trends of the post-EECO interval and would serve to evaluate if the key findings presented in this study are consistent in different settings. In addition, high-resolution semi-quantitative data of biostratigraphically important taxa are necessary in order further improve the stability of middle Eocene biostratigraphic framework. A particular attention should be deserved on the revaluation of the Base of *B. inflatus* because the present inconsistencies (Chapter 2) have grave implications for the base of the Lutetian.

ACKNOWLEDGEMENTS

First of all I would like to sincerely thank my supervisor, Claudia Agnini, who has been immensely generous with her knowledge over the last three years. This Ph.D. would not have been possible without her help. I am grateful for all the opportunities she has given me during my Ph.D. studies.

I am tremendously grateful to my co-supervisor Paul Bown, for his guidance and for giving me the opportunity to perform my studies at SEM. His support has been essential for this project. I would like to extent my thanks also to Jim Devy, for his help in teaching me how to use the SEM.

I also owe thanks to Martina de Riu and Veronica Lobba for allowing the use of their data within my thesis.

Huge thanks to the all my colleagues, especially students in my office, Chiara and Livio. I would like also to thank Hojung, for her kindness and help during my visit at UCL.

This project was supported by Fondazione Cassa di Risparmio di Padova e Rovigo and by Università degli Studi di Padova.